

NASA Contractor Report 182133
Allison EDR-13481

The Effects of Leading Edge and Downstream Film Cooling on Turbine Vane Heat Transfer

L.D. Hylton, V. Nirmalan, B.K. Sultanian,
and R.M. Kaufman

*Allison Gas Turbine Division
General Motors Corporation
Indianapolis, Indiana*

November 1988

Prepared for
Lewis Research Center
Under Contract NAS3-24619



National Aeronautics and
Space Administration

(NASA-CR-182133) THE EFFECTS OF LEADING
EDGE AND DOWNSTREAM FILM COOLING ON TURBINE
VANE HEAT TRANSFER Final Report (General
Motors Corp.) 175 p

CSCL 20D

N89-13754

G3/34 0181365
Unclass



TABLE OF CONTENTS

<u>Section</u>	<u>Title</u>	<u>Page</u>
I.	Summary	1
II.	Introduction	2
III.	Hardware and Instrumentation	3
	3.1 Facility description	3
	3.2 Facility instrumentation and geometry	4
	3.3 Cascade description	8
	3.4 Film cooling geometry description	8
	3.5 Test vane instrumentation	14
IV.	Data Acquisition and Reduction	20
	4.1 Data acquisition system	20
	4.2 Data acquisition software and data reduction procedures	20
	4.3 Heat transfer measurement technique	22
	4.4 Data uncertainties	24
V.	Test Conditions	26
	5.1 Heat transfer data test conditions	26
VI.	Discussion of Experimental Results	31
	6.1 Heat transfer results	31
	6.2 Throat passage pressure results	47
VII.	Conclusions and Recommendations	51
	Appendix A. Tabulated heat transfer data	52
	Appendix B. Heat transfer data comparison plots	108
	Appendix C. Tabulated throat passage static pressure data ..	164
	Nomenclature	169
	References	172



I. SUMMARY

This report addresses the progress under contract NAS3-24619 toward the goal of establishing a relevant data base for use in improving the predictive design capabilities for external heat transfer to turbine vanes, including the effects of downstream film cooling with and without leading edge showerhead film cooling.

Experimental measurements were made in a two-dimensional cascade previously used to obtain vane surface heat transfer distributions on non-film cooled airfoils under contract NAS3-22761 and leading edge showerhead film cooled airfoils under contract NAS3-23695. The principal independent parameters -- Mach number, Reynolds number, turbulence, wall-to-gas temperature ratio, coolant-to-gas temperature ratio, and coolant-to-gas pressure ratio -- were maintained over ranges consistent with actual engine conditions and the test matrix was structured to provide an assessment of the independent influence of parameters of interest, namely, exit Mach number, exit Reynolds number, coolant-to-gas temperature ratio, and coolant-to-gas pressure ratio. Data from this contract provide a data base for downstream film cooled turbine vanes and extends the data bases generated in the previous two studies.

The vane external heat transfer data obtained in this program indicate that considerable cooling benefits can be achieved by utilizing downstream film cooling. The downstream film cooling process was shown to be a complex function of two competing mechanisms. The thermal dilution effect, associated with the injection of relatively cold fluid, results in a decrease in the heat transfer to the airfoil. Conversely, the turbulence augmentation, produced by the injection process, results in increased heat transfer to the airfoil. The data obtained in this program and presented in this report illustrate the interaction of these variables and should provide the airfoil designer and computational analyst the information required to improve heat transfer design capabilities for film cooled turbine airfoils.

II. INTRODUCTION

The thermal design of contemporary high pressure turbine nozzle guide vanes clearly represents one of the more difficult engineering tasks in the design of any modern aircraft gas turbine. Aerodynamic and thermal analysis procedures currently available to turbine designers have deficiencies that do not permit a priori designs that achieve design goals without expensive experimental development iterations.

This study is the experimental portion of the third part of a combined analytical and experimental program initiated to address one particular aspect of the overall design problem; namely, the prediction of external convective heat transfer. In the initial program, Hylton et al (Ref 1) reported results of a study that emphasized the development of a more reliable procedure for determining convective heat transfer loads to nonfilm cooled airfoil geometries. In the first program, the experimental efforts included obtaining heat transfer data on two airfoil geometries at simulated engine conditions. In the second program, Turner et al (Ref 2) reported the study that developed a procedure to predict convective heat transfer for a leading edge film cooled airfoil geometry. As part of that program, a five-row simulated common plenum showerhead geometry was tested to determine the differences between the film cooled and non-film cooled heat transfer coefficient distribution downstream of the leading edge film cooling array. The present program examines the problem of convective heat transfer for discrete site pressure and suction surface injection with and without leading edge blowing.

The first step in the development of a prediction tool for a highly complex three-dimensional coolant jet/mainstream flow interaction is the availability of a relevant data base. Hence, this experimental study was conducted to generate a representative data base. Experiments were conducted in a 2-D linear cascade. The vane profile used is the same as the one used in the showerhead film cooled experiments in Ref 2 and the same as one of the two airfoils used in the nonfilm cooled experiments reported in Ref 1. The leading edge showerhead five row film cooling hole geometry in the present study is identical to the hole geometry of the second study. In addition, the airfoil had film cooling arrays on the suction and pressure side, each consisting of two rows of holes. The three film cooling arrays were fed by separate plenums. Hence, the data base generated in this study can therefore be viewed as extension of the data base generated in the first two programs. Heat transfer data were acquired downstream of the pressure and suction surface film cooling arrays at two exit Mach number conditions of 0.75 and 0.90 with true chord Reynolds number of order 10^6 . Also, the blowing strength and coolant temperature were varied to quantify jet turbulence production and thermal dilution mechanisms. In addition to the heat transfer data, static pressure measurements on the vane surface and near the cascade throat were acquired for all test conditions.

The description of the hardware and instrumentation is given in detail in section III. The method of data acquisition and reduction is described in section IV. The test conditions are given in section V. The experimental results are presented and discussed in detail in section VI.

III. HARDWARE AND INSTRUMENTATION

This section provides a detailed description of the facility and hardware used in acquiring the heat transfer and vane surface and cascade throat static pressure data. A complete description of the cascade is given together with the locations of all facility and cascade instrumentation.

3.1 Facility Description

This experimental investigation was performed in the Allison Aerothermo-dynamic Cascade Facility (ACF). The purpose of this facility is to conduct experimental research in high-temperature turbine component models that embody advanced cooling techniques, aerodynamics, or materials. The experimental approach employs a 2-D model technique, with full dynamic similarity in free-stream Mach number (Ma) and boundary layer Reynolds number (Re) effects, and provides an experimental method to separate the effects on local heat transfer.

The facility consists of a burner, a convergent section, a free-stream section with instrumentation and optical access, a test section with instrumentation, a quench zone with back pressure regulation and an exhaust system. The facility is shown schematically in Figure 1.

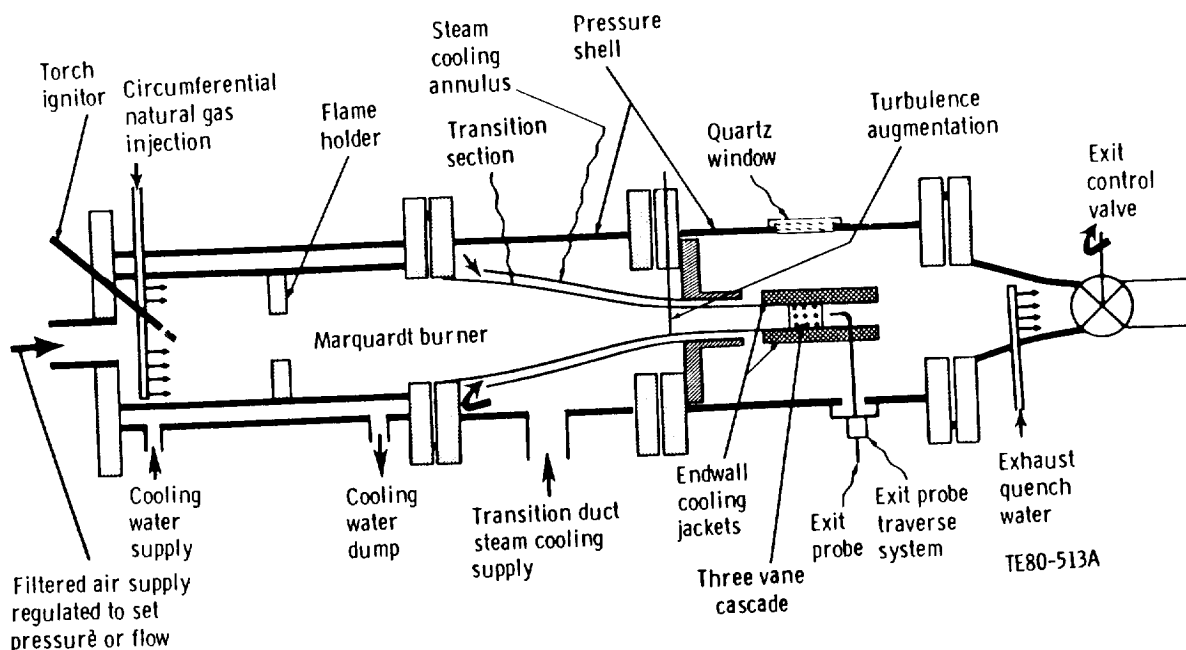


Figure 1. Schematic of the Aerothermodynamic Cascade Facility.

The Mach number and Reynolds number modeling considerations necessitate a burner with a large temperature, flow, and pressure range. This burner capability, coupled with back pressure regulating valve, allows experimental separation of free-stream Mach number and boundary layer Reynolds number effects to accurately simulate a wide range of engine designs and operating conditions.

A constant cross section is provided downstream of the burner to establish uniform inlet velocity, temperature, and turbulence profiles. This section is provided with temperature-controlled cooled walls and isolates the test section from radiant heat transfer from the primary combustion zone. The walls of the test section are cooled with steam to keep them at, or close to, the vane surface temperature to prevent radiant exchange. The test section design is unique in that it incorporates both aerodynamic and heat transfer data acquisition in a single tunnel, thereby reducing costs and ensuring the correlation of heat transfer and aerodynamic data for the single set of airfoils.

3.2 Facility Instrumentation and Geometry

The various flow circuits of the ACF incorporate standard inline instrumentation for measurement of flow rate, pressure, and temperature. American Society of Mechanical Engineers (ASME) standard sharp-edged orifices are used throughout to provide flow-rate measurements. The orifices used to meter the secondary flow systems for the current tests were calibrated to provide flow measurement accuracy to $\pm 2\%$. Facility and rig pressures were measured using two Scanivalve pressure scanners; one with six modules, each capable of handling 48 individual absolute pressures, and the other, with two modules coupled together to handle 24 differential pressures. Pressure transducers of appropriate ranges matched to the current experiment were inserted in these modules. Each time a set of data was taken, the pressure transducers were calibrated using an online pressure calibration system consisting of four dead weight testers connected to the pressure scanners. The standard pressures from three of the dead weight testers were measured by each of the pressure transducers to obtain a new calibration before each set of data was acquired. There are 300 Chromel-Alumel (CA) thermocouple circuits available in the laboratory for temperature measurement. These circuits are coupled to the data acquisition system through temperature-stabilized reference junctions.

A two-axis computer-controlled traverse system permits surveys of inlet pressure and temperature fields to be made. Access at the test section exit plane allows the installation of a three-axis computer-controlled traversing system, which enables exit pressure and/or temperature measurements to be made across the entire exit plane. Specifications regarding facility instrumentation are detailed in Table I.

The flow path upstream of the cascade in the ACF takes the burner discharge from a 31.5 cm (12.4 in.) diameter through a 50.8 cm (20. in) long transition section to a 7.6 cm x 27.9 cm (3 in. x 11 in.) rectangular section. A photograph of the transition duct is shown in Figure 2. The rectangular section upstream of the cascade is 36.83 cm (14.50 in.) long and contains inlet instrumentation. A schematic of the inlet and test section, showing the relative positions of the inlet and exit instrumentation, is shown in

Table I.
Aerothermodynamic cascade facility instrumentation

Pressure scanner	Scanivalve systems with 288 ports for absolute pressures and 24 ports for differential pressures.
Pressure transducers	Druck and Scanivalve, with ranges from 0-68.9 kPa to 0-689.4 kPa (0-10 psia to 0-100 psia)
Accuracy	+0.06% BSL
Thermocouple channels	300 CA
Accuracy	+0.3°C with calibration
Traversing gear	L.C. Smith 3-axis traversing system with computer interfaces. Discrete stepping capability to .001 of the traversing range.
Anemometers	LDA
Survey probes	Traversing CA thermocouple Traversing pressure or 5-hole cone probe

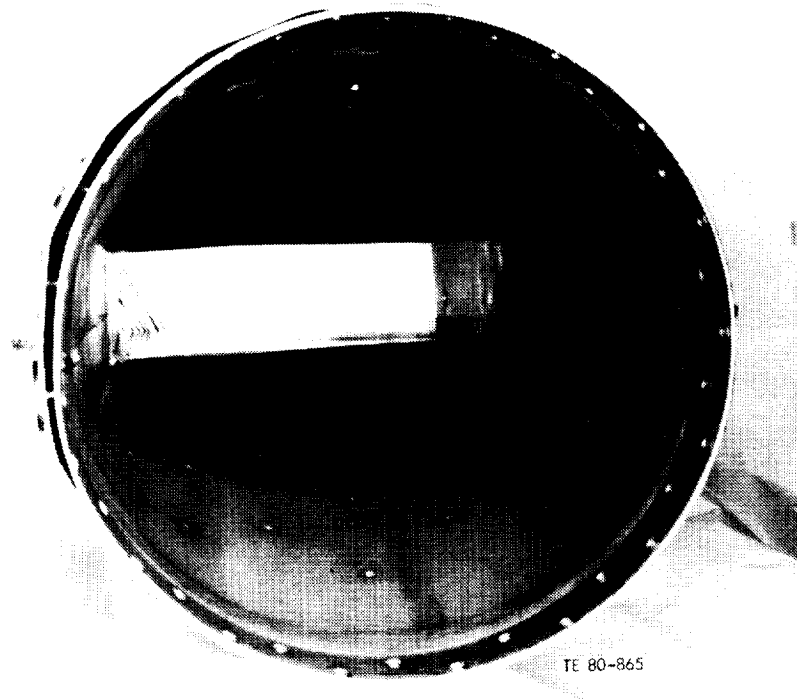
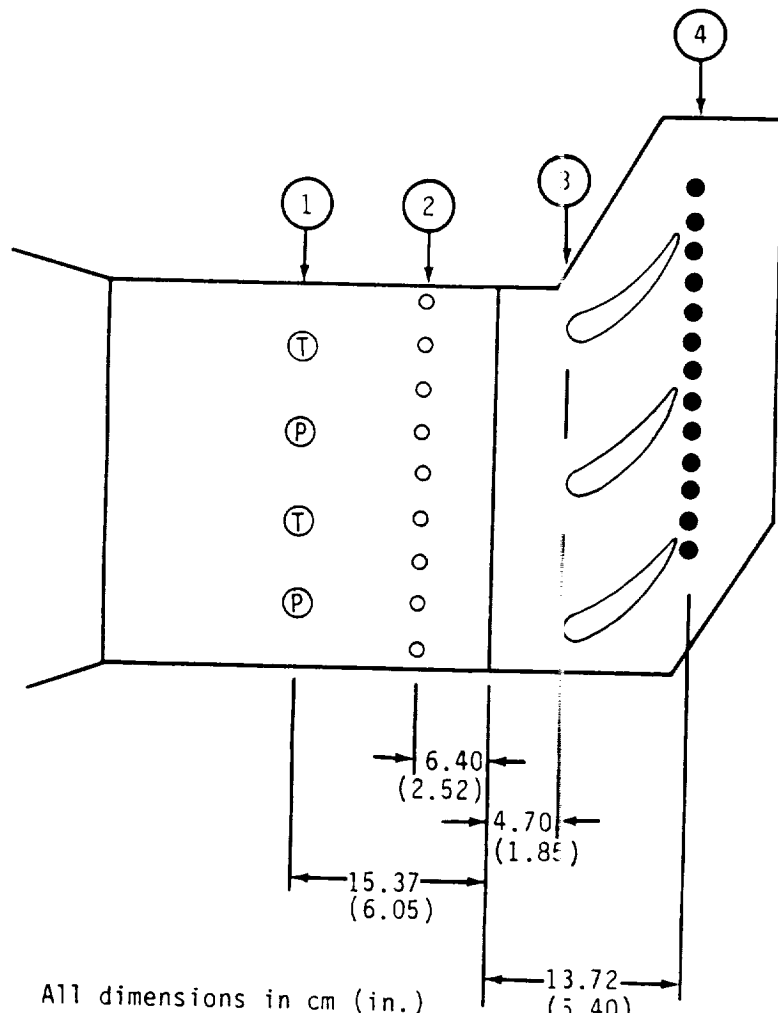


Figure 2. Burner-to-cascade inlet transition duct.

Figure 3. The inlet instrumentation consists of two inlet core total pressure rakes (each containing five total pressure probes), two inlet core temperature rakes (each containing five thermocouples), and eighteen endwall static pressure taps. The converging transition duct contains seven endwall static pressure taps. Thirty seven endwall static pressure taps are located in the endwall of the cascade at the exit plane. Six static pressure taps each are located at the cascade throat endwall to measure cascade throat pressures. Figure 4 shows a photograph giving the details of the endwall pressure taps.



- Ⓐ Core rakes
- Ⓑ Inlet static pressure taps
- Ⓒ Leading edge plane
- Ⓓ Exit static pressure taps

TE82-6020C

Figure 3. Facility instrumentation schematic.

ORIGINAL PAGE IS
OF POOR QUALITY

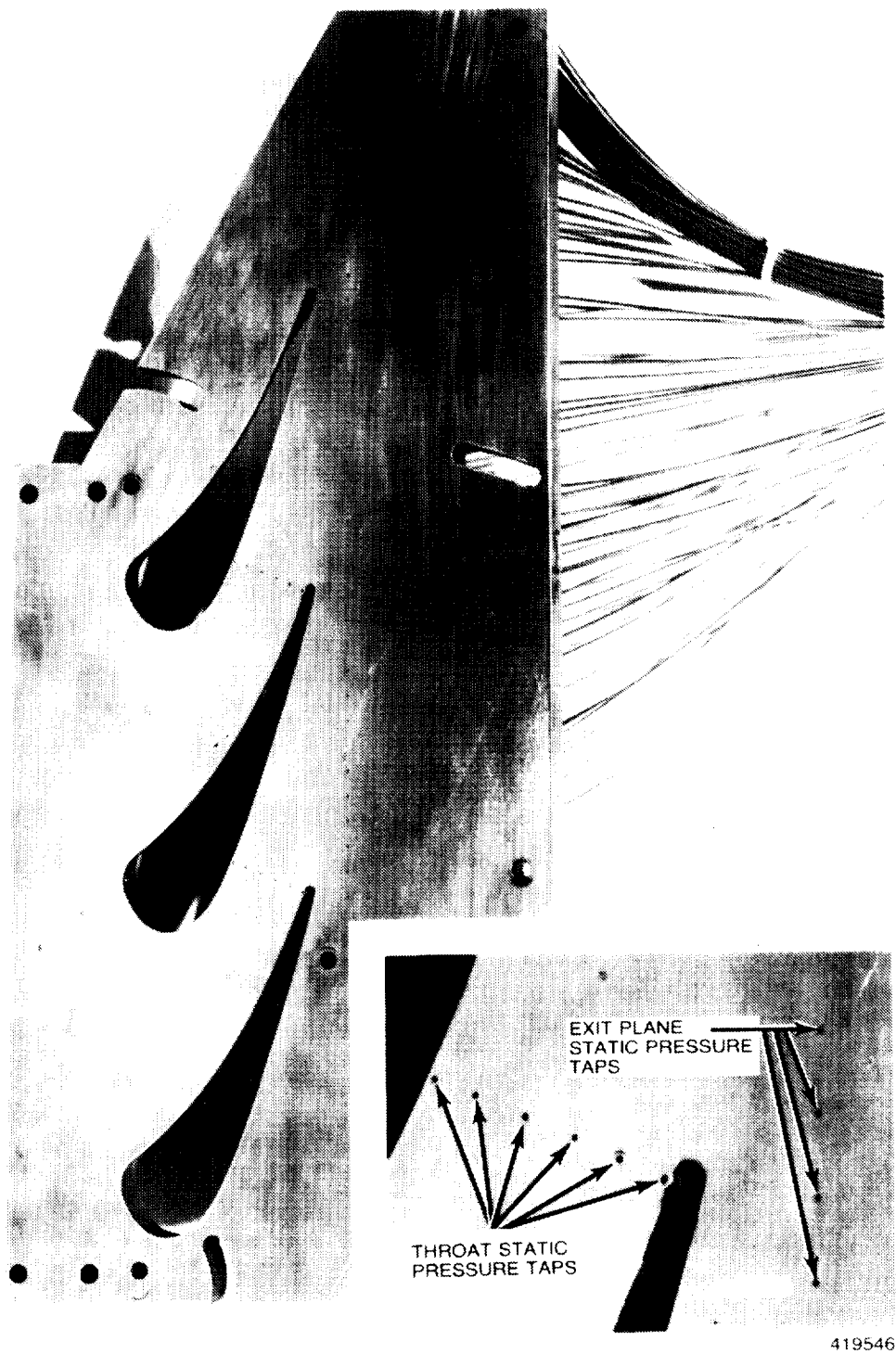


Figure 4. Details of the endwall static pressure taps at the exit plane and cascade throat.

3.3 Cascade Description

The three-vane cascade employed in this test, shown in Figure 5, was the C3X cascade previously used in the experimental studies reported in References 1 and 2. The center test vane was replaced with a new C3X vane which had suction side, leading edge, and pressure side film cooling arrays. The test vane was initially fabricated as a single piece. After all the film cooling holes and plenums and the ten radial cooling holes were machined, the vane was cut into a nose and a tail piece to form a thermal barrier between the film cooled nose piece and the rest of the vane. Photographs of the test vane are shown in Figure 6. The two pieces of the vane were held together by two pinned tabs mounted on each end of the vane. The two pin tabs were mounted before the vane was cut into two pieces in order to maintain the vane surface geometry.

The vane coordinates for the C3X airfoil are given in Table II. Figure 7 shows the cascade coordinate system used to define the airfoil shape. Table III lists additional geometry information for the cascade.

The test vane was internally cooled by an array of 10 radial cooling holes. The hole configuration is shown in Figure 8, which also depicts the finite element model (FEM) and the film cooling geometry. The radial cooling holes of each of the outer two slave vanes were supplied from a common plenum, whereas each hole in the test vane was supplied from a separate, metered line.

Flow splitters adjacent to the outer vanes and a tailboard were used to ensure periodicity. The exit plane static pressure taps provided information necessary to establish periodicity.

3.4 Film Cooling Geometry Description

The film cooling geometry for the test vane consisted of film cooling arrays on the leading edge, the suction surface, and the pressure surface. The leading edge film cooling geometry employed a showerhead array of five equally spaced rows of holes with the center row located at the predicted aerodynamic stagnation point. The hole array was staggered with the holes in the second row located midway (radially) between the holes in the first and the third rows. The holes were angled at 45 deg to the surface in the radial (spanwise) direction (slant angle). They were normal to the surface in the chordwise direction (skew angle). Coordinates of the film cooling hole rows are listed in Figure 8. The leading edge film cooling array was geometrically identical to the one tested in Reference 2. Geometry information for all film cooling arrays is detailed in Table IV.

Previous film cooling data of Reference 2 indicated that the ideal locations for the suction and pressure surface film cooling arrays would be just upstream of the suction and pressure surface recovery region respectively. These locations were determined to be 25.2% of the surface distance (as measured from the geometric stagnation point) on the suction side and 22.5% of the surface distance on the pressure side. Two cooling hole rows were centered at these points. The length-to-diameter ratio of the holes were kept the same as the showerhead hole length-to-diameter ratio. The suction surface holes were inclined at 35 degrees to the surface in the chordwise direction

**ORIGINAL PAGE IS
OF POOR QUALITY**

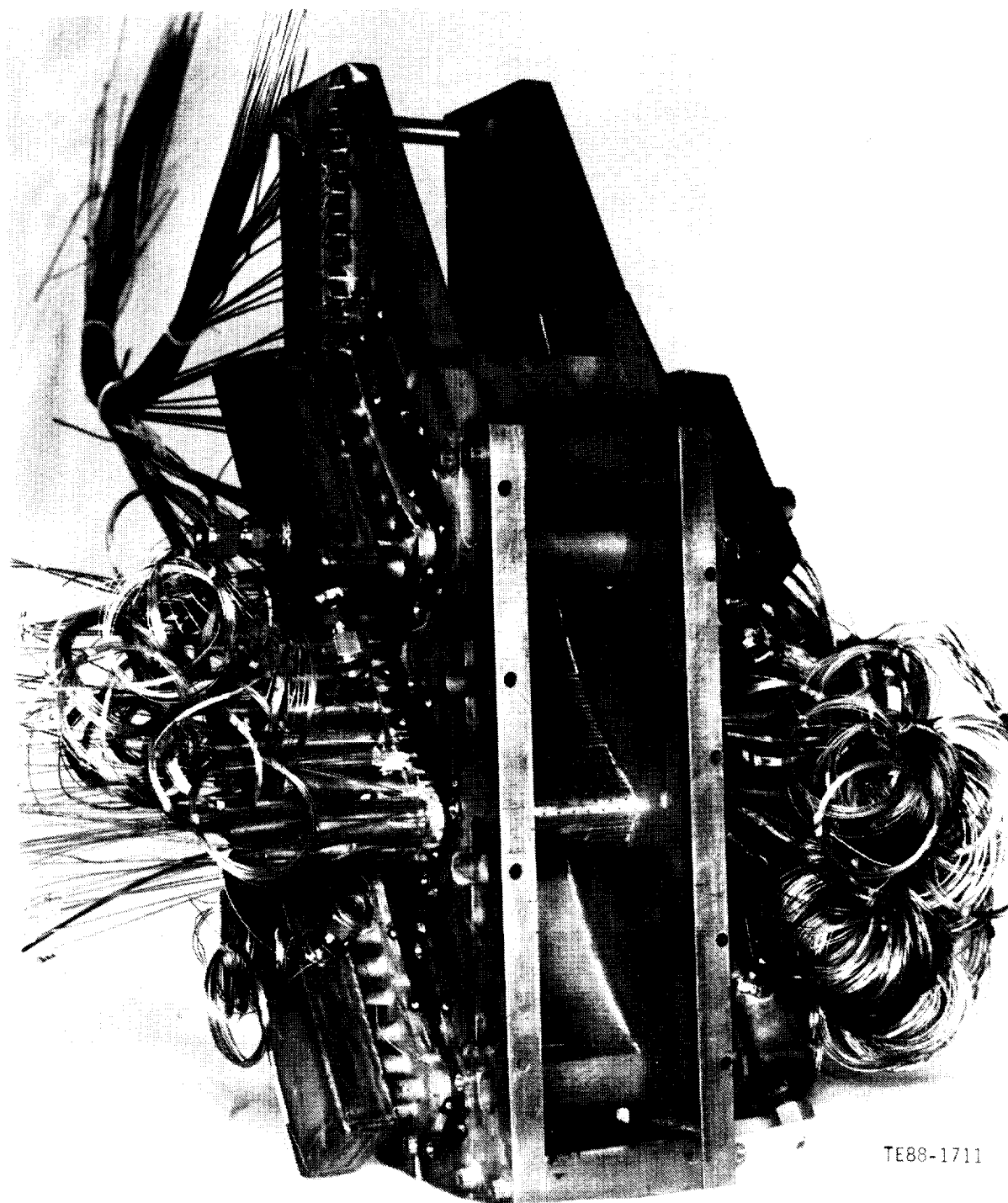
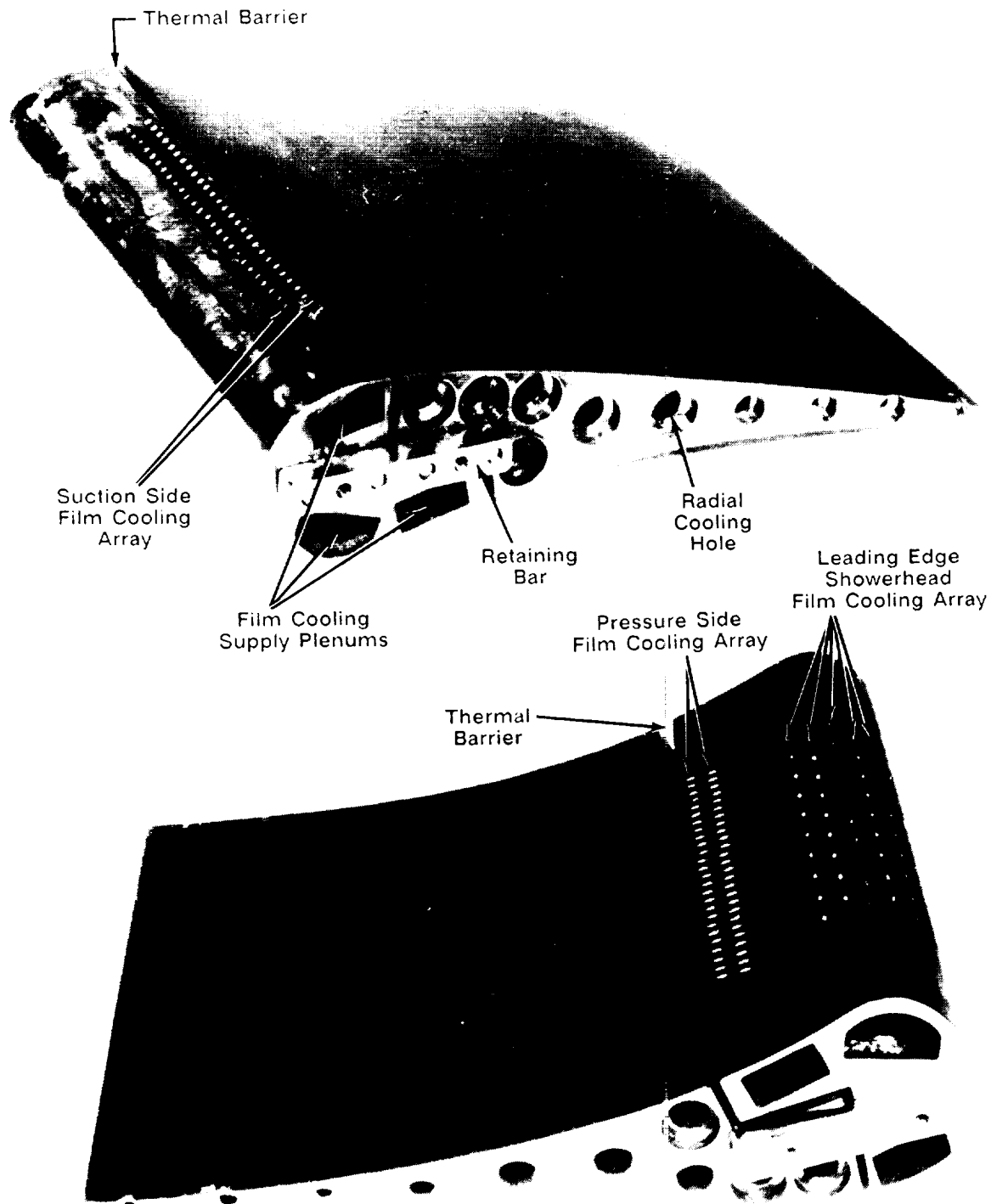


Figure 5. Photograph of the three vane C3X cascade.



TE88-1715

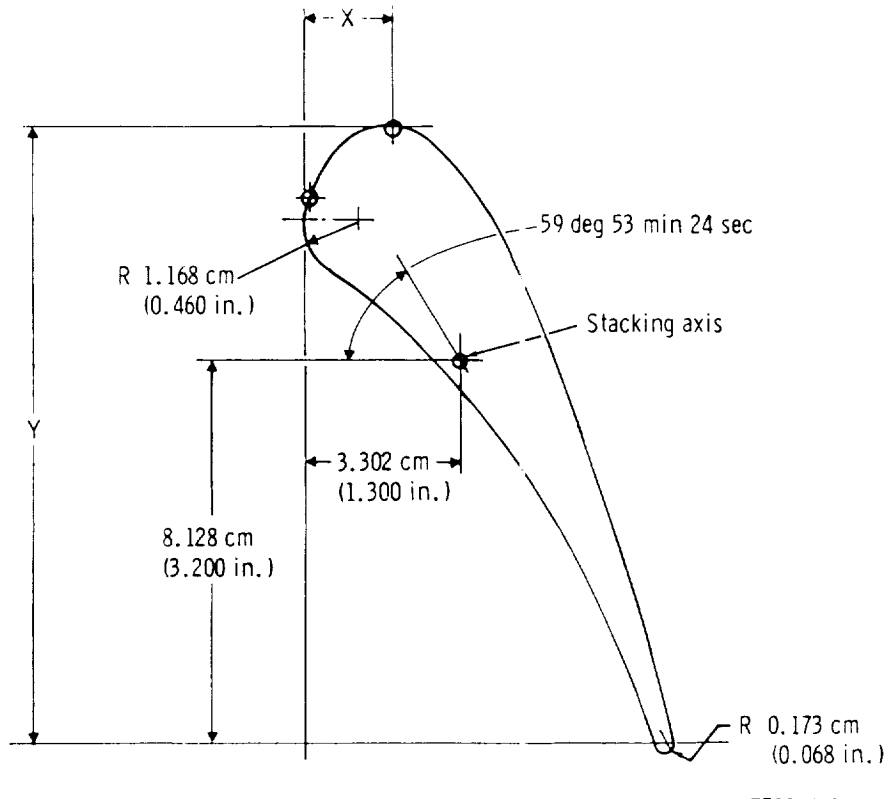
Figure 6. Leading edge and downstream film cooled C3X test vane.

ORIGINAL PAGE IS
OF POOR QUALITY

Table II
C3X vane coordinates

$$R_{LE} = 1.168 \text{ cm (0.460 in.) } R_{TE} = 0.173 \text{ cm (0.068 in.)}$$

Position number		Position number			
x--cm (in.)	y--cm (in.)	x--cm (in.)	y--cm (in.)		
1	0.1097 (0.0432)	11.6548 (4.5885)	40	7.4849 (2.9468)	-0.0617 (-0.0243)
2	0.3894 (0.1533)	12.1890 (4.7988)	41	7.3188 (2.8814)	0.3559 (0.1401)
3	0.7658 (0.3015)	12.6764 (4.9907)	42	7.1483 (2.8143)	0.7737 (0.3046)
4	1.2723 (0.5009)	13.0233 (5.1273)	43	6.9736 (2.7455)	1.1895 (0.4683)
5	1.8743 (0.7379)	13.1376 (5.1723)	44	6.7950 (2.6752)	1.6035 (0.6313)
6	2.4707 (0.9727)	12.9939 (5.1157)	45	6.6116 (2.6030)	2.0155 (0.7935)
7	2.9835 (1.1746)	12.6538 (4.9818)	46	6.4237 (2.5290)	2.4254 (0.9549)
8	3.3985 (1.3380)	12.1976 (4.8022)	47	6.2309 (2.4531)	2.8329 (1.1153)
9	3.7376 (1.4715)	11.6817 (4.5991)	48	6.0328 (2.3751)	3.2380 (1.2748)
10	4.0272 (1.5855)	11.1364 (4.3844)	49	5.8296 (2.2951)	3.6406 (1.4333)
11	4.2885 (1.6884)	10.5766 (4.1640)	50	5.6203 (2.2127)	4.0401 (1.5906)
12	4.5326 (1.7845)	10.0094 (3.9407)	51	5.4051 (2.1280)	4.4364 (1.7466)
13	4.7648 (1.8759)	9.4369 (3.7153)	52	5.1834 (2.0407)	4.8290 (1.9012)
14	4.9870 (1.9634)	8.8605 (3.4884)	53	4.9548 (1.9507)	5.2177 (2.0542)
15	5.2019 (2.0480)	8.2814 (3.2604)	54	4.7191 (1.8579)	5.6020 (2.2055)
16	5.4110 (2.1303)	7.7003 (3.0316)	55	4.4760 (1.7622)	5.9817 (2.3550)
17	5.6157 (2.2109)	7.1176 (2.8022)	56	4.2248 (1.6633)	6.3563 (2.5025)
18	5.8171 (2.2902)	6.5336 (2.5723)	57	3.9654 (1.5612)	6.7249 (2.6476)
19	6.0160 (2.3685)	5.9487 (2.3420)	58	3.6975 (1.4557)	7.0874 (2.7903)
20	6.2126 (2.4459)	5.3632 (2.1115)	59	3.4204 (1.3466)	7.4430 (2.9303)
21	6.4074 (2.5226)	4.7767 (1.8806)	60	3.1339 (1.2338)	7.7909 (3.0673)
22	6.5997 (2.5983)	4.1897 (1.6495)	61	2.8374 (1.1171)	8.1308 (3.2011)
23	6.7894 (2.6730)	3.6015 (1.4179)	62	2.5314 (0.9966)	8.4615 (3.3313)
24	6.9756 (2.7463)	3.0122 (1.1859)	63	2.2149 (0.8720)	8.7826 (3.4577)
25	7.1575 (2.8179)	2.4221 (0.9536)	64	1.8885 (0.7435)	9.0935 (3.5801)
26	7.3335 (2.8872)	1.8301 (0.7205)	65	1.5519 (0.6110)	9.3932 (3.6981)
27	7.5024 (2.9537)	1.2357 (0.4865)	66	1.2052 (0.4745)	9.6815 (3.8116)
28	7.6624 (3.0167)	0.6391 (0.2516)	67	0.8494 (0.3344)	9.9578 (3.9204)
29	7.8115 (3.0754)	0.0411 (0.0162)	68	0.4999 (0.1968)	10.2116 (4.0203)
30	7.8161 (3.0772)	-0.0053 (-0.0021)	69	0.3848 (0.1515)	10.3035 (4.0565)
31	7.8082 (3.0741)	-0.0516 (-0.0203)	70	0.2822 (0.1111)	10.4094 (4.0982)
32	7.7879 (3.0661)	-0.0935 (-0.0368)	71	0.1938 (0.0763)	10.5273 (4.1446)
33	7.7572 (3.0540)	-0.1288 (-0.0507)	72	0.1212 (0.0477)	10.6556 (4.1951)
34	7.7180 (3.0386)	-0.1542 (-0.0607)	73	0.0650 (0.0256)	10.7920 (4.2488)
35	7.6736 (3.0211)	-0.1681 (-0.0662)	74	0.0264 (0.0104)	10.9342 (4.3048)
36	7.6269 (3.0027)	-0.1699 (-0.0669)	75	0.0063 (0.0025)	11.0802 (4.3623)
37	7.5816 (2.9849)	-0.1587 (-0.0625)	76	0.0046 (0.0018)	11.2278 (4.4204)
38	7.5408 (2.9688)	-0.1356 (-0.0534)	77	0.0216 (0.0085)	11.3741 (4.4780)
39	7.5077 (2.9558)	-0.1026 (-0.0404)	78	0.0569 (0.0224)	11.5171 (4.5343)



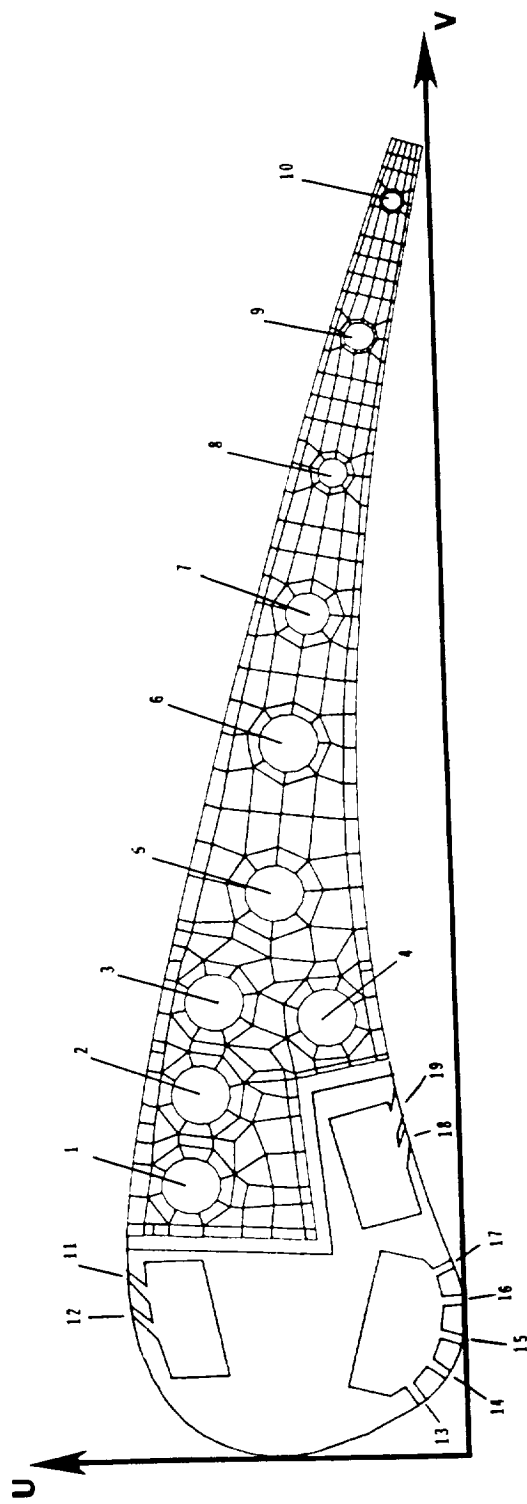
TE32-6022

Figure 7. C3X vane coordinate system.

Table III.
Cascade geometry

Setting angle, deg	59.89
Air exit angle, deg	72.38
Throat, cm (in.)	3.292 (1.296)
Vane height, cm (in.)	7.722 (3.040)
Vane spacing, cm (in.)	11.773 (4.635)
Suction surface arc, cm (in.)	18.037 (7.101)
Pressure surface arc, cm (in.)	13.982 (5.505)
True chord, cm (in.)	14.493 (5.706)
Axial chord, cm (in.)	7.816 (3.077)

ORIGINAL PAGE IS
OF POOR QUALITY.



Radial cooling holes				Film cooling holes			
Hole No.	U-cm (in.)	V-cm (in.)	Dia-cm (in.)	Cr	Hole No.	U-cm (in.)	V-cm (in.)
1	2.870 (1.130)	2.992 (1.178)	0.630 (0.248)	1.118	11	3.592 (1.414)	2.024 (0.797)
2	2.733 (1.076)	3.998 (1.574)	0.630 (0.248)	1.118	12	3.556 (1.400)	1.631 (0.642)
3	2.555 (1.006)	4.991 (1.965)	0.630 (0.248)	1.118	13	0.498 (0.196)	0.541 (0.213)
4	1.364 (0.537)	4.788 (1.885)	0.630 (0.248)	1.118	14	0.211 (0.083)	0.828 (0.326)
5	1.869 (0.736)	6.182 (2.434)	0.630 (0.248)	1.118	15	0.041 (0.016)	1.196 (0.471)
6	1.666 (0.656)	7.747 (3.050)	0.630 (0.248)	1.118	16	0.005 (0.002)	1.600 (0.630)
7	1.412 (0.556)	9.235 (3.636)	0.470 (0.185)	1.090	17	0.109 (0.043)	1.994 (0.785)
8	1.087 (0.428)	10.759 (4.236)	0.310 (0.122)	1.056	18	0.559 (0.220)	3.505 (1.380)
9	0.737 (0.290)	12.253 (4.824)	0.310 (0.122)	1.056	19	0.643 (0.253)	3.891 (1.532)
10	0.345 (0.136)	13.757 (5.416)	0.198 (0.078)	1.025			

Figure 8. Film cooled C3X finite element grid structure showing internal geometry.

Table IV.
Film cooling hole geometry

<u>Leading edge geometric parameters</u>	<u>Values</u>
Rows of holes	5
Hole diameter, cm (in.)	0.099 (0.039)
Hole length, cm (in.)	0.335 (0.132)
Hole pitch-to-diameter ratio (P/D)	4.0
Hole spacing-to-diameter (S/D)	7.5
Hole slant angle (α), deg	45
Hole skew angle (β), deg	90
<u>Downstream geometric parameters</u>	<u>Values</u>
Rows of holes	2
Hole diameter, cm (in.)	0.099 (0.039)
Hole length, cm (in.)	0.335 (0.132)
Hole pitch-to-diameter ratio (P/D)	4.0
Hole spacing-to-diameter (S/D)	3.0
Hole slant angle (α), deg	90
Hole skew angle (β), deg	
Pressure surface	20
Suction surface	35

while the pressure surface holes were at 20 degrees in the chordwise direction. Holes in both downstream arrays were normal to the surface in the spanwise direction.

Three supply plenums, each with a separate, metered line, were designed to feed the three film cooling arrays. This system was designed to provide the capability of individually controlling the blowing parameters of each array. The film coolant supply was piped through an electric heating system that provided the capability to vary the coolant supply temperature.

3.5 Test Vane Instrumentation

The heat transfer measuring technique used for this test does not make heat transfer measurements in the actual film cooled nose piece. Consequently, the film cooled area was thermally isolated from the rest of the airfoil. As mentioned before, the thermal barrier was achieved by cutting the test vane into two segments with the airfoil profile maintained in its original contour by two retaining bars pinned to the airfoil ends. Prior to testing, a thin, 0.254 mm (0.010 in.), shim was welded across the thermal barrier gap on both the pressure and suction surfaces. This provided a smooth continuous surface on the airfoil. Also, the gap was sealed at the two ends of the airfoil, thereby creating a sealed air gap between the film cooled region and the rest of the airfoil. The sealed air gap provided the thermal barrier.

The method used to obtain heat transfer measurements is based on the work of Turner (Ref 3), who employed a 2-D plane of the test piece as a fluxmeter. The technique is implemented by measuring the internal and external boundary conditions of the test piece at thermal equilibrium and solving the steady-state heat conduction equation for the internal temperature field of the test piece. The heat transfer coefficient distribution can be directly obtained from the normal temperature gradient at the surface.

For the present study, the external boundary conditions were measured using thermocouples installed in grooves on the exterior surface of the test vane and in the thermal barrier on the tail piece of test vane. Average heat transfer coefficients and coolant temperatures for each of the 10 radial cooling holes provided the internal boundary conditions for the finite element solution. The heat transfer coefficient for each cooling hole was calculated from the hole diameter, measured coolant flow rate, and coolant temperature with a correction (Cr in Figure 8) applied for thermal entry region effects.

Figure 9 shows the distribution of the thermocouples for the C3X airfoil. The airfoil surface was instrumented with 123 0.51 mm (0.020 in.) diameter sheathed CA thermocouples, while the thermal barrier region was instrumented with 18 1.02 mm (0.040 in.) CA thermocouples. Eleven of the 123 thermocouples on the vane surface were redundant or double thermocouples. They were installed in critical areas near the film cooling holes and the thermal barrier. The thermocouple junctions were located in the fully 2-D region of the airfoil in a plane 0.254 cm (0.100 in.) off midspan. The redundant thermocouple junctions were located 0.635 mm (0.250 in.) away from midspan. Thermocouples were brought off the vane in 0.58 mm (0.023 in.) deep radial grooves covered with cement, and blended by hand to provide a smooth surface. In the case of the double or redundant thermocouples, the grooves were cut to a depth of 1.092 mm (0.043 in.) to accept two thermocouples. The vane was fabricated of ASTM type 310 stainless steel, which has a relatively low thermal conductivity, thereby minimizing the error introduced by the grooves.

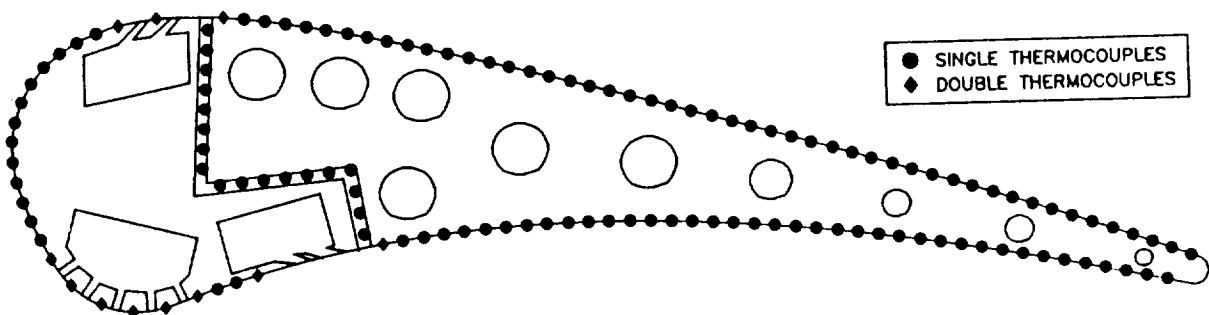


Figure 9. Surface and thermal barrier thermocouple locations for film cooled C3X airfoil.

In addition to the thermocouples on the instrumentation plane, twelve extra thermocouples were placed on the suction and pressure surfaces, 1.905 mm (0.75 in.) on either side of the instrumentation plane at three axial locations. These and the instrumentation plane temperatures at the same axial locations provided a check on the validity of the two dimensionality of the heat transfer solution.

Each of the tubes supplying the radial cooling holes of the test vane was instrumented with two static pressure taps and two thermocouples at both the vane inlet and exit. The static pressure taps were located upstream of the thermocouples in all cases. The flow to each cooling tube was measured using a calibrated orifice meter.

Each film cooling plenum was instrumented with thermocouples and pressure taps at various locations to provide the coolant supply temperature and pressure. The flow rate to each plenum was measured using a calibrated orifice meter.

The test vane surface was instrumented with surface static pressure taps in addition to the heat transfer instrumentation. Forty-six taps were located around the airfoil outer surface in a plane 0.508 cm (0.200 in.) from midspan away from the thermocouple instrumentation. The pressure taps were located so that the taps would be downstream of a film cooling hole. The spacing was varied to provide a higher density of instrumentation in high pressure gradient regions. Figure 10 illustrates the relative locations of the surface pressure taps on the C3X airfoil. As in the case of the thermocouples, eleven of the 46 pressure taps were redundant or doubles and they were located around the film cooling holes and the thermal barrier. The double pressure taps were located behind the next adjacent cooling hole so as to maintain the similarity. Figure 11 shows the technique used to install the static pressure taps. Stainless steel tubing, 0.51 mm (0.020 in.) dia, was laid in a radial surface groove, and the end of the tubing was bent 90 deg to achieve surface orientation. The tube was secured to the adjacent vane surface by laser welding.

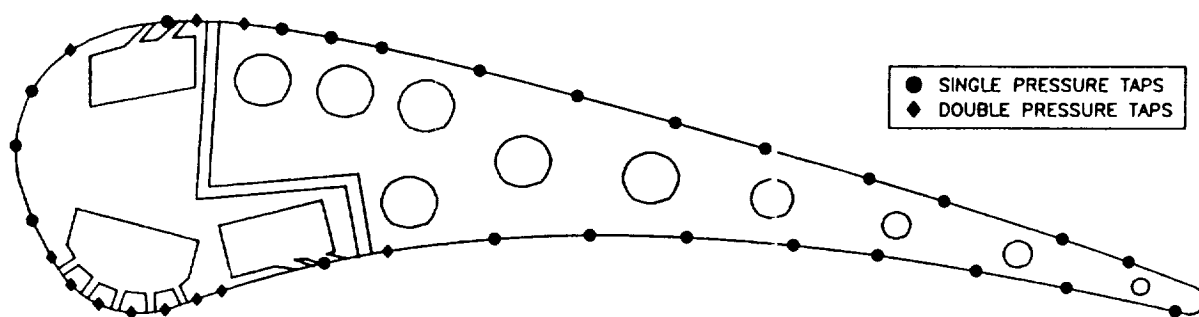


Figure 10. Surface pressure tap locations for the film cooled C3X airfoil.

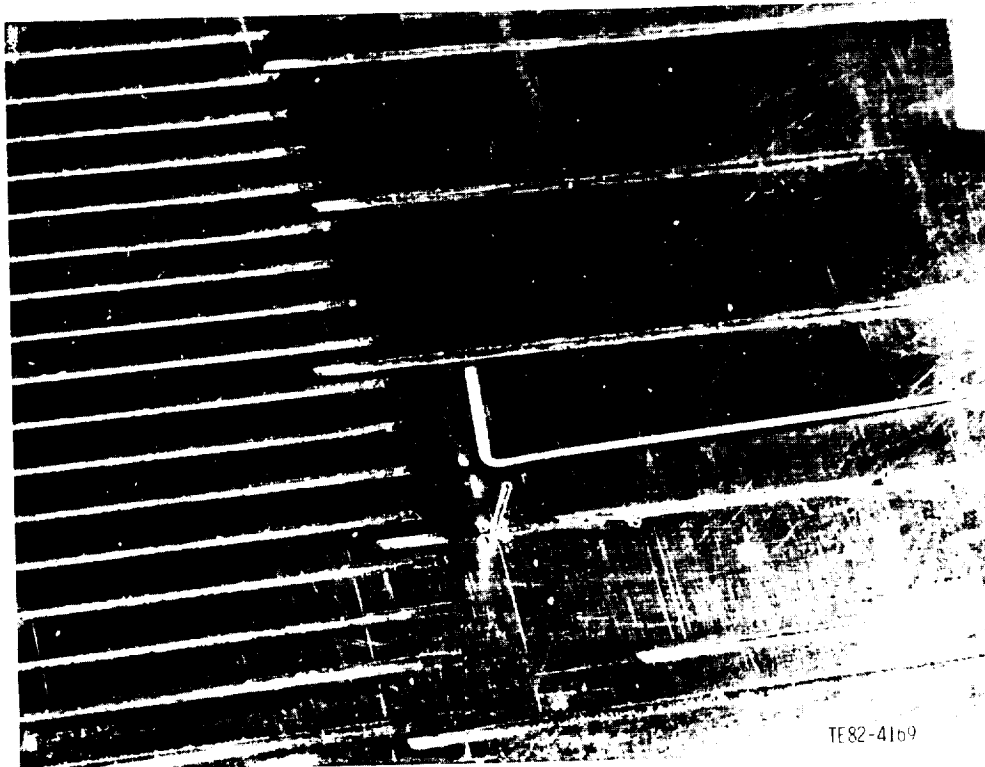


Figure 11. Installation of vane surface static pressure taps.

The excess tube length was then removed and dressed down to ensure a flush local condition. The remainder of the groove was then filled with cement and hand blended smooth with airfoil surface similar to the thermocouple installations. In cases where there were double pressure taps, a deeper groove was cut in order to lay two stainless steel tubes, one on top of the other.

In order to measure the spanwise variation of the static pressure on the airfoil at the cascade throat, 4 seven element pressure rakes were designed and fabricated using 0.51 mm (0.020 in.) stainless steel tubing. These rakes were positioned in a 2.31 mm (0.091 in.) wide and 1.45 mm (0.057 in.) deep groove at the vane throat and laser welded using a 0.254 mm (0.010 in.) shim cover. Figure 12 shows a photograph of a seven element rake before and after being installed in the vane surface. Two of these rakes were mounted on the test vane at the throat on the pressure and suction surfaces and one on each slave vane on the surfaces adjacent to the test vane. A photograph of the pressure surface of the airfoil following installation of all surface thermocouples and pressure taps is shown in Figure 13.

TE88-1713



Figure 12. A seven element rake before and after being installed in the vane surface.

ORIGINAL PAGE IS
OF POOR QUALITY

ORIGINAL PAGE IS
OF POOR QUALITY

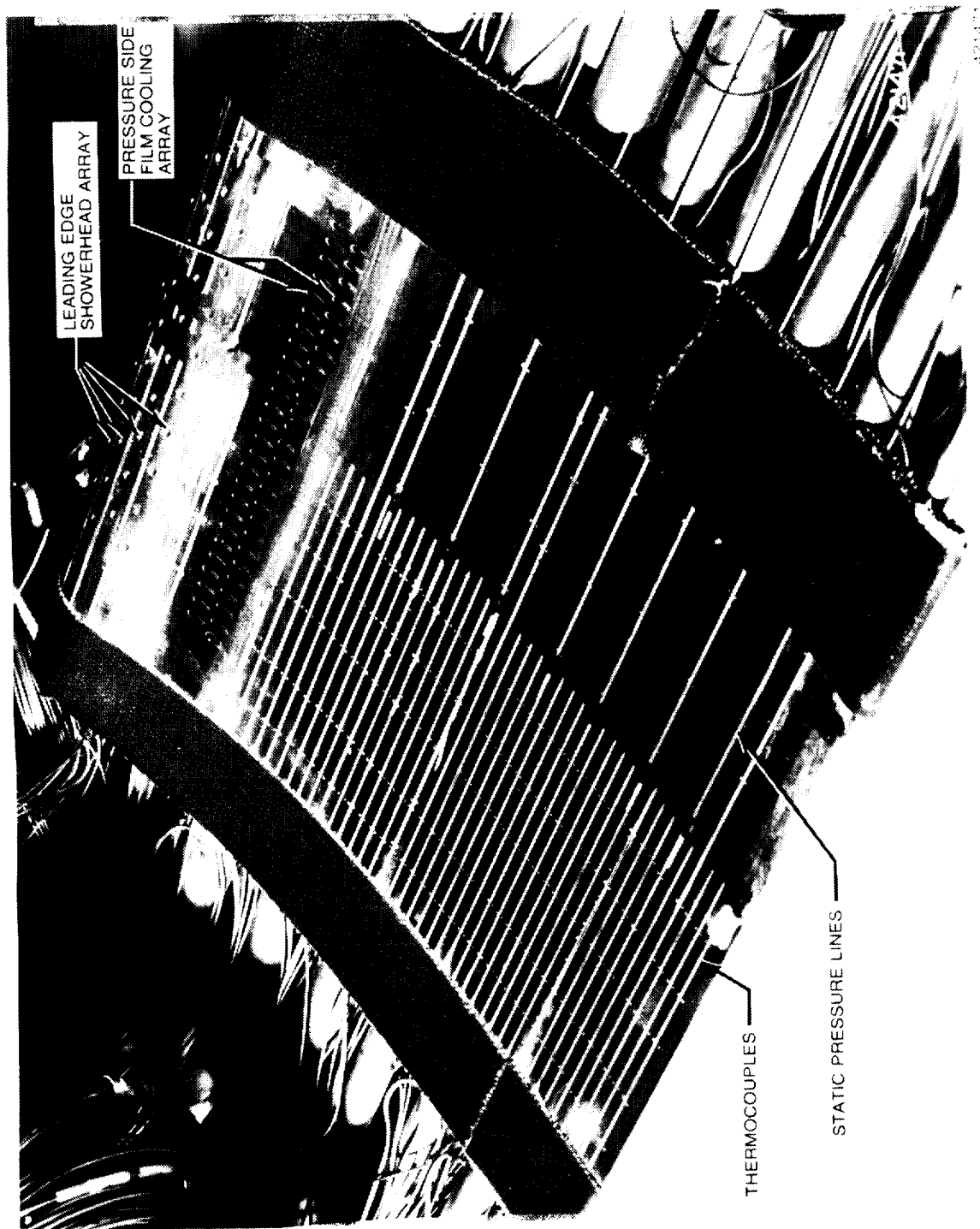


Figure 13. Pressure surface of instrumented airfoil

IV. DATA ACQUISITION AND REDUCTION

4.1 Data Acquisition System

The control room of the ACF contains a dedicated computer-controlled data acquisition system shown schematically in Figure 14. Data input signals are multiplexed by Hewlett-Packard (HP) Model 3497 440-channel random access signal scanner, with analog to digital conversion performed by an HP 3456A integrating digital voltmeter. The computer main frame is a Model HP 1000 Series A700 running under the RTE-A operating system.

Input/output devices complementing this central processing unit consist of a HP 7946 24 mega byte hard disk drive with an integral tape backup, HP 2563A graphics printer, HP 2526 graphics monitor, HP 9895 dual 9-inch floppy disk drives and a HP 7475 6-pen plotter. A multitask, facility-oriented software system that contains general subprograms to do all routine control measurement tasks exists. The system is flexible and provides for real-time facility monitoring and diagnosis of instrumentation or control problems. Software routines developed to meet specific data acquisition requirements of individual experiments are incorporated into the main system as interchangeable program segments.

4.2 Data Acquisition Software and Data Reduction Procedures

The data acquisition software written for this experimental program is menu-driven with multiple options that could be chosen by the operator. These options also include fairly standard tasks such as transducer calibrations, block or random scans of temperatures and pressures, and facility operation point monitoring. Specialized options include tasks such as individual check-out of film cooling plenum data, radial cooling tube data, plotting of surface temperature and surface static temperature profiles, full heat transfer data acquisition, and storage and analysis of all data. The heat transfer data acquisition task is operated in three phases.

The first phase of the heat transfer data acquisition task monitored and displayed the cascade operating condition as the desired run conditions were being established. The facility instrumentation used to determine the cascade operating point was described previously in Section III in sub-section "Facility Instrumentation and Geometry." Cascade inlet total pressure and temperature were based on readings of the upstream core flow rakes. The cascade inlet static pressure was defined as the average of readings at 18 endwall static pressure taps near the upstream core rakes. The average exit pressure was determined by obtaining an integrated average of the endwall static pressure taps between midlower-passage to midupper-passage at the cascade exit plane. The vane average wall temperature was defined as the average of the midspan vane surface temperatures. Coolant total pressure and temperature were taken as the average of the coolant plenum pressure and temperatures, respectively. The operating conditions of the Mach number, the Reynolds number (based on true chord), coolant-to-free-stream pressure ratio, and coolant-to-free-stream temperature ratio were calculated from these averaged quantities and displayed continuously on the monitor during the setup procedure until a satisfactory steady-state condition was achieved. The

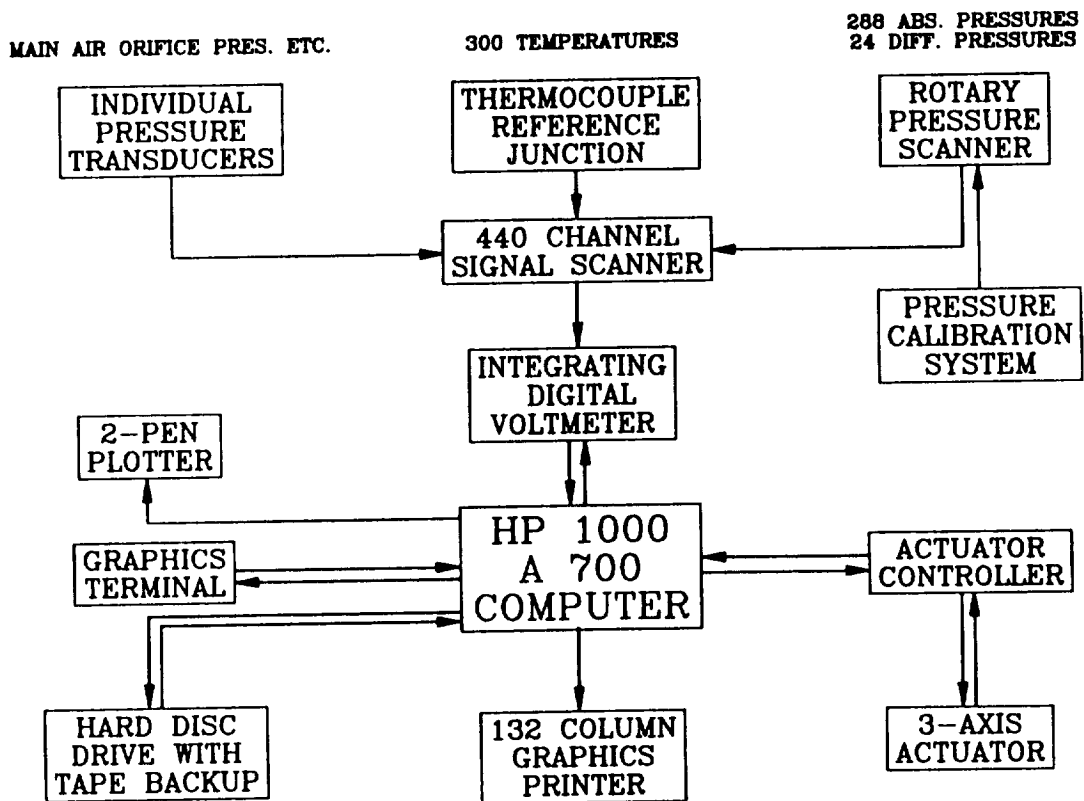


Figure 14. Schematic of the computer controlled data acquisition system.

change in temperature of the vane surface over a fixed period of time was then monitored until thermal equilibrium was established.

The second phase of the heat transfer data acquisition software sampled, averaged, and stored the raw pressure and temperature data after the desired steady-state operating conditions were achieved. All of the data were read in a single sweep that was repeated several times to provide time averaged, steady-state values. The averaged values for a given run were then stored in a permanent file on magnetic floppy disks.

All necessary calculations were performed in the third phase. The final run conditions, vane surface static pressure distributions, and temperature distributions were established. The changes in vane surface temperatures between readings were checked to verify thermal stability during data acquisition. Mass flowrates for the radial cooling tubes and the film cooling plenums were calculated from the orifice meter data.

The average coolant plenum to free-stream pressure ratio and temperature ratio were calculated. Also film cooling parameters such as discharge coefficients and blowing ratio (mass flux ratio) based on coolant plenum and local free-stream conditions were also determined.

The average coolant temperature for each radial tube at the vane surface temperature measurement plane was calculated, assuming a linear temperature rise through the vane cooling hole. The Reynolds number for each cooling tube was determined from the measured flowrate, cooling hole diameter, and viscosity based on the average coolant temperature. The Prandtl number (Pr) for the coolant flow was calculated from the average coolant temperature. The Nusselt number (Nu_D) was then calculated from the following relationship for turbulent flow in a smooth pipe:

$$Nu_D = Cr (0.022 Pr^{0.5} Re_D^{0.8}) \quad (1)$$

The correction factor (Cr) is a function of Prandtl number, the tube diameter Reynolds number (Re_D), and the streamwise coordinate at the cooling hole diameter (x/D), which corrects the Nu expression for a fully developed thermal boundary layer to account for thermal entrance region effects. The correction factor found in Ref 4 ranged from approximately 1.03 to 1.12 for the Prandtl number, tube diameter Reynolds number, and streamwise coordinate at the cooling hole diameter values encountered in this experiment. The average heat transfer coefficient for each cooling hole was then calculated from the Nusselt number, hole diameter, and thermal conductivity.

After the data acquisition task is completed, all of the data are transferred to an HP 1000 Series A900 computer in the Allison Research Laboratories for further analysis and plotting.

4.3 Heat Transfer Measurement Technique

The heat transfer measurement technique, discussed briefly in Section 3.5, used a finite element solution of the 2-D Laplacian heat conduction equation for the vane internal temperature field using measured surface temperatures and internal cooling hole heat transfer coefficients as boundary conditions. The technique is illustrated in Figure 15. Inputs to the program, in addition to the measured inlet and exit boundary conditions, were the 2-D vane cross-sectional geometry, thermal conductivity of the material, and the average coolant temperature for each radial hole.

A FEM of the midspan cross section of the airfoil was constructed by using Allison's computer aided design/computer aided manufacturing (CAD/CAM) facilities. The finite element grids used for the present film cooled airfoil were previously shown in Figure 8. A total of 179 nodes were located around the airfoil outer surface, while 41 nodes were located on the thermal barrier. A special effort was made to arrange sufficient elements in the thin trailing edge region to ensure the quality of the solution in that region. Also, the thermal barrier was designed in a "Z" shape to ease the construction of finite element grids.

A linear fit of all measured midspan surface temperatures for a given run was used to provide the temperature for each surface nodal point of the FEM. Since the finite element program was available on the Allison Data Center IBM computer, the input to the finite element program was created on the HP 1000 Series A900 computer and then transferred to IB1 using a telephone link. The

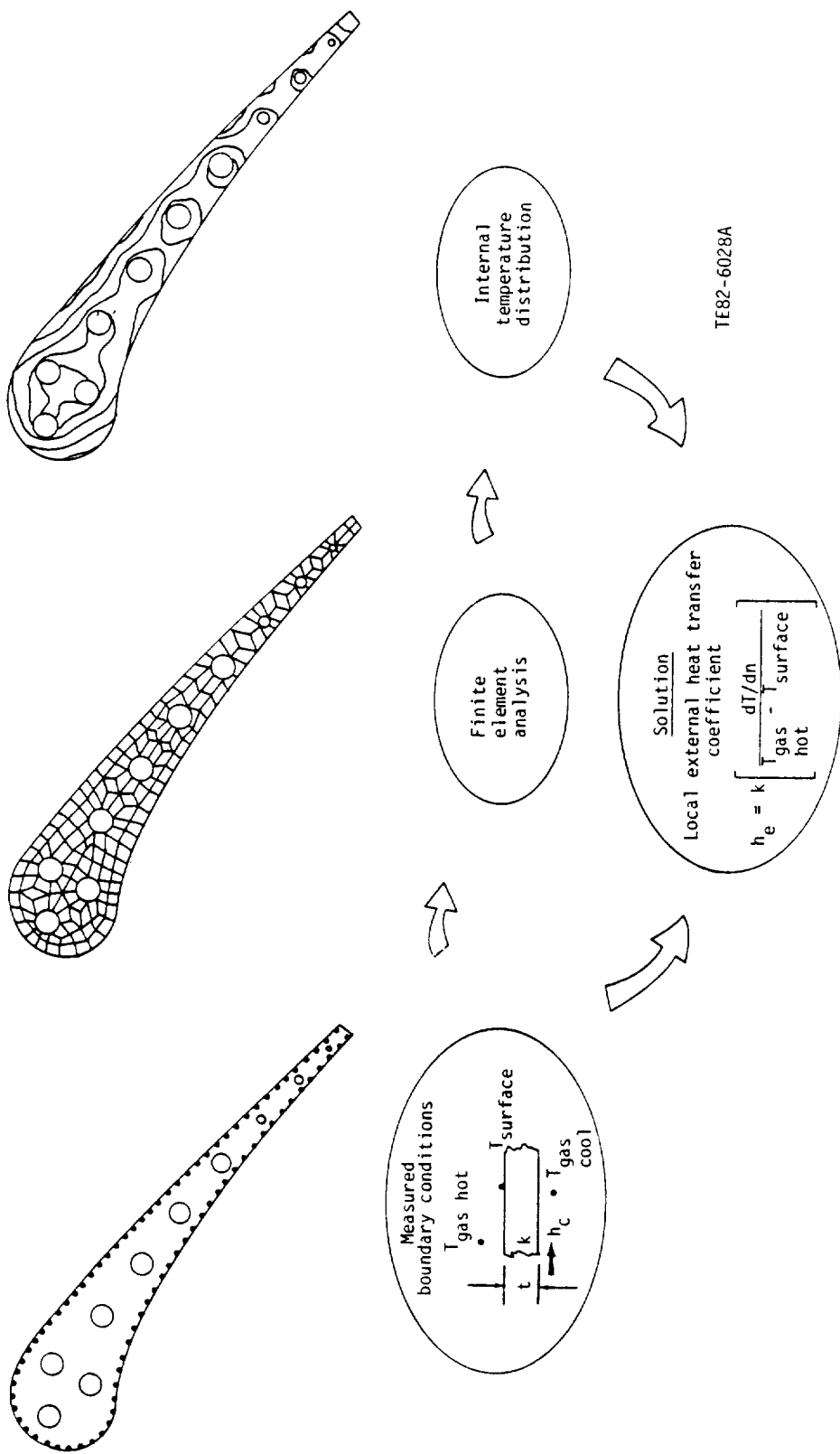


Figure 15. Heat transfer data reduction technique.

heat transfer solution from the finite element program, which is the normal heat conduction into the vane surface, is transferred back to the HP 1000 via the telephone line. The hot gas side local heat transfer coefficients were derived by equating the surface normal heat flux to the local convection.

4.4 Data Uncertainties

An uncertainty analysis was performed for the key experimental parameters, using the technique of Kline and McClintock (Ref 5). The accuracy of the external heat transfer coefficient measurement is primarily dependent on the accuracy of the external vane surface and free-stream gas temperature measurements, the geometry description for the finite element program, the calculation of the heat transfer coefficients for the radial cooling holes, and the knowledge of the thermal conductivity of the vane material. Details of the uncertainties of the individual measurements are discussed in Reference 1. Using the uncertainties of the individual measurements, a calculation of the overall uncertainty in the external heat transfer coefficient was made using the methods of Ref 5. Due to variations in the airfoil thickness along the chord, it was necessary to calculate the uncertainty at several points. The maximum uncertainty, based on minimum wall thickness (distance from cooling hole to exterior surface), was calculated at various regions on the airfoil. The values ranged from $\pm 7.1\%$ to $\pm 22.5\%$ as shown in Table V. The uncertainties increase significantly beyond midchord due to a decrease in airfoil thickness.

Table V.
Experimental Uncertainties

Uncertainty in heat transfer coefficient measurements

Pressure surface		Suction surface	
Percent surface arc	Percent uncertainty	Percent surface arc	Percent uncertainty
26-34	± 11.8	30-36	± 9.6
34-45	± 7.1	36-42	± 10.4
45-56	± 8.5	42-48	± 11.5
56-67	± 9.9	48-57	± 7.1
67-78	± 11.7	57-65	± 8.5
78-89	± 16.7	65-74	± 9.7
89-100	± 22.5	74-82	± 10.6
		82-91	± 16.8
		91-100	± 22.3

Uncertainty in test parameters

Reynolds number, Re	$\pm 3.1\%$
Mach number, Ma	$\pm 0.9\%$
Wall to gas temperature ratio, T_w/T_g	$\pm 2.0\%$
Coolant to freestream pressure ratio, P_c/P_t	$\pm 1.0\%$
Coolant to freestream temperature ratio, T_c/T_g	$\pm 4.0\%$

The uncertainty was also calculated for the test parameters, based on the methods of Reference 5. The results are given in Table V. The uncertainties presented in this subsection are intended to provide the analyst with an indication of the uncertainty in absolute levels in using the data for verification purposes. In comparing data runs for a given cascade (i.e., looking for Reynolds number trends, etc), the uncertainty in the comparisons is considerably less than the values just described. This difference is due to the fact that several of the variables contributing to the uncertainty do not change from run to run. For example, an error of 3% in the airfoil thermal conductivity would result in an error in the absolute value of the heat transfer coefficient, but would be of the same order for each run. Thus comparisons of runs from a given cascade would not be affected. Reproducibility for a given cascade is on the order of $\pm 2\%$.

V. TEST CONDITIONS

The experimental results presented in this study were obtained at different test conditions with the variable parameters being exit Reynolds number, exit Mach number, coolant-to-gas absolute temperature ratio and coolant-to-gas total pressure ratio. Each nominal test condition is represented by a five-digit numeric code. Each numeric digit of the code corresponds to one of the control variables of the experiment as shown in Figure 16. The first digit corresponds to the exit Mach number, the second to the exit Reynolds number, the third to coolant to gas temperature ratio (T_c/T_g), the fourth to the coolant to free-stream total pressure ratio of the leading edge showerhead plenum ($P_{c,le}/P_t$), and the fifth to the coolant to free-stream pressure ratio of the two downstream film cooling plenums ($P_{c,ds}/P_t$). Exit Reynolds numbers referred to in the figure are based on airfoil true chord, and exit Mach numbers are based on measured inlet total pressure and mid-passage to mid-passage average measured exit plane static pressure. All tests were conducted at a nominal gas stream temperature of 700°K (1260°R), and a turbulence intensity level of 6.5%, based on LDA measurements taken previously as reported in Reference 1.

5.1 Heat Transfer Data Test Conditions

The nominal run conditions where heat transfer data were obtained are shown in a graphical form in Figure 17. The actual run conditions corresponding to each five-digit code are given in Table VI. In Table VI-A the cascade conditions are given by the inlet total pressure, P_{t1} , the gas stream inlet total temperature, T_{t1} , the inlet and exit Mach numbers, Ma_1 and Ma_2 ,

Code No.	Control variable by position					
	Position 1-- Ma_2	Position 2-- $Re_2 \times 10^{-6}$	Position 3-- T_c/T_g	Position 4-- $P_{c,le}/P_t$	Position 5-- $P_{c,ds}/P_t$	
					ss	ps
0			No coolant flow	1.00	1.00	1.00
1			Min			
2			Med			
3	0.75	1.5	Max	1.02	1.02	1.02
4	0.90	2.0		1.05	1.05	1.05
5		2.5		1.10	1.10	1.10
6					1.30	1.30
7					1.50	1.50
8					1.70	1.70

Figure 16. Control variable code description.

the inlet and exit Reynolds number based on the true chord Re_1 and Re_2 , and the arc-distance weighted average wall-to-gas absolute temperature ratio, T_w/T_g . Table VI-B shows the actual secondary flow conditions represented by the coolant-to-gas absolute temperature ratio, T_c/T_g , the average coolant-to-free-stream total pressure ratio, P_c/P_t , and film coolant (clnt) mass flow rate for each of the three plenums supplying the suction surface, the leading edge, and the pressure surface film cooling arrays.

The cascade Reynolds number range was achieved by varying the cascade flowrate from approximately 2.27 kg/s (5 lbm/sec) to 4.54 kg/s (10 lbm/sec). At a given Reynolds number condition, exit Mach number levels were independently established by adjusting the cascade exit pressure ratio with a controllable exhaust valve. The coolant-to-free-stream total pressure ratio was varied by controlling the film cooling mass flow rate to each plenum. The coolant-to-gas absolute temperature ratio parameter was controlled by a single electric heating system for the three plenums. The coolant-to-gas absolute temperature ratio has some variation from plenum to plenum due to each plenum requiring a different coolant mass flow rate to achieve the prescribed coolant-to-gas total pressure ratio. Also, some further variations in T_c/T_g occurred between test conditions due to the changes in the influence of the test hardware on the onboard coolant supply temperature as other parameters were varied.

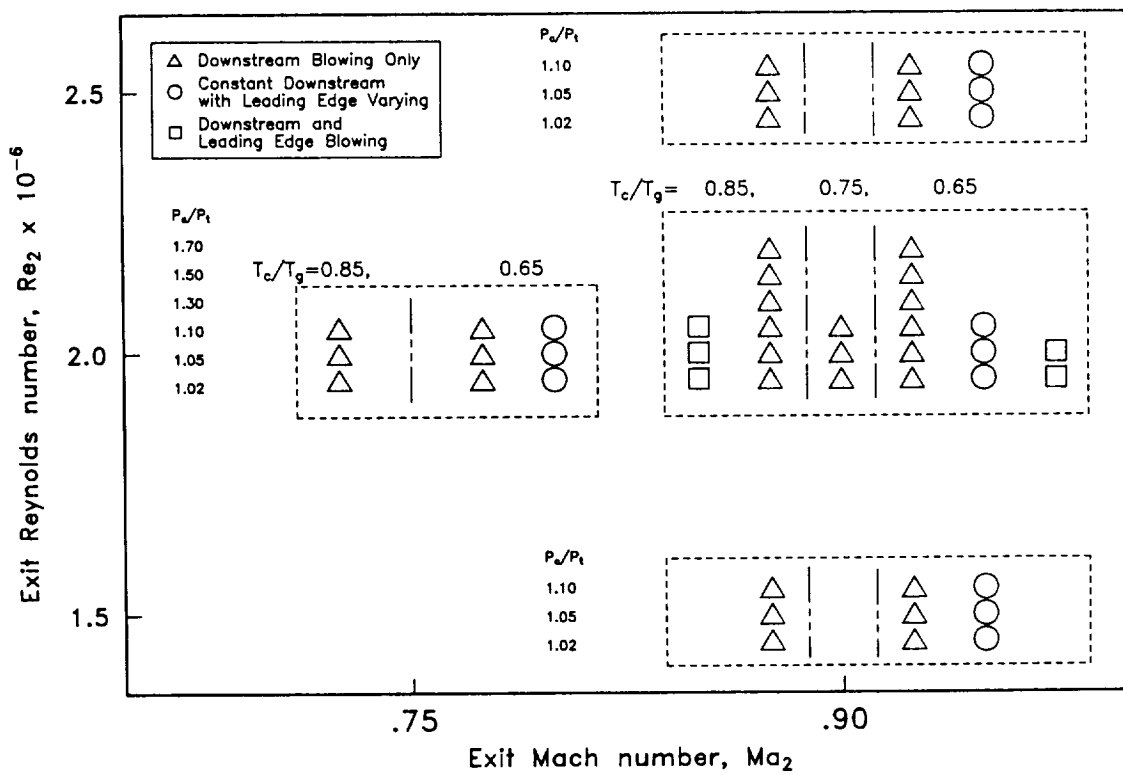


Figure 17. Test matrix for heat transfer data

Table VI
Summary of heat transfer run conditions

A. Cascade conditions

RUNCODE	PT1		TT1 °R	Ma ₁	Re ₁ x10 ⁻⁶	Ma ₂	Re ₂ x10 ⁻⁶	T _w /T _g
	kPa	psia						
34000	304.65	44.19	707.	1272.	0.17	0.57	0.75	1.99
34103	300.73	43.62	703.	1266.	0.19	0.64	0.75	1.97
34104	303.81	44.06	702.	1263.	0.19	0.63	0.75	2.00
34105	302.33	43.85	697.	1254.	0.18	0.61	0.75	2.00
34135	305.81	44.35	701.	1261.	0.18	0.62	0.75	2.01
34145	306.35	44.43	703.	1265.	0.18	0.62	0.74	2.00
34155	310.17	44.99	701.	1262.	0.19	0.65	0.75	2.05
34303	304.81	44.21	706.	1270.	0.17	0.57	0.75	2.00
34304	303.48	44.02	711.	1280.	0.17	0.56	0.75	1.97
34305	307.19	44.55	700.	1260.	0.17	0.60	0.75	2.03
43000	211.65	30.70	704.	1267.	0.19	0.46	0.91	1.51
43103	215.23	31.22	716.	1289.	0.19	0.45	0.89	1.49
43104	211.90	30.73	705.	1269.	0.19	0.45	0.91	1.51
43105	218.15	31.64	703.	1266.	0.19	0.46	0.89	1.55
43135	213.64	30.99	705.	1268.	0.19	0.45	0.90	1.52
43145	213.92	31.03	705.	1269.	0.19	0.44	0.90	1.52
43155	218.31	31.66	702.	1263.	0.19	0.46	0.89	1.55
43303	214.71	31.14	709.	1277.	0.18	0.43	0.90	1.52
43304	214.72	31.14	707.	1273.	0.19	0.44	0.90	1.52
43305	214.66	31.13	706.	1270.	0.19	0.44	0.90	1.52
44000	280.35	40.66	709.	1277.	0.19	0.59	0.89	1.97
44103	279.12	40.48	709.	1276.	0.18	0.55	0.89	1.96
44104	283.24	41.08	709.	1276.	0.18	0.56	0.90	2.00
44105	281.90	40.89	705.	1270.	0.20	0.61	0.89	1.99
44106	284.14	41.21	714.	1285.	0.21	0.64	0.90	1.99
44107	281.08	40.77	707.	1273.	0.21	0.64	0.89	1.98
44108	281.94	40.89	703.	1266.	0.20	0.63	0.89	2.00
44133	284.68	41.29	705.	1268.	0.18	0.56	0.92	2.03
44135	281.55	40.84	705.	1269.	0.20	0.62	0.90	2.00
44144	285.22	41.37	704.	1267.	0.19	0.61	0.90	2.03
44145	279.92	40.60	705.	1269.	0.20	0.61	0.89	1.98
44155	280.95	40.75	705.	1268.	0.19	0.60	0.90	2.00
44203	282.02	40.90	708.	1275.	0.17	0.54	0.90	1.99
44204	282.17	40.93	705.	1270.	0.18	0.56	0.90	2.00
44205	285.64	41.43	709.	1275.	0.18	0.56	0.90	2.01
44303	279.38	40.52	697.	1254.	0.17	0.54	0.90	2.01
44304	282.96	41.04	701.	1262.	0.17	0.53	0.89	2.01
44305	284.47	41.26	702.	1263.	0.18	0.57	0.90	2.03
44306	280.54	40.69	702.	1264.	0.21	0.64	0.90	2.00
44307	280.97	40.75	703.	1266.	0.21	0.64	0.90	2.00
44308	283.93	41.18	711.	1280.	0.21	0.64	0.89	1.98
44333	282.93	41.04	710.	1279.	0.17	0.53	0.90	1.99
44344	285.13	41.35	701.	1263.	0.17	0.54	0.89	2.03
44355	284.02	41.19	702.	1264.	0.18	0.56	0.90	2.02
45000	355.67	51.59	696.	1253.	0.19	0.76	0.92	2.58
45103	350.34	50.81	705.	1270.	0.18	0.70	0.89	2.48
45104	350.36	50.82	703.	1265.	0.18	0.68	0.89	2.49
45105	346.24	50.22	699.	1258.	0.18	0.70	0.89	2.48
45135	350.31	50.81	699.	1257.	0.18	0.72	0.90	2.51
45145	352.18	51.08	698.	1256.	0.18	0.72	0.89	2.52
45155	348.53	50.55	698.	1256.	0.18	0.71	0.90	2.50
45303	350.99	50.91	702.	1264.	0.18	0.71	0.90	2.50
45304	350.39	50.82	704.	1266.	0.18	0.70	0.89	2.49
45305	351.35	50.96	701.	1263.	0.18	0.70	0.90	2.51

Table VI (contd)
Summary of heat transfer run conditions

B. Secondary flow conditions

RUN CODE	SUCTION SIDE			LEADING EDGE			PRESSURE SIDE		
	P _c /P _t	T _c /T _g	CLNT FLOW RATE kg/sec	P _c /P _t	T _c /T _g	CLNT FLOW RATE kg/sec	P _c /P _t	T _c /T _g	CLNT FLOW RATE kg/sec
34000	1.000	1.00	0.000E+00	1.000	1.00	0.000E+00	1.000	1.00	0.000E+00
34103	1.025	0.64	0.156E-01	0.344E-01	1.000	1.00	0.000E+00	1.021	0.70
34104	1.047	0.64	0.166E-01	0.366E-01	1.000	1.00	0.000E+00	1.050	0.69
34105	1.100	0.66	0.168E-01	0.369E-01	1.000	1.00	0.000E+00	1.102	0.69
34135	1.100	0.65	0.171E-01	0.377E-01	1.019	0.75	0.506E-02	0.111E-01	0.118E-01
34145	1.097	0.65	0.169E-01	0.373E-01	1.049	0.73	0.736E-02	0.162E-01	0.116E-01
34155	1.099	0.67	0.169E-01	0.373E-01	1.099	0.73	0.102E-01	0.224E-01	1.101
34303	1.019	0.86	0.133E-01	0.292E-01	1.000	1.00	0.000E+00	0.000E+00	1.020
34304	1.048	0.86	0.137E-01	0.301E-01	1.000	1.00	0.000E+00	0.000E+00	1.050
34305	1.102	0.87	0.151E-01	0.333E-01	1.000	1.00	0.000E+00	0.000E+00	1.102
43000	1.000	1.00	0.000E+00	0.000E+00	1.000	1.00	0.000E+00	1.000	1.00
43103	1.022	0.66	0.120E-01	0.264E-01	1.000	1.00	0.000E+00	0.000E+00	1.020
43104	1.064	0.67	0.124E-01	0.272E-01	1.000	1.00	0.000E+00	0.000E+00	1.053
43105	1.100	0.67	0.132E-01	0.291E-01	1.000	1.00	0.000E+00	0.000E+00	1.098
43135	1.105	0.65	0.131E-01	0.289E-01	1.018	0.67	0.376E-02	0.829E-02	1.102
43145	1.110	0.66	0.131E-01	0.289E-01	1.051	0.68	0.557E-02	0.123E-01	1.096
43155	1.091	0.66	0.131E-01	0.289E-01	1.095	0.68	0.749E-02	0.165E-01	1.094
43303	1.022	0.85	0.106E-01	0.233E-01	1.000	1.00	0.000E+00	0.000E+00	1.021
43304	1.050	0.84	0.109E-01	0.241E-01	1.000	1.00	0.000E+00	0.000E+00	1.050
43305	1.110	0.86	0.117E-01	0.258E-01	1.000	1.00	0.000E+00	0.000E+00	1.106
44000	1.000	1.00	0.000E+00	0.000E+00	1.000	1.00	0.000E+00	0.000E+00	1.000
44103	1.020	0.68	0.139E-01	0.307E-01	1.000	1.00	0.000E+00	0.000E+00	1.019
44104	1.050	0.67	0.149E-01	0.328E-01	1.000	1.00	0.000E+00	0.000E+00	1.046
44105	1.103	0.68	0.166E-01	0.365E-01	1.000	1.00	0.000E+00	0.000E+00	1.101
44106	1.292	0.64	0.202E-01	0.444E-01	1.000	1.00	0.000E+00	0.000E+00	1.297
44107	1.524	0.63	0.246E-01	0.542E-01	1.000	1.00	0.000E+00	0.000E+00	1.505
44108	1.635	0.63	0.270E-01	0.595E-01	1.000	1.00	0.000E+00	0.000E+00	1.692

Table VI (contd)
Summary of heat transfer run conditions

B. Secondary flow conditions (contd)

RUN CODE	SUCTION SIDE				LEADING EDGE				PRESSURE SIDE			
	P_c/P_t	T_c/T_g	CNT FLOW RATE kg/sec	P_c/P_t T_c/T_g	CNT FLOW RATE kg/sec	P_c/P_t	T_c/T_g	CNT FLOW RATE kg/sec	P_c/P_t	T_c/T_g	CNT FLOW RATE kg/sec	
44133	1.020	0.67	0.145E-01	0.319E-01	1.019	0.75	0.485E-02	0.107E-01	1.020	0.71	0.608E-02	0.134E-01
44135	1.099	0.67	0.159E-01	0.351E-01	1.018	0.75	0.454E-02	0.102E-01	1.099	0.69	0.107E-01	0.236E-01
44144	1.052	0.67	0.150E-01	0.332E-01	1.051	0.74	0.704E-02	0.155E-01	1.050	0.71	0.821E-02	0.181E-01
44145	1.097	0.68	0.155E-01	0.342E-01	1.050	0.74	0.675E-02	0.149E-01	1.099	0.71	0.104E-01	0.230E-01
44155	1.101	0.66	0.160E-01	0.352E-01	1.103	0.72	0.949E-02	0.209E-01	1.101	0.69	0.107E-01	0.237E-01
44203	1.021	0.75	0.135E-01	0.298E-01	1.000	1.00	0.000E+00	0.000E+00	1.021	0.76	0.604E-02	0.133E-01
44204	1.050	0.76	0.140E-01	0.308E-01	1.000	1.00	0.000E+00	0.000E+00	1.050	0.77	0.790E-02	0.174E-01
44205	1.106	0.77	0.150E-01	0.330E-01	1.000	1.00	0.000E+00	0.000E+00	1.100	0.78	0.103E-01	0.227E-01
44303	1.024	0.84	0.128E-01	0.282E-01	1.000	1.00	0.000E+00	0.000E+00	1.021	0.82	0.582E-02	0.128E-01
44304	1.054	0.86	0.133E-01	0.294E-01	1.000	1.00	0.000E+00	0.000E+00	1.052	0.83	0.754E-02	0.166E-01
44305	1.106	0.85	0.142E-01	0.314E-01	1.000	1.00	0.000E+00	0.000E+00	1.105	0.84	0.987E-02	0.217E-01
44306	1.301	0.82	0.184E-01	0.406E-01	1.000	1.00	0.000E+00	0.000E+00	1.293	0.84	0.162E-01	0.356E-01
44307	1.493	0.85	0.209E-01	0.460E-01	1.000	1.00	0.000E+00	0.000E+00	1.476	0.86	0.200E-01	0.440E-01
44308	1.614	0.85	0.234E-01	0.516E-01	1.000	1.00	0.000E+00	0.000E+00	1.436	0.85	0.236E-01	0.523E-01
44353	1.024	0.85	0.126E-01	0.278E-01	1.021	0.86	0.474E-02	0.104E-01	1.020	0.83	0.576E-02	0.127E-01
44364	1.051	0.85	0.134E-01	0.296E-01	1.048	0.86	0.638E-02	0.141E-01	1.050	0.83	0.752E-02	0.166E-01
44355	1.101	0.84	0.143E-01	0.315E-01	1.099	0.85	0.857E-02	0.188E-01	1.102	0.83	0.982E-02	0.217E-01
45000	1.000	1.00	0.000E+00	0.000E+00	1.000	1.00	0.000E+00	0.000E+00	1.000	1.00	0.000E+00	0.000E+00
45103	1.016	0.67	0.191E-01	0.421E-01	1.000	1.00	0.000E+00	0.000E+00	1.019	0.71	0.748E-02	0.165E-01
45104	1.063	0.67	0.210E-01	0.462E-01	1.000	1.00	0.000E+00	0.000E+00	1.054	0.70	0.103E-01	0.227E-01
45105	1.102	0.66	0.226E-01	0.497E-01	1.000	1.00	0.000E+00	0.000E+00	1.102	0.69	0.135E-01	0.297E-01
45135	1.089	0.64	0.225E-01	0.499E-01	1.021	0.65	0.672E-02	0.148E-01	1.099	0.67	0.137E-01	0.301E-01
45145	1.089	0.65	0.219E-01	0.483E-01	1.046	0.64	0.908E-02	0.200E-01	1.095	0.68	0.133E-01	0.294E-01
45155	1.118	0.66	0.234E-01	0.517E-01	1.105	0.64	0.130E-01	0.287E-01	1.110	0.68	0.141E-01	0.311E-01
45303	1.021	0.87	0.170E-01	0.375E-01	1.000	1.00	0.000E+00	0.000E+00	1.019	0.82	0.668E-02	0.147E-01
45304	1.052	0.89	0.177E-01	0.390E-01	1.000	1.00	0.000E+00	0.000E+00	1.050	0.84	0.901E-02	0.199E-01
45305	1.106	0.86	0.193E-01	0.426E-01	1.000	1.00	0.000E+00	0.000E+00	1.105	0.84	0.123E-01	0.270E-01

VI. DISCUSSION OF EXPERIMENTAL RESULTS

6.1 Heat Transfer Results

Heat transfer data from this experimental program are tabulated in Appendix A. Included in the tabulation are the heat transfer coefficient distributions and vane surface temperature distributions. The location of each measurement is expressed as a percent of surface length as measured from the geometric stagnation point defined as $x=0$ point in Figure 7, and a percent of axial chord. Appendix A also contains tabulated discharge coefficient and blowing ratio data for the film coolant flow. The baseline (i.e., no discrete injection) heat transfer distribution plots and all data comparison plots showing the effects of downstream film cooling with and without leading edge film cooling are contained in Appendix B, although some representative data comparison plots are presented and discussed in this section.

The goal of presenting the heat transfer results is to isolate the differences between non-film cooled and film cooled (in this case, downstream film cooling with and without leading edge injection) heat transfer downstream of the suction and pressure side film cooling arrays. This goal is achieved, as done before in Reference 2, by calculating the ratio of the experimentally determined local Stanton number for cases where coolant is being ejected to the local Stanton number determined for the case where no coolant is added.

Rather than simply form the film cooled Stanton number to non-film cooled Stanton number ratio (St_{FC}/St_{NFC}), which would take on values about a "no difference" value of unity, an alternate parameter referred to as Stanton number reduction (SNR) is used. SNR is defined as

$$SNR = 1 - (St_{FC}/St_{NFC}) \quad (2)$$

When SNR is greater or less than zero, it implies reduced or increased heat transfer levels, respectively. When SNR is equal to zero, it implies no difference in the heat transfer level. Forming SNR values along the entire test surface gives the actual SNR distribution for the airfoil. In addition, if the film cooled Stanton number to nonfilm cooled Stanton number ratio were determined using data obtained at equivalent exit Mach number and exit Reynolds number conditions, SNR would be approximately equal to the actual heat transfer coefficient reduction,

$$SNR = 1 - (h_{FC}/h_{NFC}) \quad (3)$$

because $(\rho_\infty c_p u)_{e,NFC}/(\rho_\infty c_p u)_{e,FC}$ would be near unity. SNR results shown here and in Appendix A and B were formed by using the above equation.

Prior to obtaining film cooled heat transfer data, baseline data (i.e., without film cooling) were obtained at the four baseline conditions as shown in Figure 17. Starting first with the exit Mach number effects, typical baseline measured surface static pressure distributions corresponding to the

two cascade expansion ratios tested are shown in Figure 18 and tabulated in Table VII. The percent surface distance in Figure 18 and all figures that follow is measured from the geometric stagnation point. As observed in References 1 and 2, the primary effect of exit Mach number variations is to alter the suction surface pressure distribution downstream. The resultant effect on the measured baseline heat transfer is shown in Figure 19. In this figure and in other similar figures, the vertical dashed lines mark the locations of the film cooling hole rows and the vertical solid lines mark the locations of the thermal barrier on the pressure and suction surfaces. On the suction surface, the level of heat transfer coefficient decreases with increasing exit Mach number due to different static pressure distribution. On the pressure surface, much less variation in heat transfer due to variation in Mach number is noticed, again caused by lesser variation in the static pressure distribution.

The effect of exit Reynolds number variation on the baseline heat transfer coefficient distribution is shown in Figure 20. As expected, the overall heat transfer levels systematically increase as the exit Reynolds number increases.

The present heat transfer data matches reasonably well with the data of References 1 and 2 at surface percentage distances greater than 50% on both suction and pressure surfaces. However at surface distances less than 50%, the differences in geometry of the film cooling positions between the vane of the present study and the previous studies causes differences in absolute heat

$Ma_2=VAR$	Data	ID	Ma_2	Re_2	$P_{c,le}/P_t$	$P_{c,ds}/P_t$	T_c/T_g
$Re_2=2.0 \times 10^{+6}$	△	44000	.89	1.97E6	1.00	1.00	1.00
$P_{c,le}/P_t=1.00$	◊	34000	.75	1.99E6	1.00	1.00	1.00
$P_{c,ds}/P_t=1.00$							
$T_c/T_g=NOBLLOW$							

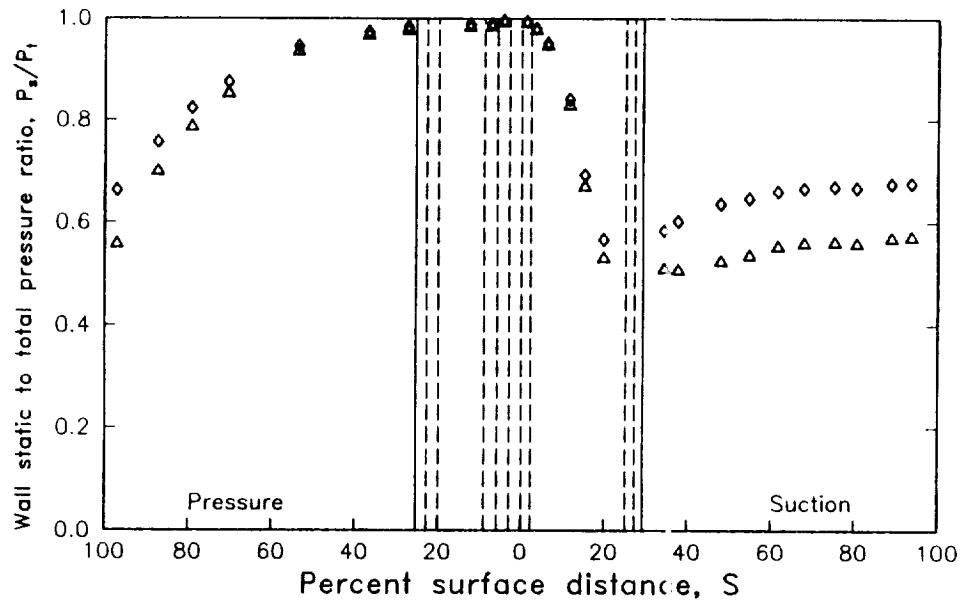


Figure 18. The effects of exit Mach number variation on the C3X vane baseline surface static pressure distribution.

Table VII.
C3X vane surface static pressure data

% Surface distance	% Axial chord	$Ma_2 = 0.75$	P_s/P_t	0.90
Suction surface				
1.22	0.27		0.9946	0.9942
3.47	2.11		0.9807	0.9804
6.29	5.23		0.9467	0.9452
11.53	13.60		0.8406	0.8287
15.26	20.91		0.6924	0.6711
19.81	30.98		0.5669	0.5333
31.81	50.00		0.5530	0.4210
34.36	52.76		0.5839	0.5106
37.73	56.08		0.6023	0.5092
47.98	65.14		0.6367	0.5271
54.81	70.65		0.6474	0.5398
61.67	75.97		0.6606	0.5564
68.00	80.74		0.6665	0.5626
75.32	86.13		0.6699	0.5639
80.63	89.94		0.6677	0.5615
89.00	95.68		0.6754	0.5717
93.74	98.68		0.6764	0.5742
Pressure surface				
1.34	0.22		1.0000	1.0000
4.25	1.99		0.9950	0.9945
7.19	5.36		0.9892	0.9873
10.11	9.62		0.9880	0.9857
27.33	33.04		0.9830	0.9814
36.77	44.32		0.9734	0.9696
53.61	61.89		0.9456	0.9386
63.02	70.51		0.9048	0.8870
70.44	76.80		0.8745	0.8488
79.23	83.76		0.8233	0.7901
87.31	89.77		0.7567	0.7014
97.06	96.51		0.6625	0.5553

transfer data. In the present study during baseline runs, there was a developing thermal boundary layer beginning at the thermal barrier at about 20-25% surface distances on both surfaces causing the differences in absolute heat transfer levels at surface distances less than 50%. The origination of the thermal boundary layer is shown by the step change in temperature across the thermal barrier in Figure 21, which gives the vane surface-to-gas absolute temperature ratio (T_w/T_g) distribution at the baseline condition corresponding to an exit Mach number (Ma_2) of 0.9 and exit Reynolds number (Re_2) of 2.0×10^6 . Also, the decreasing slope of the heat transfer coefficient, in Figures 19 and 20, downstream of the thermal barrier on both surfaces show the effect of the developing thermal boundary layer.

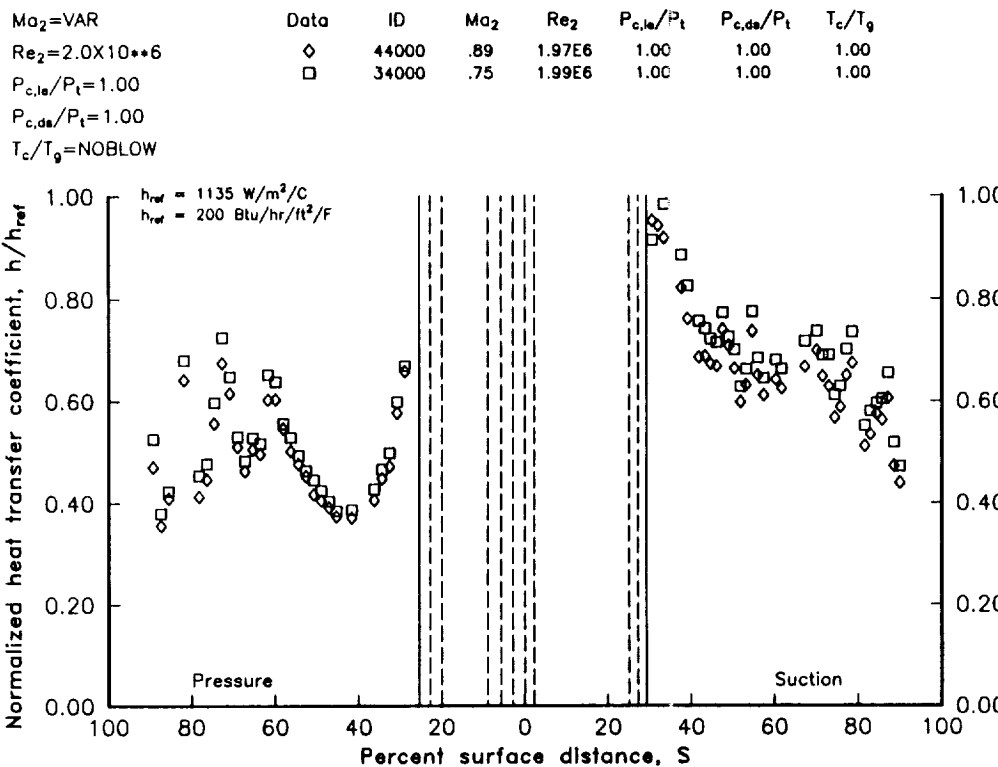


Figure 19. The effects of exit Mach number variation on the C3X vane baseline heat transfer coefficient distribution.

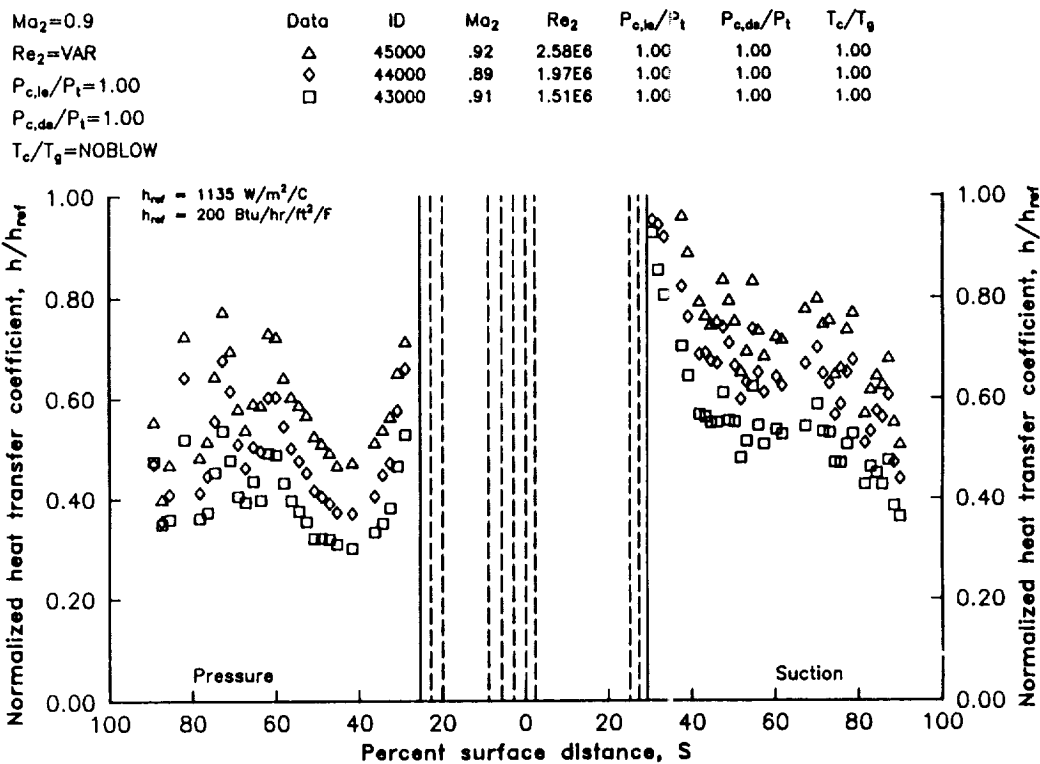


Figure 20. The effects of exit Reynolds number variation on the C3X vane baseline heat transfer coefficient distribution.

Also in Figure 21, a cyclic variation in vane surface temperatures is seen near the trailing edge on both surfaces. These variations are due to coolant air flowing through the internal cooling holes. These variations in surface temperature result in the heat transfer coefficient fluctuations seen earlier in Figures 19 and 20. Figure 22 shows the heat transfer distribution for the baseline condition of $Ma_2 = 0.9$ and $Re_2 = 2.0 \times 10^6$, which again shows the fluctuations in heat transfer coefficient over the rear 50 percent of the airfoil. Also in Figure 22, results predicted (Ref 6) for the same conditions using the Allison - STANCOOL code developed by Refs 1 and 2, are given. Here, the solid curve is the predicted results with a constant temperature boundary condition. The dashed curve is the prediction made using the actual measured condition. The comparison illustrates the significance of using the actual wall temperature boundary condition when making heat transfer predictions. It also illustrates the sensitivity of the experimental method by its demonstrated ability to track the cyclic nature of the heat transfer coefficient distribution in the trailing edge region of the airfoil.

The effect of downstream blowing on the vane surface static pressure distribution is shown in Figure 23, where the base flow conditions are at an exit Mach number of 0.9 and an exit Reynolds number of 2.0×10^6 . Figure 23 indicates that increasing the downstream blowing strength from 1.00 (no blowing) to 1.63 has no measurable effect on the vane surface static pressure distribution.

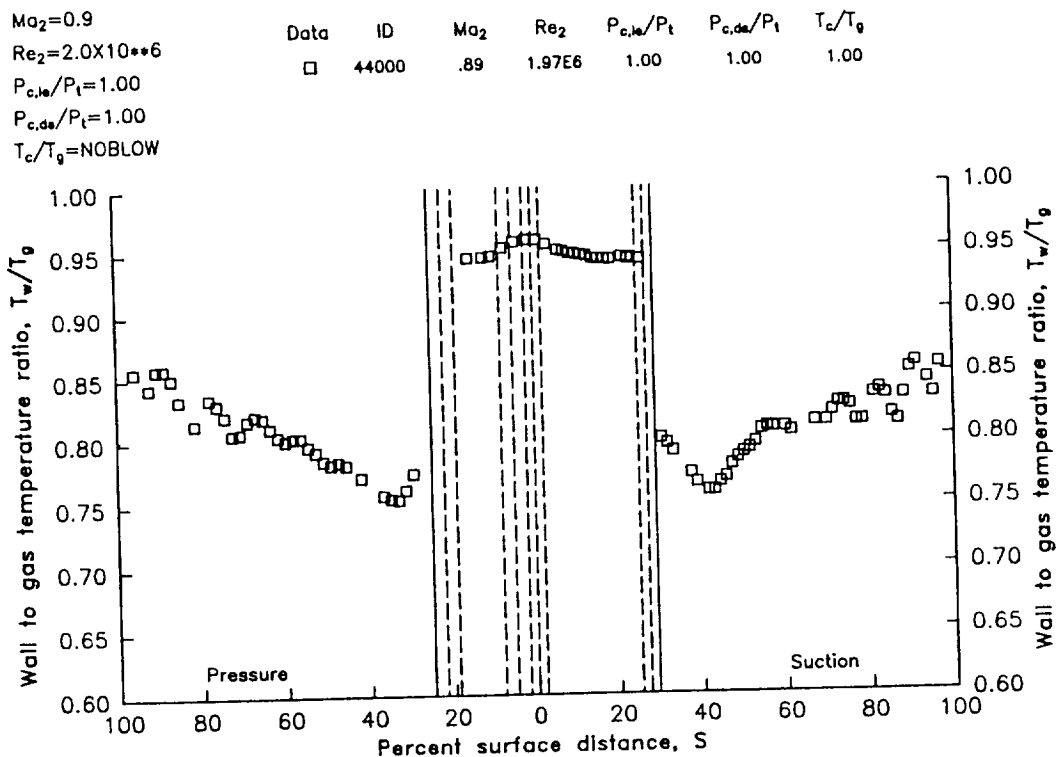


Figure 21. Vane surface-to-gas absolute temperature ratio distribution at baseline flow condition of $Ma_2 = 0.9$ and $Re_2 = 2.00 \times 10^6$.

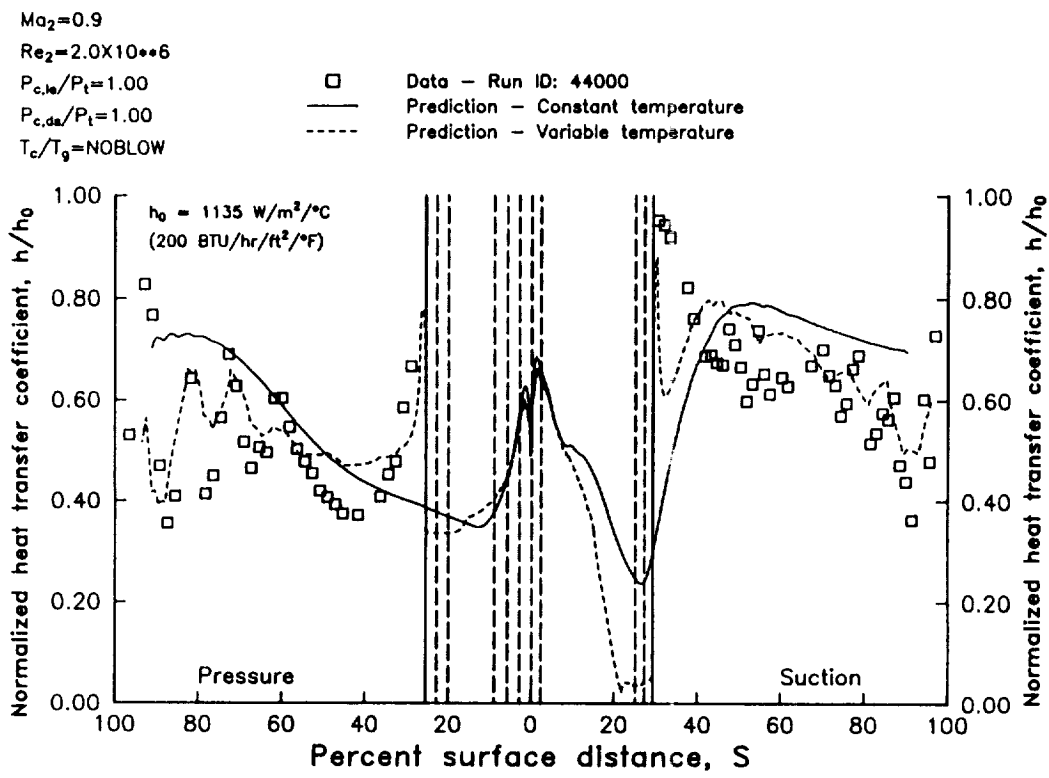


Figure 22. Vane surface local heat transfer coefficient distribution at baseline flow condition of $Ma_2 = 0.9$ and $Re_2 = 2.00 \times 10^6$.

	Data	ID	Ma_2	Re_2	$P_{c,le}/P_t$	$P_{c,de}/P_t$	T_c/T_g
$Ma_2 = 0.9$.89	2.00E6	1.00	1.64	.63
$Re_2 = 2.0 \times 10^6$.89	1.99E6	1.00	1.03	.68
$P_{c,le}/P_t = 1.00$	Δ	44108	.89	2.00E6	1.00	1.64	.63
$P_{c,de}/P_t = VAR$	\diamond	44105	.89	1.99E6	1.00	1.03	.68
$T_c/T_g = MIN$	\square	44000	.89	1.97E6	1.00	1.00	1.00

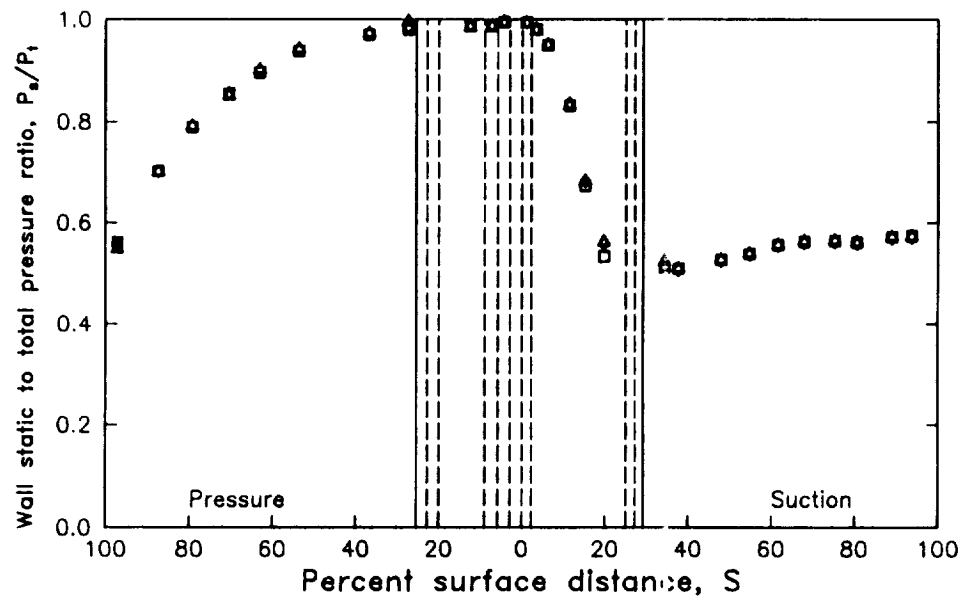


Figure 23. Effects of downstream blowing on vane surface static pressure distribution.

Figures 24, 25, and 26 show the effects of varying the blowing strength at three constant thermal dilution (T_c/T_g) levels with only the downstream film cooling arrays active. The base flow conditions are at exit Mach number of 0.9 and an exit Reynolds number of 2.0×10^6 . Figure 24 shows the effect of varying blowing strength (P_c/P_t) at the lowest coolant-to-gas temperature ratio ($T_c/T_g = 0.65$, MIN). A positive SNR is seen on both surfaces at all three blowing strengths indicating a comparatively large decrease in heat transfer due to downstream film cooling. A pronounced variation in SNR due to different blowing strengths is seen on the pressure surface. Also, on the pressure surface, as the blowing strength is increased, the effect of film cooling is felt further downstream. However, the higher turbulence level near the film cooling holes, resulting from increased blowing, tends to increase heat transfer (i.e., reduce SNR) in the near hole region. On the other hand, on the suction surface, there is no significant effect due to varying blowing strengths. This is due to the lower freestream pressure on the suction surface causing the film coolant flow on the suction surface to be choked over this range of pressure ratios. The choked conditions keep the blowing ratio almost invariant on the suction surface.

Figures 25 and 26 show similar behavior at higher T_c/T_g ratios of 0.75 (MED) and 0.85 (MAX), though, as expected, with lower values of SNR due to lower levels of thermal dilution (warmer air being injected). Also, on the pressure surface, at the lower thermal dilution levels (high T_c/T_g), the

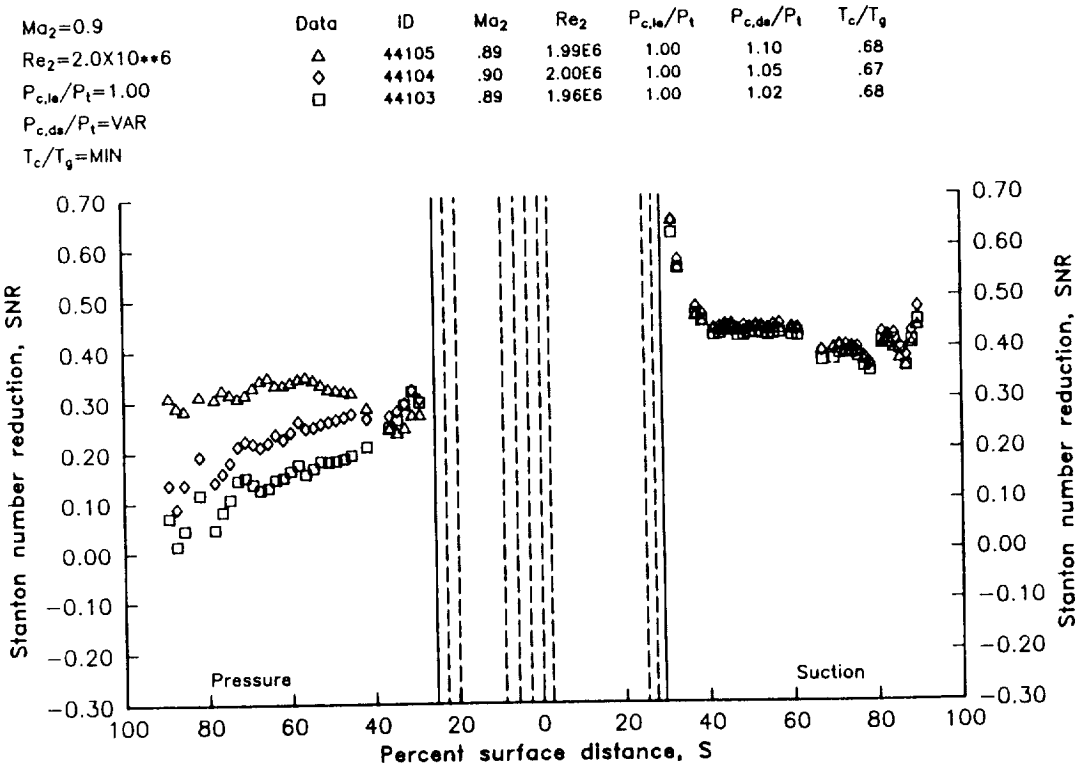


Figure 24. Effects of downstream blowing on Stanton number reduction ($T_c/T_g = MIN$).

$Ma_2=0.9$	Data	ID	Ma_2	Re_2	$P_{c,le}/P_t$	$P_{c,ds}/P_t$	T_c/T_g
$Re_2=2.0 \times 10^{6}$	△	44205	.90	2.01E6	1.00	1.11	.77
$P_{c,le}/P_t=1.00$	◊	44204	.90	2.00E6	1.00	1.05	.76
$P_{c,ds}/P_t=VAR$	□	44203	.90	1.99E6	1.00	1.02	.75
$T_c/T_g=MED$							

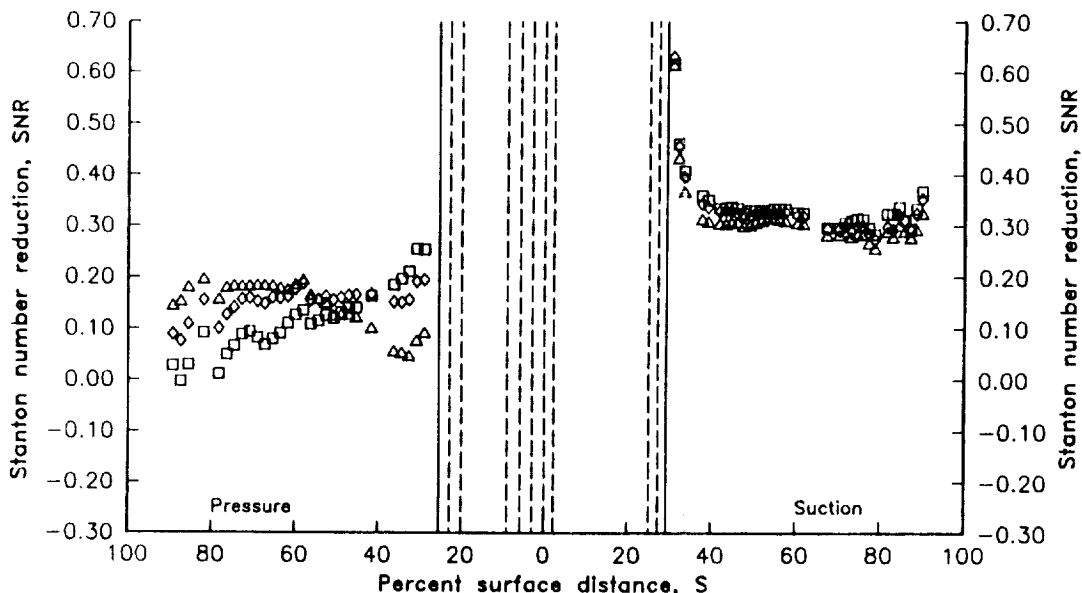


Figure 25. Effects of downstream blowing on Stanton number reduction ($T_c/T_g = MED$).

$Ma_2=0.9$	Data	ID	Ma_2	Re_2	$P_{c,le}/P_t$	$P_{c,ds}/P_t$	T_c/T_g
$Re_2=2.0 \times 10^{6}$	△	44305	.90	2.03E6	1.00	1.11	.85
$P_{c,le}/P_t=1.00$	◊	44304	.89	2.01E6	1.00	1.05	.86
$P_{c,ds}/P_t=VAR$	□	44303	.90	2.01E6	1.00	1.02	.84
$T_c/T_g=MAX$							

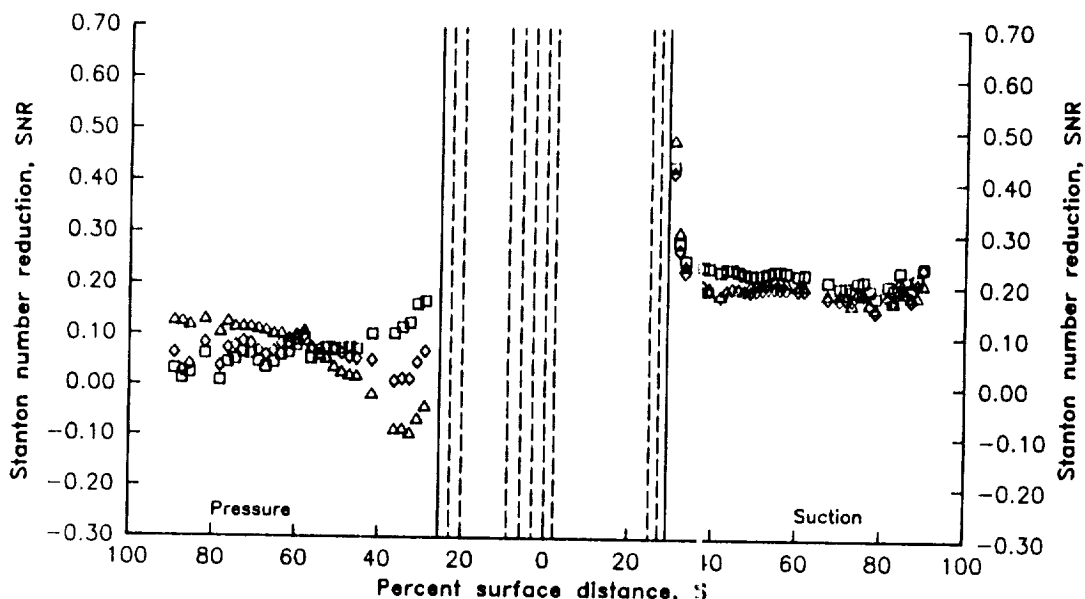


Figure 26. Effects of downstream blowing or Stanton number reduction ($T_c/T_g = MAX$).

effect of turbulence due to the higher blowing strengths increases heat transfer (i.e., decreases SNR values) just downstream of the film cooling holes to a larger extend than at higher thermal dilution levels (i.e., low T_c/T_g). It should also be noted that for the higher blowing strengths, SNR increases over the last 60% of the airfoil; whereas, for the lower blowing strengths, the SNR decreases. This is the result of the interaction of the thermal dilution and turbulence augmentation effects.

On the SNR data presented above, just downstream of the suction side film cooling holes, SNR attain high values. These high SNR values are caused by the non-film cooled and the film cooled tests having different origination of the thermal boundary layer. In the case of a vane which is uniformly cooled throughout, the hydrodynamic and the thermal boundary layer would originate simultaneously at the leading edge. However, in the present case under non-film cooled conditions, the nose piece of the vane is not cooled (radially or otherwise). This results in a step change in vane surface temperature across the thermal barrier on both surfaces as shown earlier in Figure 21. This indicates that the origin of the thermal boundary layer is at the thermal barrier, while the hydrodynamic boundary layer still originates at the leading edge. When the film cooling arrays in the nose piece are activated, the temperature in the leading edge region drops to approximately the levels on the pressure and suction surfaces just downstream of the thermal barrier, thus resulting in both the hydrodynamic and thermal boundary layers originating at the vane leading edge. This difference in thermal boundary layer origin between the film cooled and non-film cooled cases results in the high SNR values just downstream of the film cooling arrays.

The thermal dilution and turbulence augmentation trends discussed earlier are further brought out by Figures 27 and 28, which show data with downstream film cooling holes active for blowing strengths at levels up to 1.7 at MIN and MAX levels of thermal dilution, respectively. On the pressure surface, at both coolant-to-gas temperature ratios, the turbulence due to high blowing strengths decreases the SNR near the film cooling holes. At the lower coolant-to-gas temperature ratio, as shown in Figure 27, a positive value of SNR is seen, even at the highest blowing strength. However, in Figure 28, at the higher coolant-to-gas temperature ratio, almost all the data on the pressure surface at high blowing strengths ($P_c/P_t > 1.3$) show negative SNR values. (note that in Figure 28, the SNR scales are offset.) On the other hand, there is hardly any effect of coolant pressure on the suction surface due to the fact that the film coolant flow is choked and no significant variation in blowing ratio occurred. Nevertheless, at the higher coolant-to-gas temperature ratio, on the suction surface, there is slight decrease in SNR near the film cooling holes at the high blowing strengths. Although the flow is choked, increasing coolant supply pressure increases the coolant mass supply, causing an increase in turbulence level near the coolant holes, which in turn reduces SNR at very high blowing strengths. This also may be due to the damping of turbulence at increased velocity levels.

Figures 29 and 30 show the effects of both the downstream and the leading edge film cooling arrays being active with the varying blowing strengths at the MIN and MAX levels of thermal dilution, respectively. The flow conditions are at an exit Mach number of 0.9 and exit Reynolds number of 2.0×10^6 . In comparison to Figures 24 and 26, the trends and levels of SNR are very similar to the case where only the downstream film cooling holes are active. However,

$Ma_2 = 0.9$
 $Re_2 = 2.0 \times 10^{6+6}$
 $P_{c,le}/P_t = 1.00$
 $P_{c,de}/P_t = \text{VAR}$
 $T_c/T_g = \text{MIN}$

Data	ID	Ma_2	Re_2	$P_{c,le}/P_t$	$P_{c,de}/P_t$	T_c/T_g
◆	44108	.89	2.00E6	1.00	1.63	.63
■	44107	.89	1.98E6	1.00	1.52	.63
○	44108	.90	1.99E6	1.00	1.29	.64
△	44105	.89	1.99E6	1.00	1.10	.68
◊	44104	.90	2.00E6	1.00	1.05	.67
□	44103	.89	1.96E6	1.00	1.02	.68

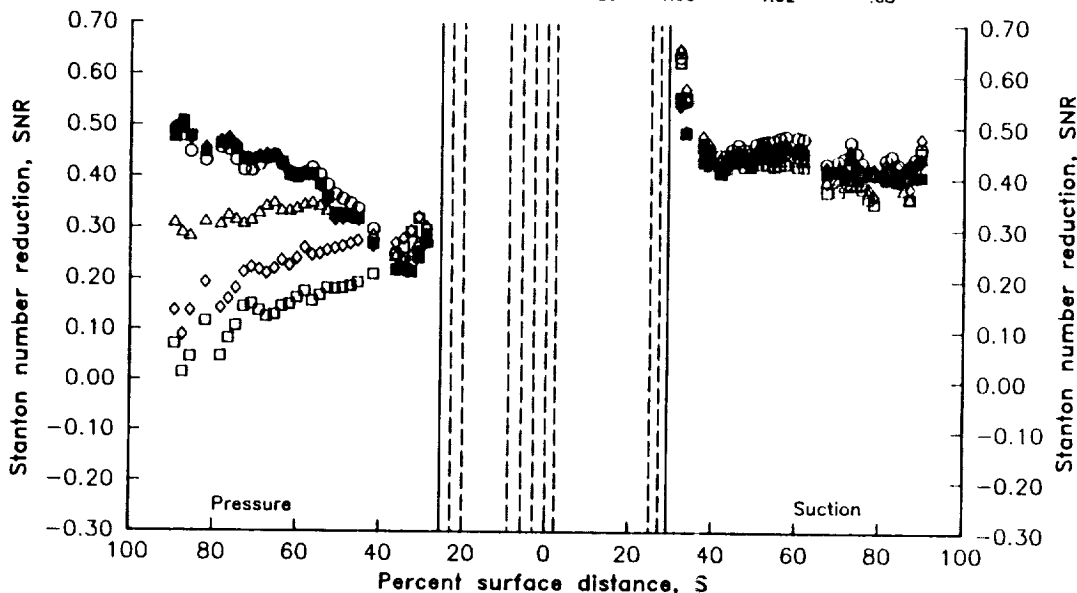


Figure 27. Effects of high downstream blowing on Stanton number reduction ($T_c/T_g = \text{MIN}$).

$Ma_2 = 0.9$
 $Re_2 = 2.0 \times 10^{6+6}$
 $P_{c,le}/P_t = 1.00$
 $P_{c,de}/P_t = \text{VAR}$
 $T_c/T_g = \text{MAX}$

Data	ID	Ma_2	Re_2	$P_{c,le}/P_t$	$P_{c,de}/P_t$	T_c/T_g
◆	44308	.89	1.98E6	1.00	1.61	.85
■	44307	.90	2.00E6	1.00	1.49	.85
○	44306	.90	2.00E6	1.00	1.30	.82
△	44305	.90	2.03E6	1.00	1.11	.85
◊	44304	.89	2.01E6	1.00	1.05	.86
□	44303	.90	2.01E6	1.00	1.02	.84

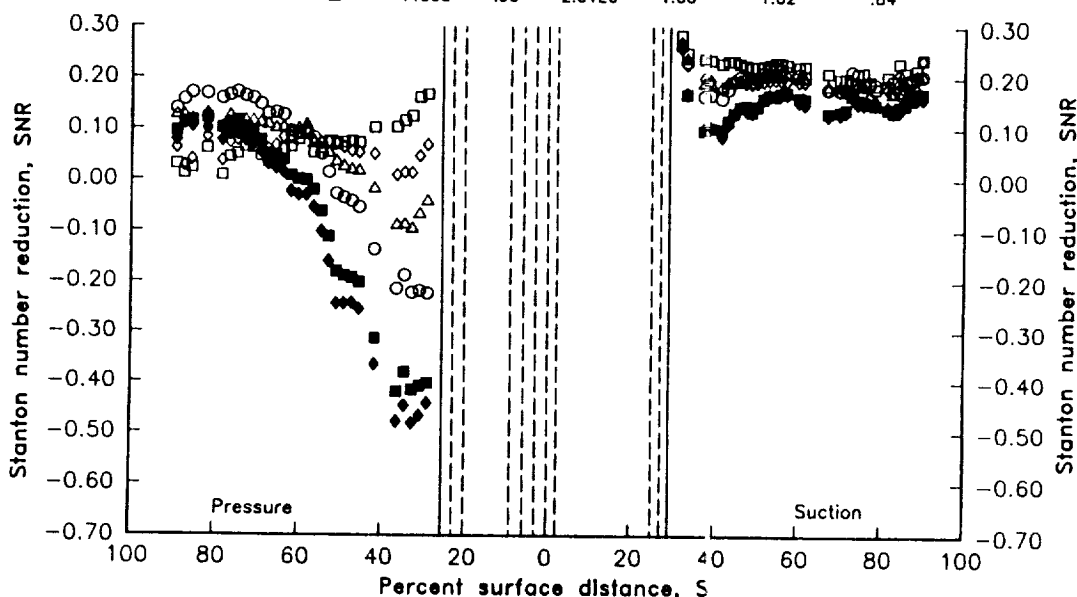


Figure 28. Effects of high downstream blowing on Stanton number reduction ($T_c/T_g = \text{MAX}$).

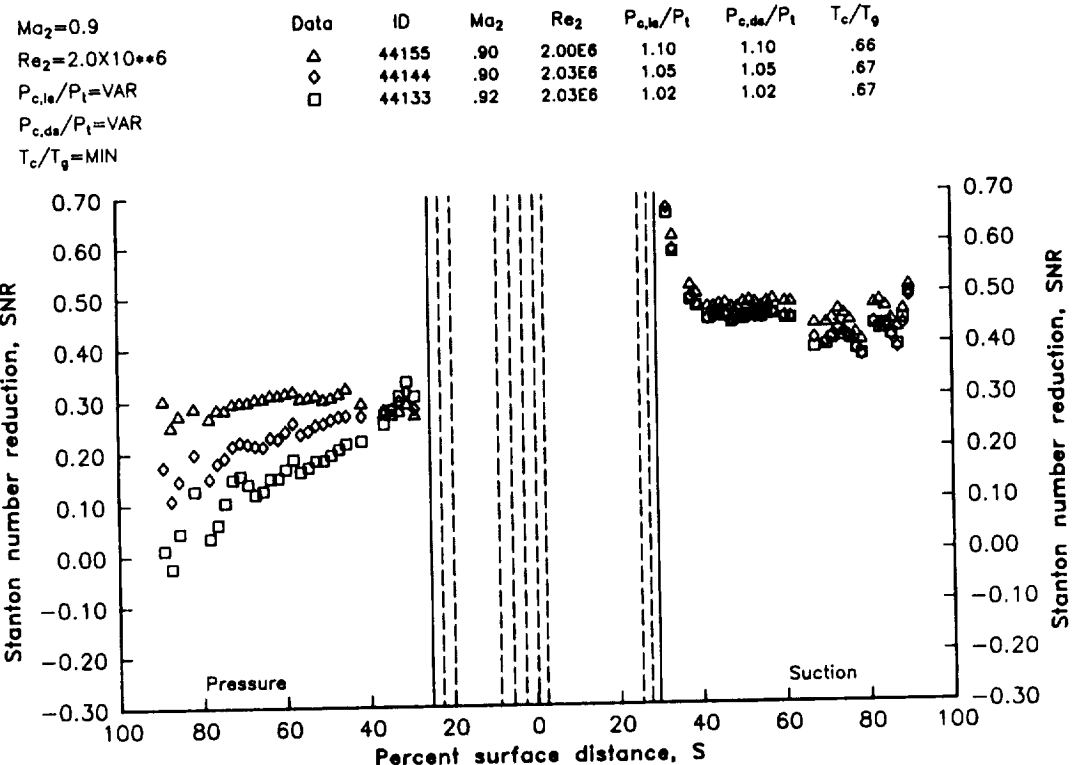


Figure 29. Effects of leading edge and downstream blowing on Stanton number reduction ($T_c/T_g = MIN$).

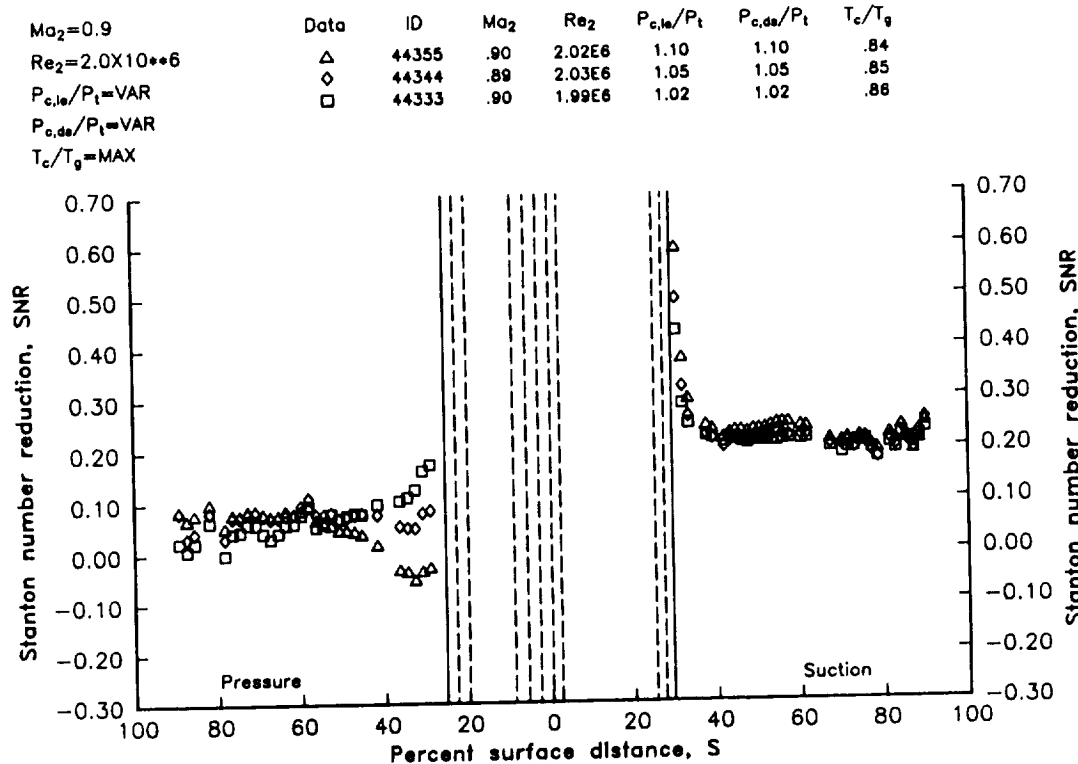


Figure 30. Effects of leading edge and downstream blowing on Stanton number reduction ($T_c/T_g = MAX$).

on the pressure surface just downstream of the film cooling holes, slightly higher values of SNR are seen due to the leading edge film cooling holes being active.

The SNR data for the case where downstream film cooling hole arrays are at a constant blowing strength of 1.10 while the leading edge film cooling blowing strength is varied from 1.00 (no leading edge blowing) to 1.10 are shown in Figure 31. These data are at the flow conditions corresponding to an exit Mach number of 0.75 and an exit Reynolds number of 2.0×10^6 . On the pressure surface, SNR is increased by low leading edge blowing values ($P_{c,le}/P_t = 1.02$). However, at higher leading edge blowing values, SNR values drop off, to the extend that SNR is lower than without any leading edge blowing. This indicates that high leading edge blowing rates can actually increase heat transfer over the entire pressure surface of the airfoil due to increased turbulence levels. On the other hand, very little effect of leading edge blowing is seen on the suction surface.

To illustrate the effects of thermal dilution, data shown earlier in Figures 24-26 were re-plotted as a function of T_c/T_g at two blowing strengths of 1.02 and 1.10 and are shown in Figures 32 and 33, respectively. On the suction surface, in both cases, there is a significant effect due to different coolant-to-gas temperature ratios. Conversely, on the pressure side, at the lower blowing strength, as shown in Figure 32, only a small effect is noticed. However, as seen in Figure 33, there is a larger effect on the pressure surface due to varying thermal dilution at the higher blowing strength of

$Ma_2=0.75$	Data	ID	Ma_2	Re_2	$P_{c,le}/P_t$	$P_{c,de}/P_t$	T_c/T_g
$Re_2=2.0 \times 10^6$	O	34155	.75	2.05E6	1.10	1.10	.67
$P_{c,le}/P_t=VAR$	△	34145	.74	2.00E6	1.05	1.10	.65
$P_{c,de}/P_t=1.10$	◊	34135	.75	2.01E6	1.02	1.10	.65
$T_c/T_g=MIN$	□	34105	.75	2.00E6	1.00	1.10	.66

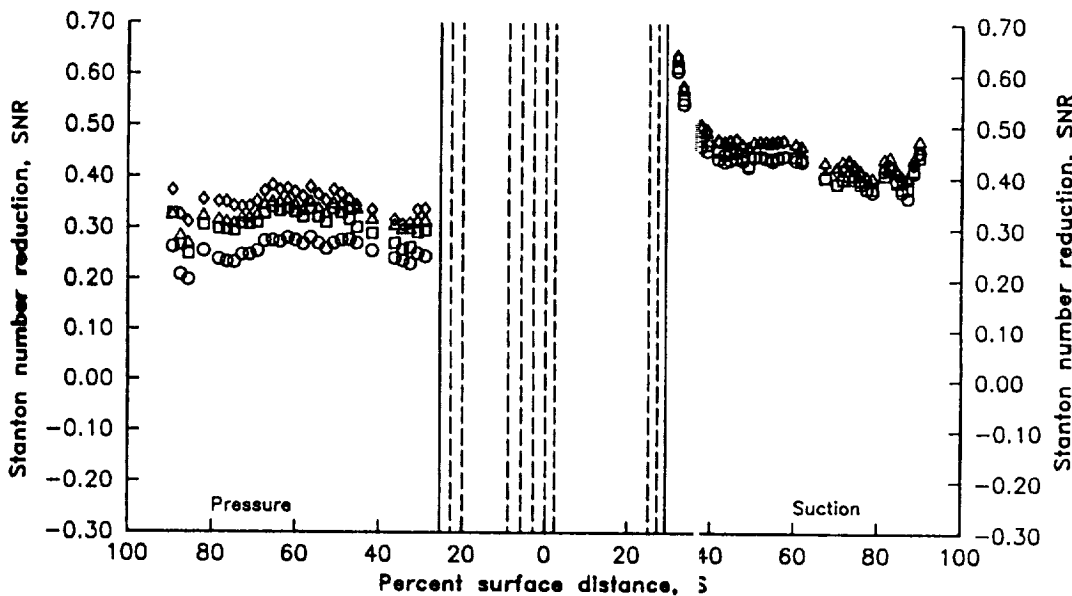


Figure 31. Effects of variable leading edge blowing with constant downstream blowing on Stanton number reduction ($T_c/T_g = MIN$).

$Ma_2=0.9$

$Re_2=2.0 \times 10^{6}$

$P_{c,le}/P_t=1.00$

$P_{c,de}/P_t=1.02$

$T_c/T_g=VAR$

Data

ID

Ma_2

Re_2

$P_{c,le}/P_t$

$P_{c,de}/P_t$

T_c/T_g

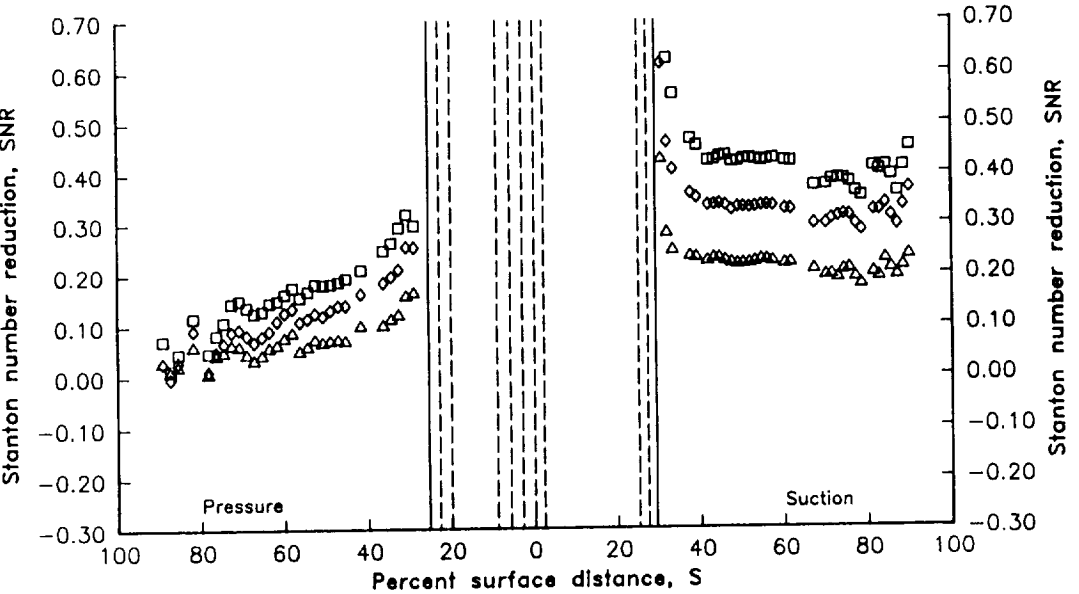


Figure 32. Effects of downstream film cooling thermal dilution on Stanton number reduction ($P_c/P_t = 1.02$).

$Ma_2=0.9$

$Re_2=2.0 \times 10^{6}$

$P_{c,le}/P_t=1.00$

$P_{c,de}/P_t=1.10$

$T_c/T_g=VAR$

Data

ID

Ma_2

Re_2

$P_{c,le}/P_t$

$P_{c,de}/P_t$

T_c/T_g

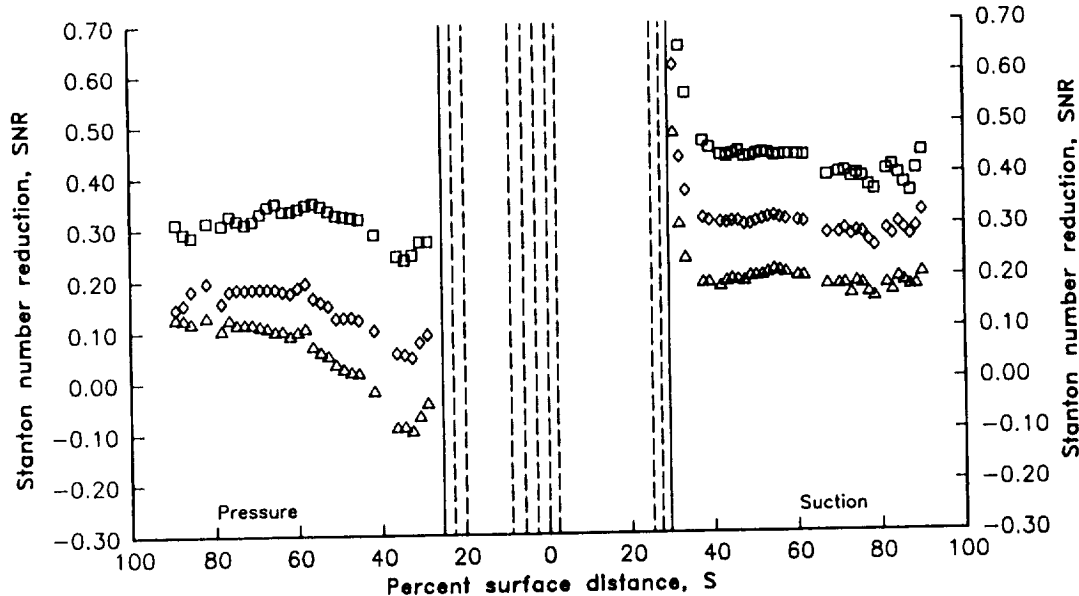


Figure 33. Effects of downstream film cooling thermal dilution on Stanton number reduction ($P_c/P_t = 1.10$).

$P_c/P_t = 1.10$. Also in Figure 33, at higher coolant-to-gas temperature ratio, SNR is negative on the pressure surface at surface distances less than 50%. As mentioned before, this increase in heat transfer is due to the high blowing strength causing a higher level of turbulence augmentation effects which offsets the thermal dilution effects in the vicinity of the film cooling holes.

Figures 34 and 35 illustrate the effect of varying the exit Mach number from 0.75 to 0.90 while keeping other flow and film cooling conditions constant. In these instances, the downstream film cooling hole arrays are at blowing strengths, $P_{c,ds}/P_t$, of 1.10 and the coolant-to-gas temperature ratios, T_c/T_g , are at MIN (Figure 34) and MAX (Figure 35) levels. In these cases, each film cooling data point is compared with the baseline at that flow condition. In other words, these SNR data show the increase or decrease of the heat transfer over the particular baseline case. Figures 34 and 35 show that there is no significant effect on SNR due to variations in Mach number on either the suction surface or pressure surfaces at the lower coolant-to-gas temperature ratio. However, on the pressure surface at the higher coolant-to-gas temperature ratio, Figure 35 shows that there is a slight Mach number effect. As pointed out earlier, at the higher coolant-to-gas temperature ratio, on the pressure surface, the favorable thermal dilution effects are offset by the adverse turbulence augmentation effects, thereby increasing heat transfer near the vicinity of the film cooling holes. At regions where this phenomenon occurs, the change in heat transfer due to film cooling seems to depend on the Mach number, suggesting that the turbulent augmentation effect may be Mach number dependent.

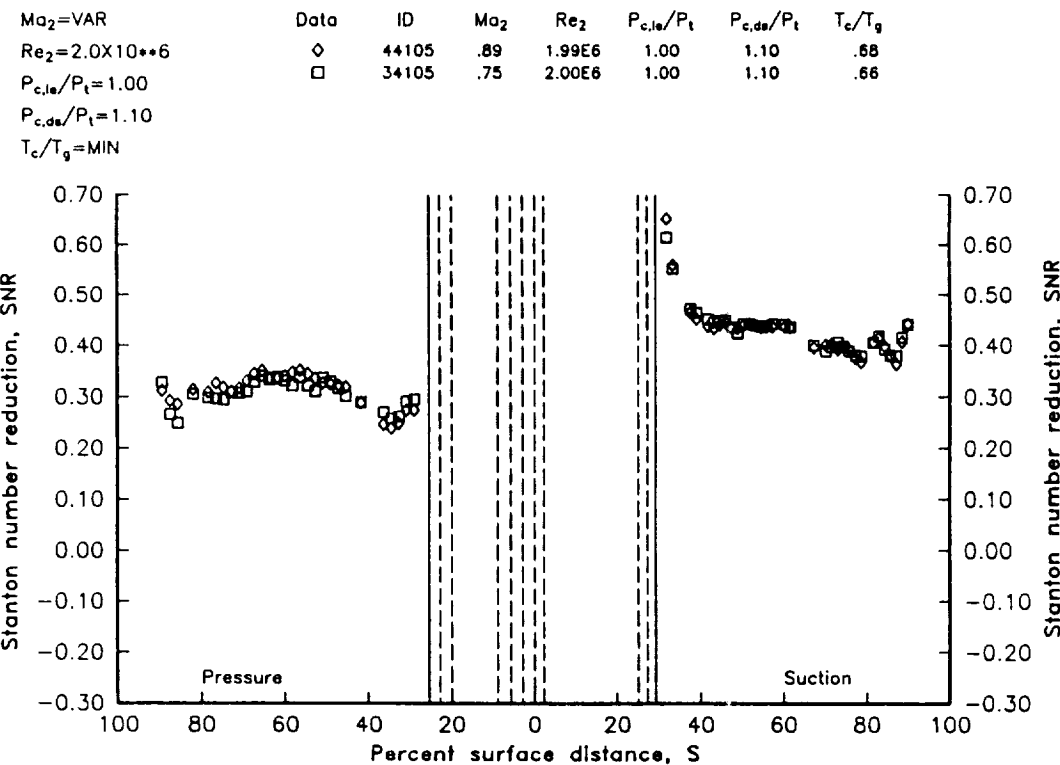


Figure 34. Effects of Mach number on Stanton number reduction ($P_c/P_t = 1.10$, $T_c/T_g = MIN$).

$Ma_2 = \text{VAR}$	Data	ID	Ma_2	Re_2	$P_{c,le}/P_t$	$P_{c,ds}/P_t$	T_c/T_g
$Re_2 = 2.0 \times 10^6$	◊	44305	.90	2.03E6	1.00	1.11	.85
$P_{c,le}/P_t = 1.00$	□	34305	.75	2.03E6	1.00	1.10	.87
$P_{c,ds}/P_t = 1.10$							
$T_c/T_g = \text{MAX}$							

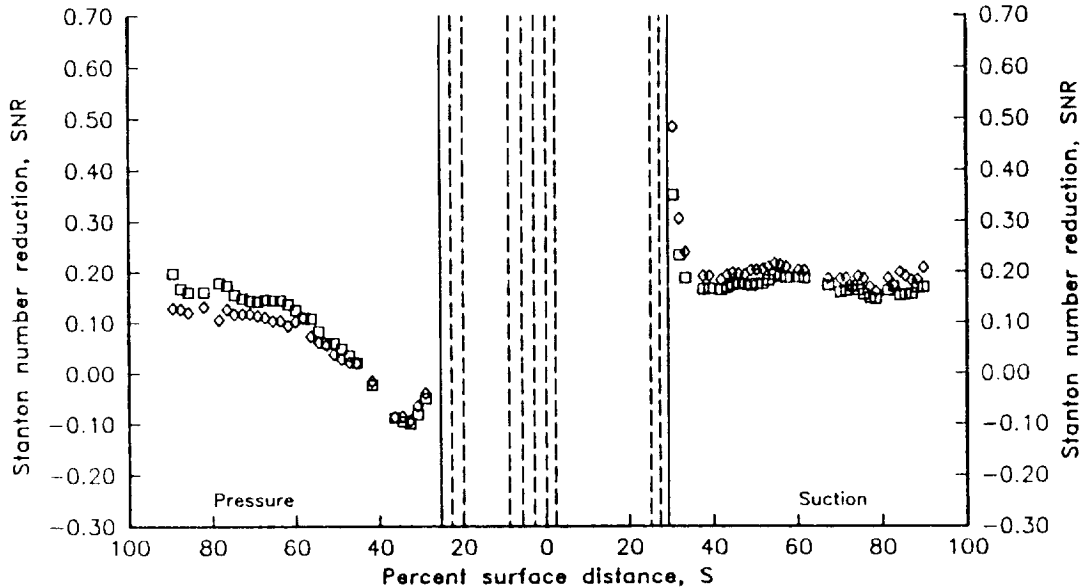


Figure 35. Effects of Mach number on Stanton number reduction ($P_c/P_t = 1.10$, $T_c/T_g = \text{MAX}$).

The effects of three different exit Reynolds numbers of 1.5×10^6 , 2.0×10^6 , and 2.5×10^6 on downstream film cooling are shown in Figures 36 and 37. As in the previous two figures, the SNR data show the change in heat transfer due to film cooling above the particular baseline. Figure 36 presents data at the MIN level of coolant-to-gas temperature ratio and coolant pressure ratio of 1.10. On both surfaces, SNR increases with increasing Reynolds number indicating that a more favorable effect of film cooling is attainable at a higher Reynolds number, though the trends are more pronounced on the pressure surface than on the suction surface. In Figure 37, where the coolant-to-gas temperature is at MAX level, the effect of Reynolds number variation is not as marked as in the case of the lower coolant-to-gas temperature ratio.

In summarizing the heat transfer results, the data indicate that considerable cooling can be attained by downstream film cooling. The downstream film cooling process is a complex function of the thermal dilution, due to the injection of relatively cold fluid, and turbulence augmentation, due to the injection process, with trends actually reversing as the coolant-to-gas temperature ratio is varied. The pressure surface of the airfoil is shown to exhibit a considerably higher degree of sensitivity to the combined effect of turbulence augmentation and thermal dilution. At regular blowing strengths ($P_{c,le}/P_t > 1.0$), the pressure surface shows considerable dependence on blowing strength, while the suction surface is insensitive to varying blowing strength, due to the coolant flow being choked. Also, the heat transfer levels are significantly dependent on the thermal dilution, to the extend that at high levels of thermal dilution, the turbulence augmentation effect is negligible. The data also indicate that, at high thermal dilution levels

$Ma_2=0.9$	Data	ID	Ma_2	Re_2	$P_{c,le}/P_t$	$P_{c,de}/P_t$	T_c/T_g
$Re_2=VAR$	Δ	45105	.89	2.48E6	1.00	1.10	.66
$P_{c,le}/P_t=1.00$	\diamond	44105	.89	1.99E6	1.00	1.10	.68
$P_{c,de}/P_t=1.10$	\square	43105	.89	1.55E6	1.00	1.10	.67
$T_c/T_g=MIN$							

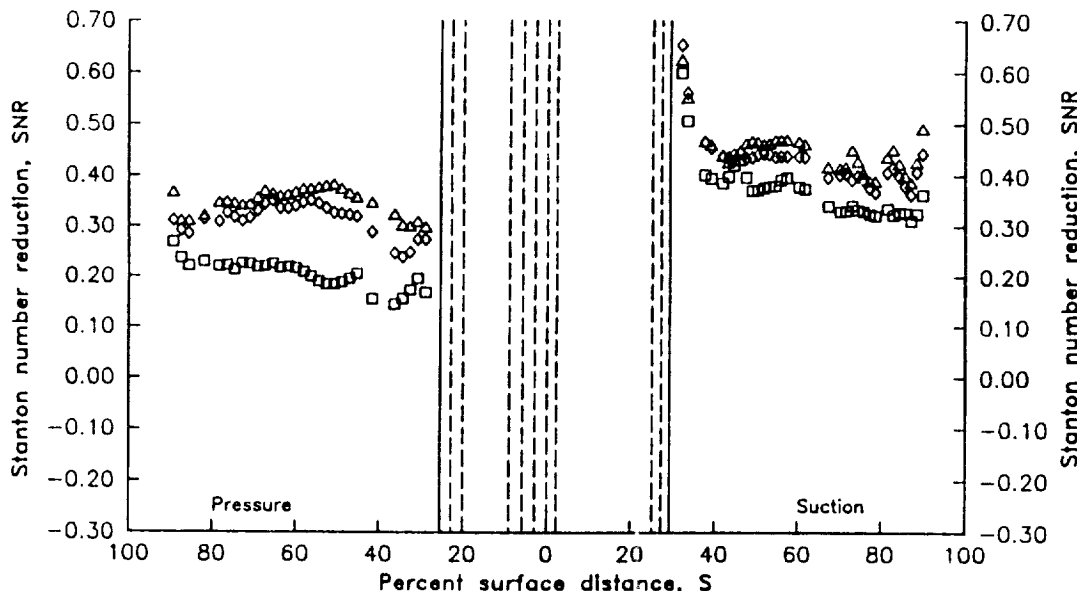


Figure 36. Effects of Reynolds number on Stanton number reduction ($P_{c}/P_t = 1.10$, $T_c/T_g = MIN$).

$Ma_2=0.9$	Data	ID	Ma_2	Re_2	$P_{c,le}/P_t$	$P_{c,de}/P_t$	T_c/T_g
$Re_2=VAR$	Δ	45305	.90	2.51E6	1.00	1.11	.86
$P_{c,le}/P_t=1.00$	\diamond	44305	.90	2.03E6	1.00	1.11	.85
$P_{c,de}/P_t=1.10$	\square	43305	.90	1.52E6	1.00	1.11	.86
$T_c/T_g=MAX$							

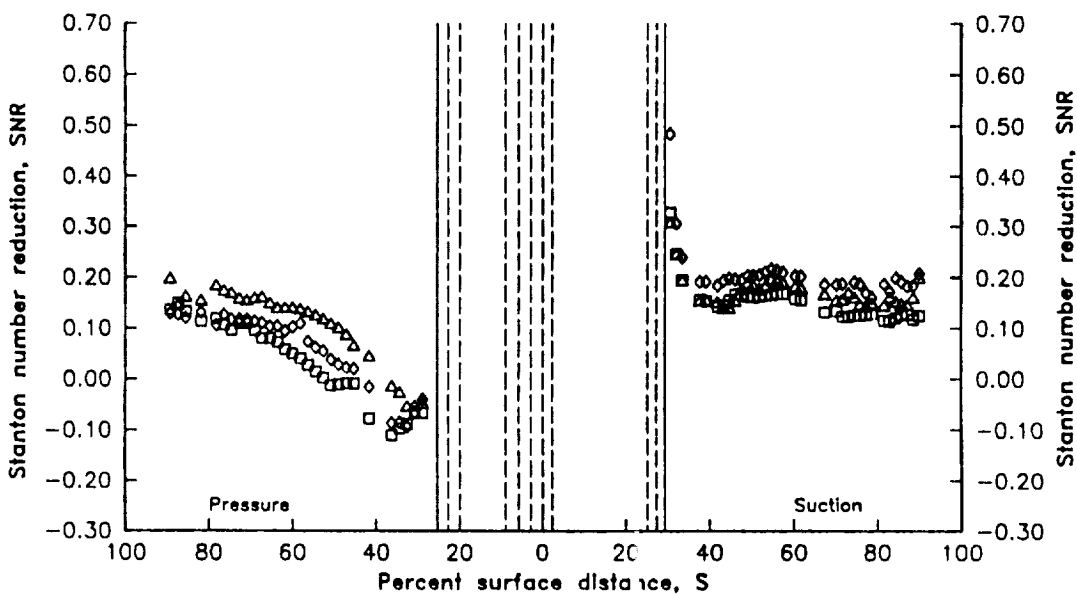


Figure 37. Effects of Reynolds number on Stanton number reduction ($P_{c}/P_t = 1.10$, $T_c/T_g = MAX$).

(i.e. low coolant-to-gas temperature ratio), the film cooling effects are relatively insensitive to exit Mach numbers, while higher favorable film cooling effects are seen at higher exit Reynolds numbers. Conversely, at low thermal dilution levels (i.e., high coolant-to-gas temperature ratio), film cooling effects are dependent on exit Mach number and lesser exit Reynolds number effects are seen and finally, the heat transfer results presented here indicate that the data is significantly dependent on the measured vane surface-to-gas temperature ratio distribution.

6.2 Throat Passage Pressure Results

During all heat transfer data acquisition runs, static pressure measurements were acquired near the cascade throat on the upper and the lower passages. These data are tabulated in Appendix C. Included in the tabulation is the run code, the percent distance of the location of the pressure tap from the midspan of the upper vane to the midspan of the lower vane, and the ratio of the local static pressure-to-inlet total pressure. Note that this distance from the upper vane midspan to the lower vane midspan is actually three dimensional, as shown in Figure 38. The distance is measured spanwise from the midspan of the upper vane suction surface to the endwall; then along the endwall to the lower vane; then spanwise from the endwall to the midspan of the lower vane along the vane pressure surface. Some representative data of the throat passage pressure are presented and discussed in this section.

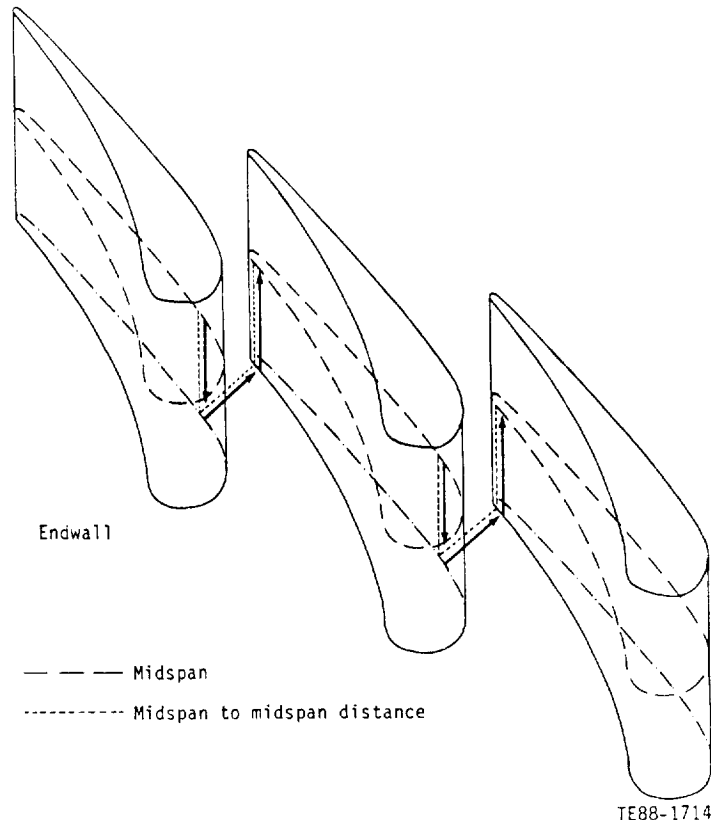


Figure 38. Isometric view of the location of the throat static pressure measurements.

Figures 39, 40, and 41 show the throat static pressure ratio for three of the baseline (i.e., no film cooling) flow conditions corresponding to an exit Mach number, Ma_2 , of 0.9 at exit Reynolds number, Re_2 , of 2.0×10^8 and 2.5×10^6 , and $Ma_2=0.75$ at $Re_2=2.0 \times 10^6$. The two dashed vertical lines in these figures indicate the corner location where the vane surface meets the endwall. Figures 39-41 show very little variation in throat static pressure ratio along the spanwise direction on either vane surface or on the endwall. Also, the upper and the lower passages have nearly identical levels on the pressure surfaces. On the endwall and on the suction surface, the throat pressures in the lower passage are about 5% less than the throat pressures on the upper passage. Comparison of Figures 39 and 40 indicate that variation of exit Reynolds number has negligible effect on the throat static pressure ratio. Comparing Figures 39 and 41, a decrease in exit Mach number increases the throat static pressure ratio. This is expected due to the different expansion ratio of the two flow conditions.

To display the effects of film cooling on the throat static pressures, the throat static pressure-to-total pressure ratios measured with film cooling were compared with the baseline case. This is shown in Figure 42 for the case of $Ma_2 = 0.9$ and $Re_2 = 2 \times 10^6$. Only the downstream film cooling arrays were active, with the coolant-to-gas pressure ratio, $P_{c,ds}/P_t$, varied from 1.02 to 1.10, and the coolant-to-gas absolute temperature ratio, T_c/T_g , kept at the MIN level. The format of Figure 42 is similar to Figures 39-41, except that the data from the lower and upper passages have been separated and the scale has been expanded. Also, it should be noted that only the center vane

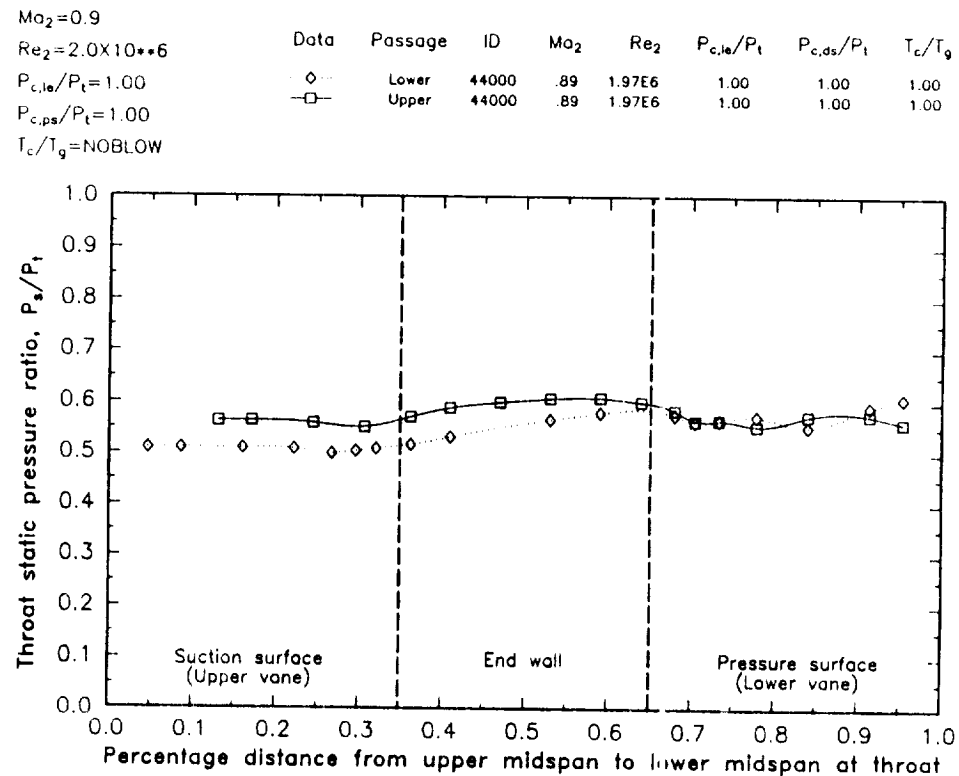


Figure 39. Throat static-to-inlet total pressure ratio at $Ma_2 = 0.9$ and $Re_2 = 2.0 \times 10^8$.

$Ma_2 = 0.9$
 $Re_2 = 2.5 \times 10^6$
 $P_{c,le}/P_t = 1.00$
 $P_{c,ps}/P_t = 1.00$
 $T_c/T_g = NOBLOW$

Data	Passage	ID	Ma_2	Re_2	$P_{c,le}/P_t$	$P_{c,ps}/P_t$	T_c/T_g
...◊...	Lower	45000	.92	2.58E6	1.00	1.00	1.00
—□—	Upper	45000	.92	2.58E6	1.00	1.00	1.00

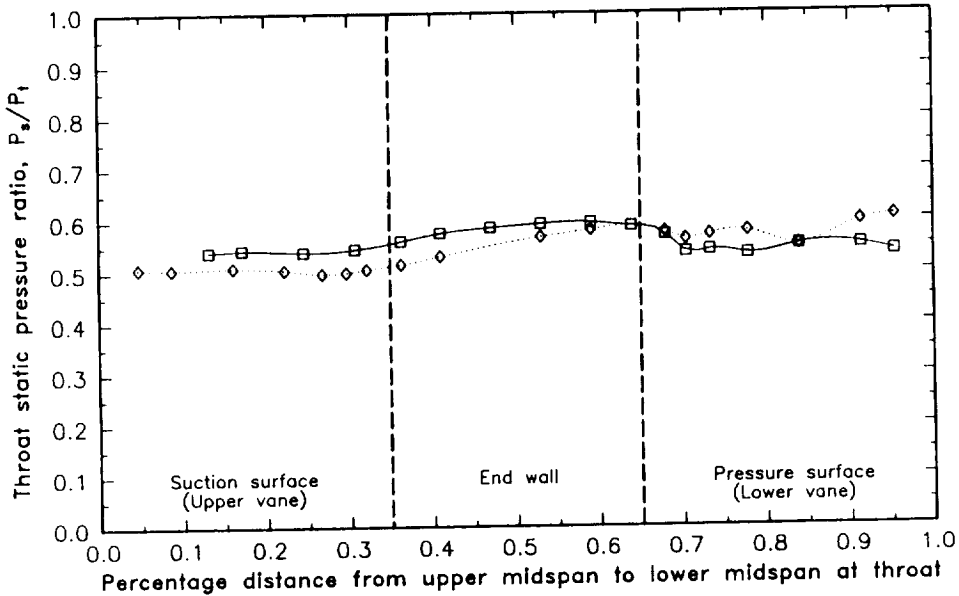


Figure 40. Throat static-to-inlet total pressure ratio at $Ma_2 = 0.9$ and $Re_2 = 2.5 \times 10^6$.

$Ma_2 = 0.75$
 $Re_2 = 2.0 \times 10^6$
 $P_{c,le}/P_t = 1.00$
 $P_{c,ps}/P_t = 1.00$
 $T_c/T_g = NOBLOW$

Data	Passage	ID	Ma_2	Re_2	$P_{c,le}/P_t$	$P_{c,ps}/P_t$	T_c/T_g
...◊...	Lower	34000	.75	1.99E6	1.00	1.00	1.00
—□—	Upper	34000	.75	1.99E6	1.00	1.00	1.00

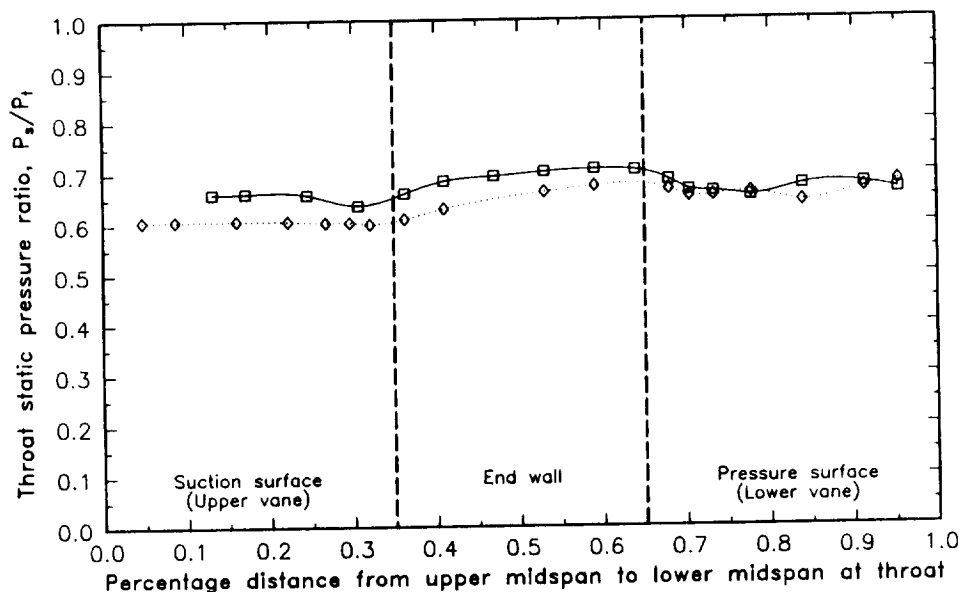


Figure 41. Throat static-to-inlet total pressure ratio at $Ma_2 = 0.75$ and $Re_2 = 2.0 \times 10^6$.

$Ma_2=0.9$	Data	Passage	ID	Ma_2	Re_2	$P_{c,le}/P_t$	$P_{c,ds}/P_t$	T_c/T_g
$Re_2=2.0 \times 10^6$	-■-	Upper	44105	.90	1.98E6	1.00	1.10	.68
$P_{c,le}/P_t=1.00$	-▲-	Upper	44104	.90	2.00E6	1.00	1.05	.67
$P_{c,ds}/P_t=VAR$	-□-	Upper	44103	.89	1.96E6	1.00	1.02	.68
$T_c/T_g=MIN$	-◆-	Lower	44105	.90	1.98E6	1.00	1.10	.68
	-○-	Lower	44104	.90	2.00E6	1.00	1.05	.67
	-◇-	Lower	44103	.89	1.96E6	1.00	1.02	.68

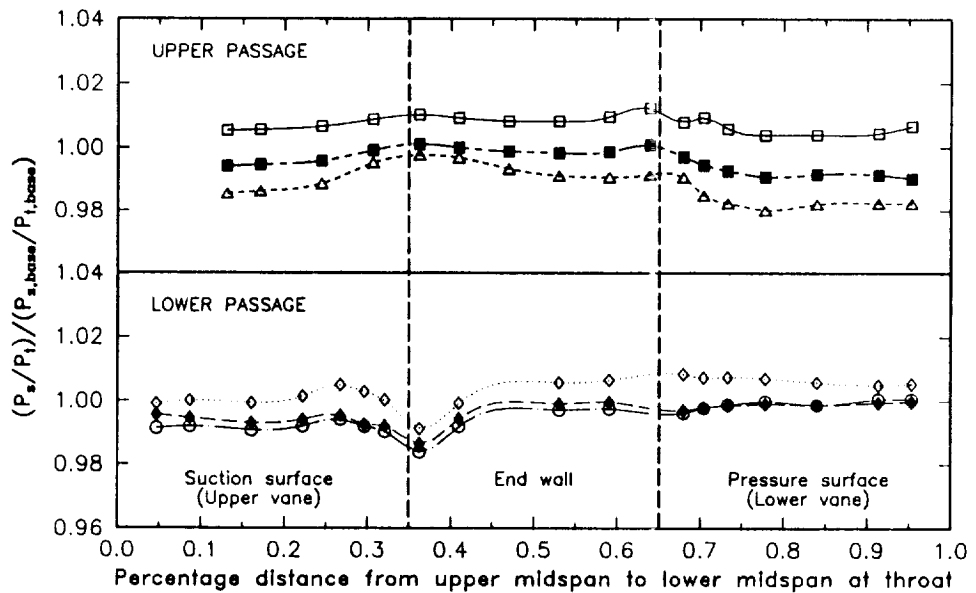


Figure 42. Effects of blowing strength on throat static-to-inlet total pressure ratio.

contains film cooling arrays. Effects of varying blowing strengths do not seem to have any significant effect on the throat static pressure ratio. However, at locations near the corner where the endwall meets the vane suction surface, there is a distinct drop in throat static pressure ratio due to film cooling, but there does not seem to be any consistent effect associated with the varying levels of film cooling.

In summary, the throat static pressure distribution from upper midspan to lower midspan via the endwall does not vary extensively. Varying downstream film cooling with and without leading edge film cooling does not show any consistent effects on the surface pressure distribution. The effects of the film cooling are essentially insignificant except at the corners of the vane suction surface and the endwall where a slight reduction in static pressure was measured.

VII. CONCLUSIONS AND RECOMMENDATIONS

The results from this experiment have provided a data base for characterizing the effects of downstream film cooling with and without leading edge (showerhead) film cooling on external heat transfer to the C3X airfoil.

The external heat transfer data indicate that considerable cooling can be attained by downstream film cooling. The downstream film cooling process is a complex function of mainly two competing mechanisms; (i) the thermal dilution, due to the injection of relatively cold fluid, which decreases heat transfer to the airfoil, and (ii) turbulence augmentation, due to the injection process, which increases heat transfer to the airfoil. It is also observed that favorable cooling effects actually reverse as the coolant-to-gas temperature ratio are varied.

The pressure surface of the airfoil is shown to exhibit a considerably higher degree of sensitivity to the combined effect of turbulence augmentation and thermal dilution. At moderate blowing strengths ($P_c/P_t > 1.0$), the pressure surface shows considerable dependence on blowing strength, while the suction surface is insensitive to variations in blowing strength, due to the coolant flow being choked. Also, the heat transfer levels are significantly dependent on thermal dilution, to the extend that at high levels of thermal dilution, the adverse turbulence augmentation effect is negligible. The data also indicate that, at high thermal dilution levels (i.e. low coolant-to-gas temperature ratio), the film cooling effects are relatively insensitive to exit Mach numbers; and higher favorable film cooling effects are seen at higher exit Reynolds numbers. Conversely, at low thermal dilution levels (i.e., high coolant-to-gas temperature ratio), film cooling effects are dependent on exit Mach number; and lesser effects due to exit Reynolds number are seen.

Static pressure data indicate that vane surface static pressure is relatively independent of downstream and leading edge blowing. Also, the throat static pressure distribution from upper midspan to lower midspan via the endwall do not vary extensively. Downstream film cooling with and without leading edge film cooling do not show any consistent effects on the passage throat static pressure distribution. And moreover, the effects of the film cooling are not significant on the static pressure except at the corners of the vane suction surface and the endwall.

After analyzing the heat transfer data obtained in this experimental program, the following recommendations should be considered for future work:

- o The heat transfer data indicate a strong dependence on the measured vane surface-to-gas temperature ratio distribution, and hence, the surface temperature distribution associated with the heat transfer data should be taken into account when predicting heat transfer results to compare with these data.
- o Further work should be carried out to fully understand the trends of the favorable effects of thermal dilution and the adverse effects of turbulence augmentation during film cooling. A better understanding of these effects would help in obtaining better predictions of film cooled vane heat transfer.

APPENDIX A

TABULATED HEAT TRANSFER DATA

Tabulated heat transfer data for each run code of the downstream and leading edge film-cooled C3X cascade are presented in Table VIII. These data sets are listed in run code order, with the actual operating conditions associated with each run code having been given previously in Table VI. Vane surface-to-gas absolute temperature ratio (T_w/T_g) data and normalized heat transfer coefficients (h/h_0) are tabulated versus percent of surface arc length and percent of axial chord. The heat transfer coefficients are normalized with respect to $1135 \text{ W/m}^2/\text{^0C}$ ($200 \text{ BTU/hr/ft}^2/\text{^0F}$). The surface arc and axial chord lengths were given in Table III.

Tabulated discharge coefficient and blowing ratio data for each heat transfer run code are presented in Table IX. The discharge coefficient is defined as the ratio of actual flow to possible ideal flow; the blowing ratio is defined as the coolant to free-stream mass flux ratio ($M = \rho_C u_C / \rho_\infty u_\infty$). Both values are averages for all holes in a given film cooling array and are based on the average local freestream conditions and total coolant mass flow rate through each cooling array.

Table VIII
Heat transfer data for each run code

RUN CODE 34000

SUCTION SURFACE				PRESSURE SURFACE			
% Surface Distance	% Axial Chord	Tw/Tg	h/ho	% Surface Distance	% Axial Chord	Tw/Tg	h/ho
30.57	49.25	.8019	.9147	28.90	34.95	.7796	.6704
31.98	50.84	.8026	1.0021	30.78	37.26	.7680	.5991
33.40	52.37	.7976	.9839	32.58	39.43	.7615	.4983
37.60	56.50	.7830	.8854	34.38	41.55	.7623	.4660
39.08	57.92	.7762	.8255	36.29	43.76	.7653	.4277
41.80	60.34	.7700	.7571	41.70	49.81	.7792	.3873
43.25	61.62	.7693	.7428	45.37	53.70	.7887	.3851
44.57	62.74	.7752	.7232	47.14	55.56	.7908	.4040
46.03	63.96	.7789	.7163	49.03	57.47	.7901	.4250
47.51	65.26	.7879	.7734	50.84	59.28	.7925	.4457
48.95	66.44	.7928	.7269	52.68	61.08	.7990	.4635
50.31	67.53	.7977	.7022	54.48	62.81	.8032	.4933
51.78	68.75	.8001	.6286	56.34	64.57	.8103	.5290
53.14	69.77	.8047	.6639	58.12	66.24	.8096	.5559
54.62	71.01	.8145	.7756	59.97	67.92	.8076	.6389
55.97	71.99	.8169	.6861	61.77	69.55	.8122	.6530
57.36	73.07	.8160	.6457	63.63	71.18	.8180	.5172
60.29	75.38	.8164	.6824	65.41	72.73	.8260	.5280
61.67	76.42	.8131	.6644	67.30	74.37	.8276	.4826
67.29	80.63	.8203	.7185	69.07	75.85	.8237	.5302
70.13	82.74	.8194	.7380	70.91	77.38	.8130	.6488
71.51	83.72	.8278	.6918	72.72	78.84	.8130	.7264
73.03	84.92	.8348	.6921	74.63	80.37	.8280	.5977
74.39	85.88	.8349	.6122	76.40	81.77	.8374	.4768
75.74	86.80	.8317	.6299	78.27	83.24	.8427	.4537
77.24	87.96	.8196	.7033	81.91	86.03	.8215	.6817
78.62	88.92	.8200	.7362	85.55	88.71	.8401	.4234
81.54	91.06	.8412	.5516	87.39	90.05	.8579	.3797
82.88	91.94	.8451	.5802	89.25	91.42	.8657	.5254
84.34	92.98	.8396	.5959	91.03	92.66	.8648	.8151
85.70	93.87	.8246	.6044	92.86	93.93	.8495	.8698
87.11	94.82	.8190	.6560	96.55	96.47	.8636	.5939
88.50	95.72	.8400	.5184				
89.92	96.63	.8601	.4714				
91.35	97.57	.8650	.3856				
94.24	99.40	.8508	.6365				
95.65	100.24	.8386	.4877				
97.03	101.02	.8635	.7888				

Table VIII (contd)
Heat transfer data for each run code

RUN CODE 34103

SUCTION SURFACE				PRESSURE SURFACE			
% Surface Distance	% Axial Chord	Tw/Tg	h/ho	% Surface Distance	% Axial Chord	Tw/Tg	h/ho
30.57	49.25	.7207	.1730	28.90	34.95	.7279	.4714
31.98	50.84	.7208	.3546	30.78	37.26	.7186	.4118
33.40	52.37	.7152	.4144	32.58	39.43	.7149	.3610
37.60	56.50	.7066	.4523	34.38	41.55	.7172	.3507
39.08	57.92	.7016	.4330	36.29	43.76	.7210	.3263
41.80	60.34	.7000	.4151	41.70	49.81	.7364	.3103
43.25	61.62	.7004	.4106	45.37	53.70	.7470	.3214
44.57	62.74	.7064	.3986	47.14	55.56	.7499	.3372
46.03	63.96	.7109	.3949	49.03	57.47	.7504	.3539
47.51	65.26	.7208	.4349	50.84	59.28	.7543	.3716
48.95	66.44	.7267	.4158	52.68	61.08	.7620	.4064
50.31	67.53	.7317	.3927	54.48	62.81	.7662	.4342
51.78	68.75	.7355	.3522	56.34	64.57	.7733	.4610
53.14	69.77	.7406	.3724	58.12	66.24	.7736	.4896
54.62	71.01	.7504	.4351	59.97	67.92	.7729	.5532
55.97	71.99	.7535	.3843	61.77	69.55	.7776	.5631
57.36	73.07	.7544	.3618	63.63	71.18	.7832	.4612
60.29	75.38	.7560	.3907	65.41	72.73	.7909	.4705
61.67	76.42	.7554	.3833	67.30	74.37	.7930	.4455
67.29	80.63	.7677	.4365	69.07	75.85	.7903	.4927
70.13	82.74	.7697	.4622	70.91	77.38	.7813	.5955
71.51	83.72	.7789	.4201	72.72	78.84	.7824	.6653
73.03	84.92	.7868	.4123	74.63	80.37	.7968	.5643
74.39	85.88	.7881	.3670	76.40	81.77	.8053	.4612
75.74	86.80	.7858	.3881	78.27	83.24	.8107	.4478
77.24	87.96	.7755	.4534	81.91	86.03	.7914	.6207
78.62	88.92	.7767	.4829	85.55	88.71	.8102	.4387
81.54	91.06	.7991	.3217	87.39	90.05	.8270	.3978
82.88	91.94	.8026	.3266	89.25	91.42	.8342	.4873
84.34	92.98	.7985	.3570	91.03	92.66	.8339	.7417
85.70	93.87	.7845	.3809	92.86	93.93	.8196	.7975
87.11	94.82	.7801	.4341	96.55	96.47	.8328	.5986
88.50	95.72	.8013	.2992				
89.92	96.63	.8213	.2482				
91.35	97.57	.8276	.2037				
94.24	99.40	.8140	.4046				
95.65	100.24	.8021	.2993				
97.03	101.02	.8269	.4823				

Table VIII (contd)
Heat transfer data for each run code

RUN CODE 34104

SUCTION SURFACE				PRESSURE SURFACE			
% Surface Distance	% Axial Chord	Tw/Tg	h/ho	% Surface Distance	% Axial Chord	Tw/Tg	h/ho
30.57	49.25	.7217	.1507	28.90	34.95	.7283	.4711
31.98	50.84	.7212	.3365	30.78	37.26	.7186	.4174
33.40	52.37	.7158	.4055	32.58	39.43	.7140	.3609
37.60	56.50	.7070	.4514	34.38	41.55	.7153	.3432
39.08	57.92	.7017	.4309	36.29	43.76	.7181	.3152
41.80	60.34	.6999	.4121	41.70	49.81	.7305	.2844
43.25	61.62	.7002	.4077	45.37	53.70	.7397	.2859
44.57	62.74	.7058	.3944	47.14	55.56	.7422	.3007
46.03	63.96	.7100	.3894	49.03	57.47	.7422	.3152
47.51	65.26	.7198	.4307	50.84	59.28	.7457	.3298
48.95	66.44	.7257	.4190	52.68	61.08	.7529	.3602
50.31	67.53	.7304	.3913	54.48	62.81	.7571	.3811
51.78	68.75	.7338	.3484	56.34	64.57	.7637	.4015
53.14	69.77	.7385	.3704	58.12	66.24	.7640	.4306
54.62	71.01	.7483	.4379	59.97	67.92	.7635	.4869
55.97	71.99	.7509	.3838	61.77	69.55	.7677	.4951
57.36	73.07	.7516	.3597	63.63	71.18	.7738	.4050
60.29	75.38	.7529	.3859	65.41	72.73	.7814	.4079
61.67	76.42	.7518	.3779	67.30	74.37	.7836	.3849
67.29	80.63	.7636	.4348	69.07	75.85	.7813	.4331
70.13	82.74	.7653	.4560	70.91	77.38	.7727	.5286
71.51	83.72	.7741	.4183	72.72	78.84	.7737	.5905
73.03	84.92	.7817	.4111	74.63	80.37	.7883	.5005
74.39	85.88	.7829	.3696	76.40	81.77	.7969	.4035
75.74	86.80	.7807	.3894	78.27	83.24	.8020	.3832
77.24	87.96	.7708	.4505	81.91	86.03	.7838	.5565
78.62	88.92	.7722	.4786	85.55	88.71	.8027	.3828
81.54	91.06	.7938	.3298	87.39	90.05	.8193	.3429
82.88	91.94	.7976	.3400	89.25	91.42	.8267	.4309
84.34	92.98	.7934	.3634	91.03	92.66	.8264	.6484
85.70	93.87	.7798	.3810	92.86	93.93	.8129	.7147
87.11	94.82	.7755	.4253	96.55	96.47	.8263	.5312
88.50	95.72	.7962	.3047				
89.92	96.63	.8159	.2599				
91.35	97.57	.8217	.2101				
94.24	99.40	.8091	.4049				
95.65	100.24	.7982	.3118				
97.03	101.02	.8218	.4780				

Table VIII (contd)
Heat transfer data for each run code

RUN CODE 34105

SUCTION SURFACE				PRESSURE SURFACE			
% Surface Distance	% Axial Chord	Tw/Tg	h/ho	% Surface Distance	% Axial Chord	Tw/Tg	h/ho
30.57	49.25	.7336	.2231	28.90	34.95	.7349	.4728
31.98	50.84	.7330	.3860	30.78	37.26	.7257	.4249
33.40	52.37	.7275	.4408	32.58	39.43	.7211	.3678
37.60	56.50	.7171	.4671	34.38	41.55	.7218	.3460
39.08	57.92	.7112	.4422	35.29	43.76	.7239	.3121
41.80	60.34	.7082	.4152	41.70	49.81	.7344	.2752
43.25	61.62	.7084	.4122	45.37	53.70	.7419	.2691
44.57	62.74	.7136	.3987	47.14	55.56	.7435	.2762
46.03	63.96	.7175	.3934	49.03	57.47	.7426	.2849
47.51	65.26	.7268	.4363	50.84	59.28	.7453	.2955
48.95	66.44	.7322	.4188	52.68	61.08	.7515	.3195
50.31	67.53	.7364	.3912	54.48	62.81	.7551	.3348
51.78	68.75	.7398	.3507	56.34	64.57	.7607	.3504
53.14	69.77	.7442	.3721	58.12	66.24	.7608	.3771
54.62	71.01	.7534	.4370	59.97	67.92	.7596	.4273
55.97	71.99	.7560	.3849	61.77	69.55	.7635	.4321
57.36	73.07	.7561	.3600	63.63	71.18	.7692	.3449
60.29	75.38	.7568	.3812	65.41	72.73	.7765	.3484
61.67	76.42	.7556	.3745	67.30	74.37	.7787	.3242
67.29	80.63	.7654	.4310	69.07	75.85	.7765	.3659
70.13	82.74	.7666	.4512	70.91	77.38	.7681	.4494
71.51	83.72	.7746	.4174	72.72	78.84	.7689	.5028
73.03	84.92	.7814	.4110	74.63	80.37	.7830	.4219
74.39	85.88	.7823	.3686	76.40	81.77	.7912	.3355
75.74	86.80	.7804	.3851	78.27	83.24	.7963	.3186
77.24	87.96	.7704	.4360	80.91	86.03	.7791	.4738
78.62	88.92	.7716	.4574	85.55	88.71	.7977	.3180
81.54	91.06	.7917	.3277	87.39	90.05	.8134	.2787
82.88	91.94	.7952	.3376	89.25	91.42	.8205	.3532
84.34	92.98	.7915	.3624	91.03	92.66	.8205	.5342
85.70	93.87	.7789	.3748	92.86	93.93	.8088	.6073
87.11	94.82	.7748	.4074	96.55	96.47	.8217	.4459
88.50	95.72	.7941	.3030				
89.92	96.63	.8124	.2634				
91.35	97.57	.8176	.2096				
94.24	99.40	.8068	.3791				
95.65	100.24	.7969	.2796				
97.03	101.02	.8190	.4567				

Table VIII (contd)
Heat transfer data for each run code

RUN CODE 34135

SUCTION SURFACE				PRESSURE SURFACE			
% Surface Distance	% Axial Chord	Tw/Tg	h/ho	% Surface Distance	% Axial Chord	Tw/Tg	h/ho
30.57	49.25	.7206	.1998	28.90	34.95	.7221	.4443
31.98	50.84	.7209	.3632	30.78	37.26	.7136	.3980
33.40	52.37	.7157	.4155	32.58	39.43	.7093	.3443
37.60	56.50	.7062	.4407	34.38	41.55	.7102	.3232
39.08	57.92	.7007	.4186	36.29	43.76	.7125	.2925
41.80	60.34	.6984	.3985	41.70	49.81	.7233	.2575
43.25	61.62	.6986	.3940	45.37	53.70	.7310	.2526
44.57	62.74	.7039	.3810	47.14	55.56	.7327	.2609
46.03	63.96	.7078	.3759	49.03	57.47	.7320	.2695
47.51	65.26	.7168	.4142	50.84	59.28	.7346	.2789
48.95	66.44	.7219	.3930	52.68	61.08	.7408	.2998
50.31	67.53	.7264	.3726	54.48	62.81	.7443	.3134
51.78	68.75	.7295	.3333	56.34	64.57	.7501	.3281
53.14	69.77	.7338	.3517	58.12	66.24	.7502	.3554
54.62	71.01	.7427	.4105	59.97	67.92	.7493	.4031
55.97	71.99	.7452	.3620	61.77	69.55	.7531	.4071
57.36	73.07	.7457	.3405	63.63	71.18	.7588	.3240
60.29	75.38	.7469	.3663	65.41	72.73	.7662	.3257
61.67	76.42	.7458	.3606	67.30	74.37	.7684	.3035
67.29	80.63	.7555	.4112	69.07	75.85	.7664	.3439
70.13	82.74	.7568	.4319	70.91	77.38	.7581	.4270
71.51	83.72	.7650	.4025	72.72	78.84	.7591	.4789
73.03	84.92	.7719	.3960	74.63	80.37	.7727	.3934
74.39	85.88	.7730	.3580	76.40	81.77	.7809	.3097
75.74	86.80	.7710	.3727	78.27	83.24	.7859	.2946
77.24	87.96	.7611	.4209	81.91	86.03	.7685	.4397
78.62	88.92	.7623	.4423	85.55	88.71	.7873	.2918
81.54	91.06	.7823	.3202	87.39	90.05	.8033	.2563
82.88	91.94	.7859	.3328	89.25	91.42	.8105	.3295
84.34	92.98	.7819	.3503	91.03	92.66	.8105	.4939
85.70	93.87	.7695	.3663	92.86	93.93	.7988	.5671
87.11	94.82	.7653	.3948	96.55	96.47	.8120	.4206
88.50	95.72	.7846	.2973				
89.92	96.63	.8030	.2595				
91.35	97.57	.8081	.2056				
94.24	99.40	.7976	.3723				
95.65	100.24	.7876	.2771				
97.03	101.02	.8095	.4364				

Table VIII (contd)
Heat transfer data for each run code

RUN CODE 34145

SUCTION SURFACE				PRESSURE SURFACE			
% Surface Distance	% Axial Chord	Tw/Tg	h/ho	% Surface Distance	% Axial Chord	Tw/Tg	h/ho
30.57	49.25	.7197	.1828	28.90	34.95	.7239	.4581
31.98	50.84	.7211	.3645	30.78	37.26	.7154	.4102
33.40	52.37	.7158	.4176	32.58	39.43	.7108	.3494
37.60	56.50	.7065	.4442	34.38	41.55	.7116	.3268
39.08	57.92	.7009	.4213	36.29	43.76	.7139	.2962
41.80	60.34	.6984	.3988	41.70	49.81	.7250	.2638
43.25	61.62	.6984	.3934	45.37	53.70	.7325	.2546
44.57	62.74	.7038	.3797	47.14	55.56	.7345	.2663
46.03	63.96	.7076	.3742	49.03	57.47	.7340	.2782
47.51	65.26	.7167	.4131	50.84	59.28	.7368	.2901
48.95	66.44	.7220	.3921	52.68	61.08	.7430	.3108
50.31	67.53	.7265	.3708	54.48	62.81	.7465	.3260
51.78	68.75	.7297	.3311	56.34	64.57	.7525	.3428
53.14	69.77	.7341	.3505	58.12	66.24	.7526	.3696
54.62	71.01	.7432	.4114	59.97	67.92	.7517	.4181
55.97	71.99	.7456	.3612	61.77	69.55	.7555	.4217
57.36	73.07	.7461	.3386	63.63	71.18	.7610	.3358
60.29	75.38	.7472	.3627	65.41	72.73	.7684	.3420
61.67	76.42	.7460	.3560	67.30	74.37	.7705	.3156
67.29	80.63	.7559	.4070	69.07	75.85	.7684	.3573
70.13	82.74	.7571	.4252	70.91	77.38	.7603	.4408
71.51	83.72	.7652	.3909	72.72	78.84	.7612	.4929
73.03	84.92	.7723	.3889	74.63	80.37	.7750	.4121
74.39	85.88	.7734	.3500	76.40	81.77	.7832	.3274
75.74	86.80	.7717	.3668	78.27	83.24	.7881	.3095
77.24	87.96	.7618	.4179	81.91	86.03	.7709	.4600
78.62	88.92	.7631	.4398	85.55	88.71	.7895	.3084
81.54	91.06	.7830	.3093	87.39	90.05	.8053	.2711
82.88	91.94	.7868	.3229	89.25	91.42	.8126	.3537
84.34	92.98	.7829	.3450	91.03	92.66	.8125	.5197
85.70	93.87	.7704	.3584	92.86	93.93	.8004	.5850
87.11	94.82	.7663	.3919	95.55	96.47	.8135	.4290
88.50	95.72	.7857	.2907				
89.92	96.63	.8039	.2478				
91.35	97.57	.8092	.1977				
94.24	99.40	.7984	.3645				
95.65	100.24	.7884	.2704				
97.03	101.02	.8108	.4433				

Table VIII (contd)
Heat transfer data for each run code

RUN CODE 34155

SUCTION SURFACE				PRESSURE SURFACE			
% Surface Distance	% Axial Chord	Tw/Tg	h/ho	% Surface Distance	% Axial Chord	Tw/Tg	h/ho
30.57	49.25	.7282	.2051	28.90	34.95	.7338	.5063
31.98	50.84	.7297	.3927	30.78	37.26	.7253	.4492
33.40	52.37	.7248	.4493	32.58	39.43	.7206	.3834
37.60	56.50	.7154	.4770	34.38	41.55	.7212	.3558
39.08	57.92	.7096	.4517	36.29	43.76	.7236	.3245
41.80	60.34	.7067	.4264	41.70	49.81	.7348	.2884
43.25	61.62	.7068	.4221	45.37	53.70	.7426	.2810
44.57	62.74	.7121	.4085	47.14	55.56	.7445	.2922
46.03	63.96	.7160	.4015	49.03	57.47	.7442	.3077
47.51	65.26	.7249	.4378	50.84	59.28	.7473	.3254
48.95	66.44	.7303	.4205	52.68	61.08	.7535	.3432
50.31	67.53	.7346	.3928	54.48	62.81	.7572	.3604
51.78	68.75	.7379	.3507	56.34	64.57	.7633	.3805
53.14	69.77	.7425	.3727	58.12	66.24	.7634	.4067
54.62	71.01	.7519	.4395	59.97	67.92	.7624	.4629
55.97	71.99	.7544	.3839	61.77	69.55	.7667	.4701
57.36	73.07	.7548	.3594	63.63	71.18	.7722	.3762
60.29	75.38	.7561	.3859	65.41	72.73	.7796	.3827
61.67	76.42	.7545	.3772	67.30	74.37	.7814	.3505
67.29	80.63	.7648	.4286	69.07	75.85	.7793	.3955
70.13	82.74	.7662	.4504	70.91	77.38	.7709	.4882
71.51	83.72	.7745	.4156	72.72	78.84	.7719	.5467
73.03	84.92	.7817	.4105	74.63	80.37	.7858	.4586
74.39	85.88	.7827	.3639	76.40	81.77	.7939	.3654
75.74	86.80	.7805	.3807	78.27	83.24	.7987	.3454
77.24	87.96	.7707	.4365	81.91	86.03	.7811	.5081
78.62	88.92	.7719	.4611	85.55	88.71	.7992	.3393
81.54	91.06	.7924	.3225	87.39	90.05	.8152	.3006
82.88	91.94	.7961	.3358	89.25	91.42	.8225	.3876
84.34	92.98	.7921	.3595	91.03	92.66	.8223	.5702
85.70	93.87	.7793	.3785	92.86	93.93	.8100	.6431
87.11	94.82	.7751	.4185	96.55	96.47	.8227	.4743
88.50	95.72	.7947	.3052				
89.92	96.63	.8132	.2586				
91.35	97.57	.8185	.2043				
94.24	99.40	.8074	.3873				
95.65	100.24	.7970	.2923				
97.03	101.02	.8192	.4510				

Table VIII (contd)
Heat transfer data for each run code

RUN CODE 34303

SUCTION SURFACE				PRESSURE SURFACE			
% Surface Distance	% Axial Chord	Tw/Tg	h/ho	% Surface Distance	% Axial Chord	Tw/Tg	h/ho
30.57	49.25	.7843	.6409	28.90	34.95	.7639	.5280
31.98	50.84	.7847	.7629	30.78	37.26	.7540	.4925
33.40	52.37	.7796	.7709	32.58	39.43	.7489	.4229
37.60	56.50	.7649	.7059	34.38	41.55	.7504	.4051
39.08	57.92	.7580	.6601	36.29	43.76	.7534	.3717
41.80	60.34	.7525	.6082	41.70	49.81	.7669	.3364
43.25	61.62	.7518	.5973	45.37	53.70	.7763	.3369
44.57	62.74	.7572	.5813	47.14	55.56	.7785	.3518
46.03	63.96	.7609	.5755	49.03	57.47	.7780	.3700
47.51	65.26	.7696	.6220	50.84	59.28	.7810	.3894
48.95	66.44	.7746	.5862	52.68	61.08	.7875	.4098
50.31	67.53	.7796	.5669	54.48	62.81	.7916	.4337
51.78	68.75	.7822	.5073	56.34	64.57	.7983	.4615
53.14	69.77	.7868	.5342	58.12	66.24	.7981	.4903
54.62	71.01	.7960	.6215	59.97	67.92	.7966	.5580
55.97	71.99	.7985	.5486	61.77	69.55	.8011	.5670
57.36	73.07	.7980	.5163	63.63	71.18	.8070	.4541
60.29	75.38	.7991	.5494	65.41	72.73	.8147	.4695
61.67	76.42	.7966	.5356	67.30	74.37	.8163	.4229
67.29	80.63	.8051	.5829	69.07	75.85	.8133	.4679
70.13	82.74	.8058	.6102	70.91	77.38	.8038	.5723
71.51	83.72	.8138	.5644	72.72	78.84	.8041	.6384
73.03	84.92	.8211	.5756	74.63	80.37	.8185	.5324
74.39	85.88	.8215	.5049	76.40	81.77	.8273	.4270
75.74	86.80	.8189	.5210	78.27	83.24	.8323	.4018
77.24	87.96	.8082	.5885	81.91	86.03	.8135	.5967
78.62	88.92	.8091	.6195	85.55	88.71	.8314	.3784
81.54	91.06	.8293	.4491	87.39	90.05	.8484	.3494
82.88	91.94	.8328	.4668	89.25	91.42	.8557	.4704
84.34	92.98	.8287	.4971	91.03	92.66	.8550	.6866
85.70	93.87	.8151	.5053	92.86	93.93	.8417	.7506
87.11	94.82	.8104	.5473	96.55	96.47	.8551	.5348
88.50	95.72	.8301	.4236				
89.92	96.63	.8491	.3807				
91.35	97.57	.8539	.3066				
94.24	99.40	.8417	.5212				
95.65	100.24	.8311	.3913				
97.03	101.02	.8542	.6537				

Table VIII (contd)
Heat transfer data for each run code

RUN CODE 34304

SUCTION SURFACE				PRESSURE SURFACE			
% Surface Distance	% Axial Chord	Tw/Tg	h/ho	% Surface Distance	% Axial Chord	Tw/Tg	h/ho
30.57	49.25	.7846	.6017	28.90	34.95	.7704	.5978
31.98	50.84	.7849	.7455	30.78	37.26	.7604	.5527
33.40	52.37	.7796	.7670	32.58	39.43	.7548	.4718
37.60	56.50	.7649	.7155	34.38	41.55	.7556	.4450
39.08	57.92	.7578	.6669	36.29	43.76	.7578	.4029
41.80	60.34	.7520	.6118	41.70	49.81	.7692	.3543
43.25	61.62	.7512	.5982	45.37	53.70	.7770	.3434
44.57	62.74	.7567	.5814	47.14	55.56	.7786	.3544
46.03	63.96	.7604	.5760	49.03	57.47	.7775	.3700
47.51	65.26	.7692	.6237	50.84	59.28	.7800	.3878
48.95	66.44	.7743	.5863	52.68	61.08	.7860	.4058
50.31	67.53	.7792	.5665	54.48	62.81	.7897	.4251
51.78	68.75	.7819	.5076	56.34	64.57	.7958	.4483
53.14	69.77	.7864	.5336	58.12	66.24	.7954	.4767
54.62	71.01	.7955	.6190	59.97	67.92	.7934	.5382
55.97	71.99	.7982	.5480	61.77	69.55	.7975	.5427
57.36	73.07	.7975	.5162	63.63	71.18	.8032	.4314
60.29	75.38	.7983	.5479	65.41	72.73	.8109	.4437
61.67	76.42	.7956	.5345	67.30	74.37	.8126	.4032
67.29	80.63	.8035	.5836	69.07	75.85	.8096	.4477
70.13	82.74	.8039	.6107	70.91	77.38	.8000	.5470
71.51	83.72	.8119	.5699	72.72	78.84	.8001	.6090
73.03	84.92	.8187	.5724	74.63	80.37	.8144	.5045
74.39	85.88	.8190	.5044	76.40	81.77	.8232	.4020
75.74	86.80	.8165	.5220	78.27	83.24	.8283	.3820
77.24	87.96	.8057	.5879	81.91	86.03	.8094	.5679
78.62	88.92	.8064	.6164	85.55	88.71	.8274	.3539
81.54	91.06	.8262	.4483	87.39	90.05	.8439	.3115
82.88	91.94	.8299	.4706	89.25	91.42	.8510	.4112
84.34	92.98	.8256	.4957	91.03	92.66	.8506	.6356
85.70	93.87	.8119	.4983	92.86	93.93	.8378	.7105
87.11	94.82	.8075	.5450	96.55	96.47	.8510	.4827
88.50	95.72	.8271	.4298				
89.92	96.63	.8461	.3946				
91.35	97.57	.8506	.3159				
94.24	99.40	.8389	.5279				
95.65	100.24	.8285	.4017				
97.03	101.02	.8512	.6588				

Table VIII (contd)
Heat transfer data for each run code

RUN CODE 34305

SUCTION SURFACE				PRESSURE SURFACE			
% Surface Distance	% Axial Chord	Tw/Tg	h/ho	% Surface Distance	% Axial Chord	Tw/Tg	h/ho
30.57	49.25	.7898	.5934	23.90	34.95	.7830	.7041
31.98	50.84	.7907	.7683	30.78	37.26	.7739	.6481
33.40	52.37	.7858	.7994	32.58	39.43	.7679	.5479
37.60	56.50	.7705	.7395	34.38	41.55	.7682	.5105
39.08	57.92	.7633	.6885	36.29	43.76	.7702	.4653
41.80	60.34	.7575	.6331	41.70	49.81	.7796	.3963
43.25	61.62	.7566	.6176	45.37	53.70	.7863	.3772
44.57	62.74	.7620	.5979	47.14	55.56	.7876	.3900
46.03	63.96	.7657	.5899	49.03	57.47	.7857	.4045
47.51	65.26	.7747	.6388	50.84	59.28	.7877	.4192
48.95	66.44	.7797	.6024	52.68	61.08	.7930	.4358
50.31	67.53	.7845	.5787	54.48	62.81	.7961	.4527
51.78	68.75	.7872	.5186	56.34	64.57	.8017	.4720
53.14	69.77	.7917	.5427	58.12	66.24	.8007	.4948
54.62	71.01	.8007	.6257	59.97	67.92	.7984	.5594
55.97	71.99	.8033	.5563	61.77	69.55	.8021	.5641
57.36	73.07	.8028	.5246	63.63	71.18	.8073	.4429
60.29	75.38	.8028	.5538	65.41	72.73	.8146	.4522
61.67	76.42	.8000	.5405	67.30	74.37	.8161	.4126
67.29	80.63	.8076	.5943	69.07	75.85	.8128	.4553
70.13	82.74	.8074	.6210	70.91	77.38	.8030	.5560
71.51	83.72	.8154	.5798	72.72	78.84	.8029	.6192
73.03	84.92	.8220	.5741	74.63	80.37	.8168	.5051
74.39	85.88	.8224	.5126	76.40	81.77	.8252	.3943
75.74	86.80	.8198	.5326	78.27	83.24	.8302	.3728
77.24	87.96	.8089	.5996	81.91	86.03	.8115	.5724
78.62	88.92	.8095	.6291	85.55	88.71	.8292	.3557
81.54	91.06	.8290	.4621	87.39	90.05	.8458	.3163
82.88	91.94	.8325	.4814	89.25	91.42	.8529	.4215
84.34	92.98	.8281	.5050	91.03	92.66	.8524	.6419
85.70	93.87	.8144	.5113	92.86	93.93	.8394	.7156
87.11	94.82	.8097	.5541	96.55	96.47	.8528	.4970
88.50	95.72	.8290	.4314				
89.92	96.63	.8478	.3920				
91.35	97.57	.8523	.3155				
94.24	99.40	.8407	.5368				
95.65	100.24	.8301	.4054				
97.03	101.02	.8528	.6603				

Table VIII (contd)
Heat transfer data for each run code

RUN CODE 43000

SUCTION SURFACE				PRESSURE SURFACE			
% Surface Distance	% Axial Chord	Tw/Tg	h/ho	% Surface Distance	% Axial Chord	Tw/Tg	h/ho
30.57	49.25	.7640	.9274	28.90	34.95	.7254	.5290
31.98	50.84	.7569	.8538	30.78	37.26	.7108	.4655
33.40	52.37	.7487	.8052	32.58	39.43	.7030	.3824
37.60	56.50	.7283	.7036	34.38	41.55	.7034	.3515
39.08	57.92	.7189	.6447	36.29	43.76	.7071	.3342
41.80	60.34	.7111	.5684	41.70	49.81	.7214	.3018
43.25	61.62	.7104	.5637	45.37	53.70	.7316	.3102
44.57	62.74	.7170	.5521	47.14	55.56	.7332	.3200
46.03	63.96	.7211	.5531	49.03	57.47	.7317	.3220
47.51	65.26	.7317	.6111	50.84	59.28	.7331	.3215
48.95	66.44	.7368	.5562	52.68	61.08	.7405	.3551
50.31	67.53	.7431	.5539	54.48	62.81	.7445	.3763
51.78	68.75	.7443	.4815	56.34	64.57	.7519	.3973
53.14	69.77	.7490	.5151	58.12	66.24	.7517	.4328
54.62	71.01	.7603	.6236	59.97	67.92	.7497	.4887
55.97	71.99	.7625	.5468	61.77	69.55	.7537	.4922
57.36	73.07	.7614	.5090	63.63	71.18	.7610	.3981
60.29	75.38	.7607	.5385	65.41	72.73	.7707	.4362
61.67	76.42	.7579	.5287	67.30	74.37	.7724	.3941
67.29	80.63	.7636	.5447	69.07	75.85	.7670	.4059
70.13	82.74	.7640	.5877	70.91	77.38	.7552	.4776
71.51	83.72	.7720	.5341	72.72	78.84	.7551	.5367
73.03	84.92	.7793	.5316	74.63	80.37	.7721	.4535
74.39	85.88	.7793	.4720	76.40	81.77	.7827	.3735
75.74	86.80	.7750	.4706	78.27	83.24	.7889	.3620
77.24	87.96	.7614	.5086	81.91	86.03	.7651	.5194
78.62	88.92	.7617	.5295	85.55	88.71	.7905	.3594
81.54	91.06	.7866	.4284	87.39	90.05	.8121	.3498
82.88	91.94	.7914	.4634	89.25	91.42	.8218	.4754
84.34	92.98	.7846	.4507	91.03	92.66	.8214	.7323
85.70	93.87	.7671	.4278	92.86	93.93	.8039	.7201
87.11	94.82	.7623	.4765	96.55	96.47	.8209	.5340
88.50	95.72	.7880	.3856				
89.92	96.63	.8124	.3640				
91.35	97.57	.8188	.2977				
94.24	99.40	.8035	.4777				
95.65	100.24	.7906	.3490				
97.03	101.02	.8192	.6200				

Table VIII (contd)
Heat transfer data for each run code

RUN CODE 43103

SUCTION SURFACE				PRESSURE SURFACE			
% Surface Distance	% Axial Chord	Tw/Tg	h/ho	% Surface Distance	% Axial Chord	Tw/Tg	h/ho
30.57	49.25	.6914	.1357	28.90	34.95	.6988	.4430
31.98	50.84	.6903	.2987	30.78	37.26	.6871	.3679
33.40	52.37	.6855	.3645	32.58	39.43	.6809	.3016
37.60	56.50	.6729	.3808	34.38	41.55	.6819	.2848
39.08	57.92	.6675	.3653	36.29	43.76	.6854	.2689
41.80	60.34	.6647	.3448	41.70	49.81	.7004	.2592
43.25	61.62	.6653	.3489	45.37	53.70	.7105	.2647
44.57	62.74	.6710	.3363	47.14	55.56	.7137	.2871
46.03	63.96	.6752	.3305	49.03	57.47	.7141	.2962
47.51	65.26	.6859	.3756	50.84	59.28	.7169	.2978
48.95	66.44	.6919	.3542	52.68	61.08	.7247	.3327
50.31	67.53	.6974	.3398	54.48	62.81	.7292	.3613
51.78	68.75	.7005	.2998	56.34	64.57	.7367	.3875
53.14	69.77	.7054	.3135	58.12	66.24	.7371	.4099
54.62	71.01	.7149	.3647	59.97	67.92	.7365	.4532
55.97	71.99	.7180	.3259	61.77	69.55	.7408	.4611
57.36	73.07	.7191	.3103	63.63	71.18	.7477	.3978
60.29	75.38	.7206	.3340	65.41	72.73	.7556	.4135
61.67	76.42	.7192	.3245	67.30	74.37	.7572	.3826
67.29	80.63	.7306	.3524	69.07	75.85	.7535	.4079
70.13	82.74	.7335	.3865	70.91	77.38	.7440	.4802
71.51	83.72	.7426	.3529	72.72	78.84	.7449	.5359
73.03	84.92	.7501	.3379	74.63	80.37	.7601	.4614
74.39	85.88	.7512	.3001	76.40	81.77	.7684	.3723
75.74	86.80	.7486	.3140	78.27	83.24	.7742	.3617
77.24	87.96	.7381	.3649	81.91	86.03	.7552	.4974
78.62	88.92	.7396	.3907	85.55	88.71	.7766	.3674
81.54	91.06	.7631	.2752	87.39	90.05	.7944	.3467
82.88	91.94	.7678	.2953	89.25	91.42	.8019	.4132
84.34	92.98	.7630	.2992	91.03	92.66	.8026	.7078
85.70	93.87	.7484	.2958	92.85	93.93	.7860	.6670
87.11	94.82	.7445	.3390	96.55	96.47	.8004	.5101
88.50	95.72	.7672	.2436				
89.92	96.63	.7880	.2061				
91.35	97.57	.7945	.1659				
94.24	99.40	.7808	.3437				
95.65	100.24	.7691	.2588				
97.03	101.02	.7946	.4185				

Table VIII (contd)
Heat transfer data for each run code

RUN CODE 43104

SUCTION SURFACE				PRESSURE SURFACE			
% Surface Distance	% Axial Chord	Tw/Tg	h/ho	% Surface Distance	% Axial Chord	Tw/Tg	h/ho
30.57	49.25	.6961	.2741	28.90	34.95	.6864	.4069
31.98	50.84	.6903	.3515	30.78	37.26	.6739	.3440
33.40	52.37	.6845	.3987	32.58	39.43	.6682	.2887
37.60	56.50	.6710	.4187	34.38	41.55	.6693	.2715
39.08	57.92	.6637	.3900	36.29	43.76	.6731	.2620
41.80	60.34	.6598	.3533	41.70	49.81	.6868	.2428
43.25	61.62	.6600	.3542	45.37	53.70	.6956	.2422
44.57	62.74	.6659	.3454	47.14	55.56	.6975	.2517
46.03	63.96	.6700	.3450	49.03	57.47	.6970	.2561
47.51	65.26	.6802	.3868	50.84	59.28	.6992	.2591
48.95	66.44	.6852	.3476	52.68	61.08	.7064	.2884
50.31	67.53	.6913	.3476	54.48	62.81	.7101	.3066
51.78	68.75	.6932	.3015	56.34	64.57	.7171	.3234
53.14	69.77	.6981	.3239	58.12	66.24	.7173	.3501
54.62	71.01	.7084	.3945	59.97	67.92	.7164	.3946
55.97	71.99	.7109	.3423	61.77	69.55	.7206	.3979
57.36	73.07	.7108	.3183	63.63	71.18	.7271	.3236
60.29	75.38	.7120	.3449	65.41	72.73	.7359	.3538
61.67	76.42	.7105	.3397	67.30	74.37	.7377	.3207
67.29	80.63	.7198	.3677	69.07	75.85	.7336	.3333
70.13	82.74	.7220	.4017	70.91	77.38	.7236	.3890
71.51	83.72	.7304	.3656	72.72	78.84	.7242	.4339
73.03	84.92	.7378	.3596	74.63	80.37	.7400	.3735
74.39	85.88	.7386	.3216	76.40	81.77	.7495	.3095
75.74	86.80	.7354	.3216	78.27	83.24	.7556	.3024
77.24	87.96	.7237	.3509	81.91	86.03	.7357	.4273
78.62	88.92	.7248	.3678	85.55	88.71	.7594	.3043
81.54	91.06	.7490	.2919	87.39	90.05	.7792	.2946
82.88	91.94	.7540	.3197	89.25	91.42	.7882	.3746
84.34	92.98	.7483	.3093	91.03	92.66	.7888	.5785
85.70	93.87	.7329	.2901	92.86	93.93	.7741	.5735
87.11	94.82	.7294	.3331	96.55	96.47	.7895	.4368
88.50	95.72	.7539	.2628				
89.92	96.63	.7759	.2338				
91.35	97.57	.7830	.1896				
94.24	99.40	.7705	.3242				
95.65	100.24	.7599	.2321				
97.03	101.02	.7860	.4288				

Table VIII (contd)
Heat transfer data for each run code

RUN CODE 43105

SUCTION SURFACE				PRESSURE SURFACE			
% Surface Distance	% Axial Chord	Tw/Tg	h/ho	% Surface Distance	% Axial Chord	Tw/Tg	h/ho
30.57	49.25	.6976	.2465	28.90	34.95	.6926	.4404
31.98	50.84	.6924	.3428	30.78	37.26	.6807	.3744
33.40	52.37	.6868	.3984	32.58	39.43	.6750	.3166
37.60	56.50	.6729	.4217	34.38	41.55	.6759	.2970
39.08	57.92	.6651	.3907	36.29	43.76	.6794	.2860
41.80	60.34	.6599	.3497	41.70	49.81	.6910	.2551
43.25	61.62	.6589	.3397	45.37	53.70	.6983	.2464
44.57	62.74	.6635	.3207	47.14	55.56	.6998	.2573
46.03	63.96	.6673	.3150	49.03	57.47	.6988	.2612
47.51	65.26	.6788	.3692	50.84	59.28	.7005	.2622
48.95	66.44	.6853	.3504	52.68	61.08	.7070	.2898
50.31	67.53	.6919	.3482	54.48	62.81	.7101	.3047
51.78	68.75	.6938	.3003	56.34	64.57	.7163	.3178
53.14	69.77	.6985	.3201	58.12	66.24	.7162	.3422
54.62	71.01	.7084	.3871	59.97	67.92	.7148	.3828
55.97	71.99	.7108	.3329	61.77	69.55	.7183	.3840
57.36	73.07	.7103	.3076	63.63	71.18	.7245	.3115
60.29	75.38	.7112	.3353	65.41	72.73	.7329	.3377
61.67	76.42	.7097	.3315	67.30	74.37	.7345	.3069
67.29	80.63	.7185	.3596	69.07	75.85	.7302	.3170
70.13	82.74	.7204	.3945	70.91	77.38	.7203	.3698
71.51	83.72	.7283	.3575	72.72	78.84	.7208	.4151
73.03	84.92	.7354	.3505	74.63	80.37	.7362	.3567
74.39	85.88	.7362	.3151	76.40	81.77	.7452	.2902
75.74	86.80	.7329	.3159	78.27	83.24	.7510	.2821
77.24	87.96	.7214	.3440	81.91	86.03	.7311	.4000
78.62	88.92	.7223	.3596	85.55	88.71	.7541	.2799
81.54	91.06	.7454	.2849	87.39	90.05	.7734	.2668
82.88	91.94	.7504	.3139	89.25	91.42	.7823	.3476
84.34	92.98	.7447	.3031	91.03	92.66	.7829	.5366
85.70	93.87	.7297	.2883	92.85	93.93	.7685	.5308
87.11	94.82	.7262	.3284	96.55	96.47	.7836	.4023
88.50	95.72	.7498	.2604				
89.92	96.63	.7713	.2321				
91.35	97.57	.7778	.1852				
94.24	99.40	.7662	.3207				
95.65	100.24	.7557	.2313				
97.03	101.02	.7807	.4108				

Table VIII (contd)
Heat transfer data for each run code

RUN CODE 43135

SUCTION SURFACE				PRESSURE SURFACE			
% Surface Distance	% Axial Chord	Tw/Tg	h/ho	% Surface Distance	% Axial Chord	Tw/Tg	h/ho
30.57	49.25	.6853	.2217	28.90	34.95	.6810	.3964
31.98	50.84	.6805	.3046	30.78	37.26	.6702	.3369
33.40	52.37	.6758	.3571	32.58	39.43	.6652	.2847
37.60	56.50	.6637	.3844	34.38	41.55	.6664	.2678
39.08	57.92	.6568	.3580	36.29	43.76	.6698	.2545
41.80	60.34	.6528	.3229	41.70	49.81	.6818	.2291
43.25	61.62	.6526	.3172	45.37	53.70	.6895	.2245
44.57	62.74	.6582	.3078	47.14	55.56	.6911	.2322
46.03	63.96	.6628	.3106	49.03	57.47	.6904	.2349
47.51	65.26	.6735	.3576	50.84	59.28	.6923	.2363
48.95	66.44	.6789	.3280	52.68	61.08	.6989	.2622
50.31	67.53	.6847	.3231	54.48	62.81	.7022	.2772
51.78	68.75	.6864	.2772	56.34	64.57	.7085	.2910
53.14	69.77	.6910	.2963	58.12	66.24	.7086	.3146
54.62	71.01	.7009	.3612	59.97	67.92	.7074	.3527
55.97	71.99	.7034	.3131	61.77	69.55	.7111	.3544
57.36	73.07	.7033	.2909	63.63	71.18	.7173	.2881
60.29	75.38	.7046	.3160	65.41	72.73	.7256	.3134
61.67	76.42	.7032	.3120	67.30	74.37	.7272	.2813
67.29	80.63	.7122	.3414	69.07	75.85	.7233	.2913
70.13	82.74	.7142	.3717	70.91	77.38	.7138	.3427
71.51	83.72	.7219	.3368	72.72	78.84	.7146	.3858
73.03	84.92	.7288	.3299	74.63	80.37	.7297	.3299
74.39	85.88	.7295	.2957	76.40	81.77	.7387	.2682
75.74	86.80	.7267	.2992	78.27	83.24	.7444	.2614
77.24	87.96	.7158	.3282	81.91	86.03	.7258	.3744
78.62	88.92	.7169	.3434	85.55	88.71	.7484	.2579
81.54	91.06	.7396	.2733	87.39	90.05	.7672	.2440
82.88	91.94	.7443	.2966	89.25	91.42	.7761	.3178
84.34	92.98	.7388	.2847	91.03	92.66	.7771	.5005
85.70	93.87	.7247	.2736	92.86	93.93	.7635	.4923
87.11	94.82	.7217	.3123	96.55	96.47	.7782	.3695
88.50	95.72	.7446	.2475				
89.92	96.63	.7657	.2240				
91.35	97.57	.7722	.1787				
94.24	99.40	.7613	.3006				
95.65	100.24	.7517	.2174				
97.03	101.02	.7759	.3936				

Table VIII (contd)
Heat transfer data for each run code

RUN CODE 43145

SUCTION SURFACE				PRESSURE SURFACE			
% Surface Distance	% Axial Chord	Tw/Tg	h/ho	% Surface Distance	% Axial Chord	Tw/Tg	h/ho
30.57	49.25	.6893	.2345	28.90	34.95	.6857	.4178
31.98	50.84	.6842	.3171	30.78	37.26	.6744	.3534
33.40	52.37	.6793	.3698	32.58	39.43	.6688	.2953
37.60	56.50	.6665	.3935	34.38	41.55	.6695	.2747
39.08	57.92	.6594	.3664	36.29	43.76	.6728	.2609
41.80	60.34	.6552	.3299	41.70	49.81	.6848	.2365
43.25	61.62	.6549	.3245	45.37	53.70	.6926	.2326
44.57	62.74	.6605	.3145	47.14	55.56	.6941	.2397
46.03	63.96	.6650	.3172	49.03	57.47	.6934	.2434
47.51	65.26	.6758	.3660	50.84	59.28	.6955	.2465
48.95	66.44	.6811	.3326	52.68	61.08	.7022	.2730
50.31	67.53	.6869	.3279	54.48	62.81	.7054	.2887
51.78	68.75	.6886	.2815	56.34	64.57	.7120	.3034
53.14	69.77	.6933	.3020	58.12	66.24	.7122	.3287
54.62	71.01	.7033	.3693	59.97	67.92	.7110	.3684
55.97	71.99	.7057	.3172	61.77	69.55	.7148	.3701
57.36	73.07	.7054	.2934	63.63	71.18	.7210	.3008
60.29	75.38	.7068	.3213	65.41	72.73	.7293	.3266
61.67	76.42	.7054	.3174	67.30	74.37	.7309	.2943
67.29	80.63	.7143	.3424	69.07	75.85	.7269	.3052
70.13	82.74	.7163	.3748	70.91	77.38	.7174	.3585
71.51	83.72	.7243	.3399	72.72	78.84	.7182	.4027
73.03	84.92	.7313	.3325	74.63	80.37	.7332	.3442
74.39	85.88	.7322	.2983	76.40	81.77	.7421	.2803
75.74	86.80	.7293	.3016	78.27	83.24	.7480	.2746
77.24	87.96	.7183	.3312	81.91	86.03	.7293	.3914
78.62	88.92	.7193	.3465	85.55	88.71	.7517	.2729
81.54	91.06	.7420	.2701	87.39	90.05	.7707	.2626
82.88	91.94	.7470	.2978	89.25	91.42	.7795	.3349
84.34	92.98	.7417	.2882	91.03	92.66	.7804	.5246
85.70	93.87	.7271	.2726	92.86	93.93	.7665	.5138
87.11	94.82	.7240	.3150	96.55	96.47	.7809	.3805
88.50	95.72	.7470	.2450				
89.92	96.63	.7680	.2163				
91.35	97.57	.7747	.1721				
94.24	99.40	.7638	.3041				
95.65	100.24	.7540	.2229				
97.03	101.02	.7782	.3945				

Table VIII (contd)
Heat transfer data for each run code

RUN CODE 43155

SUCTION SURFACE				PRESSURE SURFACE			
% Surface Distance	% Axial Chord	Tw/Tg	h/ho	% Surface Distance	% Axial Chord	Tw/Tg	h/ho
30.57	49.25	.6906	.2097	28.90	34.95	.6905	.4331
31.98	50.84	.6860	.3049	30.78	37.26	.6793	.3640
33.40	52.37	.6812	.3626	32.58	39.43	.6737	.3034
37.60	56.50	.6691	.3943	34.38	41.55	.6746	.2824
39.08	57.92	.6620	.3668	36.29	43.76	.6779	.2692
41.80	60.34	.6578	.3322	41.70	49.81	.6904	.2458
43.25	61.62	.6571	.3229	45.37	53.70	.6984	.2423
44.57	62.74	.6619	.3050	47.14	55.56	.7002	.2515
46.03	63.96	.6658	.2994	49.03	57.47	.6996	.2561
47.51	65.26	.6770	.3508	50.84	59.28	.7017	.2593
48.95	66.44	.6834	.3305	52.68	61.08	.7086	.2874
50.31	67.53	.6900	.3300	54.48	62.81	.7119	.3046
51.78	68.75	.6921	.2850	56.34	64.57	.7185	.3205
53.14	69.77	.6968	.3048	58.12	66.24	.7188	.3460
54.62	71.01	.7067	.3700	59.97	67.92	.7178	.3882
55.97	71.99	.7090	.3164	61.77	69.55	.7218	.3904
57.36	73.07	.7088	.2911	63.63	71.18	.7279	.3179
60.29	75.38	.7100	.3181	65.41	72.73	.7363	.3476
61.67	76.42	.7090	.3146	67.30	74.37	.7379	.3140
67.29	80.63	.7185	.3412	69.07	75.85	.7340	.3260
70.13	82.74	.7209	.3754	70.91	77.38	.7247	.3818
71.51	83.72	.7289	.3368	72.72	78.84	.7255	.4274
73.03	84.92	.7361	.3294	74.63	80.37	.7404	.3675
74.39	85.88	.7371	.2960	76.40	81.77	.7493	.3021
75.74	86.80	.7342	.2986	78.27	83.24	.7551	.2957
77.24	87.96	.7233	.3289	81.91	86.03	.7363	.4160
78.62	88.92	.7245	.3456	85.55	88.71	.7586	.2961
81.54	91.06	.7475	.2681	87.39	90.05	.7773	.2832
82.88	91.94	.7523	.2931	89.25	91.42	.7859	.3549
84.34	92.98	.7469	.2825	91.03	92.66	.7867	.5480
85.70	93.87	.7323	.2690	92.86	93.93	.7729	.5428
87.11	94.82	.7293	.3147	96.55	96.47	.7866	.3967
88.50	95.72	.7524	.2408				
89.92	96.63	.7734	.2092				
91.35	97.57	.7800	.1638				
94.24	99.40	.7693	.3043				
95.65	100.24	.7594	.2241				
97.03	101.02	.7832	.3891				

Table VIII (contd)
Heat transfer data for each run code

RUN CODE 43303

SUCTION SURFACE				PRESSURE SURFACE			
% Surface Distance	% Axial Chord	Tw/Tg	h/ho	% Surface Distance	% Axial Chord	Tw/Tg	h/ho
30.57	49.25	.7372	.6522	28.90	34.95	.7022	.4326
31.98	50.84	.7306	.6485	30.78	37.26	.6881	.3828
33.40	52.37	.7229	.6401	32.58	39.43	.6815	.3214
37.60	56.50	.7033	.5798	34.38	41.55	.6827	.3021
39.08	57.92	.6941	.5340	36.29	43.76	.6871	.2929
41.80	60.34	.6877	.4783	41.70	49.81	.7026	.2742
43.25	61.62	.6870	.4748	45.37	53.70	.7128	.2801
44.57	62.74	.6928	.4626	47.14	55.56	.7148	.2919
46.03	63.96	.6967	.4604	49.03	57.47	.7138	.2972
47.51	65.26	.7070	.5085	50.84	59.28	.7159	.3002
48.95	66.44	.7122	.4623	52.68	61.08	.7235	.3317
50.31	67.53	.7185	.4625	54.48	62.81	.7277	.3527
51.78	68.75	.7201	.4025	56.34	64.57	.7352	.3741
53.14	69.77	.7249	.4317	58.12	66.24	.7355	.4084
54.62	71.01	.7360	.5240	59.97	67.92	.7341	.4630
55.97	71.99	.7384	.4578	61.77	69.55	.7384	.4678
57.36	73.07	.7375	.4264	63.63	71.18	.7454	.3792
60.29	75.38	.7378	.4561	65.41	72.73	.7549	.4144
61.67	76.42	.7354	.4482	67.30	74.37	.7566	.3781
67.29	80.63	.7428	.4711	69.07	75.85	.7513	.3851
70.13	82.74	.7437	.5080	70.91	77.38	.7393	.4467
71.51	83.72	.7526	.4686	72.72	78.84	.7397	.5026
73.03	84.92	.7601	.4616	74.53	80.37	.7569	.4337
74.39	85.88	.7603	.4098	76.40	81.77	.7673	.3583
75.74	86.80	.7562	.4067	78.27	83.24	.7732	.3444
77.24	87.96	.7429	.4413	81.91	86.03	.7503	.4938
78.62	88.92	.7436	.4628	85.55	88.71	.7753	.3435
81.54	91.06	.7689	.3728	87.39	90.05	.7969	.3370
82.88	91.94	.7738	.4053	89.25	91.42	.8066	.4488
84.34	92.98	.7671	.3915	91.03	92.66	.8066	.6986
85.70	93.87	.7499	.3709	92.86	93.93	.7889	.6655
87.11	94.82	.7452	.4157	96.55	96.47	.8060	.5083
88.50	95.72	.7713	.3352				
89.92	96.63	.7955	.3104				
91.35	97.57	.8023	.2538				
94.24	99.40	.7872	.4112				
95.65	100.24	.7745	.2889				
97.03	101.02	.8033	.5440				

Table VIII (contd)
Heat transfer data for each run code

RUN CODE 43304

SUCTION SURFACE				PRESSURE SURFACE			
% Surface Distance	% Axial Chord	T _w /T _g	h/h _o	% Surface Distance	% Axial Chord	T _w /T _g	h/h _o
30.57	49.25	.7380	.6154	28.90	34.95	.7099	.4799
31.98	50.84	.7312	.6246	30.78	37.26	.6959	.4208
33.40	52.37	.7237	.6261	32.58	39.43	.6888	.3505
37.60	56.50	.7045	.5767	34.38	41.55	.6895	.3265
39.08	57.92	.6954	.5310	36.29	43.76	.6932	.3126
41.80	60.34	.6889	.4743	41.70	49.81	.7068	.2848
43.25	61.62	.6883	.4720	45.37	53.70	.7157	.2838
44.57	62.74	.6940	.4582	47.14	55.56	.7173	.2943
46.03	63.96	.6977	.4541	49.03	57.47	.7159	.2990
47.51	65.26	.7081	.5037	50.84	59.28	.7177	.3015
48.95	66.44	.7133	.4577	52.68	61.08	.7248	.3315
50.31	67.53	.7196	.4571	54.48	62.81	.7285	.3505
51.78	68.75	.7211	.3967	56.34	64.57	.7357	.3695
53.14	69.77	.7259	.4266	58.12	66.24	.7357	.4017
54.62	71.01	.7370	.5204	59.97	67.92	.7341	.4545
55.97	71.99	.7393	.4524	61.77	69.55	.7381	.4580
57.36	73.07	.7383	.4194	63.63	71.18	.7448	.3691
60.29	75.38	.7382	.4482	65.41	72.73	.7540	.4036
61.67	76.42	.7359	.4412	67.30	74.37	.7555	.3633
67.29	80.63	.7431	.4661	69.07	75.85	.7503	.3715
70.13	82.74	.7438	.5018	70.91	77.38	.7385	.4885
71.51	83.72	.7523	.4604	72.72	78.84	.7388	.4205
73.03	84.92	.7599	.4617	74.63	80.37	.7558	.3460
74.39	85.88	.7600	.4066	76.40	81.77	.7659	.3334
75.74	86.80	.7559	.4035	78.27	83.24	.7719	.4788
77.24	87.96	.7427	.4360	81.91	86.03	.7493	.3299
78.62	88.92	.7431	.4548	85.55	88.71	.7739	.3223
81.54	91.06	.7681	.3689	87.39	90.05	.7952	.4335
82.88	91.94	.7728	.3976	89.25	91.42	.8048	.6621
84.34	92.98	.7663	.3869	91.03	92.66	.8047	.6511
85.70	93.87	.7494	.3671	92.86	93.93	.7879	
87.11	94.82	.7449	.4119	96.55	96.47	.8049	.4977
88.50	95.72	.7705	.3332				
89.92	96.63	.7942	.3069				
91.35	97.57	.8008	.2480				
94.24	99.40	.7862	.4069				
95.65	100.24	.7740	.2931				
97.03	101.02	.8022	.5309				

Table VIII (contd)
Heat transfer data for each run code

RUN CODE 43305

SUCTION SURFACE				PRESSURE SURFACE			
% Surface Distance	% Axial Chord	Tw/Tg	h/ho	% Surface Distance	% Axial Chord	Tw/Tg	h/ho
30.57	49.25	.7424	.6239	28.90	34.95	.7220	.5640
31.98	50.84	.7359	.6440	30.78	37.26	.7090	.4966
33.40	52.37	.7283	.6489	32.58	39.43	.7021	.4162
37.60	56.50	.7085	.5938	34.38	41.55	.7026	.3857
39.08	57.92	.6992	.5461	36.29	43.76	.7061	.3710
41.80	60.34	.6924	.4874	41.70	49.81	.7174	.3252
43.25	61.62	.6915	.4821	45.37	53.70	.7246	.3130
44.57	62.74	.6972	.4666	47.14	55.56	.7255	.3227
46.03	63.96	.7010	.4611	49.03	57.47	.7233	.3255
47.51	65.26	.7116	.5098	50.84	59.28	.7243	.3256
48.95	66.44	.7170	.4662	52.68	61.08	.7307	.3545
50.31	67.53	.7234	.4648	54.48	62.81	.7338	.3710
51.78	68.75	.7249	.4033	56.34	64.57	.7402	.3866
53.14	69.77	.7297	.4306	58.12	66.24	.7395	.4155
54.62	71.01	.7406	.5206	59.97	67.92	.7371	.4646
55.97	71.99	.7431	.4550	61.77	69.55	.7403	.4637
57.36	73.07	.7423	.4237	63.63	71.18	.7464	.3694
60.29	75.38	.7417	.4537	65.41	72.73	.7552	.4016
61.67	76.42	.7391	.4467	67.30	74.37	.7564	.3626
67.29	80.63	.7458	.4731	69.07	75.85	.7508	.3674
70.13	82.74	.7459	.5092	70.91	77.38	.7384	.4253
71.51	83.72	.7543	.4685	72.72	78.84	.7383	.4781
73.03	84.92	.7616	.4668	74.63	80.37	.7551	.4099
74.39	85.88	.7616	.4127	76.40	81.77	.7651	.3336
75.74	86.80	.7575	.4122	78.27	83.24	.7707	.3189
77.24	87.96	.7439	.4446	81.91	86.03	.7476	.4604
78.62	88.92	.7440	.4616	85.55	88.71	.7718	.3117
81.54	91.06	.7686	.3790	87.39	90.05	.7928	.2977
82.88	91.94	.7733	.4110	89.25	91.42	.8023	.4108
84.34	92.98	.7665	.3967	91.03	92.66	.8019	.6174
85.70	93.87	.7494	.3741	92.86	93.93	.7852	.6137
87.11	94.82	.7446	.4160	96.55	96.47	.8024	.4677
88.50	95.72	.7697	.3404				
89.92	96.63	.7933	.3188				
91.35	97.57	.7997	.2619				
94.24	99.40	.7851	.4176				
95.65	100.24	.7729	.3001				
97.03	101.02	.8008	.5417				

Table VIII (contd)
Heat transfer data for each run code

RUN CODE 44000

SUCTION SURFACE				PRESSURE SURFACE			
% Surface Distance	% Axial Chord	Tw/Tg	h/ho	% Surface Distance	% Axial Chord	Tw/Tg	h/ho
30.57	49.25	.8009	.9518	28.90	34.95	.7749	.6593
31.98	50.84	.7969	.9428	30.78	37.26	.7620	.5766
33.40	52.37	.7907	.9186	32.58	39.43	.7545	.4717
37.60	56.50	.7736	.8219	34.38	41.55	.7554	.4483
39.08	57.92	.7661	.7615	36.29	43.76	.7580	.4059
41.80	60.34	.7596	.6871	41.70	49.81	.7720	.3713
43.25	61.62	.7595	.6895	45.37	53.70	.7818	.3738
44.57	62.74	.7661	.6742	47.14	55.56	.7842	.3914
46.03	63.96	.7700	.6696	49.03	57.47	.7824	.4051
47.51	65.26	.7799	.7406	50.84	59.28	.7852	.4171
48.95	66.44	.7851	.7095	52.68	61.08	.7924	.4526
50.31	67.53	.7893	.6648	54.48	62.81	.7965	.4763
51.78	68.75	.7923	.5978	56.34	64.57	.8033	.5017
53.14	69.77	.7968	.6320	58.12	66.24	.8033	.5461
54.62	71.01	.8067	.7374	59.97	67.92	.8011	.6035
55.97	71.99	.8091	.6512	61.77	69.55	.8046	.6030
57.36	73.07	.8082	.6113	63.63	71.18	.8113	.4959
60.29	75.38	.8083	.6425	65.41	72.73	.8194	.5052
61.67	76.42	.8052	.6247	67.30	74.37	.8211	.4626
67.29	80.63	.8126	.6683	69.07	75.85	.8174	.5102
70.13	82.74	.8125	.7004	70.91	77.38	.8073	.6156
71.51	83.72	.8206	.6491	72.72	78.84	.8063	.6761
73.03	84.92	.8272	.6291	74.63	80.37	.8210	.5563
74.39	85.88	.8275	.5668	76.40	81.77	.8303	.4463
75.74	86.80	.8249	.5878	78.27	83.24	.8349	.4128
77.24	87.96	.8124	.6512	81.91	86.03	.8149	.6423
78.62	88.92	.8127	.6758	85.55	88.71	.8340	.4094
81.54	91.06	.8340	.5112	87.39	90.05	.8512	.3556
82.88	91.94	.8374	.5342	89.25	91.42	.8587	.4699
84.34	92.98	.8331	.5744	91.03	92.66	.8584	.7674
85.70	93.87	.8176	.5625	92.86	93.93	.8438	.8270
87.11	94.82	.8122	.6059	96.55	96.47	.8567	.5305
88.50	95.72	.8329	.4721				
89.92	96.63	.8533	.4392				
91.35	97.57	.8583	.3630				
94.24	99.40	.8448	.6028				
95.65	100.24	.8331	.4791				
97.03	101.02	.8568	.7286				

Table VIII (contd)
Heat transfer data for each run code

RUN CODE 44103

SUCTION SURFACE				PRESSURE SURFACE			
% Surface Distance	% Axial Chord	Tw/Tg	h/ho	% Surface Distance	% Axial Chord	Tw/Tg	h/ho
30.57	49.25	.7257	.2206	28.90	34.95	.7272	.4636
31.98	50.84	.7232	.3531	30.78	37.26	.7175	.3924
33.40	52.37	.7178	.4079	32.58	39.43	.7131	.3335
37.60	56.50	.7075	.4377	34.38	41.55	.7155	.3305
39.08	57.92	.7020	.4156	36.29	43.76	.7191	.3052
41.80	60.34	.6999	.3956	41.70	49.81	.7342	.2932
43.25	61.62	.7005	.3954	45.37	53.70	.7443	.3013
44.57	62.74	.7063	.3823	47.14	55.56	.7472	.3182
46.03	63.96	.7106	.3785	49.03	57.47	.7473	.3310
47.51	65.26	.7208	.4279	50.84	59.28	.7506	.3415
48.95	66.44	.7265	.4095	52.68	61.08	.7577	.3700
50.31	67.53	.7309	.3804	54.48	62.81	.7617	.3961
51.78	68.75	.7348	.3417	56.34	64.57	.7687	.4229
53.14	69.77	.7397	.3625	58.12	66.24	.7691	.4500
54.62	71.01	.7493	.4251	59.97	67.92	.7682	.5049
55.97	71.99	.7524	.3735	61.77	69.55	.7728	.5122
57.36	73.07	.7526	.3495	63.63	71.18	.7786	.4233
60.29	75.38	.7541	.3705	65.41	72.73	.7863	.4395
61.67	76.42	.7529	.3611	67.30	74.37	.7880	.4044
67.29	80.63	.7652	.4188	69.07	75.85	.7852	.4399
70.13	82.74	.7670	.4375	70.91	77.38	.7765	.5227
71.51	83.72	.7757	.3983	72.72	78.84	.7771	.5779
73.03	84.92	.7831	.3850	74.63	80.37	.7912	.4963
74.39	85.88	.7845	.3474	76.40	81.77	.7996	.4093
75.74	86.80	.7826	.3641	78.27	83.24	.8047	.3932
77.24	87.96	.7722	.4159	81.91	86.03	.7878	.5673
78.62	88.92	.7734	.4380	85.55	88.71	.8059	.3906
81.54	91.06	.7947	.3008	87.39	90.05	.8220	.3504
82.88	91.94	.7987	.3179	89.25	91.42	.8293	.4365
84.34	92.98	.7947	.3372	91.03	92.66	.8295	.6713
85.70	93.87	.7811	.3408	92.86	93.93	.8164	.6990
87.11	94.82	.7772	.3873	96.55	96.47	.8287	.5169
88.50	95.72	.7980	.2776				
89.92	96.63	.8176	.2408				
91.35	97.57	.8237	.1968				
94.24	99.40	.8117	.3637				
95.65	100.24	.8009	.2531				
97.03	101.02	.8242	.4543				

Table VIII (contd)
Heat transfer data for each run code

RUN CODE 44104

SUCTION SURFACE				PRESSURE SURFACE			
% Surface Distance	% Axial Chord	Tw/Tg	h/ho	% Surface Distance	% Axial Chord	Tw/Tg	h/ho
30.57	49.25	.7254	.1934	28.90	34.95	.7270	.4596
31.98	50.84	.7224	.3293	30.78	37.26	.7171	.3910
33.40	52.37	.7171	.3922	32.58	39.43	.7124	.3325
37.60	56.50	.7067	.4273	34.38	41.55	.7140	.3230
39.08	57.92	.7012	.4065	36.29	43.76	.7168	.2960
41.80	60.34	.6990	.3863	41.70	49.81	.7297	.2727
43.25	61.62	.6995	.3857	45.37	53.70	.7385	.2709
44.57	62.74	.7051	.3738	47.14	55.56	.7411	.2860
46.03	63.96	.7094	.3711	49.03	57.47	.7410	.2981
47.51	65.26	.7192	.4178	50.84	59.28	.7443	.3086
48.95	66.44	.7247	.3957	52.68	61.08	.7511	.3365
50.31	67.53	.7292	.3729	54.48	62.81	.7550	.3574
51.78	68.75	.7326	.3330	56.34	64.57	.7615	.3777
53.14	69.77	.7374	.3530	58.12	66.24	.7619	.4034
54.62	71.01	.7466	.4151	59.97	67.92	.7612	.4582
55.97	71.99	.7494	.3623	61.77	69.55	.7659	.4663
57.36	73.07	.7495	.3383	63.63	71.18	.7716	.3785
60.29	75.38	.7512	.3604	65.41	72.73	.7791	.3939
61.67	76.42	.7497	.3513	67.30	74.37	.7811	.3649
67.29	80.63	.7613	.4064	69.07	75.85	.7783	.3987
70.13	82.74	.7630	.4237	70.91	77.38	.7704	.4782
71.51	83.72	.7714	.3872	72.72	78.84	.7711	.5320
73.03	84.92	.7785	.3756	74.63	80.37	.7850	.4555
74.39	85.88	.7798	.3402	76.40	81.77	.7935	.3748
75.74	86.80	.7777	.3534	78.27	83.24	.7982	.3541
77.24	87.96	.7679	.4035	81.91	86.03	.7819	.5183
78.62	88.92	.7694	.4278	85.55	88.71	.7998	.3533
81.54	91.06	.7897	.2924	87.39	90.05	.8159	.3238
82.88	91.94	.7937	.3088	89.25	91.42	.8232	.4056
84.34	92.98	.7900	.3302	91.03	92.66	.8237	.6231
85.70	93.87	.7772	.3374	92.86	93.93	.8113	.6561
87.11	94.82	.7732	.3748	96.55	96.47	.8232	.4783
88.50	95.72	.7932	.2690				
89.92	96.63	.8120	.2294				
91.35	97.57	.8177	.1806				
94.24	99.40	.8066	.3418				
95.65	100.24	.7967	.2465				
97.03	101.02	.8190	.4270				

Table VIII (contd)
Heat transfer data for each run code

RUN CODE 44105

SUCTION SURFACE				PRESSURE SURFACE			
% Surface Distance	% Axial Chord	Tw/Tg	h/ho	% Surface Distance	% Axial Chord	Tw/Tg	h/ho
30.57	49.25	.7214	.0941	28.90	34.95	.7339	.5200
31.98	50.84	.7214	.2995	30.78	37.26	.7244	.4519
33.40	52.37	.7186	.3970	32.58	39.43	.7189	.3777
37.60	56.50	.7072	.4369	34.38	41.55	.7196	.3559
39.08	57.92	.7017	.4178	36.29	43.76	.7225	.3381
41.80	60.34	.6991	.3965	41.70	49.81	.7324	.2905
43.25	61.62	.6996	.3972	45.37	53.70	.7392	.2719
44.57	62.74	.7047	.3841	47.14	55.56	.7416	.2989
46.03	63.96	.7089	.3757	49.03	57.47	.7414	.3155
47.51	65.26	.7181	.4106	50.84	59.28	.7435	.3233
48.95	66.44	.7236	.3844	52.68	61.08	.7490	.3361
50.31	67.53	.7291	.3752	54.48	62.81	.7523	.3489
51.78	68.75	.7313	.3262	56.34	64.57	.7581	.3640
53.14	69.77	.7360	.3417	58.12	66.24	.7581	.3837
54.62	71.01	.7448	.4023	59.97	67.92	.7575	.4429
55.97	71.99	.7473	.3535	61.77	69.55	.7620	.4530
57.36	73.07	.7481	.3344	63.63	71.18	.7669	.3575
60.29	75.38	.7495	.3637	65.41	72.73	.7741	.3711
61.67	76.42	.7477	.3549	67.30	74.37	.7756	.3411
67.29	80.63	.7585	.4000	69.07	75.85	.7727	.3711
70.13	82.74	.7601	.4192	70.91	77.38	.7646	.4619
71.51	83.72	.7680	.3817	72.72	78.84	.7665	.5300
73.03	84.92	.7749	.3815	74.63	80.37	.7794	.4312
74.39	85.88	.7756	.3327	76.40	81.77	.7867	.3324
75.74	86.80	.7732	.3500	78.27	83.24	.7922	.3250
77.24	87.96	.7646	.4103	81.91	86.03	.7748	.4544
78.62	88.92	.7658	.4392	85.55	88.71	.7933	.3161
81.54	91.06	.7856	.3009	87.39	90.05	.8082	.2752
82.88	91.94	.7897	.3166	89.25	91.42	.8152	.3567
84.34	92.98	.7855	.3242	91.03	92.66	.8152	.5354
85.70	93.87	.7735	.3428	92.86	93.93	.8031	.5905
87.11	94.82	.7701	.3859	96.55	96.47	.8156	.4339
88.50	95.72	.7886	.2778				
89.92	96.63	.8064	.2347				
91.35	97.57	.8109	.1747				
94.24	99.40	.8010	.3650				
95.65	100.24	.7910	.2744				
97.03	101.02	.8124	.4245				

Table VIII (contd)
Heat transfer data for each run code

RUN CODE 44106

SUCTION SURFACE				PRESSURE SURFACE			
% Surface Distance	% Axial Chord	Tw/Tg	h/ho	% Surface Distance	% Axial Chord	Tw/Tg	h/ho
30.57	49.25	.7168	.1201	28.90	34.95	.7293	.5143
31.98	50.84	.7185	.3361	30.78	37.26	.7206	.4588
33.40	52.37	.7151	.4197	32.58	39.43	.7160	.3996
37.60	56.50	.7028	.4458	34.38	41.55	.7165	.3791
39.08	57.92	.6957	.4165	36.29	43.76	.7182	.3455
41.80	60.34	.6919	.3821	41.70	49.81	.7258	.2874
43.25	61.62	.6919	.3820	45.37	53.70	.7319	.2782
44.57	62.74	.6972	.3677	47.14	55.56	.7334	.2880
46.03	63.96	.7008	.3608	49.03	57.47	.7312	.2914
47.51	65.26	.7105	.4045	50.84	59.28	.7331	.2926
48.95	66.44	.7160	.3909	52.68	61.08	.7388	.3218
50.31	67.53	.7194	.3533	54.48	62.81	.7411	.3283
51.78	68.75	.7230	.3170	56.34	64.57	.7458	.3308
53.14	69.77	.7270	.3330	58.12	66.24	.7455	.3566
54.62	71.01	.7359	.3852	59.97	67.92	.7438	.3919
55.97	71.99	.7383	.3385	61.77	69.55	.7465	.3910
57.36	73.07	.7385	.3158	63.63	71.18	.7518	.3219
60.29	75.38	.7384	.3336	65.41	72.73	.7583	.3210
61.67	76.42	.7370	.3278	67.30	74.37	.7597	.2933
67.29	80.63	.7471	.3818	69.07	75.85	.7568	.3268
70.13	82.74	.7475	.3923	70.91	77.38	.7488	.4014
71.51	83.72	.7546	.3556	72.72	78.84	.7489	.4458
73.03	84.92	.7607	.3390	74.63	80.37	.7613	.3626
74.39	85.88	.7617	.3123	76.40	81.77	.7688	.2823
75.74	86.80	.7597	.3319	78.27	83.24	.7727	.2577
77.24	87.96	.7506	.3850	81.91	86.03	.7562	.3918
78.62	88.92	.7517	.4106	85.55	88.71	.7731	.2538
81.54	91.06	.7698	.2862	87.39	90.05	.7874	.2099
82.88	91.94	.7729	.2934	89.25	91.42	.7937	.2548
84.34	92.98	.7691	.3127	91.03	92.66	.7938	.3952
85.70	93.87	.7573	.3284	92.86	93.93	.7834	.4805
87.11	94.82	.7533	.3583	96.55	96.47	.7944	.3037
88.50	95.72	.7706	.2622				
89.92	96.63	.7881	.2329				
91.35	97.57	.7926	.1857				
94.24	99.40	.7833	.3421				
95.65	100.24	.7745	.2780				
97.03	101.02	.7941	.4026				

Table VIII (contd)
Heat transfer data for each run code

RUN CODE 44107

SUCTION SURFACE				PRESSURE SURFACE			
% Surface Distance	% Axial Chord	Tw/Tg	h/ho	% Surface Distance	% Axial Chord	Tw/Tg	h/ho
30.57	49.25	.7047	.1947	28.90	34.95	.7115	.5126
31.98	50.84	.7074	.4087	30.78	37.26	.7027	.4701
33.40	52.37	.7036	.4778	32.58	39.43	.6980	.4091
37.60	56.50	.6885	.4697	34.38	41.55	.6990	.3878
39.08	57.92	.6808	.4391	36.29	43.76	.7012	.3602
41.80	60.34	.6764	.4060	41.70	49.81	.7086	.2989
43.25	61.62	.6758	.3997	45.37	53.70	.7143	.2860
44.57	62.74	.6808	.3837	47.14	55.56	.7154	.2978
46.03	63.96	.6844	.3770	49.03	57.47	.7125	.3048
47.51	65.26	.6945	.4192	50.84	59.28	.7141	.3095
48.95	66.44	.7001	.4051	52.68	61.08	.7197	.3345
50.31	67.53	.7039	.3701	54.43	62.81	.7213	.3380
51.78	68.75	.7067	.3271	56.34	64.57	.7261	.3375
53.14	69.77	.7107	.3443	58.12	66.24	.7250	.3589
54.62	71.01	.7201	.4035	59.97	67.92	.7227	.3955
55.97	71.99	.7222	.3531	61.77	69.55	.7250	.3943
57.36	73.07	.7220	.3297	63.63	71.18	.7304	.3197
60.29	75.38	.7211	.3518	65.41	72.73	.7374	.3238
61.67	76.42	.7187	.3455	67.30	74.37	.7384	.2936
67.29	80.63	.7278	.3944	69.07	75.85	.7343	.3194
70.13	82.74	.7272	.4058	70.91	77.38	.7244	.3865
71.51	83.72	.7351	.3743	72.72	78.84	.7238	.4280
73.03	84.92	.7416	.3593	74.63	80.37	.7376	.3497
74.39	85.88	.7424	.3324	76.40	81.77	.7463	.2767
75.74	86.80	.7394	.3457	78.27	83.24	.7504	.2537
77.24	87.96	.7280	.3886	81.91	86.03	.7300	.3803
78.62	88.92	.7285	.4101	85.55	88.71	.7485	.2397
81.54	91.06	.7490	.3054	87.39	90.05	.7650	.1985
82.88	91.94	.7523	.3169	89.25	91.42	.7723	.2629
84.34	92.98	.7473	.3313	91.03	92.66	.7720	.4123
85.70	93.87	.7329	.3354	92.85	93.93	.7588	.4754
87.11	94.82	.7275	.3599	96.55	96.47	.7713	.2971
88.50	95.72	.7475	.2790				
89.92	96.63	.7675	.2566				
91.35	97.57	.7721	.2062				
94.24	99.40	.7597	.3500				
95.65	100.24	.7488	.2717				
97.03	101.02	.7717	.4233				

Table VIII (contd)
Heat transfer data for each run code

RUN CODE 44108

SUCTION SURFACE				PRESSURE SURFACE			
% Surface Distance	% Axial Chord	Tw/Tg	h/ho	% Surface Distance	% Axial Chord	Tw/Tg	h/ho
30.57	49.25	.7057	.2083	28.90	34.95	.7130	.5048
31.98	50.84	.7095	.4237	30.78	37.26	.7053	.4640
33.40	52.37	.7047	.4758	32.58	39.43	.7014	.4074
37.60	56.50	.6900	.4538	34.38	41.55	.7029	.3899
39.08	57.92	.6828	.4260	36.29	43.76	.7051	.3598
41.80	60.34	.6791	.3977	41.70	49.81	.7126	.2998
43.25	61.62	.6784	.3895	45.37	53.70	.7182	.2873
44.57	62.74	.6835	.3742	47.14	55.56	.7193	.3000
46.03	63.96	.6872	.3691	49.03	57.47	.7165	.3085
47.51	65.26	.6973	.4110	50.84	59.28	.7180	.3148
48.95	66.44	.7029	.3979	52.68	61.08	.7233	.3369
50.31	67.53	.7066	.3626	54.48	62.81	.7245	.3395
51.78	68.75	.7095	.3203	56.34	64.57	.7292	.3382
53.14	69.77	.7132	.3380	58.12	66.24	.7279	.3565
54.62	71.01	.7227	.3978	59.97	67.92	.7254	.3940
55.97	71.99	.7247	.3480	61.77	69.55	.7278	.3942
57.36	73.07	.7246	.3243	63.63	71.18	.7328	.3192
60.29	75.38	.7234	.3458	65.41	72.73	.7395	.3209
61.67	76.42	.7213	.3408	67.30	74.37	.7404	.2899
67.29	80.63	.7300	.3868	69.07	75.85	.7364	.3174
70.13	82.74	.7295	.4022	70.91	77.38	.7266	.3876
71.51	83.72	.7372	.3704	72.72	78.84	.7260	.4296
73.03	84.92	.7433	.3502	74.63	80.37	.7390	.3451
74.39	85.88	.7439	.3246	76.40	81.77	.7472	.2708
75.74	86.80	.7411	.3400	78.27	83.24	.7515	.2518
77.24	87.96	.7298	.3835	81.91	86.03	.7314	.3745
78.62	88.92	.7300	.4037	85.55	88.71	.7495	.2414
81.54	91.06	.7497	.2948	87.39	90.05	.7656	.2038
82.88	91.94	.7532	.3109	89.25	91.42	.7724	.2536
84.34	92.98	.7483	.3263	91.03	92.66	.7721	.4088
85.70	93.87	.7339	.3262	92.86	93.93	.7591	.4718
87.11	94.82	.7284	.3492	96.55	96.47	.7712	.2947
88.50	95.72	.7479	.2677				
89.92	96.63	.7673	.2435				
91.35	97.57	.7719	.1978				
94.24	99.40	.7598	.3432				
95.65	100.24	.7490	.2684				
97.03	101.02	.7714	.4096				

Table VIII (contd)
Heat transfer data for each run code

RUN CODE 44133

SUCTION SURFACE				PRESSURE SURFACE			
% Surface Distance	% Axial Chord	Tw/Tg	h/ho	% Surface Distance	% Axial Chord	Tw/Tg	h/ho
30.57	49.25	.7132	.1782	28.90	34.95	.7172	.4569
31.98	50.84	.7115	.3206	30.78	37.26	.7082	.3832
33.40	52.37	.7068	.3830	32.58	39.43	.7045	.3264
37.60	56.50	.6976	.4208	34.38	41.55	.7072	.3224
39.08	57.92	.6923	.3994	36.29	43.76	.7112	.3028
41.80	60.34	.6902	.3781	41.70	49.81	.7266	.2890
43.25	61.62	.6906	.3738	45.37	53.70	.7365	.2928
44.57	62.74	.6965	.3638	47.14	55.56	.7395	.3106
46.03	63.96	.7014	.3653	49.03	57.47	.7398	.3261
47.51	65.26	.7118	.4127	50.84	59.28	.7434	.3402
48.95	66.44	.7174	.3884	52.68	61.08	.7507	.3693
50.31	67.53	.7222	.3663	54.48	62.81	.7545	.3948
51.78	68.75	.7256	.3252	56.34	64.57	.7616	.4199
53.14	69.77	.7306	.3439	58.12	66.24	.7619	.4437
54.62	71.01	.7401	.4042	59.97	67.92	.7612	.5020
55.97	71.99	.7432	.3534	61.77	69.55	.7661	.5119
57.36	73.07	.7434	.3308	63.63	71.18	.7717	.4212
60.29	75.38	.7453	.3536	65.41	72.73	.7795	.4414
61.67	76.42	.7438	.3440	67.30	74.37	.7813	.4071
67.29	80.63	.7568	.4066	69.07	75.85	.7781	.4389
70.13	82.74	.7585	.4225	70.91	77.38	.7695	.5197
71.51	83.72	.7675	.3842	72.72	78.84	.7701	.5755
73.03	84.92	.7748	.3629	74.63	80.37	.7845	.4985
74.39	85.88	.7764	.3325	76.40	81.77	.7934	.4189
75.74	86.80	.7743	.3480	78.27	83.24	.7982	.3982
77.24	87.96	.7638	.3980	81.91	86.03	.7802	.5606
78.62	88.92	.7651	.4210	85.55	88.71	.7986	.3911
81.54	91.06	.7870	.2880	87.39	90.05	.8157	.3639
82.88	91.94	.7912	.3062	89.25	91.42	.8235	.4641
84.34	92.98	.7869	.3238	91.03	92.66	.8236	.6983
85.70	93.87	.7729	.3294	92.36	93.93	.8095	.7073
87.11	94.82	.7683	.3671	96.55	96.47	.8219	.5313
88.50	95.72	.7899	.2621				
89.92	96.63	.8099	.2208				
91.35	97.57	.8161	.1734				
94.24	99.40	.8036	.3419				
95.65	100.24	.7923	.2378				
97.03	101.02	.8160	.4189				

Table VIII (contd)
Heat transfer data for each run code

RUN CODE 44135

SUCTION SURFACE				PRESSURE SURFACE			
% Surface Distance	% Axial Chord	Tw/Tg	h/ho	% Surface Distance	% Axial Chord	Tw/Tg	h/ho
30.57	49.25	.7187	.1437	28.90	34.95	.7238	.4592
31.98	50.84	.7168	.2920	30.78	37.26	.7147	.3900
33.40	52.37	.7125	.3640	32.58	39.43	.7099	.3300
37.60	56.50	.7029	.4057	34.38	41.55	.7108	.3138
39.08	57.92	.6977	.3868	36.29	43.76	.7128	.2838
41.80	60.34	.6955	.3676	41.70	49.81	.7233	.2501
43.25	61.62	.6961	.3680	45.37	53.70	.7306	.2404
44.57	62.74	.7015	.3561	47.14	55.56	.7327	.2523
46.03	63.96	.7055	.3519	49.03	57.47	.7321	.2615
47.51	65.26	.7148	.3945	50.84	59.28	.7348	.2693
48.95	66.44	.7199	.3732	52.68	61.08	.7409	.2903
50.31	67.53	.7242	.3509	54.48	62.81	.7442	.3059
51.78	68.75	.7274	.3138	56.34	64.57	.7502	.3212
53.14	69.77	.7320	.3329	58.12	66.24	.7502	.3403
54.62	71.01	.7408	.3912	59.97	67.92	.7492	.3841
55.97	71.99	.7434	.3412	61.77	69.55	.7534	.3901
57.36	73.07	.7433	.3183	63.63	71.18	.7591	.3172
60.29	75.38	.7449	.3382	65.41	72.73	.7661	.3202
61.67	76.42	.7433	.3300	67.30	74.37	.7680	.2936
67.29	80.63	.7541	.3851	69.07	75.85	.7657	.3255
70.13	82.74	.7557	.3999	70.91	77.38	.7582	.3975
71.51	83.72	.7631	.3653	72.72	78.84	.7589	.4432
73.03	84.92	.7696	.3535	74.63	80.37	.7720	.3715
74.39	85.88	.7709	.3241	76.40	81.77	.7803	.2998
75.74	86.80	.7692	.3393	78.27	83.24	.7846	.2772
77.24	87.96	.7601	.3865	81.91	86.03	.7698	.4252
78.62	88.92	.7616	.4086	85.55	88.71	.7866	.2670
81.54	91.06	.7802	.2836	87.39	90.05	.8020	.2371
82.88	91.94	.7836	.2927	89.25	91.42	.8092	.3074
84.34	92.98	.7805	.3177	91.03	92.66	.8099	.4785
85.70	93.87	.7690	.3270	92.86	93.93	.7992	.5253
87.11	94.82	.7654	.3547	96.55	96.47	.8107	.3666
88.50	95.72	.7838	.2673				
89.92	96.63	.8017	.2391				
91.35	97.57	.8065	.1843				
94.24	99.40	.7976	.3360				
95.65	100.24	.7890	.2592				
97.03	101.02	.8089	.4032				

Table VIII (contd)
Heat transfer data for each run code

RUN CODE 44144

SUCTION SURFACE				PRESSURE SURFACE			
% Surface Distance	% Axial Chord	Tw/Tg	h/ho	% Surface Distance	% Axial Chord	Tw/Tg	h/ho
30.57	49.25	.7194	.1488	28.90	34.95	.7256	.4727
31.98	50.84	.7181	.3101	30.78	37.26	.7159	.3949
33.40	52.37	.7133	.3786	32.58	39.43	.7111	.3315
37.60	56.50	.7037	.4174	34.38	41.55	.7128	.3221
39.08	57.92	.6985	.3977	36.29	43.76	.7155	.2921
41.80	60.34	.6966	.3786	41.70	49.81	.7286	.2713
43.25	61.62	.6973	.3787	45.37	53.70	.7376	.2727
44.57	62.74	.7031	.3673	47.14	55.56	.7402	.2862
46.03	63.96	.7074	.3646	49.03	57.47	.7400	.2985
47.51	65.26	.7172	.4100	50.84	59.28	.7434	.3104
48.95	66.44	.7227	.3913	52.68	61.08	.7503	.3379
50.31	67.53	.7270	.3645	54.48	62.81	.7542	.3609
51.78	68.75	.7307	.3274	56.34	64.57	.7608	.3832
53.14	69.77	.7354	.3466	58.12	66.24	.7611	.4053
54.62	71.01	.7445	.4051	59.97	67.92	.7603	.4579
55.97	71.99	.7473	.3533	61.77	69.55	.7650	.4660
57.36	73.07	.7473	.3296	63.63	71.18	.7707	.3818
60.29	75.38	.7489	.3515	65.41	72.73	.7782	.3980
61.67	76.42	.7476	.3428	67.30	74.37	.7800	.3636
67.29	80.63	.7593	.3946	69.07	75.85	.7774	.3990
70.13	82.74	.7615	.4194	70.91	77.38	.7694	.4796
71.51	83.72	.7697	.3818	72.72	78.84	.7700	.5313
73.03	84.92	.7766	.3599	74.63	80.37	.7836	.4502
74.39	85.88	.7780	.3287	76.40	81.77	.7917	.3657
75.74	86.80	.7762	.3463	78.27	83.24	.7967	.3506
77.24	87.96	.7665	.3986	81.91	86.03	.7805	.5148
78.62	88.92	.7679	.4225	85.55	88.71	.7981	.3494
81.54	91.06	.7881	.2867	87.39	90.05	.8140	.3169
82.88	91.94	.7921	.3034	89.25	91.42	.8211	.3885
84.34	92.98	.7884	.3255	91.03	92.66	.8216	.6047
85.70	93.87	.7755	.3315	92.86	93.93	.8094	.6440
87.11	94.82	.7716	.3702	96.55	96.47	.8212	.4601
88.50	95.72	.7915	.2667				
89.92	96.63	.8100	.2245				
91.35	97.57	.8160	.1835				
94.24	99.40	.8049	.3417				
95.65	100.24	.7950	.2475				
97.03	101.02	.8174	.4296				

Table VIII (contd)
Heat transfer data for each run code

RUN CODE 44145

SUCTION SURFACE				PRESSURE SURFACE			
% Surface Distance	% Axial Chord	Tw/Tg	h/ho	% Surface Distance	% Axial Chord	Tw/Tg	h/ho
30.57	49.25	.7234	.1462	28.90	34.95	.7306	.4908
31.98	50.84	.7217	.3065	30.78	37.26	.7208	.4131
33.40	52.37	.7168	.3777	32.58	39.43	.7154	.3453
37.60	56.50	.7066	.4156	34.38	41.55	.7161	.3282
39.08	57.92	.7013	.3961	36.29	43.76	.7179	.2929
41.80	60.34	.6991	.3775	41.70	49.81	.7285	.2613
43.25	61.62	.6996	.3768	45.37	53.70	.7362	.2572
44.57	62.74	.7051	.3635	47.14	55.56	.7382	.2669
46.03	63.96	.7091	.3593	49.03	57.47	.7375	.2761
47.51	65.26	.7187	.4065	50.84	59.28	.7403	.2855
48.95	66.44	.7240	.3881	52.68	61.08	.7464	.3073
50.31	67.53	.7278	.3574	54.48	62.81	.7500	.3250
51.78	68.75	.7314	.3218	56.34	64.57	.7559	.3436
53.14	69.77	.7360	.3408	58.12	66.24	.7561	.3667
54.62	71.01	.7447	.3980	59.97	67.92	.7549	.4108
55.97	71.99	.7474	.3480	61.77	69.55	.7590	.4145
57.36	73.07	.7473	.3245	63.63	71.18	.7646	.3378
60.29	75.38	.7485	.3429	65.41	72.73	.7717	.3463
61.67	76.42	.7469	.3344	67.30	74.37	.7735	.3172
67.29	80.63	.7576	.3878	69.07	75.85	.7711	.3523
70.13	82.74	.7591	.4055	70.91	77.38	.7634	.4254
71.51	83.72	.7667	.3699	72.72	78.84	.7637	.4699
73.03	84.92	.7731	.3520	74.63	80.37	.7769	.3955
74.39	85.88	.7744	.3211	76.40	81.77	.7848	.3172
75.74	86.80	.7728	.3405	78.27	83.24	.7895	.3001
77.24	87.96	.7635	.3897	81.91	86.03	.7744	.4525
78.62	88.92	.7647	.4096	85.55	88.71	.7920	.3077
81.54	91.06	.7835	.2825	87.39	90.05	.8071	.2739
82.88	91.94	.7871	.2941	89.25	91.42	.8141	.3472
84.34	92.98	.7837	.3131	91.03	92.66	.8146	.5214
85.70	93.87	.7718	.3207	92.86	93.93	.8037	.5740
87.11	94.82	.7683	.3566	96.55	96.47	.8153	.4217
88.50	95.72	.7869	.2565				
89.92	96.63	.8043	.2148				
91.35	97.57	.8096	.1682				
94.24	99.40	.7999	.3172				
95.65	100.24	.7910	.2349				
97.03	101.02	.8116	.3835				

Table VIII (contd)
Heat transfer data for each run code

RUN CODE 44155

SUCTION SURFACE				PRESSURE SURFACE			
% Surface Distance	% Axial Chord	Tw/Tg	h/ho	% Surface Distance	% Axial Chord	Tw/Tg	h/ho
30.57	49.25	.7177	.1240	28.90	34.95	.7268	.4794
31.98	50.84	.7155	.2755	30.78	37.26	.7178	.4072
33.40	52.37	.7112	.3514	32.58	39.43	.7127	.3396
37.60	56.50	.7012	.3950	34.38	41.55	.7138	.3258
39.08	57.92	.6962	.3781	36.29	43.76	.7159	.2935
41.80	60.34	.6942	.3594	41.70	49.81	.7268	.2613
43.25	61.62	.6949	.3609	45.37	53.70	.7344	.2524
44.57	62.74	.7006	.3498	47.14	55.56	.7368	.2682
46.03	63.96	.7049	.3460	49.03	57.47	.7364	.2804
47.51	65.26	.7144	.3888	50.84	59.28	.7394	.2902
48.95	66.44	.7197	.3729	52.58	61.08	.7457	.3114
50.31	67.53	.7237	.3426	54.48	62.81	.7492	.3292
51.78	68.75	.7273	.3061	56.34	64.57	.7553	.3480
53.14	69.77	.7319	.3265	58.12	66.24	.7556	.3712
54.62	71.01	.7411	.3868	59.97	67.92	.7546	.4121
55.97	71.99	.7438	.3353	61.77	69.55	.7586	.4142
57.36	73.07	.7439	.3117	63.53	71.18	.7643	.3405
60.29	75.38	.7454	.3314	65.41	72.73	.7714	.3503
61.67	76.42	.7439	.3224	67.30	74.37	.7733	.3211
67.29	80.63	.7552	.3734	69.07	75.85	.7712	.3570
70.13	82.74	.7571	.3914	70.91	77.38	.7638	.4311
71.51	83.72	.7649	.3565	72.72	78.84	.7642	.4750
73.03	84.92	.7714	.3346	74.53	80.37	.7770	.3976
74.39	85.88	.7728	.3068	76.40	81.77	.7848	.3185
75.74	86.80	.7715	.3253	78.27	83.24	.7894	.3015
77.24	87.96	.7623	.3770	81.91	86.03	.7751	.4563
78.62	88.92	.7640	.4008	85.55	88.71	.7915	.2967
81.54	91.06	.7825	.2662	87.39	90.05	.8065	.2656
82.88	91.94	.7860	.2753	89.25	91.42	.8134	.3267
84.34	92.98	.7832	.3029	91.03	92.66	.8142	.5170
85.70	93.87	.7715	.3113	92.36	93.93	.8033	.5447
87.11	94.82	.7682	.3451	96.55	96.47	.8143	.3843
88.50	95.72	.7867	.2520				
89.92	96.63	.8040	.2136				
91.35	97.57	.8093	.1649				
94.24	99.40	.8007	.3223				
95.65	100.24	.7921	.2473				
97.03	101.02	.8115	.3820				

Table VIII (contd)
Heat transfer data for each run code

RUN CODE 44203

SUCTION SURFACE				PRESSURE SURFACE			
% Surface Distance	% Axial Chord	Tw/Tg	h/ho	% Surface Distance	% Axial Chord	Tw/Tg	h/ho
30.57	49.25	.7444	.3658	28.90	34.95	.7372	.4919
31.98	50.84	.7436	.5081	30.78	37.26	.7263	.4294
33.40	52.37	.7377	.5444	32.58	39.43	.7215	.3722
37.60	56.50	.7236	.5266	34.38	41.55	.7232	.3600
39.08	57.92	.7168	.4948	36.29	43.76	.7264	.3308
41.80	60.34	.7127	.4571	41.70	49.81	.7407	.3106
43.25	61.62	.7129	.4578	45.37	53.70	.7508	.3213
44.57	62.74	.7189	.4466	47.14	55.56	.7533	.3366
46.03	63.96	.7233	.4457	49.03	57.47	.7530	.3518
47.51	65.26	.7336	.5000	50.84	59.28	.7563	.3672
48.95	66.44	.7391	.4747	52.68	61.08	.7634	.3959
50.31	67.53	.7436	.4449	54.48	62.81	.7675	.4215
51.78	68.75	.7471	.4005	56.34	64.57	.7746	.4471
53.14	69.77	.7519	.4227	58.12	66.24	.7746	.4722
54.62	71.01	.7614	.4913	59.97	67.92	.7734	.5271
55.97	71.99	.7642	.4336	61.77	69.55	.7779	.5363
57.36	73.07	.7640	.4076	63.63	71.18	.7845	.4510
60.29	75.38	.7649	.4329	65.41	72.73	.7924	.4648
61.67	76.42	.7629	.4215	67.30	74.37	.7943	.4310
67.29	80.63	.7738	.4700	69.07	75.85	.7911	.4684
70.13	82.74	.7751	.4927	70.91	77.38	.7821	.5578
71.51	83.72	.7838	.4504	72.72	78.84	.7822	.6161
73.03	84.92	.7911	.4336	74.63	80.37	.7964	.5196
74.39	85.88	.7922	.3887	76.40	81.77	.8049	.4244
75.74	86.80	.7897	.4038	78.27	83.24	.8101	.4082
77.24	87.96	.7787	.4587	81.91	86.03	.7913	.5834
78.62	88.92	.7798	.4842	85.55	88.71	.8097	.3975
81.54	91.06	.8017	.3460	87.39	90.05	.8264	.3567
82.88	91.94	.8056	.3615	89.25	91.42	.8340	.4571
84.34	92.98	.8010	.3810	91.03	92.66	.8338	.6862
85.70	93.87	.7868	.3871	92.86	93.93	.8202	.7338
87.11	94.82	.7820	.4275	96.55	96.47	.8329	.5358
88.50	95.72	.8032	.3148				
89.92	96.63	.8233	.2778				
91.35	97.57	.8291	.2255				
94.24	99.40	.8161	.3990				
95.65	100.24	.8047	.2803				
97.03	101.02	.8287	.4966				

Table VIII (contd)
Heat transfer data for each run code

RUN CODE 44204

SUCTION SURFACE				PRESSURE SURFACE			
% Surface Distance	% Axial Chord	Tw/Tg	h/ho	% Surface Distance	% Axial Chord	Tw/Tg	h/ho
30.57	49.25	.7471	.3526	28.90	34.95	.7428	.5308
31.98	50.84	.7466	.5129	30.78	37.26	.7317	.4662
33.40	52.37	.7407	.5554	32.58	39.43	.7260	.3980
37.60	56.50	.7263	.5397	34.38	41.55	.7270	.3807
39.08	57.92	.7192	.5052	36.29	43.76	.7293	.3442
41.80	60.34	.7145	.4612	41.70	49.81	.7411	.3092
43.25	61.62	.7145	.4617	45.37	53.70	.7499	.3119
44.57	62.74	.7205	.4522	47.14	55.56	.7521	.3271
46.03	63.96	.7249	.4524	49.03	57.47	.7513	.3403
47.51	65.26	.7350	.5041	50.84	59.28	.7540	.3525
48.95	66.44	.7405	.4823	52.68	61.08	.7607	.3791
50.31	67.53	.7448	.4490	54.48	62.81	.7645	.4020
51.78	68.75	.7481	.4026	56.34	64.57	.7711	.4238
53.14	69.77	.7527	.4255	58.12	66.24	.7707	.4436
54.62	71.01	.7622	.4971	59.97	67.92	.7692	.4971
55.97	71.99	.7648	.4385	61.77	69.55	.7736	.5054
57.36	73.07	.7646	.4117	63.63	71.18	.7798	.4172
60.29	75.38	.7650	.4367	65.41	72.73	.7875	.4244
61.67	76.42	.7629	.4261	67.30	74.37	.7895	.3941
67.29	80.63	.7727	.4714	69.07	75.85	.7863	.4324
70.13	82.74	.7738	.4944	70.91	77.38	.7773	.5176
71.51	83.72	.7822	.4544	72.72	78.84	.7772	.5705
73.03	84.92	.7895	.4475	74.63	80.37	.7915	.4781
74.39	85.88	.7903	.3964	76.40	81.77	.8004	.3898
75.74	86.80	.7879	.4119	78.27	83.24	.8054	.3714
77.24	87.96	.7770	.4666	81.91	86.03	.7867	.5425
78.62	88.92	.7780	.4909	85.55	88.71	.8054	.3649
81.54	91.06	.7995	.3589	87.39	90.05	.8222	.3287
82.88	91.94	.8034	.3781	89.25	91.42	.8298	.4280
84.34	92.98	.7987	.3898	91.03	92.66	.8298	.6552
85.70	93.87	.7843	.3879	92.86	93.93	.8162	.6948
87.11	94.82	.7797	.4292	96.55	96.47	.8287	.4877
88.50	95.72	.8004	.3194				
89.92	96.63	.8202	.2844				
91.35	97.57	.8259	.2332				
94.24	99.40	.8129	.3956				
95.65	100.24	.8018	.2813				
97.03	101.02	.8258	.5081				

Table VIII (contd)
Heat transfer data for each run code

RUN CODE 44205

SUCTION SURFACE				PRESSURE SURFACE			
% Surface Distance	% Axial Chord	Tw/Tg	h/ho	% Surface Distance	% Axial Chord	Tw/Tg	h/ho
30.57	49.25	.7505	.3671	28.90	34.95	.7494	.5980
31.98	50.84	.7496	.5341	30.78	37.26	.7385	.5317
33.40	52.37	.7435	.5811	32.58	39.43	.7322	.4493
37.60	56.50	.7281	.5637	34.38	41.55	.7327	.4243
39.08	57.92	.7206	.5262	36.29	43.76	.7345	.3829
41.80	60.34	.7154	.4772	41.70	49.81	.7444	.3334
43.25	61.62	.7154	.4795	45.37	53.70	.7518	.3280
44.57	62.74	.7212	.4670	47.14	55.56	.7534	.3415
46.03	63.96	.7254	.4636	49.03	57.47	.7517	.3537
47.51	65.26	.7357	.5178	50.84	59.28	.7539	.3647
48.95	66.44	.7413	.4955	52.68	61.08	.7597	.3845
50.31	67.53	.7455	.4609	54.48	62.81	.7630	.4012
51.78	68.75	.7487	.4119	56.34	64.57	.7689	.4186
53.14	69.77	.7532	.4332	58.12	66.24	.7682	.4393
54.62	71.01	.7626	.5037	59.97	67.92	.7663	.4909
55.97	71.99	.7653	.4473	61.77	69.55	.7702	.4969
57.36	73.07	.7650	.4217	63.63	71.18	.7762	.4069
60.29	75.38	.7649	.4454	65.41	72.73	.7837	.4123
61.67	76.42	.7623	.4343	67.30	74.37	.7854	.3774
67.29	80.63	.7713	.4797	69.07	75.85	.7820	.4161
70.13	82.74	.7718	.5024	70.91	77.38	.7729	.5024
71.51	83.72	.7800	.4607	72.72	78.84	.7724	.5525
73.03	84.92	.7871	.4537	74.63	80.37	.7863	.4541
74.39	85.88	.7878	.4050	76.40	81.77	.7951	.3658
75.74	86.80	.7854	.4214	78.27	83.24	.8001	.3478
77.24	87.96	.7743	.4771	81.91	86.03	.7810	.5161
78.62	88.92	.7751	.5023	85.55	88.71	.7993	.3352
81.54	91.06	.7958	.3632	87.39	90.05	.8163	.3009
82.88	91.94	.7997	.3854	89.25	91.42	.8240	.4015
84.34	92.98	.7950	.4012	91.03	92.66	.8236	.6075
85.70	93.87	.7805	.3994	92.86	93.93	.8097	.6443
87.11	94.82	.7756	.4380	96.55	96.47	.8228	.4525
88.50	95.72	.7962	.3338				
89.92	96.63	.8158	.2966				
91.35	97.57	.8211	.2391				
94.24	99.40	.8085	.4154				
95.65	100.24	.7974	.3071				
97.03	101.02	.8210	.5153				

Table VIII (contd)
Heat transfer data for each run code

RUN CODE 44303

SUCTION SURFACE				PRESSURE SURFACE			
% Surface Distance	% Axial Chord	Tw/Tg	h/ho	% Surface Distance	% Axial Chord	Tw/Tg	h/ho
30.57	49.25	.7685	.5420	28.90	34.95	.7550	.5493
31.98	50.84	.7684	.6758	30.78	37.26	.7434	.4836
33.40	52.37	.7624	.6898	32.58	39.43	.7378	.4132
37.60	56.50	.7461	.6271	34.38	41.55	.7392	.3966
39.08	57.92	.7384	.5827	36.29	43.76	.7421	.3641
41.80	60.34	.7331	.5305	41.70	49.81	.7556	.3334
43.25	61.62	.7329	.5288	45.37	53.70	.7655	.3468
44.57	62.74	.7390	.5172	47.14	55.56	.7678	.3622
46.03	63.96	.7433	.5167	49.03	57.47	.7670	.3756
47.51	65.26	.7534	.5749	50.84	59.28	.7698	.3883
48.95	66.44	.7590	.5527	52.68	61.08	.7767	.4186
50.31	67.53	.7633	.5171	54.48	62.81	.7809	.4472
51.78	68.75	.7666	.4646	56.34	64.57	.7877	.4751
53.14	69.77	.7710	.4892	58.12	66.24	.7873	.4975
54.62	71.01	.7806	.5679	59.97	67.92	.7858	.5561
55.97	71.99	.7833	.5021	61.77	69.55	.7899	.5643
57.36	73.07	.7826	.4729	63.63	71.18	.7963	.4665
60.29	75.38	.7832	.5002	65.41	72.73	.8043	.4826
61.67	76.42	.7803	.4854	67.30	74.37	.8061	.4465
67.29	80.63	.7896	.5282	69.07	75.85	.8026	.4866
70.13	82.74	.7907	.5619	70.91	77.38	.7929	.5773
71.51	83.72	.7993	.5197	72.72	78.84	.7923	.6327
73.03	84.92	.8065	.5080	74.63	80.37	.8068	.5282
74.39	85.88	.8070	.4486	76.40	81.77	.8155	.4265
75.74	86.80	.8042	.4638	78.27	83.24	.8208	.4093
77.24	87.96	.7929	.5250	81.91	86.03	.8015	.6028
78.62	88.92	.7937	.5543	85.55	88.71	.8202	.3999
81.54	91.06	.8154	.4074	87.39	90.05	.8370	.3513
82.88	91.94	.8194	.4301	89.25	91.42	.8445	.4555
84.34	92.98	.8144	.4425	91.03	92.66	.8442	.7101
85.70	93.87	.7997	.4434	92.86	93.93	.8301	.7582
87.11	94.82	.7947	.4865	96.56	96.47	.8427	.5121
88.50	95.72	.8159	.3703				
89.92	96.63	.8360	.3349				
91.35	97.57	.8418	.2846				
94.24	99.40	.8282	.4667				
95.65	100.24	.8164	.3327				
97.03	101.02	.8410	.6000				

Table VIII (contd)
Heat transfer data for each run code

RUN CODE 44304

SUCTION SURFACE				PRESSURE SURFACE			
% Surface Distance	% Axial Chord	Tw/Tg	h/ho	% Surface Distance	% Axial Chord	Tw/Tg	h/ho
30.57	49.25	.7766	.5537	28.90	34.95	.7668	.6144
31.98	50.84	.7764	.6897	30.78	37.26	.7561	.5500
33.40	52.37	.7704	.7113	32.58	39.43	.7500	.4656
37.60	56.50	.7547	.6576	34.38	41.55	.7509	.4423
39.08	57.92	.7473	.6128	36.29	43.76	.7532	.4025
41.80	60.34	.7421	.5637	41.70	49.81	.7643	.3527
43.25	61.62	.7416	.5580	45.37	53.70	.7728	.3540
44.57	62.74	.7473	.5423	47.14	55.56	.7747	.3698
46.03	63.96	.7514	.5392	49.03	57.47	.7731	.3796
47.51	65.26	.7613	.5993	50.84	59.28	.7753	.3868
48.95	66.44	.7668	.5754	52.68	61.08	.7818	.4194
50.31	67.53	.7710	.5377	54.48	62.81	.7857	.4426
51.78	68.75	.7741	.4819	56.34	64.57	.7918	.4646
53.14	69.77	.7786	.5081	58.12	66.24	.7914	.4932
54.62	71.01	.7881	.5920	59.97	67.92	.7896	.5495
55.97	71.99	.7908	.5239	61.77	69.55	.7933	.5539
57.36	73.07	.7900	.4926	63.63	71.18	.7995	.4551
60.29	75.38	.7903	.5187	65.41	72.73	.8074	.4716
61.67	76.42	.7873	.5043	67.30	74.37	.8091	.4354
67.29	80.63	.7957	.5498	69.07	75.85	.8056	.4759
70.13	82.74	.7962	.5783	70.91	77.38	.7960	.5652
71.51	83.72	.8043	.5342	72.72	78.84	.7952	.6180
73.03	84.92	.8110	.5193	74.63	80.37	.8094	.5135
74.39	85.88	.8115	.4607	76.40	81.77	.8181	.4139
75.74	86.80	.8088	.4789	78.27	83.24	.8233	.3976
77.24	87.96	.7978	.5433	81.91	86.03	.8041	.5889
78.62	88.92	.7985	.5733	85.55	88.71	.8226	.3934
81.54	91.06	.8192	.4193	87.39	90.05	.8390	.3461
82.88	91.94	.8229	.4413	89.25	91.42	.8462	.4407
84.34	92.98	.8180	.4545	91.03	92.66	.8460	.6896
85.70	93.87	.8036	.4557	92.86	93.93	.8325	.7507
87.11	94.82	.7987	.5007	96.55	96.47	.8452	.5256
88.50	95.72	.8188	.3756				
89.92	96.63	.8383	.3356				
91.35	97.57	.8438	.2818				
94.24	99.40	.8309	.4719				
95.65	100.24	.8196	.3450				
97.03	101.02	.8431	.5808				

Table VIII (contd)
Heat transfer data for each run code

RUN CODE 44305

SUCTION SURFACE				PRESSURE SURFACE			
% Surface Distance	% Axial Chord	Tw/Tg	h/ho	% Surface Distance	% Axial Chord	Tw/Tg	h/ho
30.57	49.25	.7759	.4916	28.90	34.95	.7734	.6857
31.98	50.84	.7755	.6550	30.78	37.26	.7633	.6142
33.40	52.37	.7703	.6990	32.58	39.43	.7570	.5159
37.60	56.50	.7550	.6647	34.38	41.55	.7575	.4867
39.08	57.92	.7472	.6156	36.29	43.76	.7593	.4410
41.80	60.34	.7419	.5611	41.70	49.81	.7687	.3772
43.25	61.62	.7415	.5561	45.37	53.70	.7758	.3665
44.57	62.74	.7473	.5411	47.14	55.56	.7774	.3830
46.03	63.96	.7515	.5385	49.03	57.47	.7753	.3939
47.51	65.26	.7615	.5972	50.84	59.28	.7772	.4016
48.95	66.44	.7667	.5656	52.68	61.08	.7829	.4280
50.31	67.53	.7709	.5296	54.48	62.81	.7862	.4472
51.78	68.75	.7740	.4754	56.34	64.57	.7918	.4651
53.14	69.77	.7785	.4996	58.12	66.24	.7908	.4867
54.62	71.01	.7878	.5784	59.97	67.92	.7886	.5421
55.97	71.99	.7905	.5125	61.77	69.55	.7919	.5465
57.36	73.07	.7899	.4833	63.63	71.18	.7976	.4445
60.29	75.38	.7901	.5124	65.41	72.73	.8050	.4532
61.67	76.42	.7869	.4986	67.30	74.37	.8064	.4118
67.29	80.63	.7948	.5443	69.07	75.85	.8029	.4525
70.13	82.74	.7949	.5707	70.91	77.38	.7933	.5437
71.51	83.72	.8029	.5278	72.72	78.84	.7925	.5970
73.03	84.92	.8097	.5242	74.63	80.37	.8063	.4916
74.39	85.88	.8099	.4591	76.40	81.77	.8148	.3899
75.74	86.80	.8074	.4784	78.27	83.24	.8196	.3692
77.24	87.96	.7963	.5415	81.91	86.03	.8007	.5581
78.62	88.92	.7967	.5676	85.55	88.71	.8189	.3604
81.54	91.06	.8168	.4160	87.39	90.05	.8352	.3106
82.88	91.94	.8206	.4422	89.25	91.42	.8425	.4097
84.34	92.98	.8159	.4606	91.03	92.66	.8422	.6425
85.70	93.87	.8016	.4553	92.86	93.93	.8290	.7059
87.11	94.82	.7966	.4955	96.55	96.47	.8415	.4737
88.50	95.72	.8168	.3856				
89.92	96.63	.8360	.3483				
91.35	97.57	.8413	.2915				
94.24	99.40	.8286	.4782				
95.65	100.24	.8174	.3501				
97.03	101.02	.8407	.5971				

Table VIII (contd)
Heat transfer data for each run code

RUN CODE 44306

SUCTION SURFACE				PRESSURE SURFACE			
% Surface Distance	% Axial Chord	Tw/Tg	h/ho	% Surface Distance	% Axial Chord	Tw/Tg	h/ho
30.57	49.25	.7516	.3771	28.90	34.95	.7669	.8652
31.98	50.84	.7535	.6314	30.78	37.26	.7556	.7559
33.40	52.37	.7498	.7171	32.58	39.43	.7488	.6367
37.60	56.50	.7325	.6910	34.38	41.55	.7489	.5927
39.08	57.92	.7234	.6369	36.29	43.76	.7515	.5599
41.80	60.34	.7174	.5778	41.70	49.81	.7590	.4658
43.25	61.62	.7163	.5661	45.37	53.70	.7645	.4431
44.57	62.74	.7221	.5452	47.14	55.56	.7653	.4606
46.03	63.96	.7264	.5381	49.03	57.47	.7617	.4692
47.51	65.26	.7380	.5973	50.84	59.28	.7627	.4742
48.95	66.44	.7442	.5724	52.68	61.08	.7688	.5149
50.31	67.53	.7486	.5301	54.48	62.81	.7702	.5223
51.78	68.75	.7518	.4727	56.34	64.57	.7754	.5210
53.14	69.77	.7562	.4937	58.12	66.24	.7734	.5450
54.62	71.01	.7666	.5694	59.97	67.92	.7701	.5986
55.97	71.99	.7693	.5084	61.77	69.55	.7725	.5979
57.36	73.07	.7691	.4795	63.63	71.18	.7779	.4878
60.29	75.38	.7669	.5082	65.41	72.73	.7856	.5001
61.67	76.42	.7639	.4992	67.30	74.37	.7861	.4534
67.29	80.63	.7723	.5486	69.07	75.85	.7807	.4830
70.13	82.74	.7708	.5700	70.91	77.38	.7685	.5743
71.51	83.72	.7796	.5230	72.72	78.84	.7675	.6352
73.03	84.92	.7868	.5045	74.63	80.37	.7829	.5297
74.39	85.88	.7872	.4591	76.40	81.77	.7926	.4304
75.74	86.80	.7829	.4737	78.27	83.24	.7971	.3987
77.24	87.96	.7698	.5331	81.91	86.03	.7725	.5728
78.62	88.92	.7696	.5632	85.55	88.71	.7929	.3816
81.54	91.06	.7926	.4134	87.39	90.05	.8119	.3399
82.88	91.94	.7964	.4352	89.25	91.42	.8196	.4331
84.34	92.98	.7900	.4505	91.03	92.66	.8185	.6794
85.70	93.87	.7728	.4554	92.86	93.93	.8015	.7387
87.11	94.82	.7659	.4904	96.55	96.47	.8156	.4913
88.50	95.72	.7890	.3728				
89.92	96.63	.8117	.3424				
91.35	97.57	.8173	.2846				
94.24	99.40	.8006	.4828				
95.65	100.24	.7866	.3677				
97.03	101.02	.8137	.5821				

Table VIII (contd)
Heat transfer data for each run code

RUN CODE 44307

SUCTION SURFACE				PRESSURE SURFACE			
% Surface Distance	% Axial Chord	Tw/Tg	h/ho	% Surface Distance	% Axial Chord	Tw/Tg	h/ho
30.57	49.25	.7568	.4031	28.90	34.95	.7781	.9920
31.98	50.84	.7596	.6788	30.78	37.26	.7685	.8740
33.40	52.37	.7571	.7766	32.58	39.43	.7621	.7378
37.60	56.50	.7397	.7465	34.38	41.55	.7627	.6893
39.08	57.92	.7305	.6861	36.29	43.76	.7655	.6547
41.80	60.34	.7242	.6193	41.70	49.81	.7724	.5380
43.25	61.62	.7233	.6087	45.37	53.70	.7772	.5047
44.57	62.74	.7294	.5869	47.14	55.56	.7779	.5266
46.03	63.96	.7339	.5775	49.03	57.47	.7737	.5381
47.51	65.26	.7456	.6357	50.84	59.28	.7745	.5440
48.95	66.44	.7521	.6145	52.68	61.08	.7800	.5807
50.31	67.53	.7566	.5671	54.48	62.81	.7807	.5841
51.78	68.75	.7597	.5031	56.34	64.57	.7856	.5792
53.14	69.77	.7643	.5267	58.12	66.24	.7831	.6020
54.62	71.01	.7750	.6111	59.97	67.92	.7794	.6573
55.97	71.99	.7776	.5389	61.77	69.55	.7812	.6550
57.36	73.07	.7771	.5048	63.63	71.18	.7863	.5363
60.29	75.38	.7747	.5375	65.41	72.73	.7938	.5477
61.67	76.42	.7712	.5271	67.30	74.37	.7939	.4942
67.29	80.63	.7794	.5800	69.07	75.85	.7880	.5227
70.13	82.74	.7773	.5994	70.91	77.38	.7752	.6181
71.51	83.72	.7861	.5470	72.72	78.84	.7738	.6812
73.03	84.92	.7934	.5309	74.63	80.37	.7891	.5654
74.39	85.88	.7935	.4781	76.40	81.77	.7986	.4582
75.74	86.80	.7891	.4937	78.27	83.24	.8030	.4258
77.24	87.96	.7753	.5580	81.91	86.03	.7773	.6054
78.62	88.92	.7750	.5910	85.55	88.71	.7976	.4067
81.54	91.06	.7984	.4369	87.39	90.05	.8166	.3581
82.88	91.94	.8020	.4572	89.25	91.42	.8241	.4547
84.34	92.98	.7951	.4685	91.03	92.66	.8227	.7067
85.70	93.87	.7773	.4749	92.86	93.93	.8051	.7704
87.11	94.82	.7701	.5149	96.55	96.47	.8191	.5090
88.50	95.72	.7932	.3875				
89.92	96.63	.8163	.3574				
91.35	97.57	.8219	.2999				
94.24	99.40	.8044	.5068				
95.65	100.24	.7896	.3792				
97.03	101.02	.8174	.6095				

Table VIII (contd)
Heat transfer data for each run code

RUN CODE 44308

SUCTION SURFACE				PRESSURE SURFACE			
% Surface Distance	% Axial Chord	Tw/Tg	h/ho	% Surface Distance	% Axial Chord	Tw/Tg	h/ho
30.57	49.25	.7554	.3954	28.90	34.95	.7790	1.0201
31.98	50.84	.7587	.6844	30.78	37.26	.7703	.9107
33.40	52.37	.7553	.7750	32.58	39.43	.7643	.7721
37.60	56.50	.7382	.7424	34.38	41.55	.7650	.7222
39.08	57.92	.7291	.6852	36.29	43.76	.7677	.6818
41.80	60.34	.7235	.6290	41.70	49.81	.7742	.5593
43.25	61.62	.7223	.6130	45.37	53.70	.7789	.5271
44.57	62.74	.7283	.5882	47.14	55.56	.7795	.5487
46.03	63.96	.7327	.5790	49.03	57.47	.7752	.5632
47.51	65.26	.7447	.6414	50.84	59.28	.7760	.5735
48.95	66.44	.7511	.6147	52.68	61.08	.7813	.6060
50.31	67.53	.7556	.5667	54.48	62.81	.7815	.6062
51.78	68.75	.7588	.5034	56.34	64.57	.7862	.5987
53.14	69.77	.7634	.5267	58.12	66.24	.7834	.6197
54.62	71.01	.7743	.6105	59.97	67.92	.7795	.6781
55.97	71.99	.7770	.5397	61.77	69.55	.7813	.6762
57.36	73.07	.7765	.5063	63.63	71.18	.7860	.5504
60.29	75.38	.7740	.5428	65.41	72.73	.7934	.5629
61.67	76.42	.7707	.5342	67.30	74.37	.7932	.5044
67.29	80.63	.7784	.5833	69.07	75.85	.7873	.5357
70.13	82.74	.7759	.6025	70.91	77.38	.7742	.6357
71.51	83.72	.7848	.5495	72.72	78.84	.7727	.7011
73.03	84.92	.7922	.5356	74.63	80.37	.7880	.5821
74.39	85.88	.7923	.4827	76.40	81.77	.7974	.4697
75.74	86.80	.7877	.4968	78.27	83.24	.8017	.4373
77.24	87.96	.7733	.5585	81.91	86.03	.7753	.6197
78.62	88.92	.7728	.5899	85.55	88.71	.7952	.4114
81.54	91.06	.7965	.4349	87.39	90.05	.8142	.3588
82.88	91.94	.8000	.4572	89.25	91.42	.8219	.4633
84.34	92.98	.7931	.4728	91.03	92.66	.8203	.7268
85.70	93.87	.7744	.4705	92.86	93.93	.8020	.7848
87.11	94.82	.7670	.5148	96.55	96.47	.8160	.5050
88.50	95.72	.7908	.3924				
89.92	96.63	.8140	.3613				
91.35	97.57	.8197	.3055				
94.24	99.40	.8011	.5099				
95.65	100.24	.7858	.3815				
97.03	101.02	.8146	.6279				

Table VIII (contd)
Heat transfer data for each run code

RUN CODE 44333

SUCTION SURFACE				PRESSURE SURFACE			
% Surface Distance	% Axial Chord	Tw/Tg	h/ho	% Surface Distance	% Axial Chord	Tw/Tg	h/ho
30.57	49.25	.7669	.5424	28.90	34.95	.7523	.5450
31.98	50.84	.7665	.6716	30.78	37.26	.7410	.4833
33.40	52.37	.7607	.6904	32.58	39.43	.7353	.4128
37.60	56.50	.7449	.6370	34.38	41.55	.7369	.3990
39.08	57.92	.7374	.5935	36.29	43.76	.7398	.3639
41.80	60.34	.7320	.5421	41.70	49.81	.7536	.3350
43.25	61.62	.7317	.5382	45.37	53.70	.7634	.3447
44.57	62.74	.7378	.5266	47.14	55.56	.7658	.3600
46.03	63.96	.7422	.5274	49.03	57.47	.7649	.3743
47.51	65.26	.7523	.5859	50.84	59.28	.7678	.3883
48.95	66.44	.7576	.5566	52.68	61.08	.7747	.4166
50.31	67.53	.7620	.5230	54.48	62.81	.7791	.4457
51.78	68.75	.7652	.4700	56.34	64.57	.7861	.4748
53.14	69.77	.7699	.4970	58.12	66.24	.7857	.4955
54.62	71.01	.7795	.5803	59.97	67.92	.7842	.5568
55.97	71.99	.7820	.5102	61.77	69.55	.7886	.5667
57.36	73.07	.7815	.4783	63.63	71.18	.7949	.4671
60.29	75.38	.7818	.5041	65.41	72.73	.8030	.4842
61.67	76.42	.7790	.4891	67.30	74.37	.8048	.4484
67.29	80.63	.7886	.5346	69.07	75.85	.8014	.4889
70.13	82.74	.7898	.5690	70.91	77.38	.7916	.5796
71.51	83.72	.7981	.5208	72.72	78.84	.7911	.6356
73.03	84.92	.8050	.5041	74.63	80.37	.8056	.5315
74.39	85.88	.8056	.4484	76.40	81.77	.8142	.4278
75.74	86.80	.8027	.4627	78.27	83.24	.8197	.4132
77.24	87.96	.7915	.5242	81.91	86.03	.8001	.6013
78.62	88.92	.7923	.5549	85.55	88.71	.8187	.4001
81.54	91.06	.8140	.4059	87.39	90.05	.8354	.3530
82.88	91.94	.8180	.4302	89.25	91.42	.8428	.4589
84.34	92.98	.8131	.4443	91.03	92.66	.8423	.6913
85.70	93.87	.7983	.4420	92.86	93.93	.8284	.7507
87.11	94.82	.7931	.4820	96.55	96.47	.8412	.5267
88.50	95.72	.8143	.3686				
89.92	96.63	.8345	.3365				
91.35	97.57	.8400	.2778				
94.24	99.40	.8264	.4618				
95.65	100.24	.8147	.3289				
97.03	101.02	.8389	.5806				

Table VIII (contd)
Heat transfer data for each run code

RUN CODE 44344

SUCTION SURFACE				PRESSURE SURFACE			
% Surface Distance	% Axial Chord	Tw/Tg	h/ho	% Surface Distance	% Axial Chord	Tw/Tg	h/ho
30.57	49.25	.7711	.4825	28.90	34.95	.7627	.6039
31.98	50.84	.7707	.6403	30.78	37.26	.7516	.5309
33.40	52.37	.7654	.6783	32.58	39.43	.7455	.4482
37.60	56.50	.7499	.6371	34.38	41.55	.7463	.4256
39.08	57.92	.7427	.5951	36.29	43.76	.7485	.3840
41.80	60.34	.7377	.5485	41.70	49.81	.7602	.3429
43.25	61.62	.7374	.5431	45.37	53.70	.7689	.3442
44.57	62.74	.7432	.5284	47.14	55.56	.7710	.3614
46.03	63.96	.7473	.5256	49.03	57.47	.7700	.3759
47.51	65.26	.7572	.5826	50.84	59.28	.7724	.3886
48.95	66.44	.7625	.5553	52.68	61.08	.7789	.4160
50.31	67.53	.7667	.5207	54.48	62.81	.7827	.4395
51.78	68.75	.7699	.4690	56.34	64.57	.7890	.4628
53.14	69.77	.7745	.4931	58.12	66.24	.7886	.4862
54.62	71.01	.7837	.5703	59.97	67.92	.7868	.5464
55.97	71.99	.7864	.5057	61.77	69.55	.7911	.5558
57.36	73.07	.7857	.4761	63.63	71.18	.7972	.4579
60.29	75.38	.7858	.4997	65.41	72.73	.8050	.4690
61.67	76.42	.7829	.4849	67.30	74.37	.8066	.4304
67.29	80.63	.7918	.5310	69.07	75.85	.8033	.4714
70.13	82.74	.7925	.5592	70.91	77.38	.7939	.5647
71.51	83.72	.8008	.5140	72.72	78.84	.7935	.6220
73.03	84.92	.8078	.5055	74.63	80.37	.8075	.5161
74.39	85.88	.8084	.4481	76.40	81.77	.8160	.4140
75.74	86.80	.8058	.4653	78.27	83.24	.8213	.3998
77.24	87.96	.7948	.5277	81.91	86.03	.8023	.5895
78.62	88.92	.7956	.5561	85.55	88.71	.8205	.3922
81.54	91.06	.8162	.4022	87.39	90.05	.8368	.3442
82.88	91.94	.8202	.4274	89.25	91.42	.8437	.4308
84.34	92.98	.8152	.4385	91.03	92.66	.8434	.6847
85.70	93.87	.8010	.4442	92.86	93.93	.8295	.7208
87.11	94.82	.7961	.4885	96.55	96.47	.8419	.4893
88.50	95.72	.8163	.3647				
89.92	96.63	.8359	.3281				
91.35	97.57	.8413	.2744				
94.24	99.40	.8286	.4686				
95.65	100.24	.8172	.3410				
97.03	101.02	.8406	.5873				

Table VIII (contd)
Heat transfer data for each run code

RUN CODE 44355

SUCTION SURFACE				PRESSURE SURFACE			
% Surface Distance	% Axial Chord	Tw/Tg	h/ho	% Surface Distance	% Axial Chord	Tw/Tg	h/ho
30.57	49.25	.7689	.3857	28.90	34.95	.7704	.6774
31.98	50.84	.7693	.5866	30.78	37.26	.7602	.5964
33.40	52.37	.7644	.6446	32.58	39.43	.7537	.4964
37.60	56.50	.7493	.6197	34.38	41.55	.7539	.4641
39.08	57.92	.7423	.5797	36.29	43.76	.7556	.4187
41.80	60.34	.7375	.5345	41.70	49.81	.7655	.3644
43.25	61.62	.7373	.5307	45.37	53.70	.7731	.3593
44.57	62.74	.7432	.5160	47.14	55.56	.7748	.3738
46.03	63.96	.7474	.5123	49.03	57.47	.7731	.3860
47.51	65.26	.7572	.5684	50.84	59.28	.7755	.3973
48.95	66.44	.7626	.5414	52.68	61.08	.7817	.4267
50.31	67.53	.7668	.5066	54.48	62.81	.7851	.4475
51.78	68.75	.7699	.4547	56.34	64.57	.7910	.4675
53.14	69.77	.7744	.4781	58.12	66.24	.7905	.4938
54.62	71.01	.7837	.5542	59.97	67.92	.7887	.5512
55.97	71.99	.7863	.4885	61.77	69.55	.7924	.5559
57.36	73.07	.7858	.4588	63.63	71.18	.7981	.4529
60.29	75.38	.7860	.4866	65.41	72.73	.8056	.4658
61.67	76.42	.7834	.4740	67.30	74.37	.8071	.4273
67.29	80.63	.7924	.5236	69.07	75.85	.8037	.4690
70.13	82.74	.7930	.5514	70.91	77.38	.7945	.5618
71.51	83.72	.8011	.5073	72.72	78.84	.7940	.6174
73.03	84.92	.8080	.4948	74.63	80.37	.8078	.5127
74.39	85.88	.8086	.4414	76.40	81.77	.8162	.4107
75.74	86.80	.8060	.4590	78.27	83.24	.8211	.3904
77.24	87.96	.7950	.5179	81.91	86.03	.8026	.5780
78.62	88.92	.7956	.5433	85.55	88.71	.8204	.3772
81.54	91.06	.8162	.3956	87.39	90.05	.8367	.3311
82.88	91.94	.8202	.4204	89.25	91.42	.8439	.4294
84.34	92.98	.8155	.4357	91.03	92.66	.8435	.6498
85.70	93.87	.8016	.4385	92.86	93.93	.8305	.7319
87.11	94.82	.7971	.4886	96.55	96.47	.8423	.4822
88.50	95.72	.8172	.3712				
89.92	96.63	.8362	.3300				
91.35	97.57	.8416	.2730				
94.24	99.40	.8291	.4688				
95.65	100.24	.8181	.3520				
97.03	101.02	.8409	.5769				

Table VIII (contd)
Heat transfer data for each run code

RUN CODE 45000

SUCTION SURFACE				PRESSURE SURFACE			
% Surface Distance	% Axial Chord	Tw/Tg	h/ho	% Surface Distance	% Axial Chord	Tw/Tg	h/ho
30.57	49.25	.7978	1.0654	28.90	34.95	.7631	.7144
31.98	50.84	.7923	1.0570	30.78	37.26	.7513	.6525
33.40	52.37	.7860	1.0467	32.58	39.43	.7463	.5658
37.60	56.50	.7684	.9615	34.38	41.55	.7489	.5399
39.08	57.92	.7597	.8896	36.29	43.76	.7538	.5145
41.80	60.34	.7515	.7933	41.70	49.81	.7701	.4737
43.25	61.62	.7498	.7653	45.37	53.70	.7799	.4683
44.57	62.74	.7561	.7468	47.14	55.56	.7817	.4936
46.03	63.96	.7613	.7541	49.03	57.47	.7801	.5124
47.51	65.26	.7731	.8371	50.84	59.28	.7818	.5274
48.95	66.44	.7790	.7959	52.68	61.08	.7892	.5691
50.31	67.53	.7843	.7547	54.48	62.81	.7921	.5888
51.78	68.75	.7858	.6546	56.34	64.57	.7990	.6055
53.14	69.77	.7898	.6951	58.12	66.24	.7975	.6436
54.62	71.01	.8021	.8346	59.97	67.92	.7945	.7241
55.97	71.99	.8044	.7364	61.77	69.55	.7979	.7315
57.36	73.07	.8034	.6853	63.63	71.18	.8045	.5885
60.29	75.38	.8011	.7245	65.41	72.73	.8134	.5924
61.67	76.42	.7992	.7180	67.30	74.37	.8149	.5404
67.29	80.63	.8063	.7795	69.07	75.85	.8098	.5816
70.13	82.74	.8040	.8000	70.91	77.38	.7966	.6962
71.51	83.72	.8139	.7491	72.72	78.84	.7957	.7746
73.03	84.92	.8222	.7567	74.63	80.37	.8128	.6462
74.39	85.88	.8217	.6496	76.40	81.77	.8230	.5171
75.74	86.80	.8182	.6623	78.27	83.24	.8281	.4849
77.24	87.96	.8027	.7382	81.91	86.03	.8012	.7258
78.62	88.92	.8030	.7716	85.55	88.71	.8232	.4699
81.54	91.06	.8264	.5720	87.39	90.05	.8433	.4008
82.88	91.94	.8308	.6192	89.25	91.42	.8520	.5560
84.34	92.98	.8240	.6467	91.03	92.66	.8505	.8606
85.70	93.87	.8044	.6280	92.86	93.93	.8316	.9145
87.11	94.82	.7969	.6814	96.55	96.47	.8469	.5942
88.50	95.72	.8224	.5545				
89.92	96.63	.8463	.5100				
91.35	97.57	.8513	.4108				
94.24	99.40	.8338	.6813				
95.65	100.24	.8190	.5520				
97.03	101.02	.8469	.8080				

Table VIII (contd)
Heat transfer data for each run code

RUN CODE 45103

SUCTION SURFACE				PRESSURE SURFACE			
% Surface Distance	% Axial Chord	Tw/Tg	h/ho	% Surface Distance	% Axial Chord	Tw/Tg	h/ho
30.57	49.25	.7253	.2794	28.90	34.95	.7202	.4758
31.98	50.84	.7209	.3824	30.78	37.26	.7125	.4243
33.40	52.37	.7168	.4512	32.58	39.43	.7107	.3820
37.60	56.50	.7073	.5002	34.38	41.55	.7145	.3772
39.08	57.92	.7015	.4743	36.29	43.76	.7196	.3602
41.80	60.34	.6991	.4465	41.70	49.81	.7367	.3454
43.25	61.62	.6994	.4420	45.37	53.70	.7468	.3521
44.57	62.74	.7053	.4293	47.14	55.56	.7494	.3699
46.03	63.96	.7097	.4239	49.03	57.47	.7496	.3838
47.51	65.26	.7195	.4612	50.34	59.28	.7524	.3965
48.95	66.44	.7254	.4390	52.58	61.08	.7600	.4362
50.31	67.53	.7307	.4179	54.48	62.81	.7628	.4582
51.78	68.75	.7337	.3652	56.34	64.57	.7697	.4763
53.14	69.77	.7383	.3890	58.12	66.24	.7694	.5057
54.62	71.01	.7492	.4668	59.97	67.92	.7682	.5712
55.97	71.99	.7519	.4087	61.77	69.55	.7725	.5825
57.36	73.07	.7526	.3787	63.63	71.18	.7784	.4800
60.29	75.38	.7525	.4090	65.41	72.73	.7862	.4851
61.67	76.42	.7532	.4093	67.30	74.37	.7878	.4457
67.29	80.63	.7647	.4703	69.07	75.85	.7845	.4830
70.13	82.74	.7654	.4910	70.91	77.38	.7745	.5754
71.51	83.72	.7751	.4535	72.72	78.84	.7748	.6374
73.03	84.92	.7832	.4409	74.63	80.37	.7896	.5428
74.39	85.88	.7841	.3826	76.40	81.77	.7985	.4438
75.74	86.80	.7820	.4027	78.27	83.24	.8033	.4204
77.24	87.96	.7703	.4649	81.91	86.03	.7837	.6201
78.62	88.92	.7713	.4895	85.55	88.71	.8030	.4264
81.54	91.06	.7933	.3309	87.39	90.05	.8204	.3786
82.88	91.94	.7976	.3549	89.25	91.42	.8281	.4657
84.34	92.98	.7930	.3835	91.03	92.66	.8281	.7440
85.70	93.87	.7776	.3903	92.86	93.93	.8125	.7529
87.11	94.82	.7726	.4432	96.55	96.47	.8254	.5332
88.50	95.72	.7956	.3285				
89.92	96.63	.8156	.2641				
91.35	97.57	.8222	.2156				
94.24	99.40	.8089	.4260				
95.65	100.24	.7974	.3497				
97.03	101.02	.8209	.4875				

Table VIII (contd)
Heat transfer data for each run code

RUN CODE 45104

SUCTION SURFACE				PRESSURE SURFACE			
% Surface Distance	% Axial Chord	Tw/Tg	h/ho	% Surface Distance	% Axial Chord	Tw/Tg	h/ho
30.57	49.25	.7299	.2948	28.90	34.95	.7218	.4801
31.98	50.84	.7249	.3963	30.78	37.26	.7131	.4345
33.40	52.37	.7208	.4680	32.58	39.43	.7099	.3831
37.60	56.50	.7097	.5107	34.38	41.55	.7124	.3679
39.08	57.92	.7031	.4814	36.29	43.76	.7164	.3464
41.80	60.34	.6997	.4461	41.70	49.81	.7302	.3154
43.25	61.62	.6997	.4420	45.37	53.70	.7392	.3165
44.57	62.74	.7053	.4297	47.14	55.56	.7412	.3306
46.03	63.96	.7094	.4246	49.03	57.47	.7409	.3412
47.51	65.26	.7188	.4617	50.84	59.28	.7434	.3508
48.95	66.44	.7242	.4336	52.68	61.08	.7505	.3857
50.31	67.53	.7292	.4143	54.48	62.81	.7533	.4028
51.78	68.75	.7318	.3627	56.34	64.57	.7599	.4172
53.14	69.77	.7362	.3847	58.12	66.24	.7597	.4487
54.62	71.01	.7464	.4585	59.97	67.92	.7586	.5100
55.97	71.99	.7490	.4042	61.77	69.55	.7628	.5198
57.36	73.07	.7494	.3762	63.63	71.18	.7688	.4238
60.29	75.38	.7491	.4031	65.41	72.73	.7766	.4263
61.67	76.42	.7493	.4028	67.30	74.37	.7783	.3894
67.29	80.63	.7599	.4631	69.07	75.85	.7752	.4264
70.13	82.74	.7605	.4827	70.91	77.38	.7658	.5140
71.51	83.72	.7698	.4482	72.72	78.84	.7661	.5714
73.03	84.92	.7773	.4339	74.63	80.37	.7808	.4830
74.39	85.88	.7781	.3781	76.40	81.77	.7897	.3915
75.74	86.80	.7761	.3964	78.27	83.24	.7945	.3691
77.24	87.96	.7649	.4583	81.91	86.03	.7756	.5555
78.62	88.92	.7662	.4852	85.55	88.71	.7952	.3780
81.54	91.06	.7870	.3271	87.39	90.05	.8123	.3345
82.88	91.94	.7913	.3520	89.25	91.42	.8196	.4035
84.34	92.98	.7869	.3783	91.03	92.66	.8195	.6266
85.70	93.87	.7720	.3827	92.86	93.93	.8056	.6804
87.11	94.82	.7673	.4294	96.55	96.47	.8188	.4851
88.50	95.72	.7896	.3249				
89.92	96.63	.8092	.2672				
91.35	97.57	.8153	.2166				
94.24	99.40	.8028	.4062				
95.65	100.24	.7921	.3296				
97.03	101.02	.8152	.4727				

Table VIII (contd)
Heat transfer data for each run code

RUN CODE 45105

SUCTION SURFACE				PRESSURE SURFACE			
% Surface Distance	% Axial Chord	Tw/Tg	h/ho	% Surface Distance	% Axial Chord	Tw/Tg	h/ho
30.57	49.25	.7315	.2942	28.90	34.95	.7244	.5008
31.98	50.84	.7263	.3974	30.78	37.26	.7153	.4502
33.40	52.37	.7219	.4702	32.58	39.43	.7116	.3957
37.60	56.50	.7101	.5129	34.38	41.55	.7133	.3766
39.08	57.92	.7031	.4805	36.29	43.76	.7165	.3480
41.80	60.34	.6995	.4454	41.70	49.81	.7282	.3093
43.25	61.62	.6993	.4395	45.37	53.70	.7356	.3008
44.57	62.74	.7045	.4248	47.14	55.56	.7371	.3133
46.03	63.96	.7081	.4166	49.03	57.47	.7361	.3205
47.51	65.26	.7171	.4501	50.84	59.28	.7378	.3256
48.95	66.44	.7223	.4241	52.68	61.08	.7440	.3526
50.31	67.53	.7271	.4038	54.48	62.81	.7466	.3667
51.78	68.75	.7295	.3534	56.34	64.57	.7526	.3789
53.14	69.77	.7335	.3735	58.12	66.24	.7520	.4029
54.62	71.01	.7434	.4431	59.97	67.92	.7504	.4577
55.97	71.99	.7459	.3911	61.77	69.55	.7544	.4661
57.36	73.07	.7461	.3636	63.63	71.18	.7603	.3764
60.29	75.38	.7454	.3872	65.41	72.73	.7679	.3763
61.67	76.42	.7454	.3877	67.30	74.37	.7696	.3401
67.29	80.63	.7557	.4548	69.07	75.85	.7666	.3742
70.13	82.74	.7559	.4688	70.91	77.38	.7574	.4566
71.51	83.72	.7647	.4370	72.72	78.84	.7577	.5093
73.03	84.92	.7718	.4167	74.63	80.37	.7719	.4223
74.39	85.88	.7727	.3718	76.40	81.77	.7806	.3363
75.74	86.80	.7711	.3941	78.27	83.24	.7854	.3164
77.24	87.96	.7600	.4505	81.91	86.03	.7673	.4918
78.62	88.92	.7610	.4712	85.55	88.71	.7862	.3235
81.54	91.06	.7807	.3226	87.39	90.05	.8027	.2757
82.88	91.94	.7845	.3403	89.25	91.42	.8104	.3515
84.34	92.98	.7807	.3730	91.03	92.66	.8109	.5648
85.70	93.87	.7665	.3769	92.86	93.93	.7976	.6029
87.11	94.82	.7619	.4177	96.55	96.47	.8101	.4062
88.50	95.72	.7829	.3183				
89.92	96.63	.8014	.2592				
91.35	97.57	.8073	.2091				
94.24	99.40	.7961	.3865				
95.65	100.24	.7862	.3197				
97.03	101.02	.8081	.4553				

Table VIII (contd)
Heat transfer data for each run code

RUN CODE 45135							
SUCTION SURFACE				PRESSURE SURFACE			
% Surface Distance	% Axial Chord	Tw/Tg	h/ho	% Surface Distance	% Axial Chord	Tw/Tg	h/ho
30.57	49.25	.7154	.2042	28.90	34.95	.7110	.4465
31.98	50.84	.7117	.3197	30.78	37.26	.7033	.3949
33.40	52.37	.7085	.3990	32.58	39.43	.7005	.3477
37.60	56.50	.6992	.4549	34.38	41.55	.7027	.3325
39.08	57.92	.6933	.4297	36.29	43.76	.7061	.3061
41.80	60.34	.6905	.4022	41.70	49.81	.7187	.2745
43.25	61.62	.6908	.3973	45.37	53.70	.7266	.2693
44.57	62.74	.6960	.3843	47.14	55.56	.7283	.2780
46.03	63.96	.6998	.3769	49.03	57.47	.7279	.2856
47.51	65.26	.7085	.4077	50.84	59.28	.7302	.2937
48.95	66.44	.7137	.3886	52.68	61.08	.7366	.3201
50.31	67.53	.7181	.3649	54.48	62.81	.7391	.3310
51.78	68.75	.7208	.3202	56.34	64.57	.7450	.3403
53.14	69.77	.7250	.3392	58.12	66.24	.7450	.3678
54.62	71.01	.7345	.4029	59.97	67.92	.7437	.4169
55.97	71.99	.7367	.3530	61.77	69.55	.7479	.4237
57.36	73.07	.7375	.3276	63.63	71.18	.7539	.3439
60.29	75.38	.7376	.3522	65.41	72.73	.7612	.3403
61.67	76.42	.7380	.3525	67.30	74.37	.7633	.3111
67.29	80.63	.7485	.4101	69.07	75.85	.7609	.3453
70.13	82.74	.7494	.4272	70.91	77.38	.7526	.4215
71.51	83.72	.7581	.3985	72.72	78.84	.7531	.4695
73.03	84.92	.7650	.3804	74.63	80.37	.7668	.3908
74.39	85.88	.7660	.3358	76.40	81.77	.7751	.3096
75.74	86.80	.7649	.3581	78.27	83.24	.7796	.2879
77.24	87.96	.7548	.4141	81.91	86.03	.7631	.4508
78.62	88.92	.7562	.4352	85.55	88.71	.7811	.2914
81.54	91.06	.7750	.2940	87.39	90.05	.7970	.2506
82.88	91.94	.7789	.3115	89.25	91.42	.8042	.3097
84.34	92.98	.7753	.3396	91.03	92.66	.8047	.4815
85.70	93.87	.7623	.3464	92.86	93.93	.7933	.5391
87.11	94.82	.7583	.3834	96.55	96.47	.8055	.3848
88.50	95.72	.7782	.2917				
89.92	96.63	.7959	.2388				
91.35	97.57	.8016	.1904				
94.24	99.40	.7923	.3625				
95.65	100.24	.7834	.3055				
97.03	101.02	.8030	.3950				

Table VIII (contd)
Heat transfer data for each run code

RUN CODE 45145

SUCTION SURFACE				PRESSURE SURFACE			
% Surface Distance	% Axial Chord	Tw/Tg	h/ho	% Surface Distance	% Axial Chord	Tw/Tg	h/ho
30.57	49.25	.7165	.1982	28.90	34.95	.7149	.4752
31.98	50.84	.7131	.3242	30.78	37.26	.7071	.4188
33.40	52.37	.7098	.4057	32.58	39.43	.7039	.3631
37.60	56.50	.7007	.4637	34.38	41.55	.7061	.3466
39.08	57.92	.6950	.4393	36.29	43.76	.7093	.3161
41.80	60.34	.6926	.4152	41.70	49.81	.7224	.2875
43.25	61.62	.6928	.4084	45.37	53.70	.7305	.2843
44.57	62.74	.6982	.3945	47.14	55.56	.7323	.2943
46.03	63.96	.7020	.3865	49.03	57.47	.7318	.3028
47.51	65.26	.7108	.4166	50.84	59.28	.7342	.3114
48.95	66.44	.7161	.3968	52.68	61.08	.7408	.3397
50.31	67.53	.7208	.3756	54.48	62.81	.7433	.3520
51.78	68.75	.7235	.3284	56.34	64.57	.7494	.3624
53.14	69.77	.7276	.3484	58.12	66.24	.7492	.3899
54.62	71.01	.7375	.4156	59.97	67.92	.7478	.4427
55.97	71.99	.7399	.3638	61.77	69.55	.7522	.4505
57.36	73.07	.7404	.3371	63.63	71.18	.7580	.3655
60.29	75.38	.7404	.3626	65.41	72.73	.7654	.3617
61.67	76.42	.7409	.3634	67.30	74.37	.7671	.3261
67.29	80.63	.7515	.4231	69.07	75.85	.7647	.3650
70.13	82.74	.7523	.4403	70.91	77.38	.7564	.4487
71.51	83.72	.7613	.4129	72.72	78.84	.7569	.4995
73.03	84.92	.7682	.3895	74.63	80.37	.7706	.4141
74.39	85.88	.7692	.3464	76.40	81.77	.7788	.3272
75.74	86.80	.7678	.3672	78.27	83.24	.7834	.3062
77.24	87.96	.7574	.4222	81.91	86.03	.7667	.4792
78.62	88.92	.7586	.4434	85.55	88.71	.7850	.3140
81.54	91.06	.7781	.3002	87.39	90.05	.8009	.2675
82.88	91.94	.7818	.3161	89.25	91.42	.8082	.3286
84.34	92.98	.7782	.3449	91.03	92.66	.8087	.5227
85.70	93.87	.7648	.3530	92.86	93.93	.7966	.5749
87.11	94.82	.7608	.3934	96.55	96.47	.8086	.3978
88.50	95.72	.7811	.2957				
89.92	96.63	.7996	.2470				
91.35	97.57	.8050	.1937				
94.24	99.40	.7948	.3673				
95.65	100.24	.7857	.3144				
97.03	101.02	.8060	.4132				

Table VIII (contd)
Heat transfer data for each run code

RUN CODE 45155

SUCTION SURFACE				PRESSURE SURFACE			
% Surface Distance	% Axial Chord	Tw/Tg	h/ho	% Surface Distance	% Axial Chord	Tw/Tg	h/ho
30.57	49.25	.7201	.2227	28.90	34.95	.7189	.5070
31.98	50.84	.7171	.3538	30.78	37.26	.7107	.4440
33.40	52.37	.7138	.4349	32.58	39.43	.7073	.3836
37.60	56.50	.7035	.4846	34.38	41.55	.7092	.3629
39.08	57.92	.6971	.4558	36.29	43.76	.7127	.3350
41.80	60.34	.6939	.4242	41.70	49.81	.7259	.3062
43.25	61.62	.6938	.4173	45.37	53.70	.7339	.3002
44.57	62.74	.6991	.4022	47.14	55.56	.7358	.3133
46.03	63.96	.7028	.3938	49.03	57.47	.7354	.3254
47.51	65.26	.7118	.4265	50.84	59.28	.7379	.3375
48.95	66.44	.7169	.4014	52.68	61.08	.7445	.3666
50.31	67.53	.7215	.3798	54.48	62.81	.7469	.3802
51.78	68.75	.7242	.3324	56.34	64.57	.7531	.3918
53.14	69.77	.7284	.3507	58.12	66.24	.7528	.4187
54.62	71.01	.7382	.4149	59.97	67.92	.7515	.4757
55.97	71.99	.7408	.3663	61.77	69.55	.7557	.4841
57.36	73.07	.7412	.3408	63.63	71.18	.7612	.3911
60.29	75.38	.7409	.3657	65.41	72.73	.7686	.3904
61.67	76.42	.7414	.3664	67.30	74.37	.7702	.3561
67.29	80.63	.7518	.4211	69.07	75.85	.7675	.3934
70.13	82.74	.7524	.4383	70.91	77.38	.7586	.4766
71.51	83.72	.7614	.4063	72.72	78.84	.7589	.5282
73.03	84.92	.7689	.3937	74.63	80.37	.7728	.4419
74.39	85.88	.7697	.3417	76.40	81.77	.7812	.3555
75.74	86.80	.7682	.3632	78.27	83.24	.7859	.3353
77.24	87.96	.7574	.4217	81.91	86.03	.7683	.5086
78.62	88.92	.7587	.4438	85.55	88.71	.7866	.3408
81.54	91.06	.7786	.2955	87.39	90.05	.8027	.2945
82.88	91.94	.7824	.3109	89.25	91.42	.8099	.3577
84.34	92.98	.7785	.3399	91.03	92.66	.8104	.5619
85.70	93.87	.7646	.3494	92.86	93.93	.7978	.6188
87.11	94.82	.7603	.3926	96.55	96.47	.8096	.4337
88.50	95.72	.7813	.2923				
89.92	96.63	.7996	.2326				
91.35	97.57	.8055	.1837				
94.24	99.40	.7947	.3668				
95.65	100.24	.7851	.3144				
97.03	101.02	.8057	.3997				

Table VIII (contd)
Heat transfer data for each run code

RUN CODE 45303

SUCTION SURFACE				PRESSURE SURFACE			
% Surface Distance	% Axial Chord	Tw/Tg	h/ho	% Surface Distance	% Axial Chord	Tw/Tg	h/ho
30.57	49.25	.7804	.7929	28.90	34.95	.7482	.5637
31.98	50.84	.7745	.8023	30.78	37.26	.7373	.5228
33.40	52.37	.7693	.8223	32.58	39.43	.7334	.4635
37.60	56.50	.7532	.7849	34.38	41.55	.7363	.4487
39.08	57.92	.7446	.7274	36.29	43.76	.7412	.4298
41.80	60.34	.7384	.6585	41.70	49.81	.7571	.3955
43.25	61.62	.7375	.6471	45.37	53.70	.7673	.4041
44.57	62.74	.7435	.6320	47.14	55.56	.7692	.4199
46.03	63.96	.7475	.6282	49.03	57.47	.7681	.4343
47.51	65.26	.7573	.6767	50.84	59.28	.7703	.4488
48.95	66.44	.7627	.6366	52.68	61.08	.7776	.4859
50.31	67.53	.7679	.6120	54.48	62.81	.7805	.5057
51.78	68.75	.7700	.5389	56.34	64.57	.7875	.5237
53.14	69.77	.7743	.5676	58.12	66.24	.7866	.5600
54.62	71.01	.7850	.6679	59.97	67.92	.7842	.6313
55.97	71.99	.7875	.5948	61.77	69.55	.7881	.6395
57.36	73.07	.7871	.5574	63.63	71.18	.7945	.5183
60.29	75.38	.7857	.5931	65.41	72.73	.8030	.5208
61.67	76.42	.7847	.5900	67.30	74.37	.8046	.4756
67.29	80.63	.7928	.6476	69.07	75.85	.8002	.5144
70.13	82.74	.7920	.6745	70.91	77.38	.7886	.6162
71.51	83.72	.8015	.6322	72.72	78.84	.7880	.6829
73.03	84.92	.8093	.6237	74.63	80.37	.8039	.5689
74.39	85.88	.8094	.5421	76.40	81.77	.8137	.4573
75.74	86.80	.8065	.5611	78.27	83.24	.8187	.4278
77.24	87.96	.7931	.6319	81.91	86.03	.7958	.6538
78.62	88.92	.7935	.6609	85.55	88.71	.8166	.4262
81.54	91.06	.8199	.4808	87.39	90.05	.8355	.3719
82.88	91.94	.8199	.5116	89.25	91.42	.8436	.4928
84.34	92.98	.8144	.5445	91.03	92.66	.8425	.7633
85.70	93.87	.7971	.5372	92.86	93.93	.8257	.8121
87.11	94.82	.7907	.5828	96.55	96.47	.8398	.5315
88.50	95.72	.8147	.4685				
89.92	96.63	.8365	.4159				
91.35	97.57	.8418	.3351				
94.24	99.40	.8267	.5835				
95.65	100.24	.8137	.4738				
97.03	101.02	.8393	.6912				

Table VIII (contd)
Heat transfer data for each run code

RUN CODE 45304

SUCTION SURFACE				PRESSURE SURFACE			
% Surface Distance	% Axial Chord	Tw/Tg	h/h ₀	% Surface Distance	% Axial Chord	Tw/Tg	h/h ₀
30.57	49.25	.7883	.8312	28.90	34.95	.7606	.6490
31.98	50.84	.7824	.8476	30.78	37.26	.7499	.6046
33.40	52.37	.7771	.8705	32.58	39.43	.7451	.5266
37.60	56.50	.7608	.8330	34.38	41.55	.7470	.4985
39.08	57.92	.7521	.7700	36.29	43.76	.7510	.4731
41.80	60.34	.7454	.6927	41.70	49.81	.7641	.4175
43.25	61.62	.7443	.6782	45.37	53.70	.7726	.4109
44.57	62.74	.7502	.6624	47.14	55.56	.7739	.4273
46.03	63.96	.7542	.6585	49.03	57.47	.7723	.4395
47.51	65.26	.7638	.7059	50.84	59.28	.7737	.4498
48.95	66.44	.7690	.6613	52.68	61.08	.7803	.4823
50.31	67.53	.7742	.6372	54.48	62.81	.7831	.4996
51.78	68.75	.7761	.5600	56.34	64.57	.7895	.5160
53.14	69.77	.7803	.5912	58.12	66.24	.7884	.5510
54.62	71.01	.7911	.6985	59.97	67.92	.7857	.6200
55.97	71.99	.7934	.6203	61.77	69.55	.7891	.6265
57.36	73.07	.7929	.5805	63.63	71.18	.7955	.5049
60.29	75.38	.7913	.6191	65.41	72.73	.8038	.5017
61.67	76.42	.7901	.6166	67.30	74.37	.8053	.4551
67.29	80.63	.7972	.6733	69.07	75.85	.8009	.4939
70.13	82.74	.7960	.7005	70.91	77.38	.7892	.5984
71.51	83.72	.8054	.6593	72.72	78.84	.7887	.6674
73.03	84.92	.8131	.6608	74.63	80.37	.8045	.5503
74.39	85.88	.8129	.5694	76.40	81.77	.8144	.4392
75.74	86.80	.8102	.5888	78.27	83.24	.8194	.4115
77.24	87.96	.7963	.6590	81.91	86.03	.7961	.6312
78.62	88.92	.7966	.6850	85.55	88.71	.8169	.4042
81.54	91.06	.8184	.5042	87.39	90.05	.8359	.3538
82.88	91.94	.8224	.5375	89.25	91.42	.8439	.4694
84.34	92.98	.8169	.5698	91.03	92.66	.8429	.7276
85.70	93.87	.7994	.5537	92.86	93.93	.8265	.8000
87.11	94.82	.7930	.5999	96.55	96.47	.8411	.5257
88.50	95.72	.8166	.4865				
89.92	96.63	.8382	.4380				
91.35	97.57	.8435	.3593				
94.24	99.40	.8284	.6013				
95.65	100.24	.8155	.4870				
97.03	101.02	.8411	.7138				

Table VIII (contd)
Heat transfer data for each run code

RUN CODE 45305

SUCTION SURFACE				PRESSURE SURFACE			
% Surface Distance	% Axial Chord	Tw/Tg	h/ho	% Surface Distance	% Axial Chord	Tw/Tg	h/ho
30.57	49.25	.7829	.7370	28.90	34.95	.7671	.7480
31.98	50.84	.7779	.7966	30.78	37.26	.7570	.6859
33.40	52.37	.7734	.8428	32.58	39.43	.7521	.5954
37.60	56.50	.7569	.8130	34.38	41.55	.7532	.5535
39.08	57.92	.7481	.7504	36.29	43.76	.7567	.5213
41.80	60.34	.7414	.6728	41.70	49.81	.7679	.4522
43.25	61.62	.7403	.6584	45.37	53.70	.7750	.4373
44.57	62.74	.7462	.6418	47.14	55.56	.7758	.4503
46.03	63.96	.7504	.6378	49.03	57.47	.7735	.4604
47.51	65.26	.7604	.6882	50.84	59.28	.7745	.4699
48.95	66.44	.7657	.6454	52.68	61.08	.7806	.5015
50.31	67.53	.7707	.6154	54.48	62.81	.7826	.5145
51.78	68.75	.7726	.5385	56.34	64.57	.7885	.5250
53.14	69.77	.7767	.5674	58.12	66.24	.7869	.5547
54.62	71.01	.7875	.6704	59.97	67.92	.7839	.6222
55.97	71.99	.7898	.5935	61.77	69.55	.7871	.6281
57.36	73.07	.7894	.5548	63.63	71.18	.7931	.5056
60.29	75.38	.7875	.5922	65.41	72.73	.8010	.5034
61.67	76.42	.7859	.5890	67.30	74.37	.8022	.4526
67.29	80.63	.7933	.6490	69.07	75.85	.7975	.4884
70.13	82.74	.7919	.6756	70.91	77.38	.7857	.5879
71.51	83.72	.8011	.6318	72.72	78.84	.7848	.6515
73.03	84.92	.8087	.6283	74.63	80.37	.8004	.5364
74.39	85.88	.8085	.5447	76.40	81.77	.8101	.4269
75.74	86.80	.8057	.5651	78.27	83.24	.8148	.3953
77.24	87.96	.7920	.6321	81.91	86.03	.7918	.6129
78.62	88.92	.7920	.6563	85.55	88.71	.8122	.3932
81.54	91.06	.8141	.4890	87.39	90.05	.8310	.3421
82.88	91.94	.8179	.5193	89.25	91.42	.8389	.4459
84.34	92.98	.8123	.5478	91.03	92.66	.8379	.7005
85.70	93.87	.7950	.5351	92.86	93.93	.8217	.7635
87.11	94.82	.7886	.5817	96.55	96.47	.8359	.4972
88.50	95.72	.8117	.4653				
89.92	96.63	.8327	.4081				
91.35	97.57	.8383	.3381				
94.24	99.40	.8239	.5859				
95.65	100.24	.8112	.4816				
97.03	101.02	.8360	.6772				

Table IX.
Discharge coefficient and blowing ratio data for
heat transfer runs

RUN CODE	SUCTION SIDE CD	SIDE BLR	LEADING EDGE CD	EDGE BLR	PRESSURE SIDE CD	SIDE BLR
34000	0.000	0.000	0.000	0.000	0.000	0.000
34103	0.668	0.862	0.000	0.000	0.796	1.486
34104	0.685	0.906	0.000	0.000	0.779	1.982
34105	0.667	0.916	0.000	0.000	0.748	2.538
34135	0.672	0.928	0.738	1.509	0.746	2.556
34145	0.666	0.917	0.735	2.197	0.743	2.528
34155	0.668	0.904	0.737	2.990	0.745	2.509
34303	0.656	0.724	0.000	0.000	0.732	1.246
34304	0.661	0.752	0.000	0.000	0.735	1.700
34305	0.682	0.813	0.000	0.000	0.738	2.265
43000	0.000	0.000	0.000	0.000	0.000	0.000
43103	0.734	0.930	0.000	0.000	0.753	1.345
43104	0.743	0.966	0.000	0.000	0.761	1.908
43105	0.744	1.000	0.000	0.000	0.758	2.449
43135	0.743	1.017	0.755	1.542	0.756	2.517
43145	0.748	1.015	0.755	2.285	0.755	2.449
43155	0.741	0.992	0.756	3.003	0.757	2.418
43303	0.740	0.820	0.000	0.000	0.779	1.344
43304	0.741	0.846	0.000	0.000	0.772	1.760
43305	0.761	0.905	0.000	0.000	0.767	2.353
44000	0.000	0.000	0.000	0.000	0.000	0.000
44103	0.668	0.830	0.000	0.000	0.760	1.338
44104	0.679	0.874	0.000	0.000	0.758	1.801
44105	0.730	0.974	0.000	0.000	0.778	2.531
44106	0.759	1.184	0.000	0.000	0.762	4.110
44107	0.823	1.453	0.000	0.000	0.754	5.267
44108	0.853	1.584	0.000	0.000	0.777	6.328
44133	0.673	0.843	0.756	1.493	0.765	1.375
44135	0.697	0.936	0.745	1.444	0.750	2.444
44144	0.680	0.873	0.749	2.163	0.757	1.852
44145	0.693	0.919	0.741	2.115	0.747	2.404
44155	0.697	0.941	0.743	2.962	0.748	2.463
44203	0.674	0.796	0.000	0.000	0.789	1.383
44204	0.679	0.821	0.000	0.000	0.770	1.805
44205	0.694	0.870	0.000	0.000	0.752	2.327
44303	0.672	0.753	0.000	0.000	0.785	1.333
44304	0.685	0.778	0.000	0.000	0.750	1.712
44305	0.695	0.827	0.000	0.000	0.734	2.229
44306	0.789	1.085	0.000	0.000	0.768	3.703
44307	0.828	1.230	0.000	0.000	0.768	4.571
44308	0.875	1.373	0.000	0.000	0.783	5.374
44333	0.669	0.742	0.776	1.474	0.788	1.316
44344	0.685	0.777	0.748	1.959	0.755	1.695
44355	0.696	0.832	0.732	2.641	0.735	2.223
45000	0.000	0.000	0.000	0.000	0.000	0.000
45103	0.723	0.904	0.000	0.000	0.772	1.375
45104	0.760	0.990	0.000	0.000	0.751	1.893
45105	0.796	1.075	0.000	0.000	0.759	2.497
45135	0.780	1.059	0.761	1.673	0.759	2.502
45145	0.759	1.025	0.753	2.248	0.752	2.426
45155	0.808	1.109	0.763	3.260	0.758	2.597
45303	0.730	0.802	0.000	0.000	0.744	1.223
45304	0.751	0.836	0.000	0.000	0.736	1.654
45305	0.770	0.909	0.000	0.000	0.738	2.241

APPENDIX B

HEAT TRANSFER DATA COMPARISON PLOTS

Figures 43-97 contain data comparison plots for the downstream and leading edge film-cooled C3X cascade. Figures 43 and 44 show normalized heat transfer coefficient distribution plots for the baseline (i.e., non-film cooling) runs. The remaining figures contain Stanton number reduction (SNR) plots for all combinations of the parametric variation. The figure titles describe which parameter is varied and display the run codes for the data series. For a complete explanation of the run code, refer to Test Conditions (Section III). The values of all parameters indicating which are kept constant and which ones are varied, are shown by the plot descriptor.

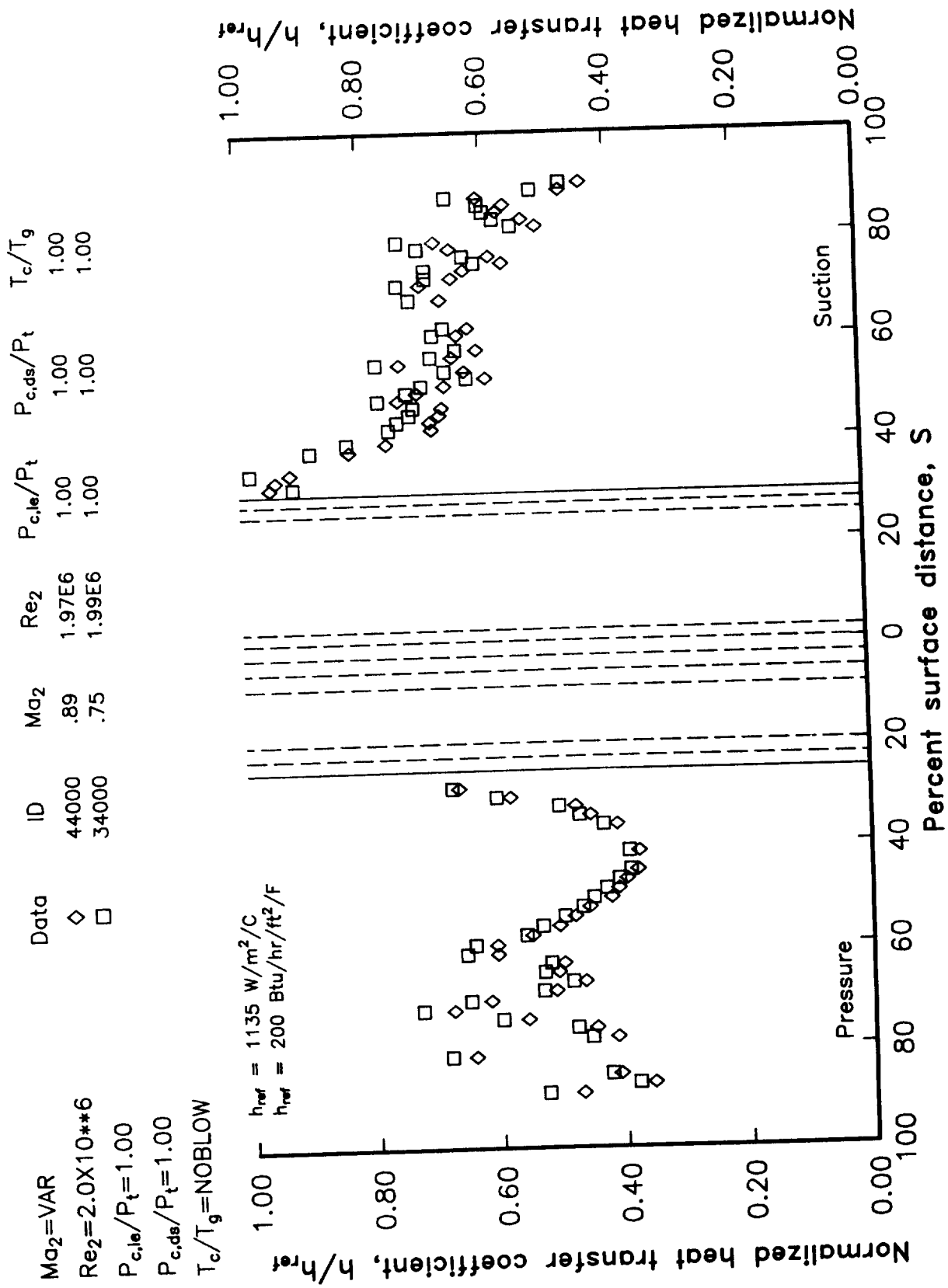


Figure 43. Heat transfer coefficient distribution for baseline runs 34000 and 44000.

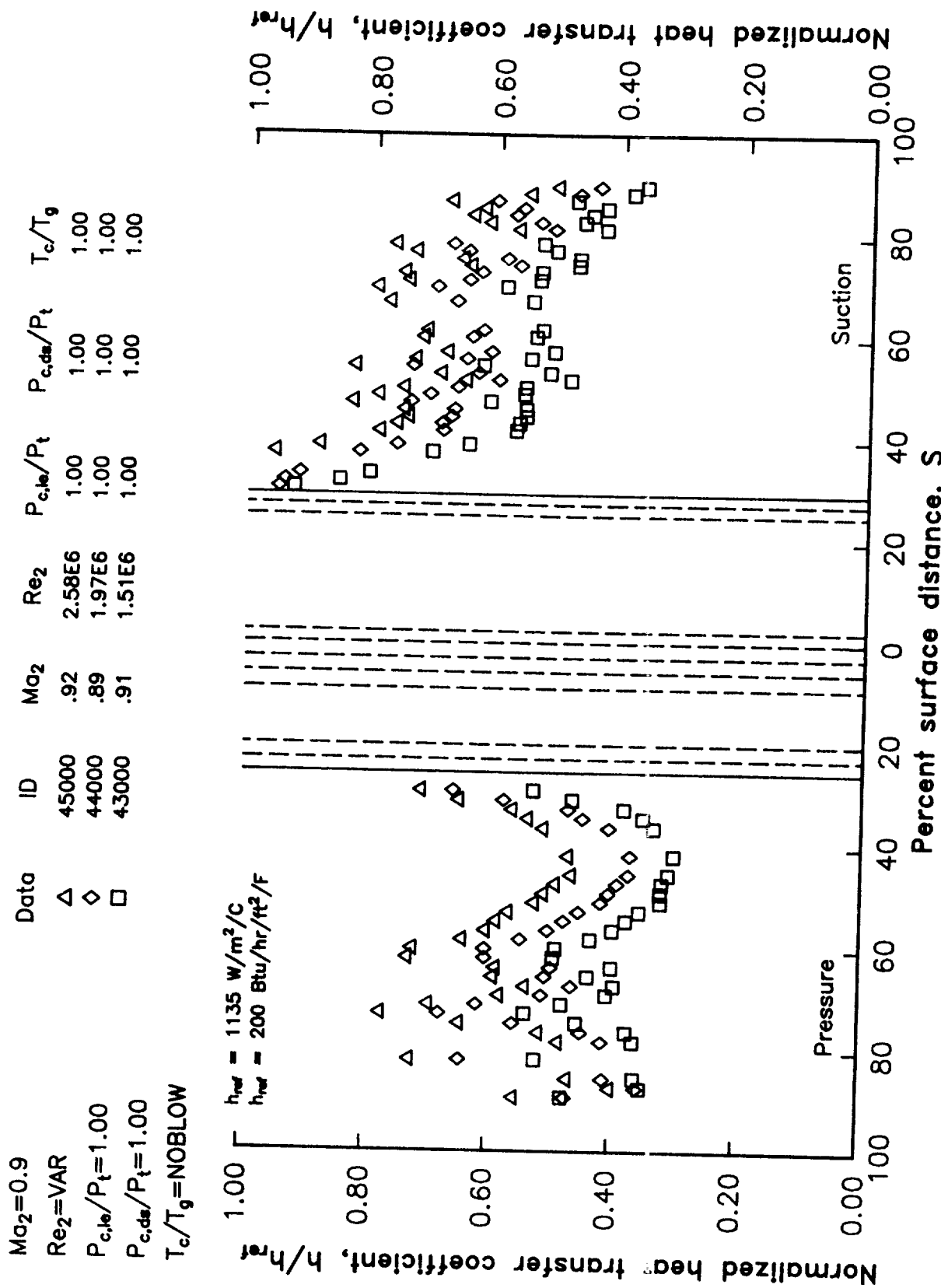


Figure 44. Heat transfer coefficient distribution for baseline runs 43000, 44000, and 45000.

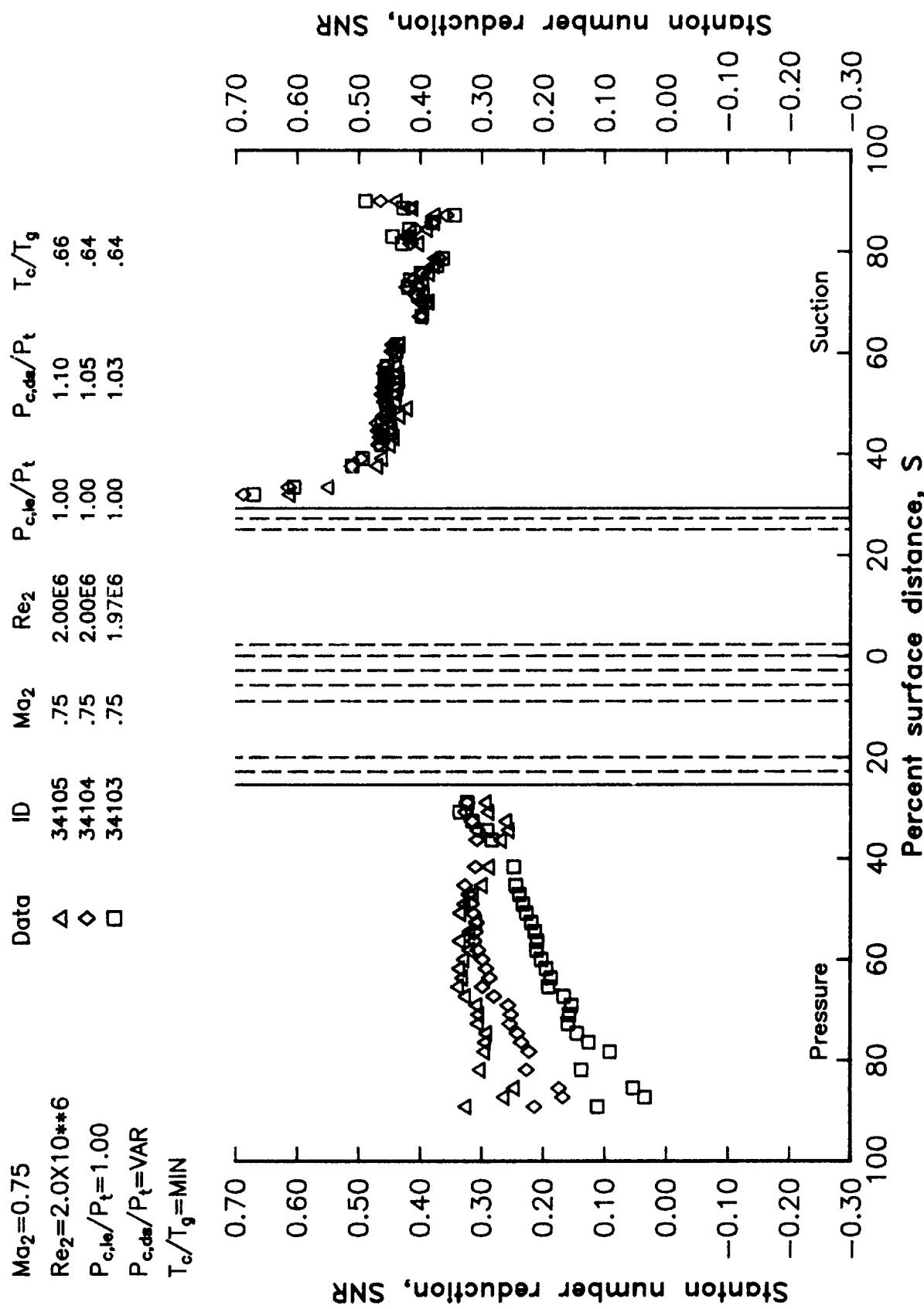


Figure 45. Effects of downstream coolant-to-gas pressure ratio variation on SNR distribution -- series 3410X.

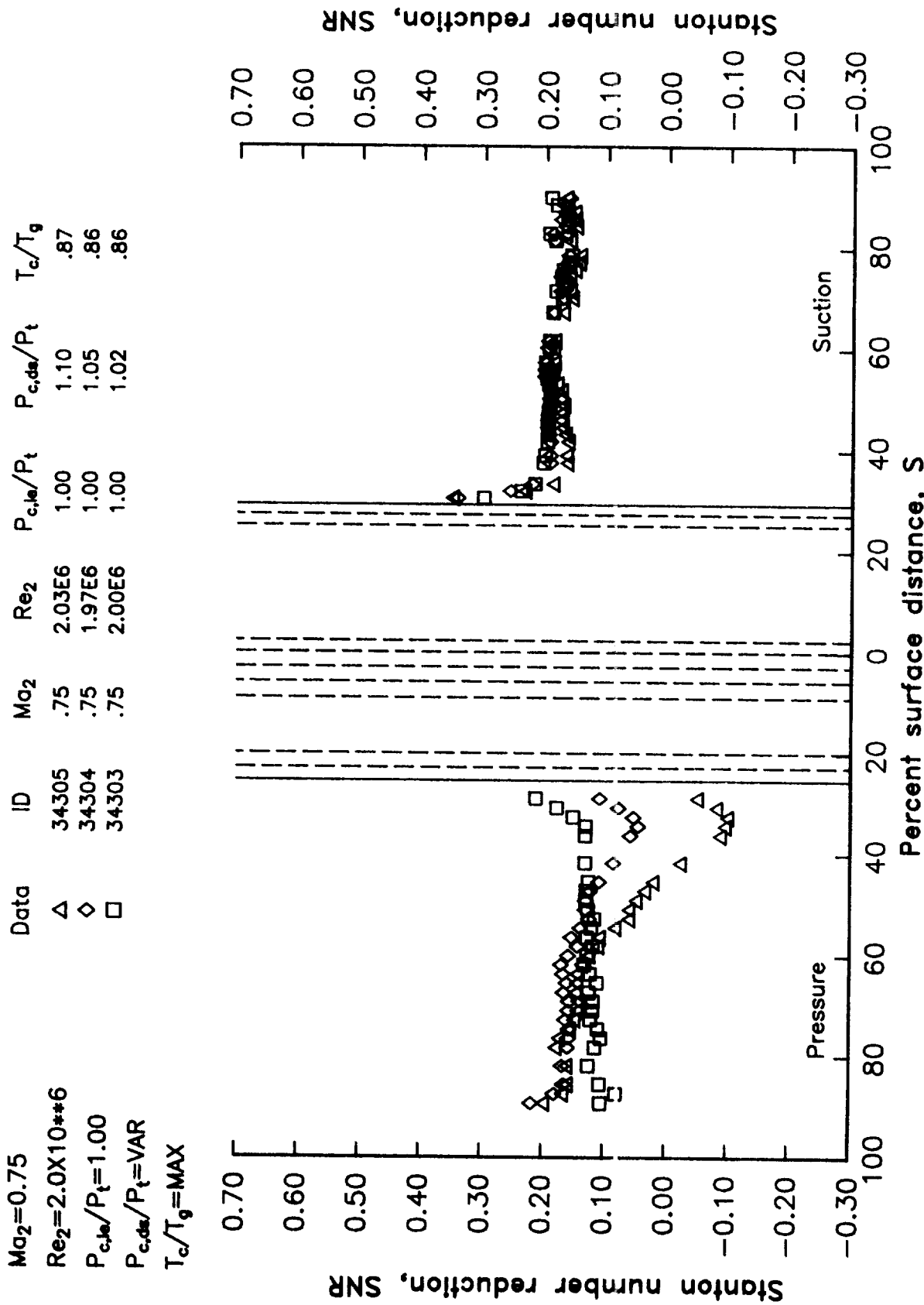


Figure 46. Effects of downstream coolant-to-gas pressure ratio variation on SNR distribution -- series 3430X .

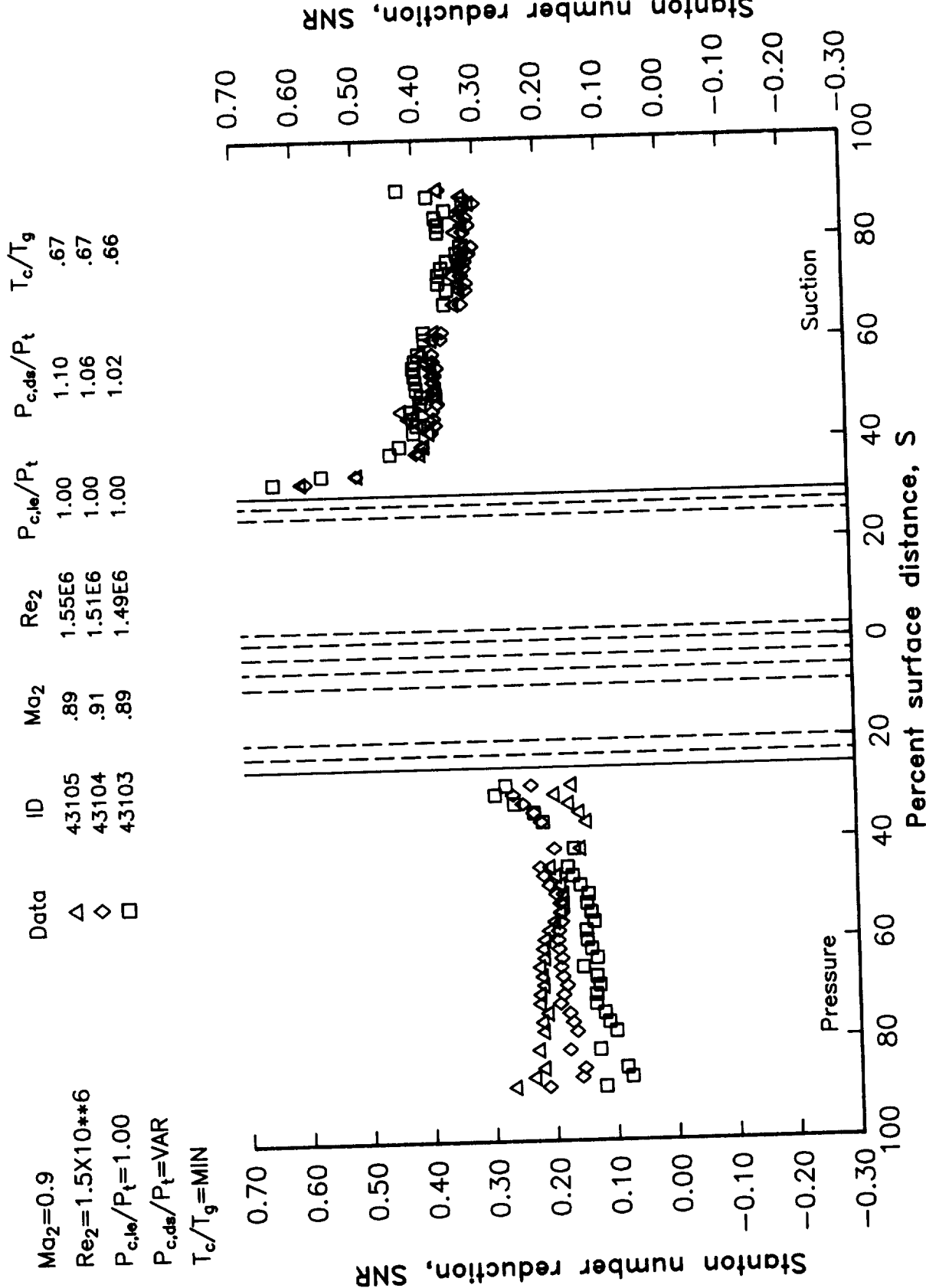


Figure 47. Effects of downstream coolant-to-gas pressure ratio variation on SNR distribution -- series 4310X.

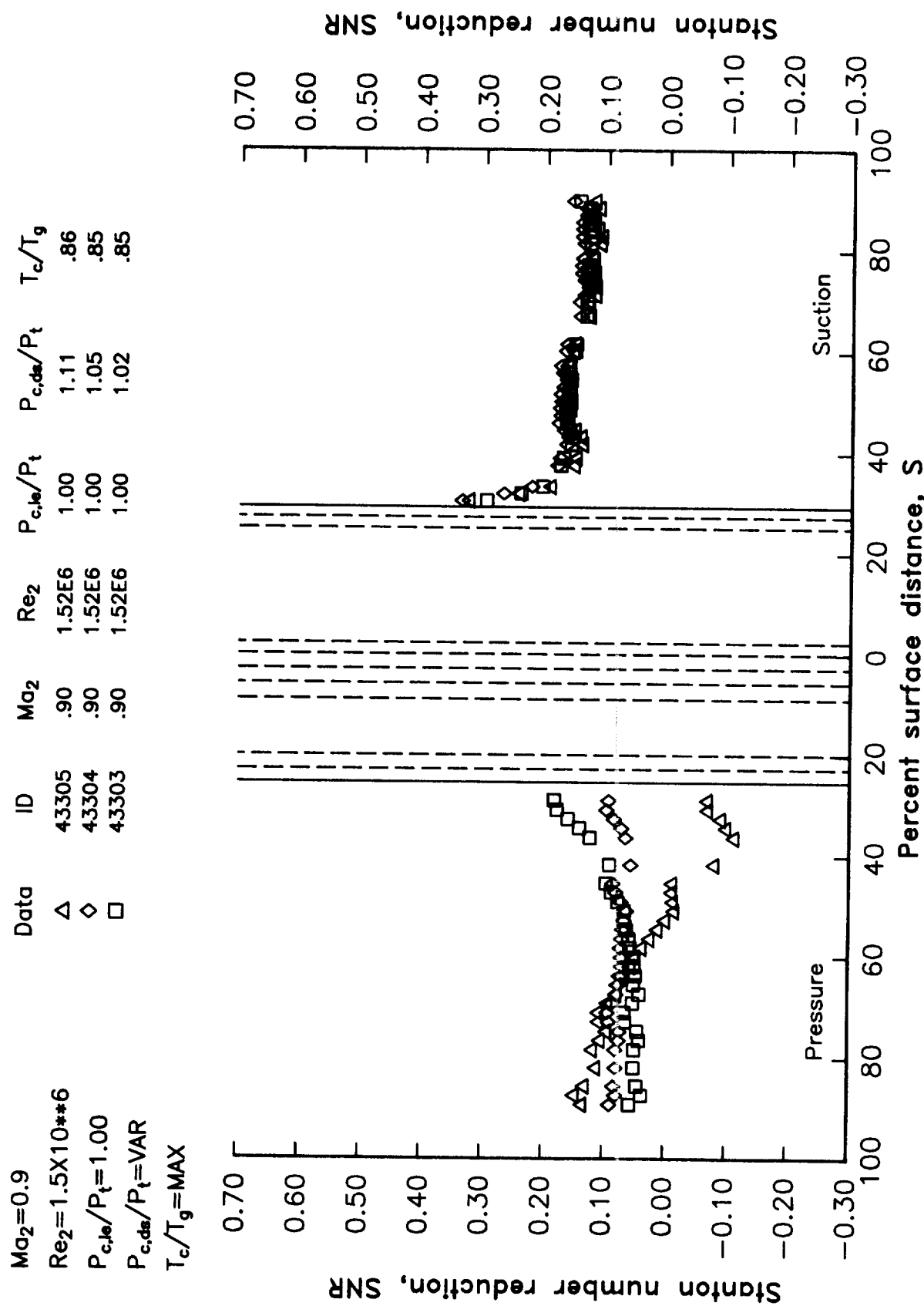


Figure 48. Effects of downstream coolant-to-gas pressure ratio variation on SNR distribution -- series 4330X.

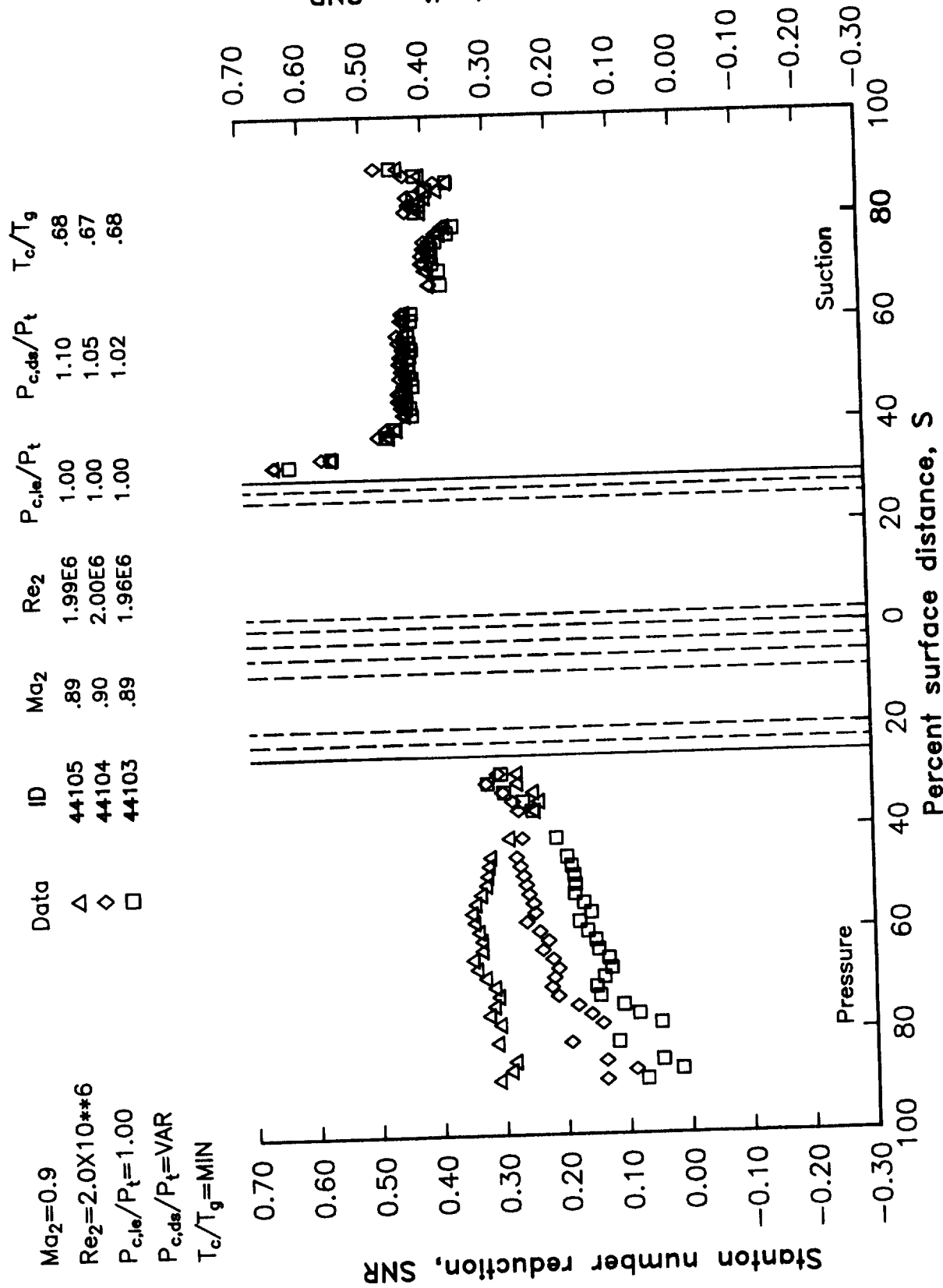


Figure 49. Effects of downstream coolant-to-gas pressure ratio variation on SNR distribution -- series 4410X ($P_c/P_t <= 1.10$).

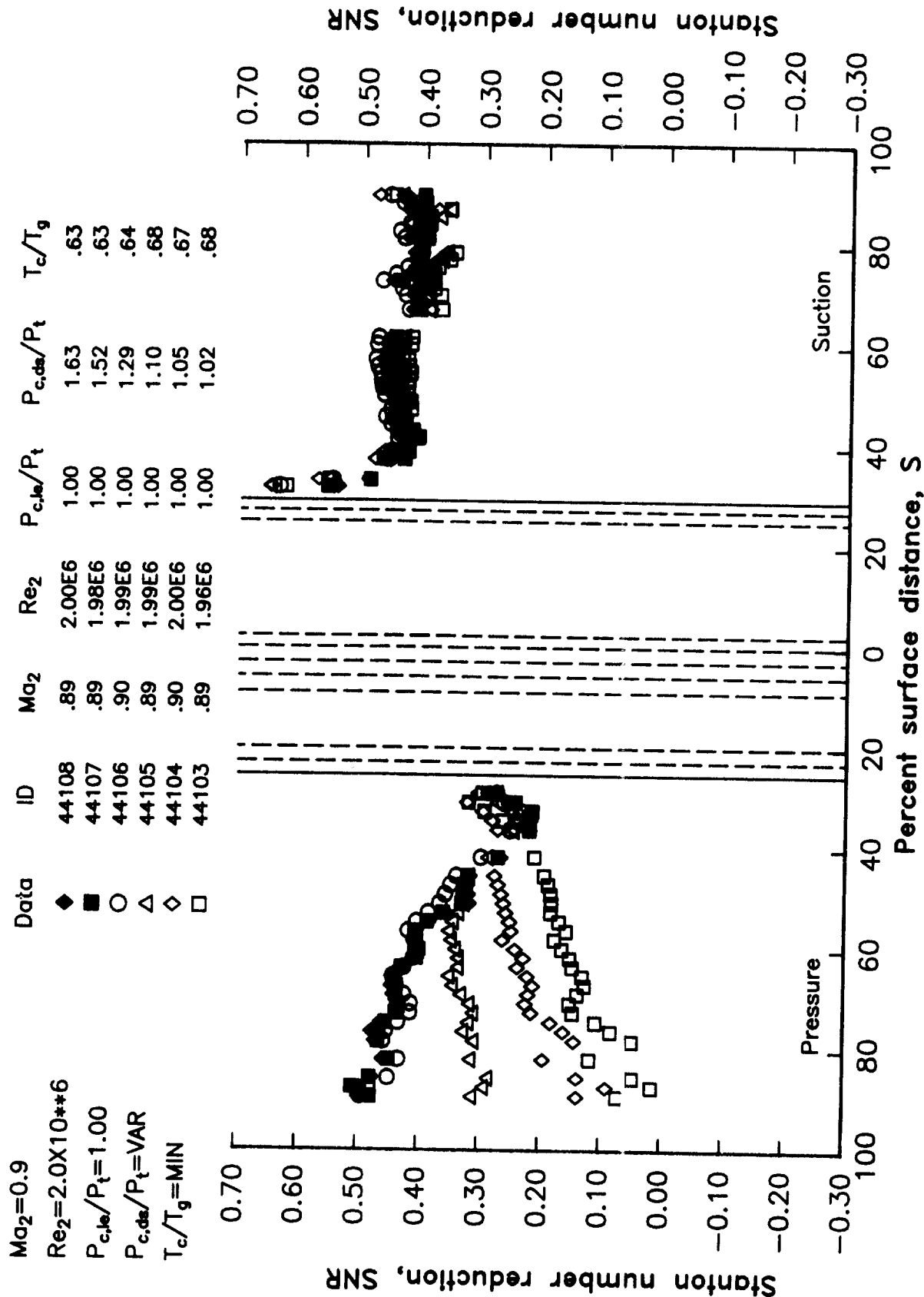


Figure 50. Effects of downstream coolant-to-gas pressure ratio variation on SNR distribution -- series 4410X.

$Ma_2 = 0.9$
 $Re_2 = 2.0 \times 10^{6}$
 $P_{c,le}/P_t = 1.00$
 $P_{c,de}/P_t = VAR$
 $T_c/T_g = MED$

Data	ID	Ma_2	Re_2	$P_{c,le}/P_t$	$P_{c,de}/P_t$	T_c/T_g
△	44205	.90	2.01E6	1.00	1.11	.77
◇	44204	.90	2.00E6	1.00	1.05	.76
□	44203	.90	1.99E6	1.00	1.02	.75

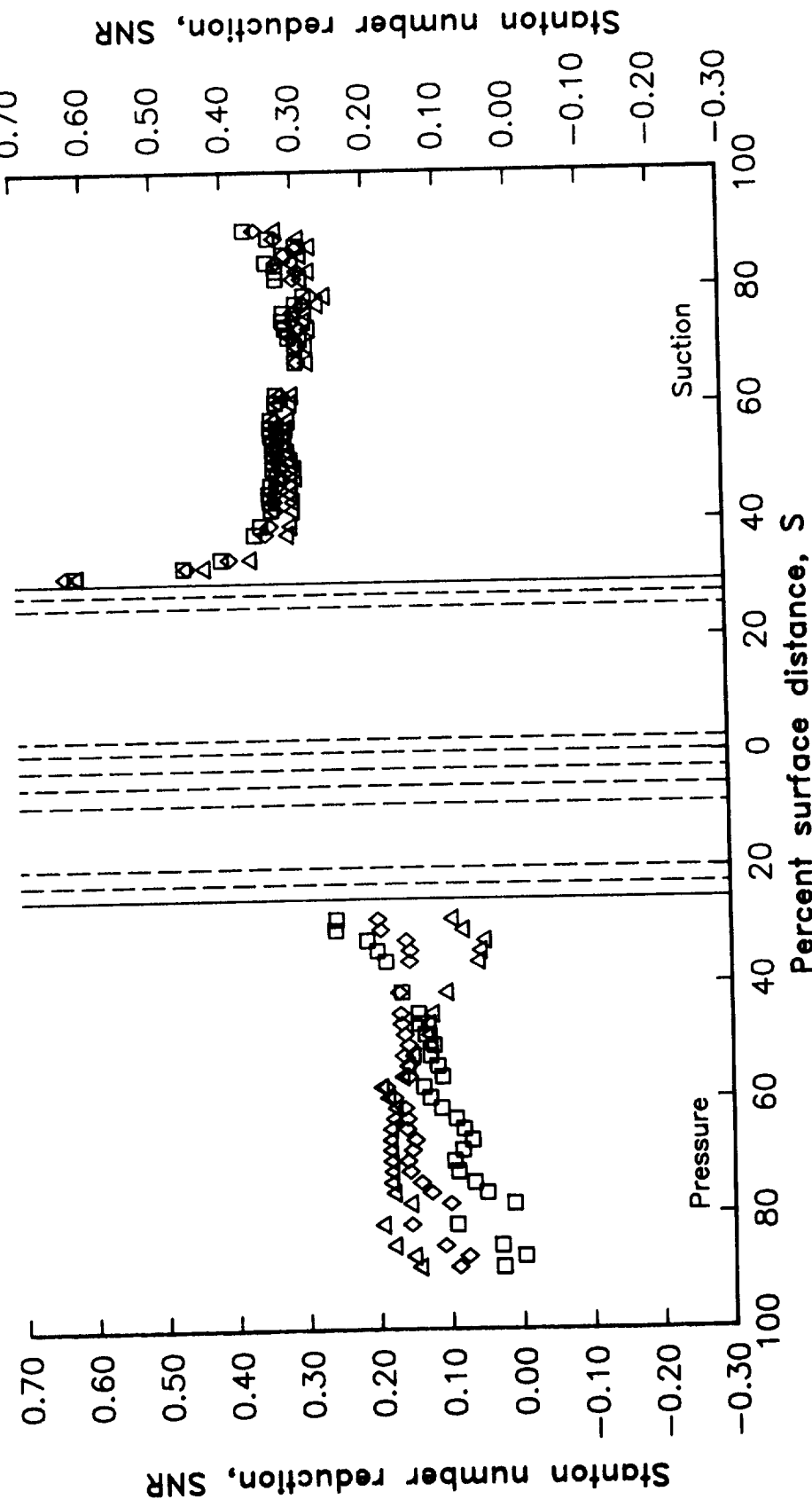


Figure 51. Effects of downstream coolant-to-gas pressure ratio variation on
SNR distribution -- series 4420X.

$Ma_2 = 0.9$
 $Re_2 = 2.0 \times 10^{**6}$
 $P_{c,lo}/P_t = 1.00$
 $P_{c,ds}/P_t = VAR$
 $T_c/T_g = MAX$

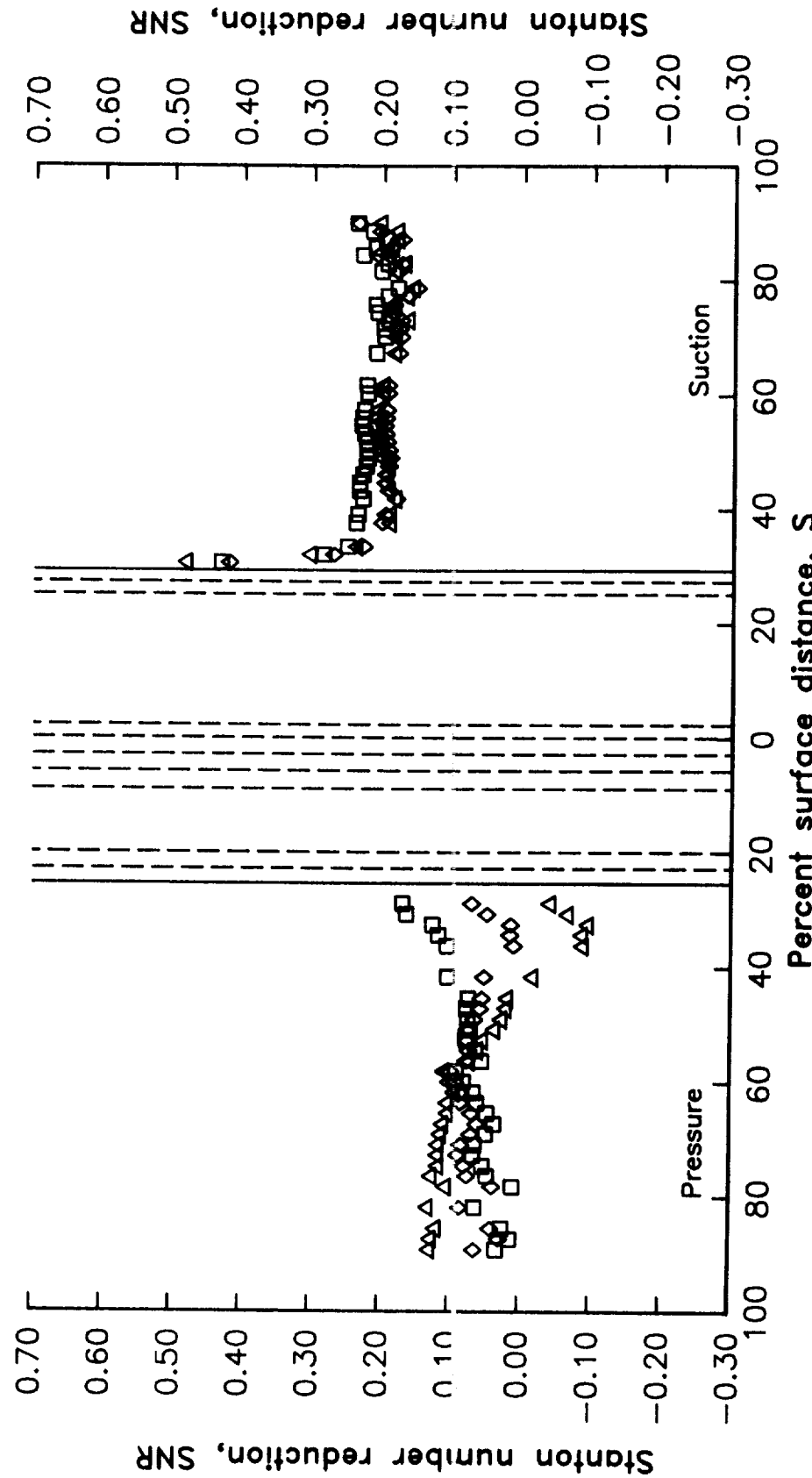


Figure 52. Effects of downstream coolant-to-gas pressure ratio variation on SNR distribution -- series 4430X ($P_c/P_t \leq 1.10$).

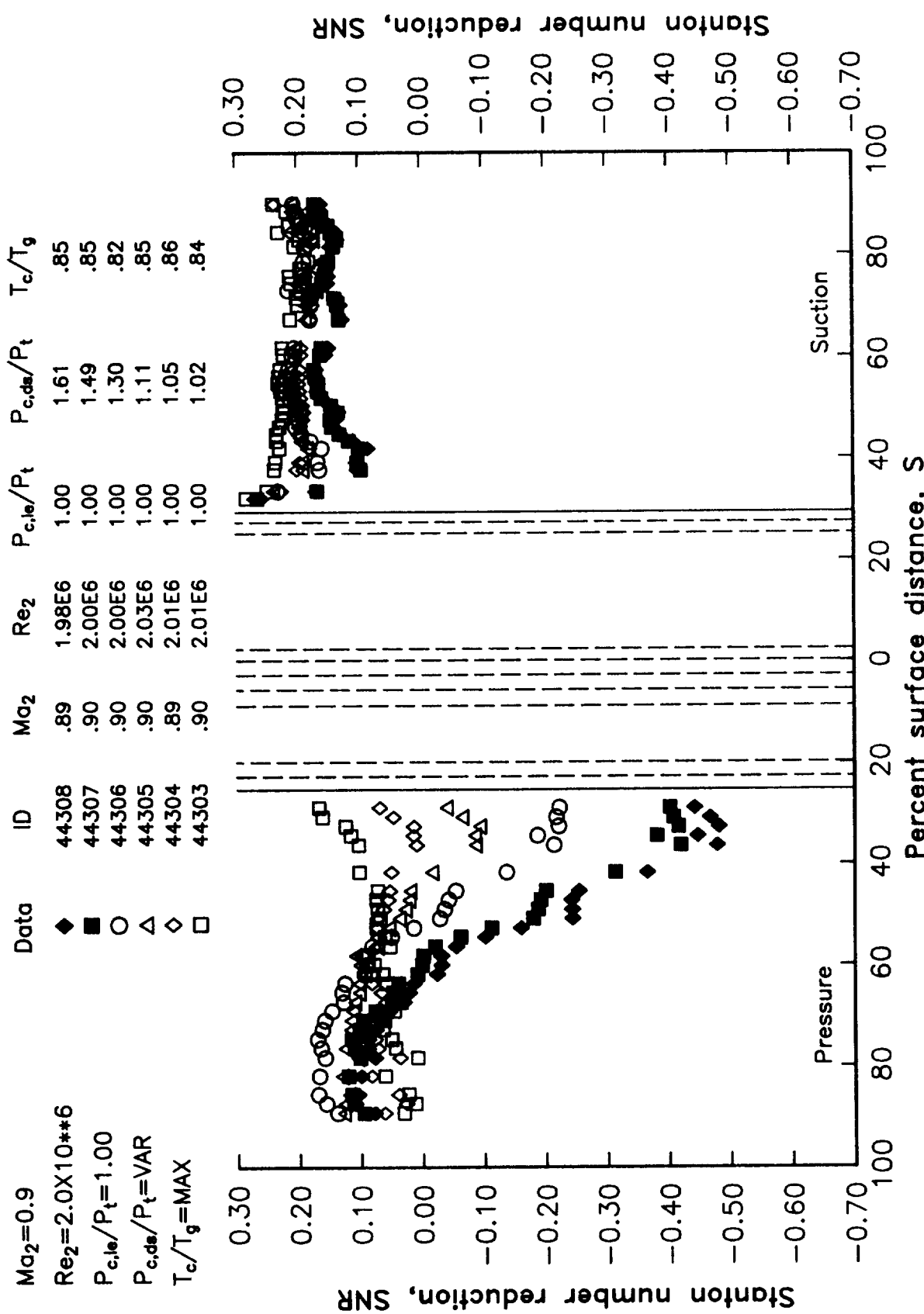


Figure 53. Effects of downstream coolant-to-gas pressure ratio variation on SNR distribution -- series 4430X.

$Ma_2 = 0.9$
 $Re_2 = 2.5 \times 10^{**6}$
 $P_{c,le}/P_t = 1.00$
 $P_{c,ds}/P_t = VAR$
 $T_c/T_g = MIN$

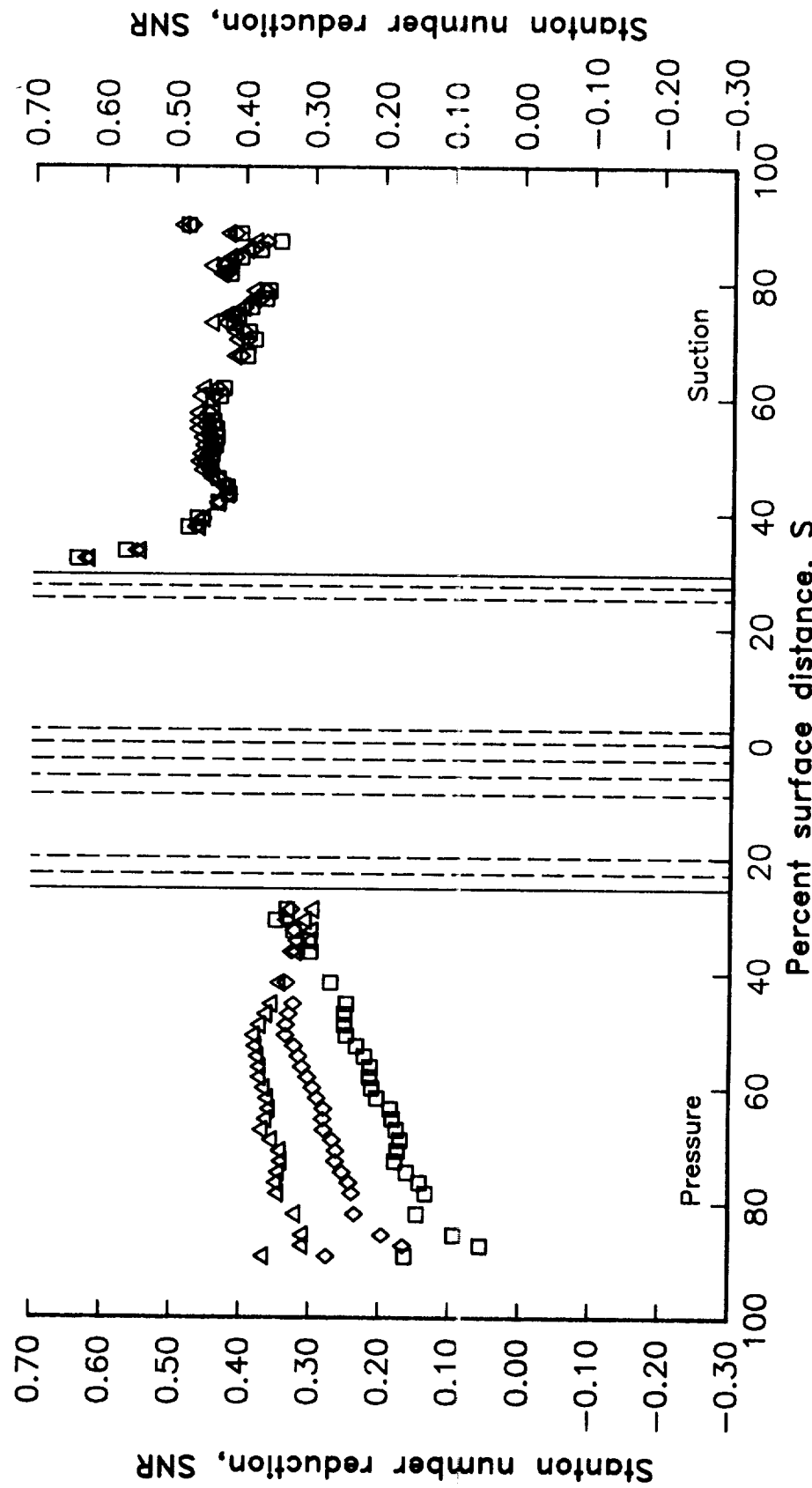


Figure 54. Effects of downstream coolant-to-gas pressure ratio variation on
SNR distribution -- series 4510X.

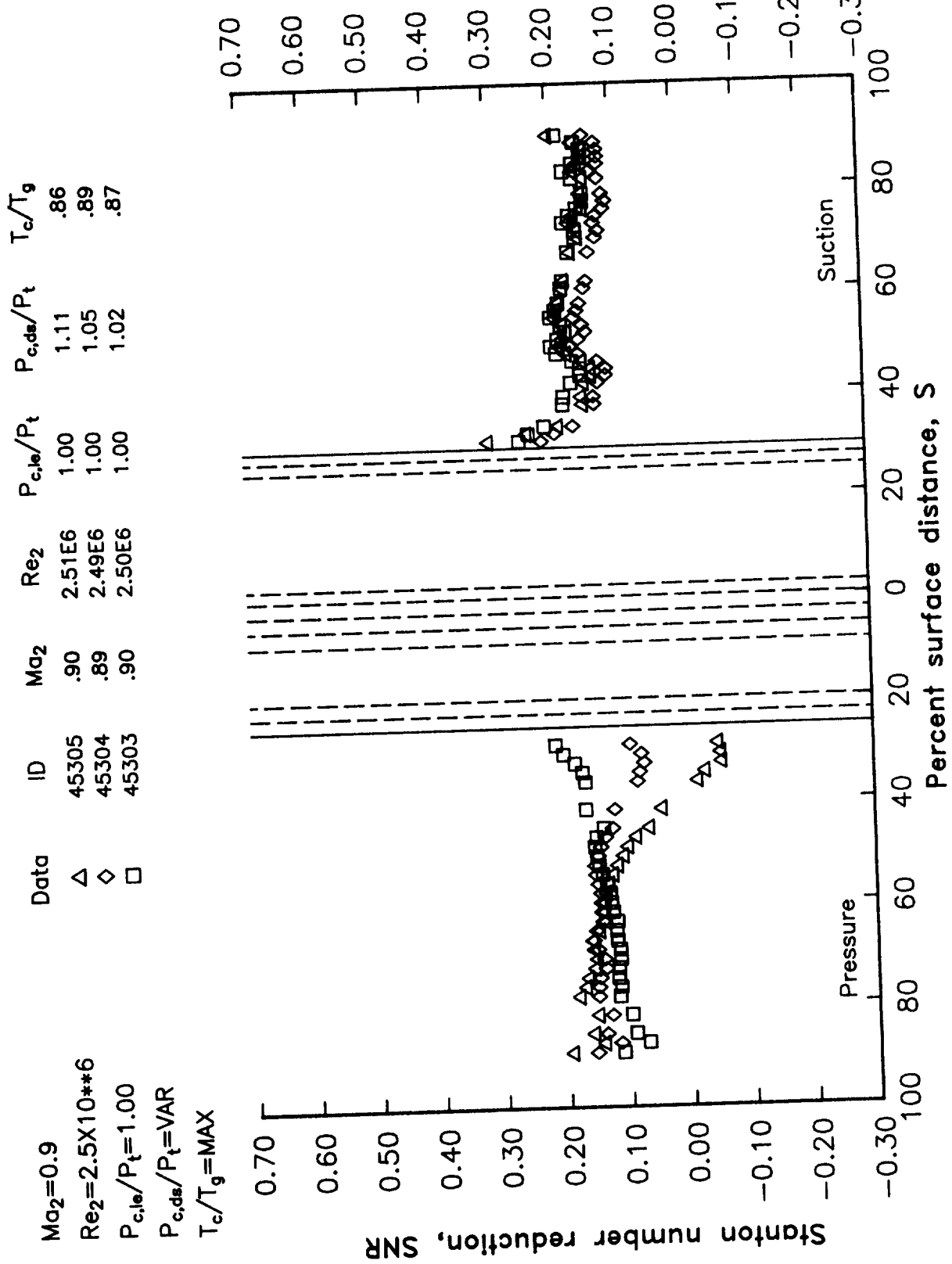


Figure 55. Effects of downstream coolant-to-gas pressure ratio variation on
SNR distribution -- series 4530X.

$Ma_2 = 0.9$
 $Re_2 = 2.0 \times 10^{**6}$
 $P_{c,le}/P_t = VAR$
 $P_{c,de}/P_t = VAR$
 $T_c/T_g = MIN$

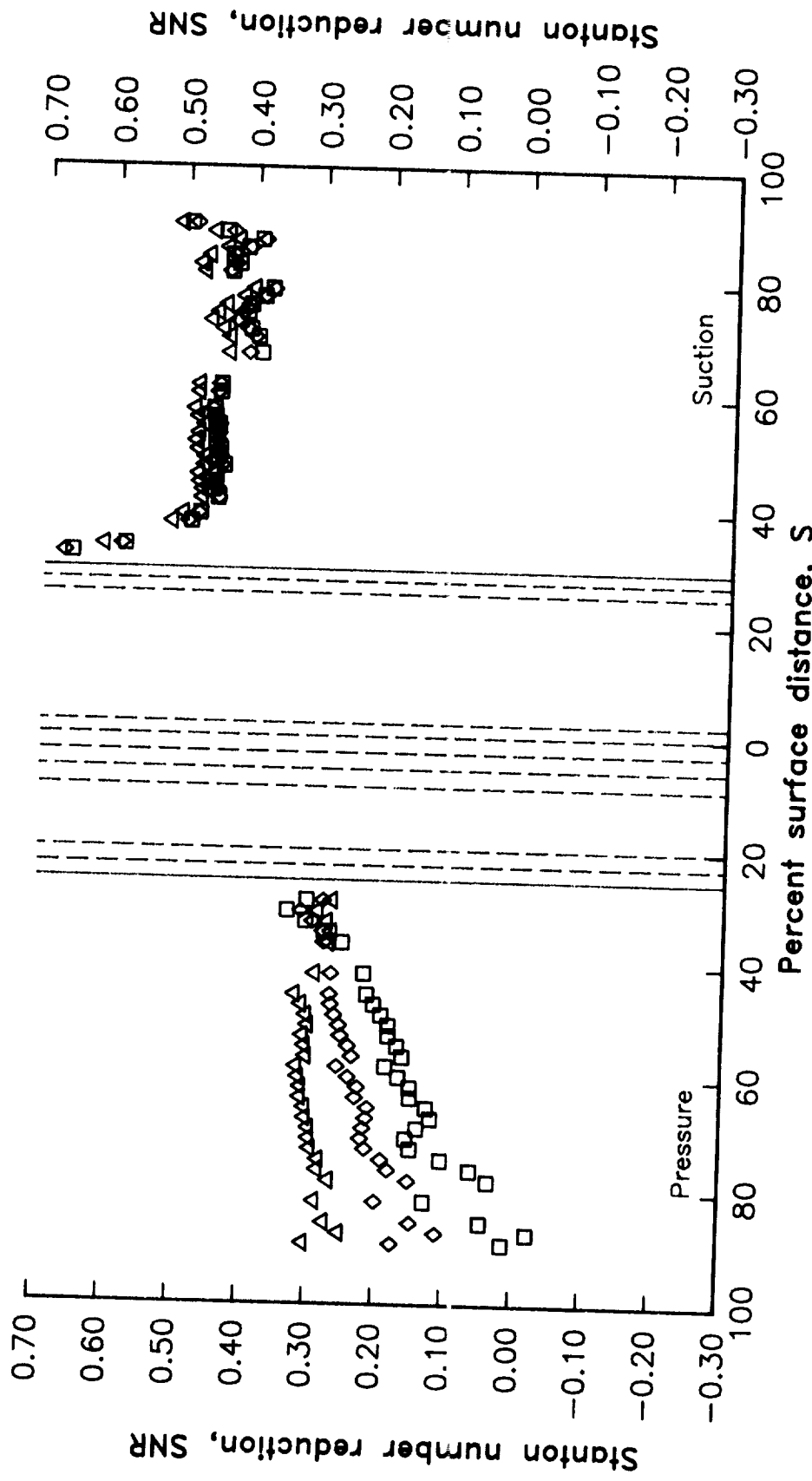


Figure 56. Effects of leading edge and downstream coolant-to-gas pressure ratio variation on SNR distribution -- series 441XX.

$Ma_2 = 0.9$
 $Re_2 = 2.0 \times 10^{**6}$
 $P_{c,le}/P_t = VAR$
 $P_{c,ds}/P_t = MAX$
 $T_c/T_g = MAX$

Data	ID	Ma_2	Re_2	$P_{c,le}/P_t$	$P_{c,ds}/P_t$	T_c/T_g
△	44355	.90	2.02E6	1.10	1.10	.84
◊	44344	.89	2.03E6	1.05	1.05	.85
□	44333	.90	1.99E6	1.02	1.02	.86

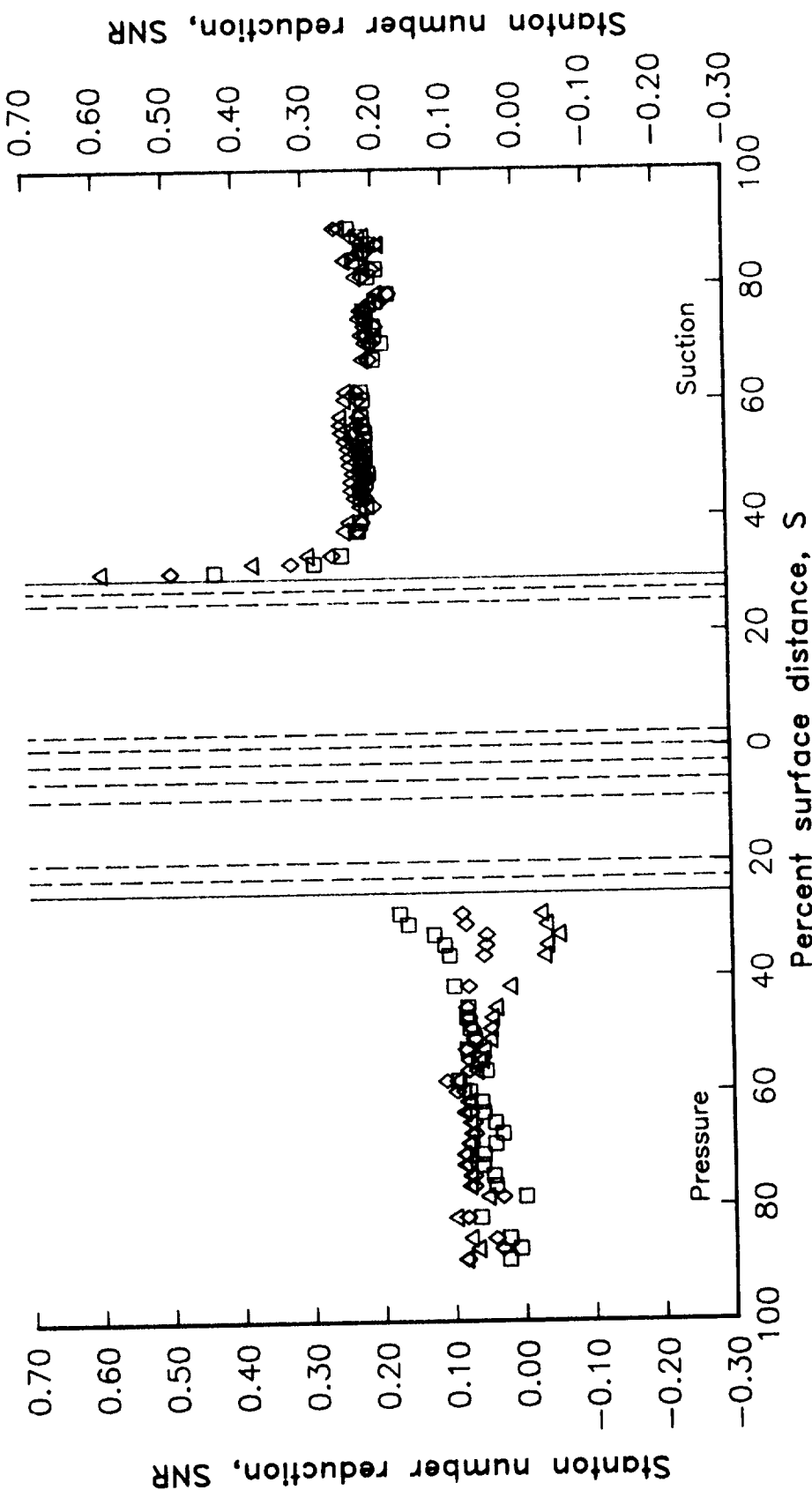


Figure 57. Effects of leading edge and downstream coolant-to-gas pressure ratio variation on SNR distribution -- series 443XX.

$Ma_2 = 0.75$	Data	ID	Ma_2	Re_2	$P_{c,le}/P_t$	$P_{c,ds}/P_t$	T_c/T_g
$Re_2 = 2.0 \times 10^{**6}$	O	34155	.75	2.05E6	1.10	1.10	.67
$P_{c,le}/P_t = VAR$	△	34145	.74	2.00E6	1.05	1.10	.65
$P_{c,ds}/P_t = 1.10$	◊	34135	.75	2.01E6	1.02	1.10	.65
$T_c/T_g = MIN$	□	34105	.75	2.00E6	1.00	1.10	.66

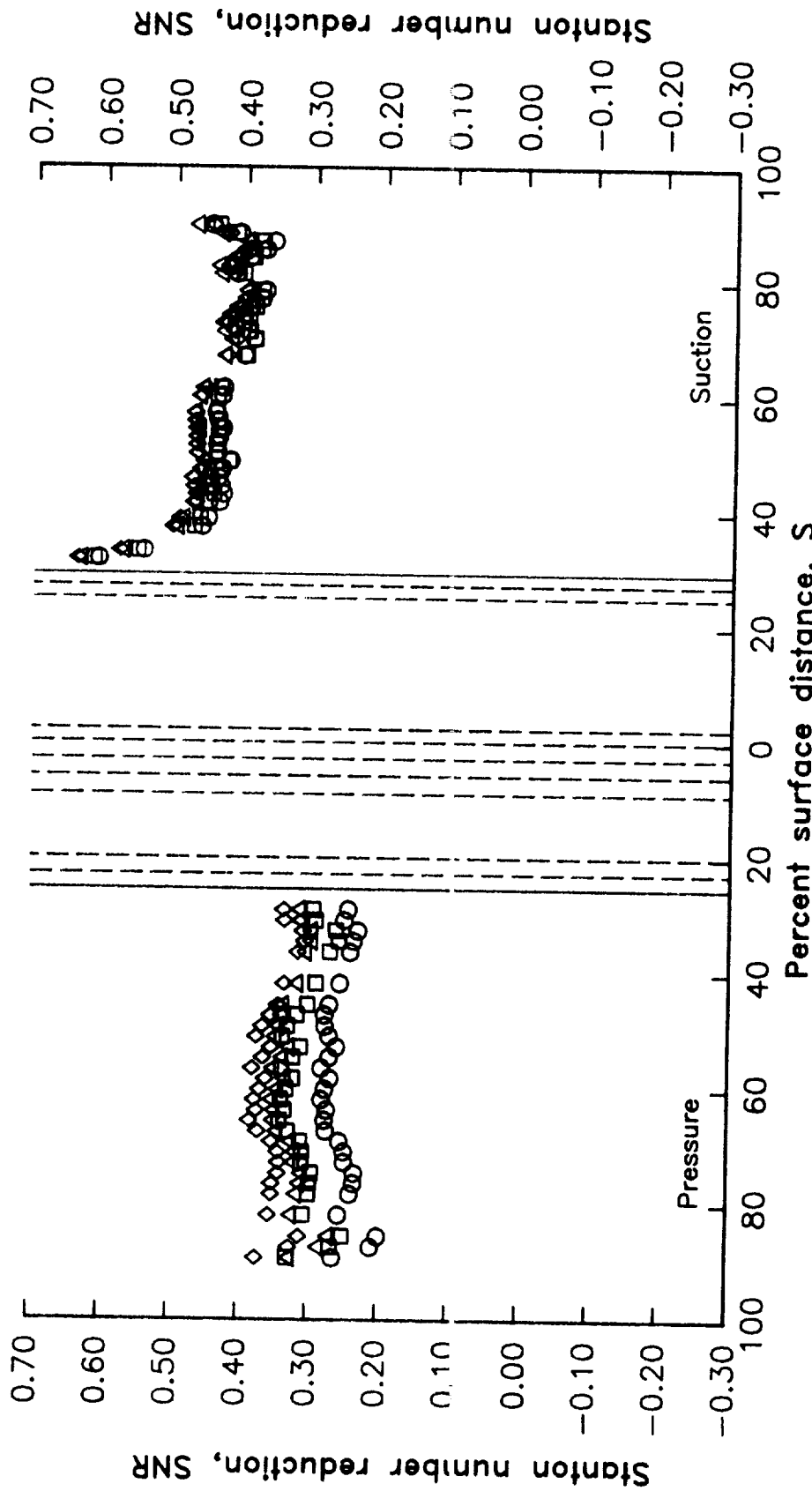


Figure 58. Effects of leading edge blowing variation with constant downstream coolant-to-gas pressure ratio on SNR distribution -- series 341X5.

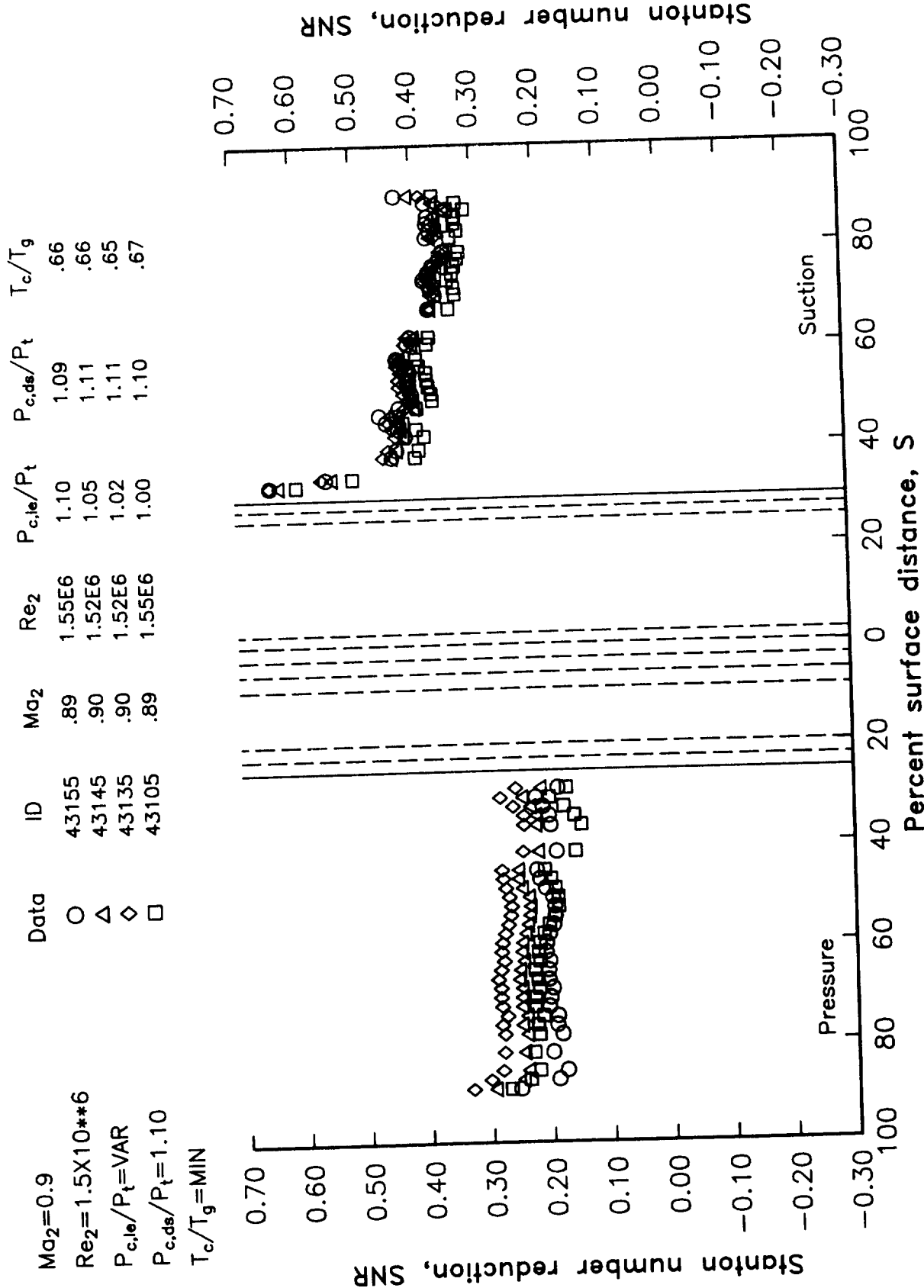


Figure 59. Effects of leading edge blowing variation with constant downstream coolant-to-gas pressure ratio on SNR distribution -- series 431X5.

$Ma_2 = 0.9$	$Re_2 = 2.0 \times 10^{**6}$	Data	ID	Ma_2	Re_2	$P_{c,le}/P_t$	T_c/T_g
$P_{c,le}/P_t = VAR$	O	44155	.90	2.00E6	1.10	1.10	.66
$P_{c,ds}/P_t = 1.10$	△	44145	.89	1.98E6	1.05	1.10	.68
$T_c/T_g = MIN$	◊	44135	.90	2.00E6	1.02	1.10	.67
	□	44105	.89	1.99E6	1.00	1.10	.68

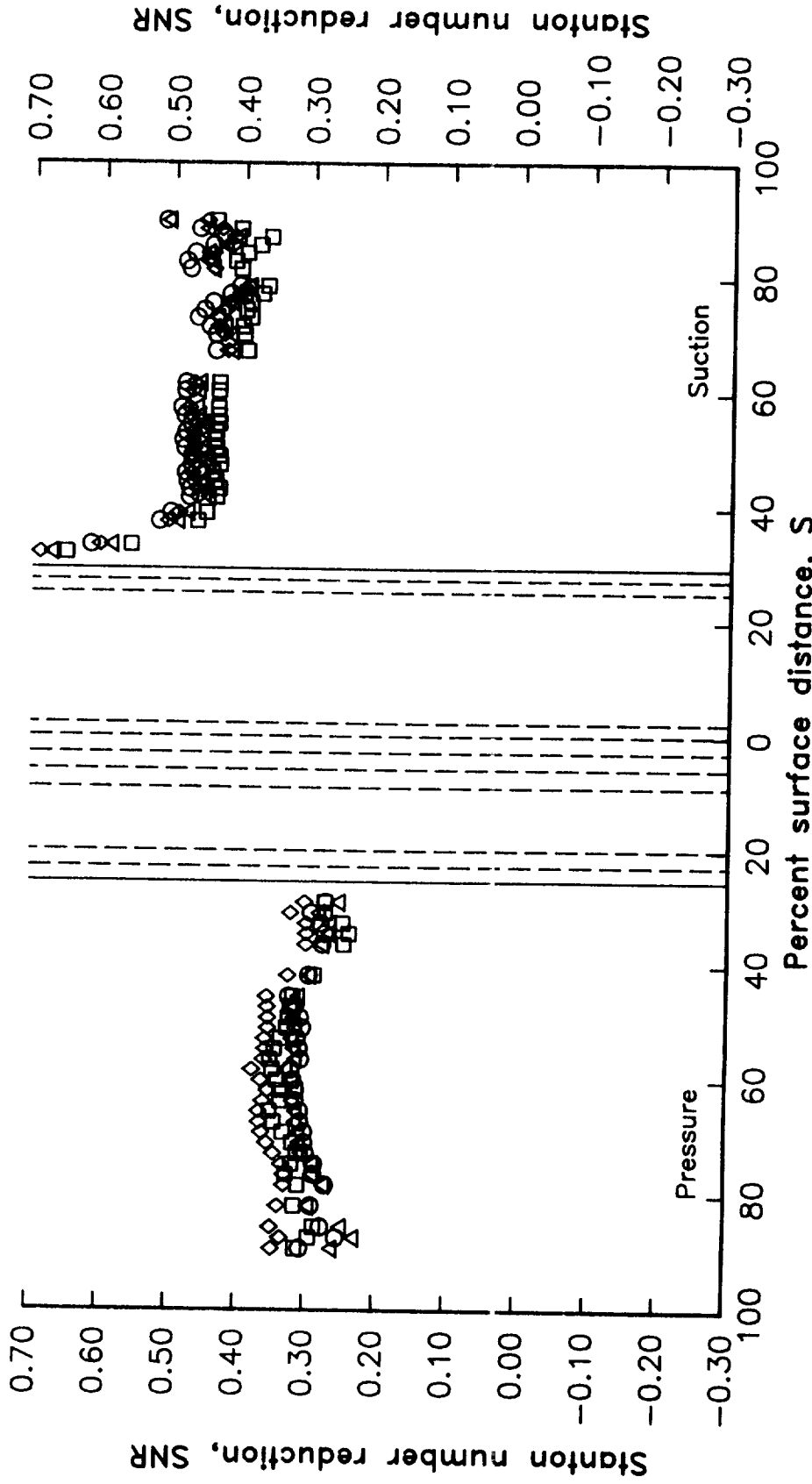


Figure 60. Effects of leading edge blowing variation with constant downstream coolant-to-gas pressure ratio on SNR distribution -- series 441X5.

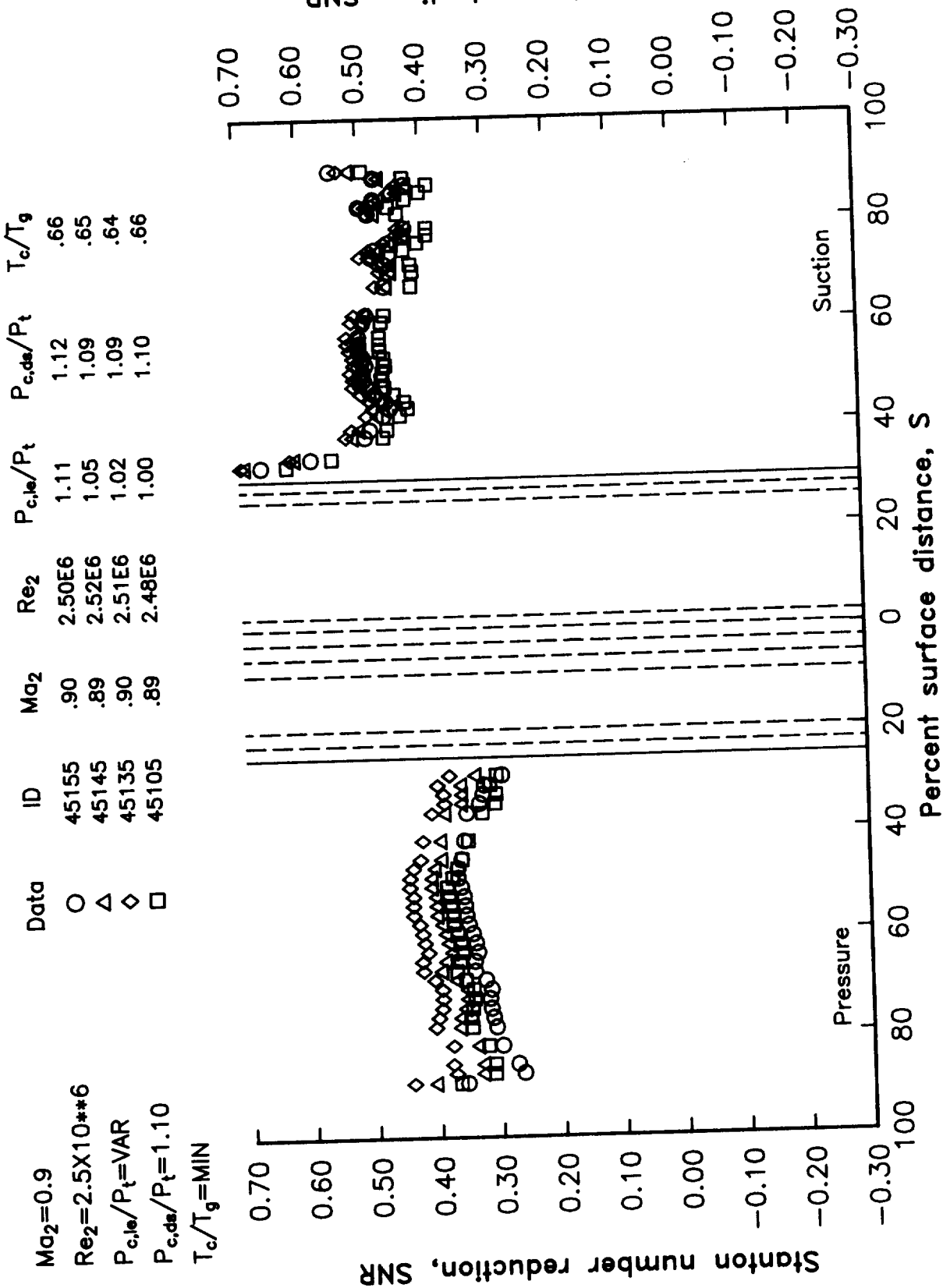


Figure 61. Effects of leading edge blowing variation with constant downstream coolant-to-gas pressure ratio on SNR distribution -- series 451X5.

$Ma_2 = 0.75$
 $Re_2 = 2.0 \times 10^{6}$
 $P_{c,le}/P_t = 1.00$
 $P_{c,ds}/P_t = 1.02$
 $T_c/T_g = VAR$

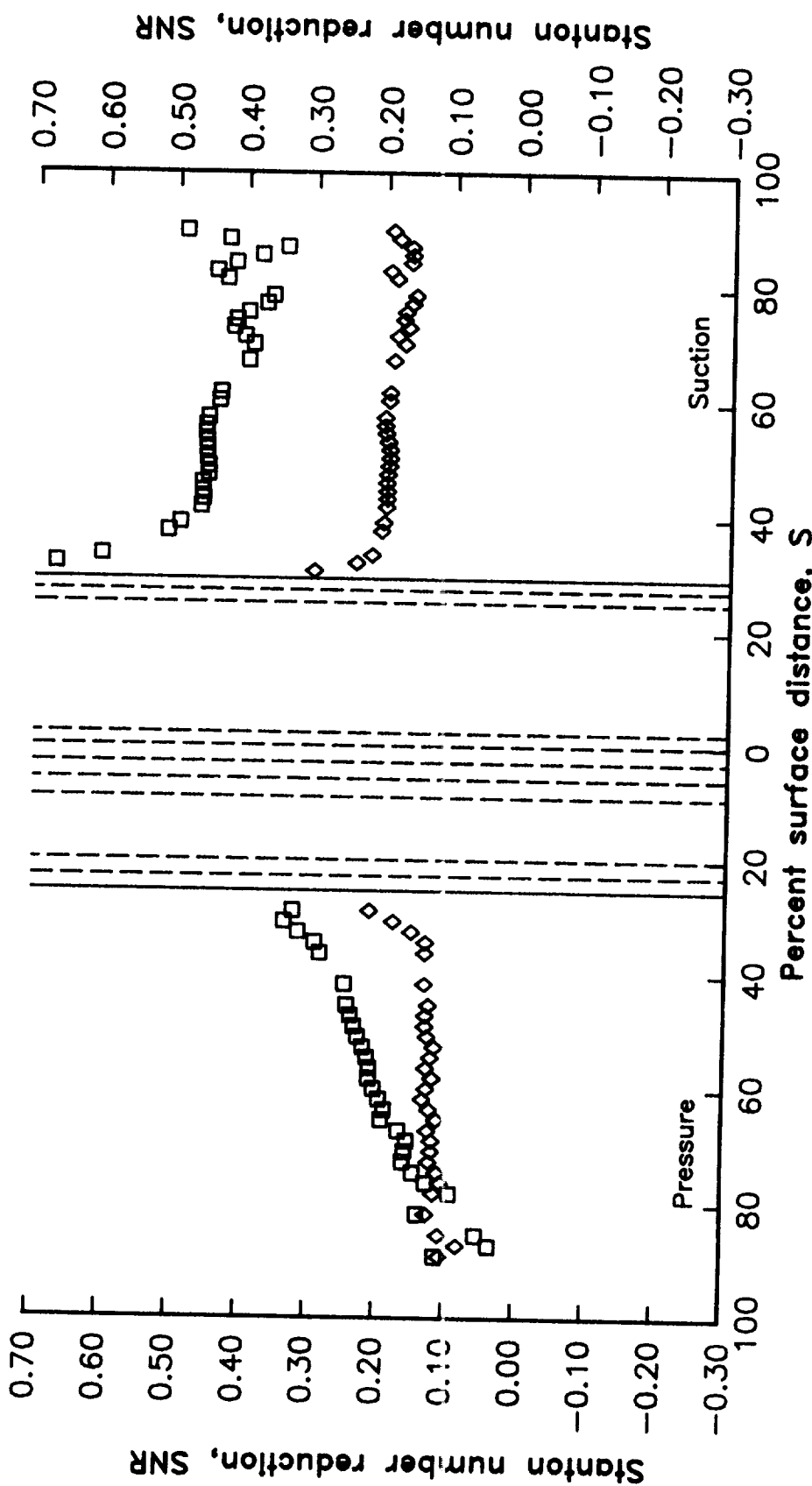


Figure 62. Effects of coolant-to-gas absolute temperature ratio variation on SNR distribution -- series 34X03.

$Ma_2 = 0.75$
 $Re_2 = 2.0 \times 10^{4*6}$
 $P_{c,le}/P_t = 1.00$
 $P_{c,ds}/P_t = 1.05$
 $T_c/T_g = VAR$

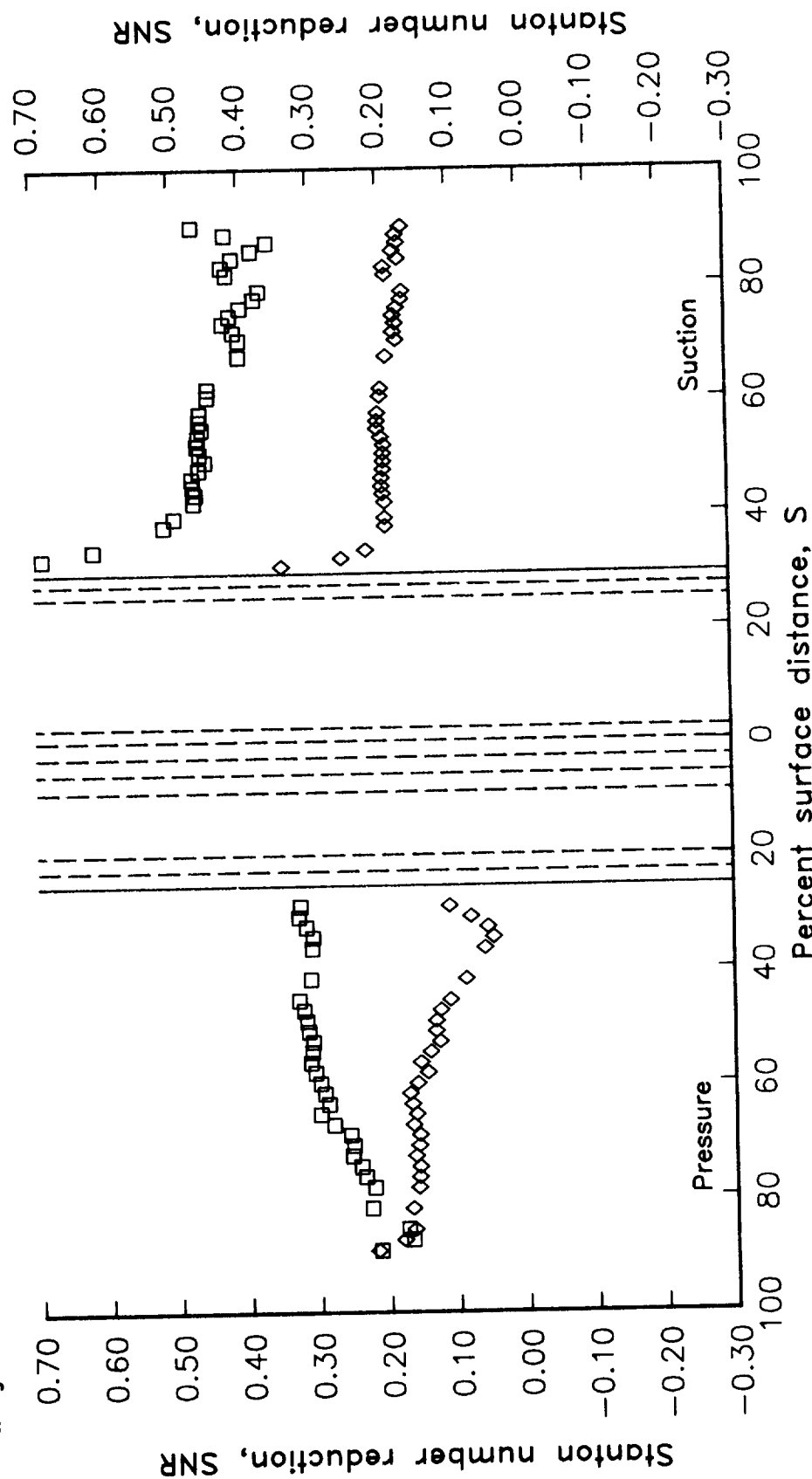


Figure 63. Effects of coolant-to-gas absolute temperature ratio variation on
SNR distribution -- series 34X04.

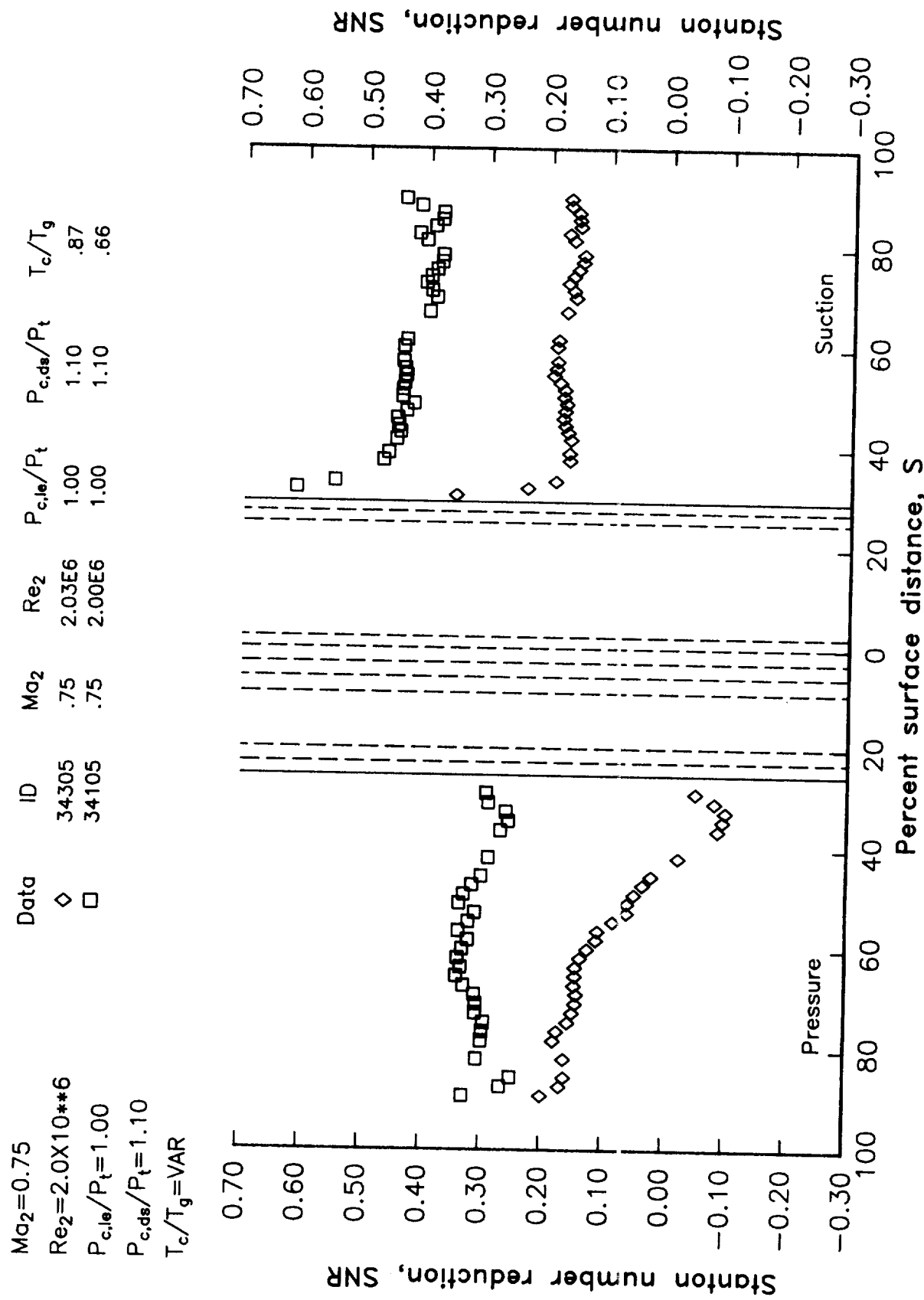


Figure 64. Effects of coolant-to-gas absolute temperature ratio variation on SNR distribution -- series 34X05.

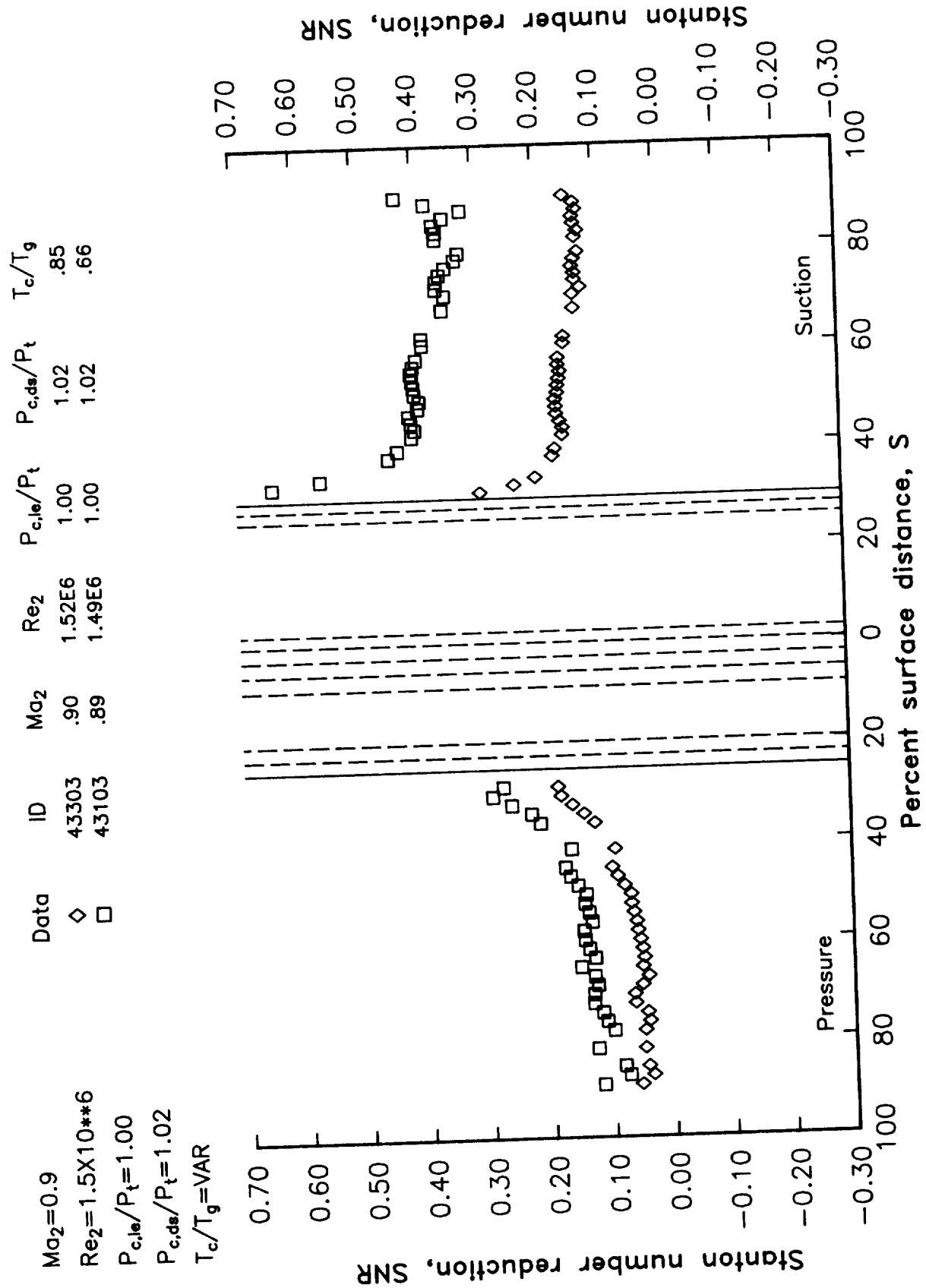


Figure 65. Effects of coolant-to-gas absolute temperature ratio variation on
SNR distribution -- series 43X03.

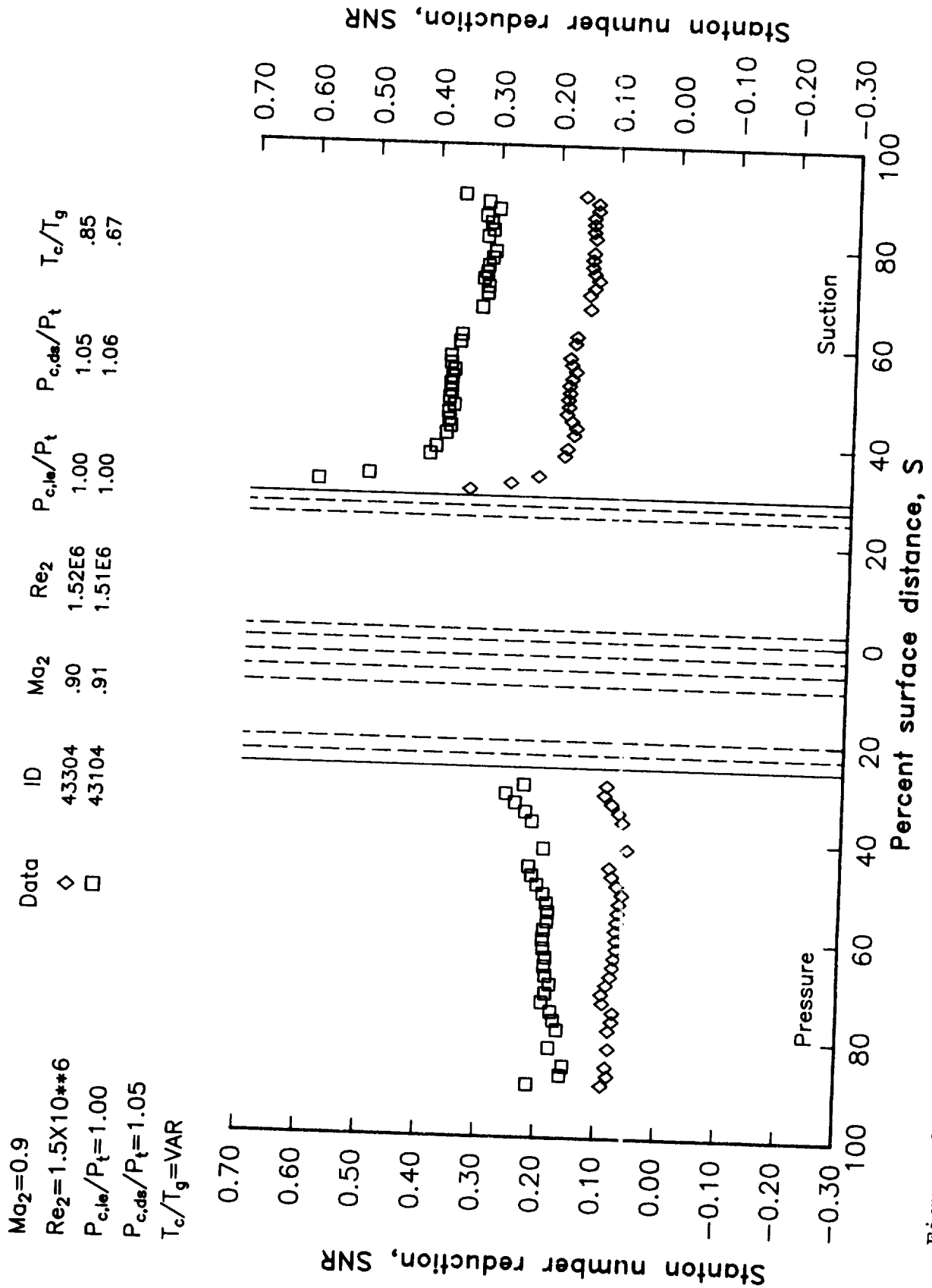


Figure 66. Effects of coolant-to-gas absolute temperature ratio variation on SNR distribution -- series 43X04

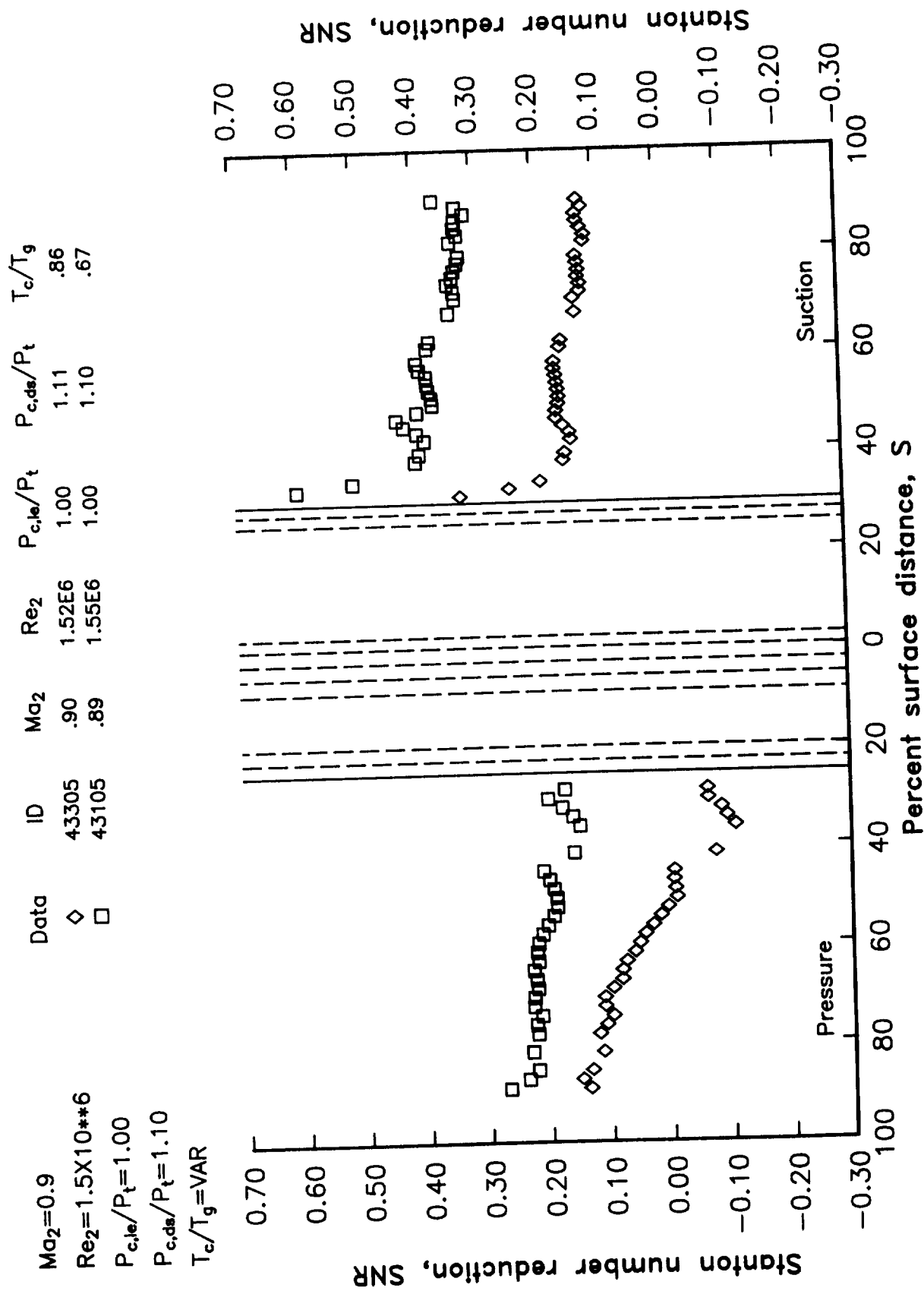


Figure 67. Effects of coolant-to-gas absolute temperature ratio variation on SNR distribution -- series 43X05.

$Ma_2=0.9$	Data	ID	Ma_2	Re_2	$P_{c,le}/P_t$	$P_{c,de}/P_t$	T_c/T_g
$Re_2=2.0 \times 10^{**6}$	△	44303	.90	2.01E6	1.00	1.02	.84
$P_{c,le}/P_t=1.00$	◇	44203	.90	1.99E6	1.00	1.02	.75
$P_{c,de}/P_t=1.02$	□	44103	.89	1.96E6	1.00	1.02	.68
$T_c/T_g=VAR$							

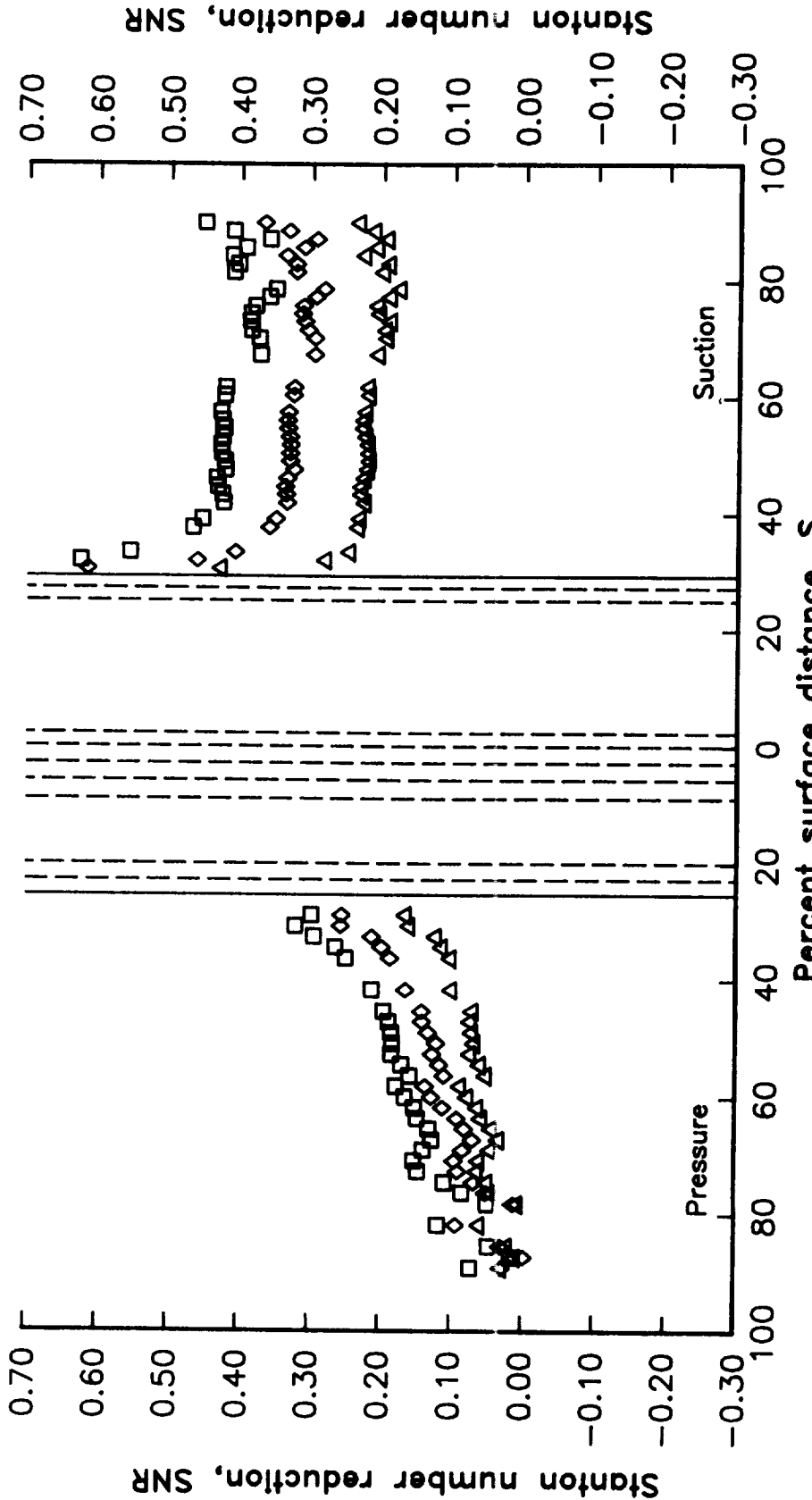


Figure 68. Effects of coolant-to-gas absolute temperature ratio variation on SNR distribution -- series 44X03.

$Ma_2 = 0.9$	Data	ID	Ma_2	Re_2	$P_{c,le}/P_t$	$P_{c,ds}/P_t$	T_c/T_g
$Re_2 = 2.0 \times 10^{**6}$	△	44304	.89	2.01E6	1.00	1.05	.86
$P_{c,le}/P_t = 1.00$	◇	44204	.90	2.00E6	1.00	1.05	.76
$P_{c,ds}/P_t = 1.05$	□	44104	.90	2.00E6	1.00	1.05	.67
$T_c/T_g = VAR$							

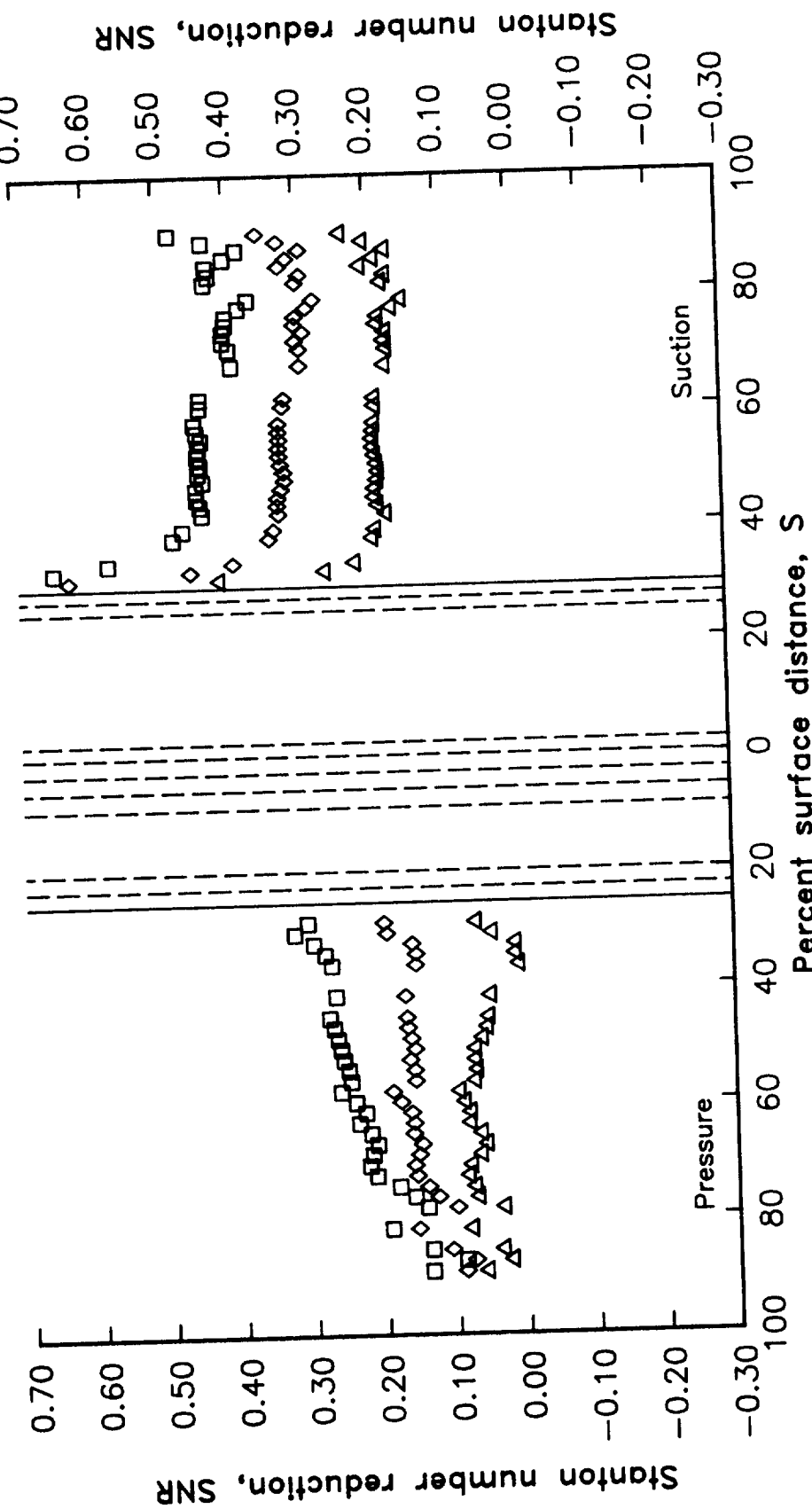


Figure 69. Effects of coolant-to-gas absolute temperature ratio variation on
SNR distribution -- series 44X04.

$Ma_2 = 0.9$	Data	ID	Ma_2	Re_2	$P_{c,le}/P_t$	$P_{c,de}/P_t$	T_c/T_g
$Re_2 = 2.0 \times 10^{**6}$	△	44305	.90	2.03E6	1.00	1.11	.85
$P_{c,le}/P_t = 1.00$	◇	44205	.90	2.01E6	1.00	1.11	.77
$P_{c,de}/P_t = 1.10$	□	44105	.89	1.99E6	1.00	1.10	.68
$T_c/T_g = VAR$							

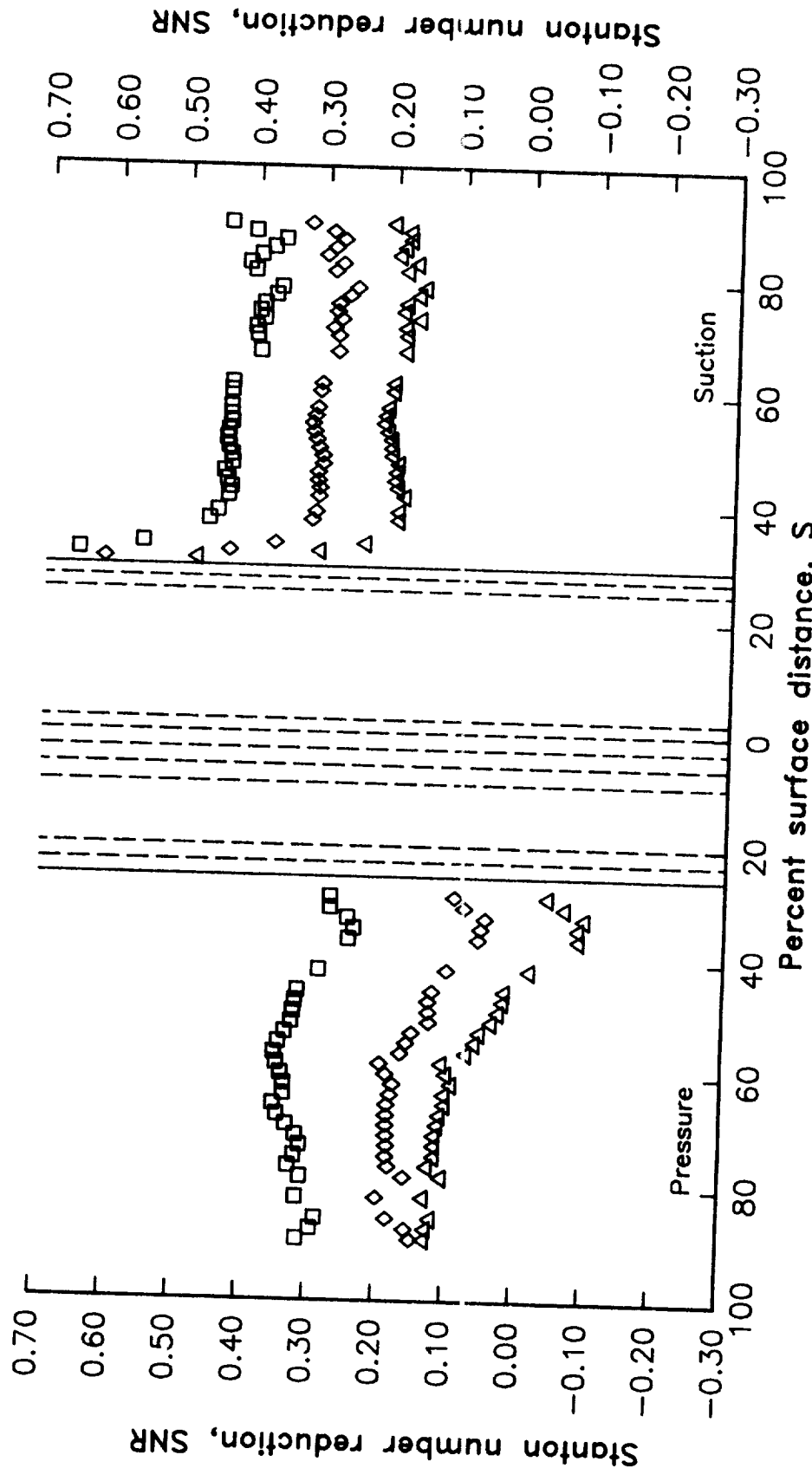


Figure 70. Effects of coolant-to-gas absolute temperature ratio variation on
SNR distribution -- series 44X05.

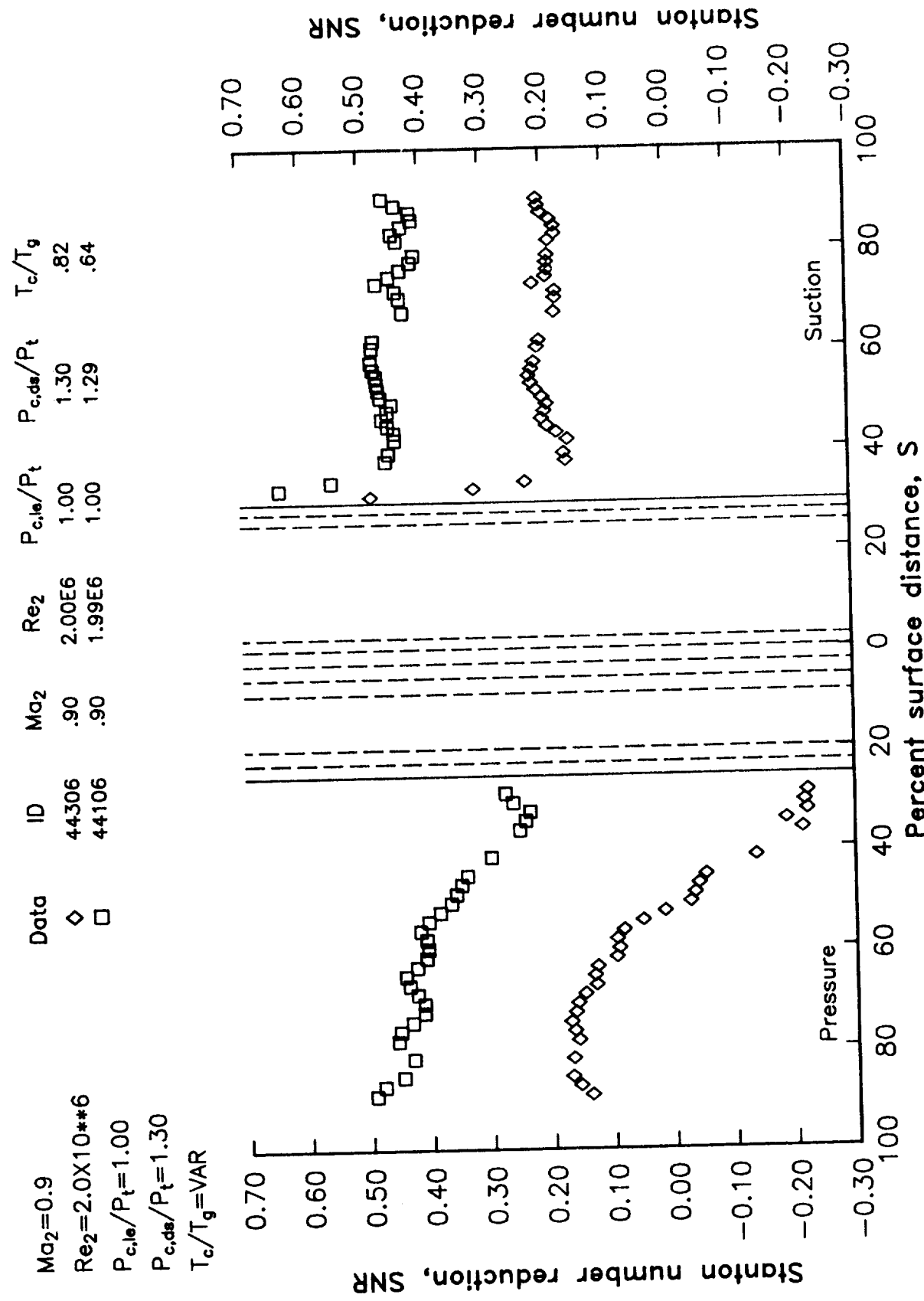


Figure 71. Effects of coolant-to-gas absolute temperature ratio variation on
SNR distribution -- series 44X06.

$Ma_2 = 0.9$
 $Re_2 = 2.0 \times 10^{4*6}$
 $P_{c,le}/P_t = 1.00$
 $P_{c,de}/P_t = 1.50$
 $T_c/T_g = VAR$

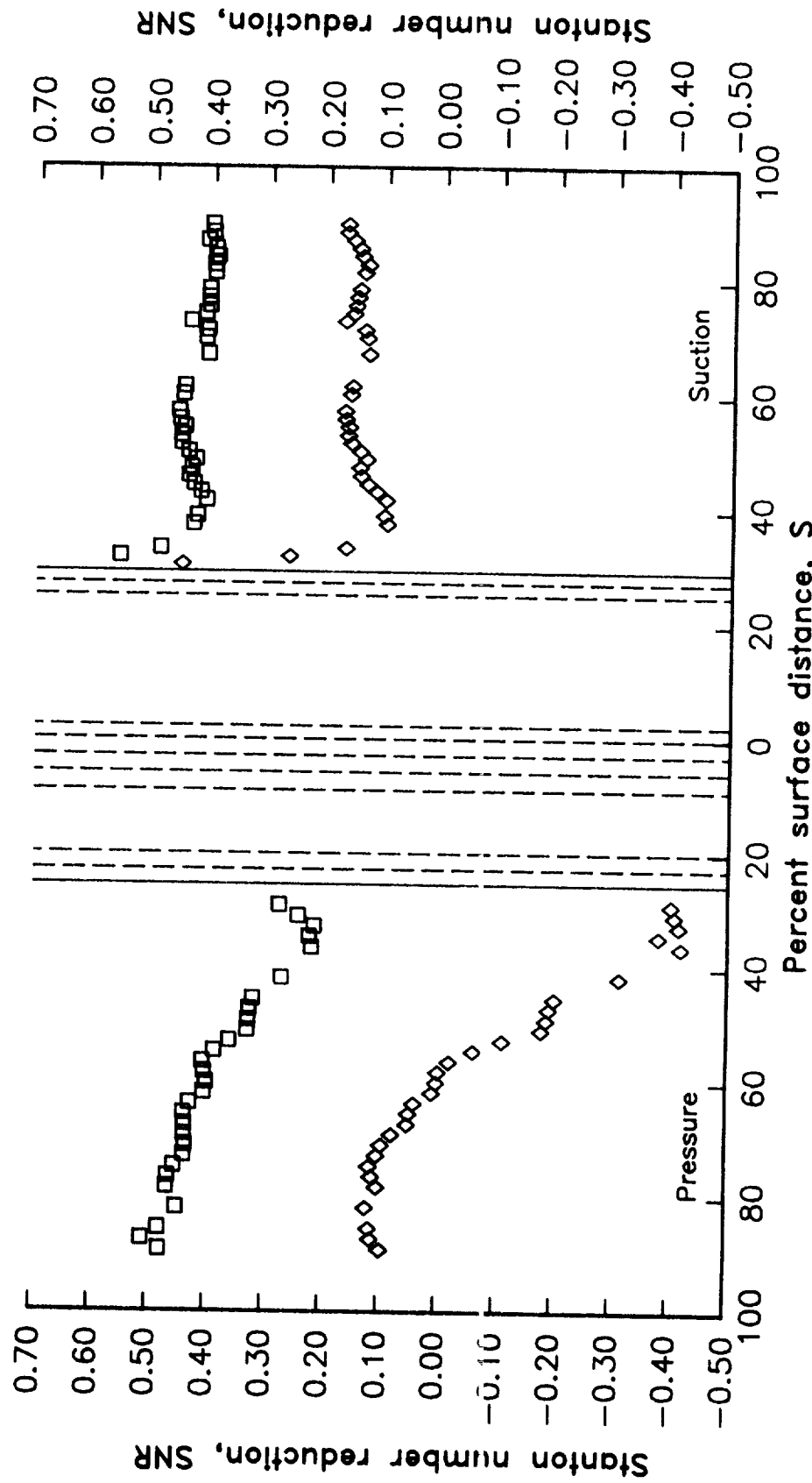


Figure 72. Effects of coolant-to-gas absolute temperature ratio variation on SNR distribution -- series 44X07.

$Ma_2 = 0.9$
 $Re_2 = 2.0 \times 10^{*6}$
 $P_{c,le}/P_t = 1.00$
 $P_{c,ds}/P_t = 1.70$
 $T_c/T_g = VAR$

Data	ID	Ma_2	Re_2	$P_{c,le}/P_t$	$P_{c,ds}/P_t$	T_c/T_g
◊	44308	.89	1.98E6	1.00	1.61	.85
□	44108	.89	2.00E6	1.00	1.63	.63

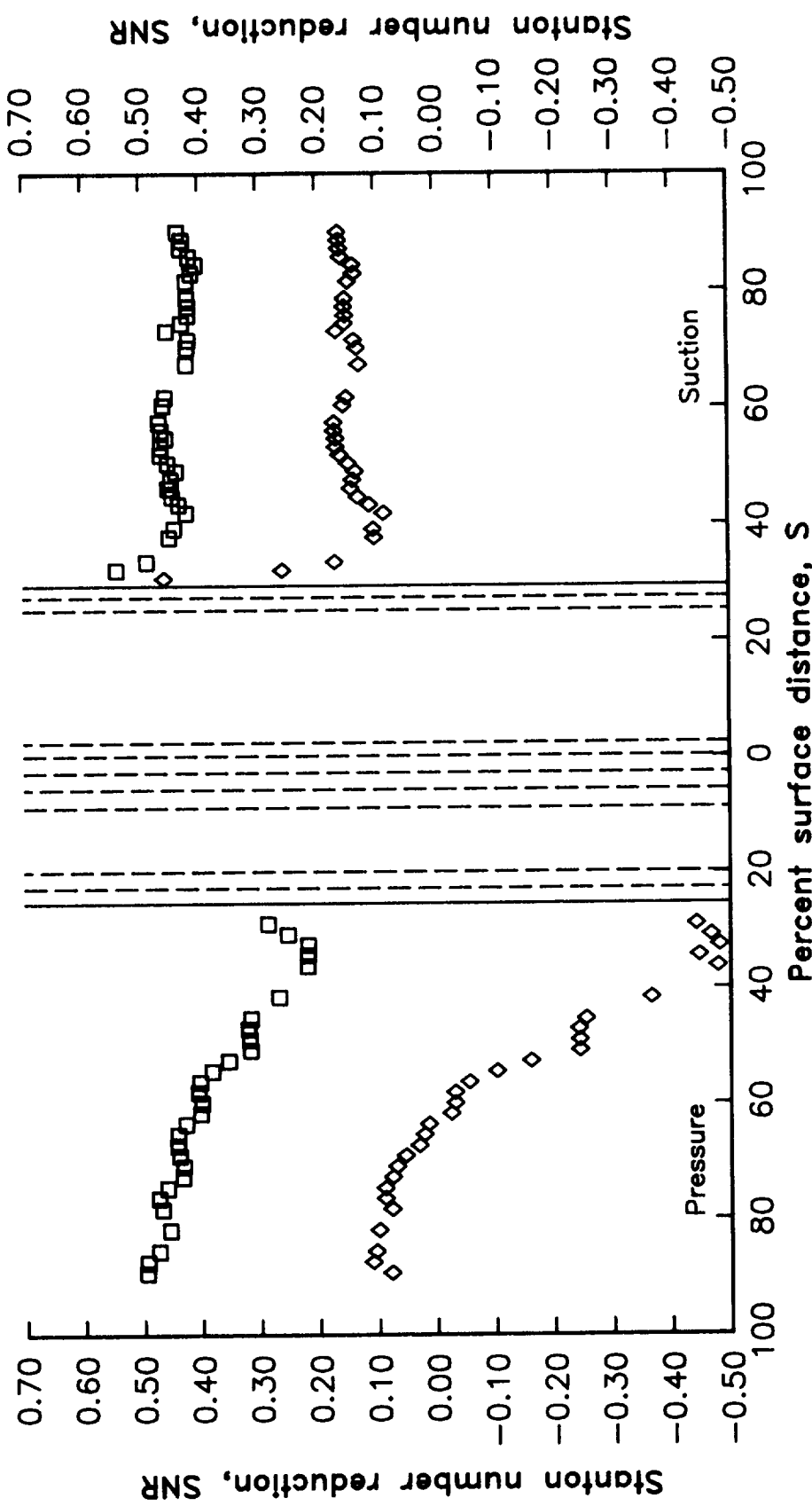


Figure 73. Effects of coolant-to-gas absolute temperature ratio variation on SNR distribution -- series 44X08.

$Ma_2 = 0.9$
 $Re_2 = 2.0 \times 10^{11*6}$
 $P_{c,le}/P_t = 1.02$
 $P_{c,ds}/P_t = 1.02$
 $T_c/T_g = VAR$

Data	ID	Ma_2	Re_2	$P_{c,le}/P_t$	$P_{c,ds}/P_t$	T_c/T_g
◊	44333	.90	1.99E6	1.02	1.02	.86
□	44133	.92	2.03E6	1.02	1.02	.67

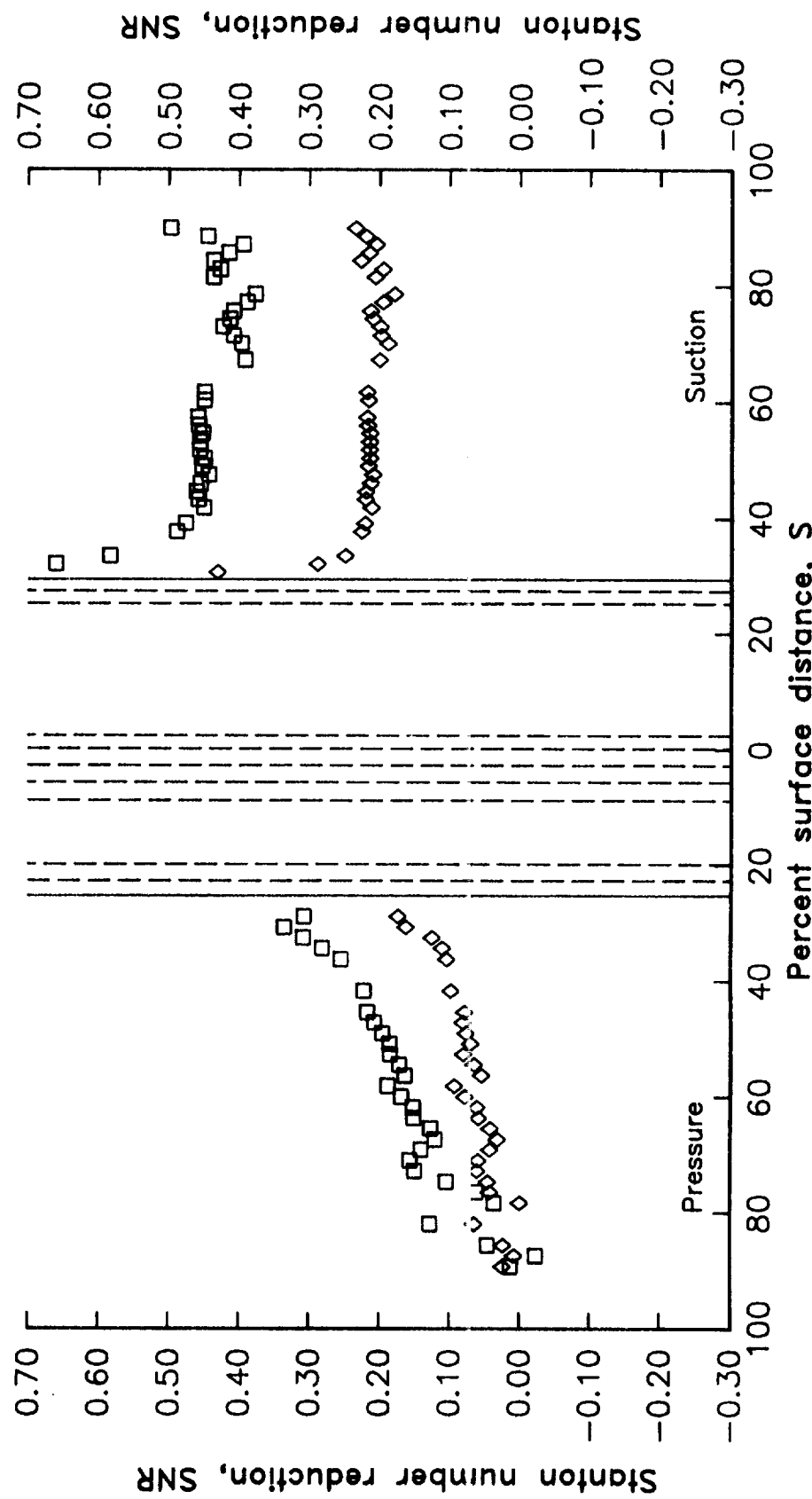


Figure 74. Effects of coolant-to-gas absolute temperature ratio variation on SNR distribution -- series 44X33.

	Data	ID	Ma_2	Re_2	$P_{c,le}/P_t$	T_c/T_g
$Ma_2=0.9$	◊	44344	.89	2.03E6	1.05	.85
$Re_2=2.0\times 10^{11}$	□	44144	.90	2.03E6	1.05	.67
$P_{c,le}/P_t=1.05$						
$T_c/T_g=VAR$						

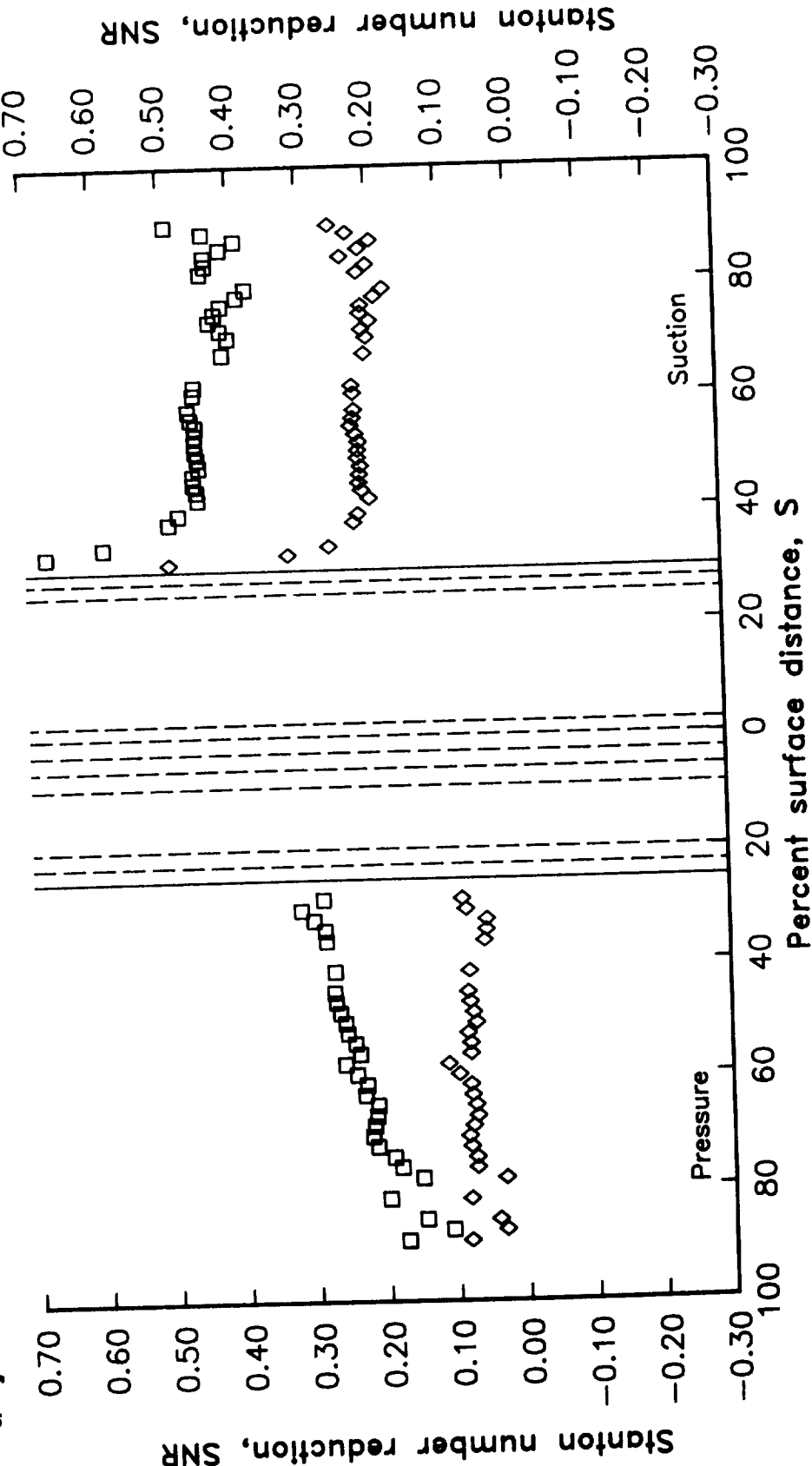


Figure 75. Effects of coolant-to-gas absolute temperature ratio variation on
SNR distribution -- series 44X44.

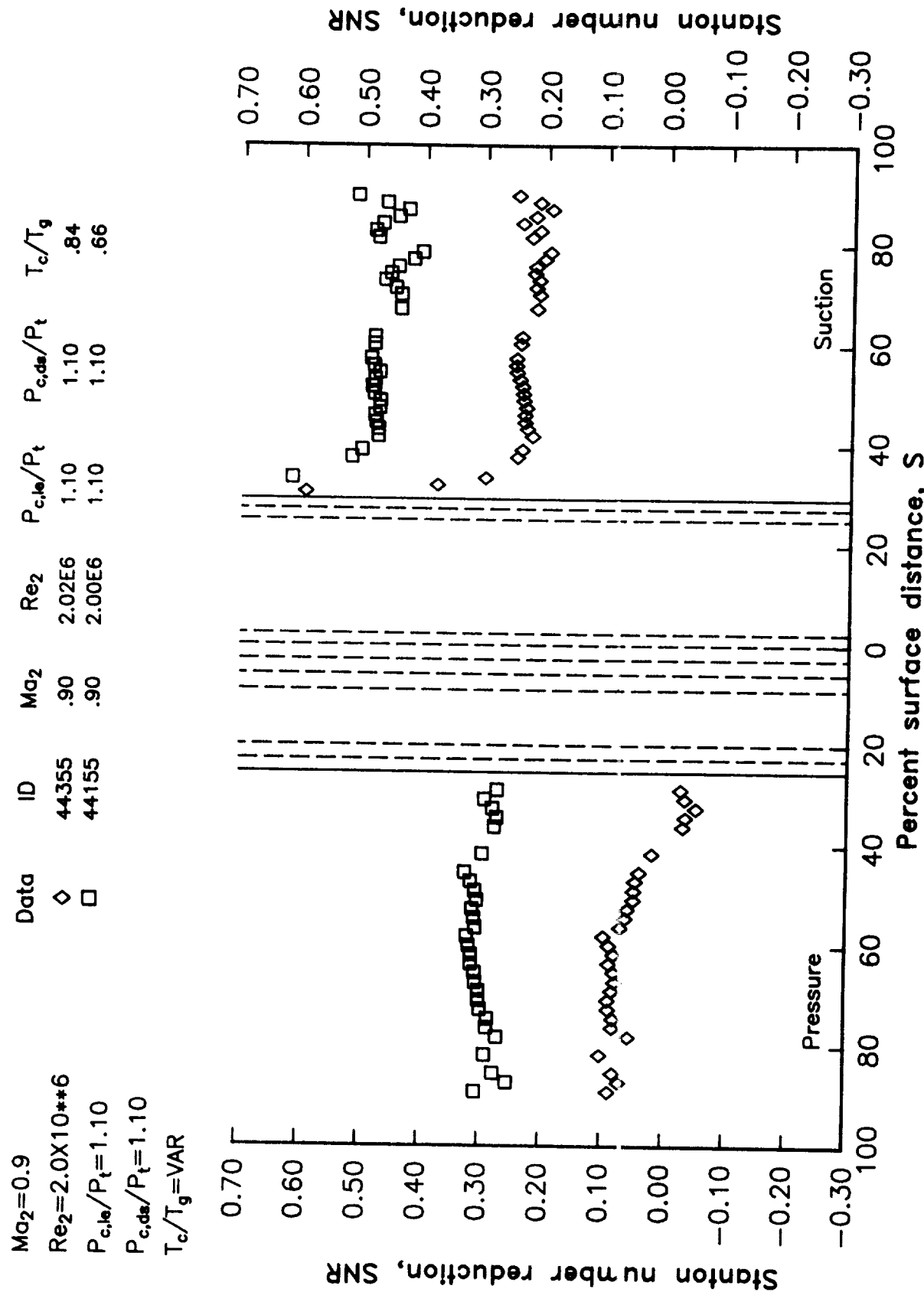


Figure 76. Effects of coolant-to-gas absolute temperature ratio variation on SNR distribution -- series 44X55.

$Ma_2 = 0.9$
 $Re_2 = 2.5 \times 10^{10} * 6$
 $P_{c,le}/P_t = 1.00$
 $P_{c,ds}/P_t = 1.02$
 $T_c/T_g = VAR$

Data	ID	Ma_2	Re_2	$P_{c,le}/P_t$	$P_{c,ds}/P_t$	T_c/T_g
◊	45303	.90	2.50E6	1.00	1.02	.87
□	45103	.89	2.48E6	1.00	1.02	.67

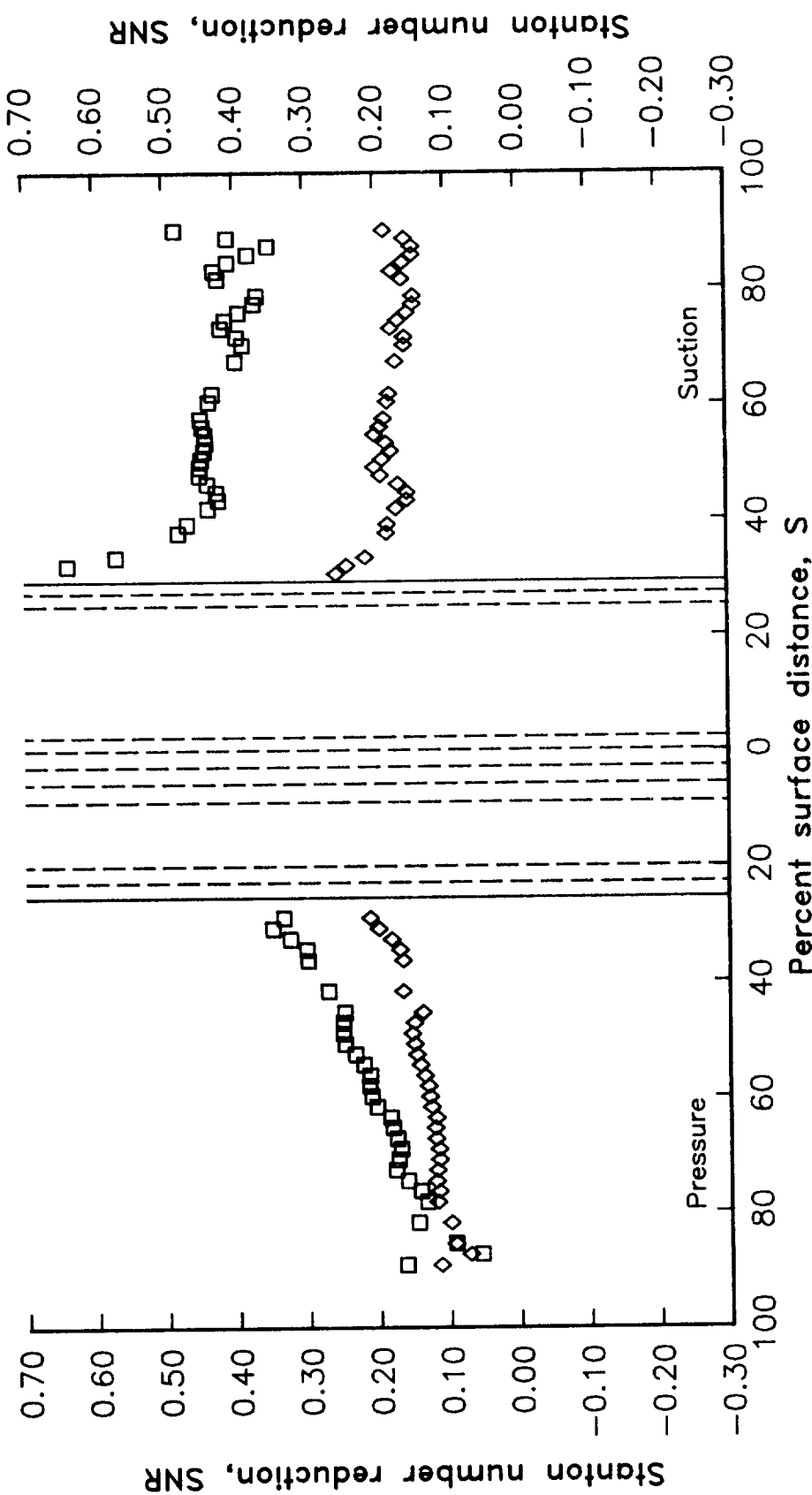


Figure 77. Effects of coolant-to-gas absolute temperature ratio variation on SNR distribution -- series 45X03.

$Ma_2 = 0.9$
 $Re_2 = 2.5 \times 10^{**6}$
 $P_{c,le}/P_t = 1.00$
 $P_{c,ds}/P_t = 1.05$
 $T_c/T_g = VAR$

Data	ID	Ma_2	Re_2	$P_{c,le}/P_t$	$P_{c,ds}/P_t$	T_c/T_g
◊	45304	.89	2.49E6	1.00	1.05	.89
□	45104	.89	2.49E6	1.00	1.06	.67

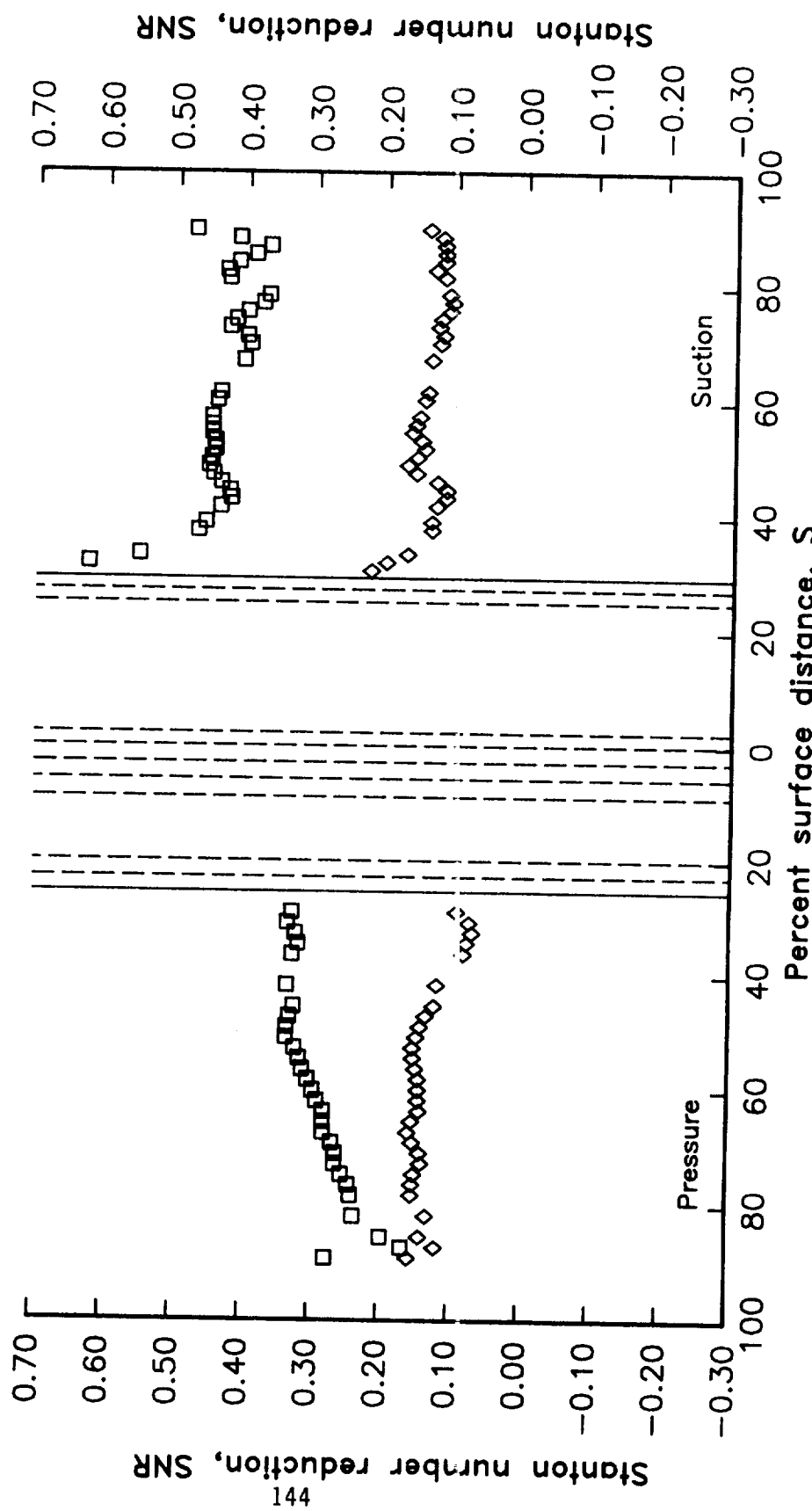


Figure 78. Effects of coolant-to-gas absolute temperature ratio variation on
SNR distribution -- series 45X04.

Figure 78.

$Ma_2 = 0.9$
 $Re_2 = 2.5 \times 10^{**6}$
 $P_{c,le}/P_t = 1.00$
 $P_{c,ds}/P_t = 1.10$
 $T_c/T_g = VAR$

Data	ID	Ma_2	Re_2	$P_{c,le}/P_t$	$P_{c,ds}/P_t$	T_c/T_g
◊	45305	.90	2.51E6	1.00	1.11	.86
□	45105	.89	2.48E6	1.00	1.10	.66

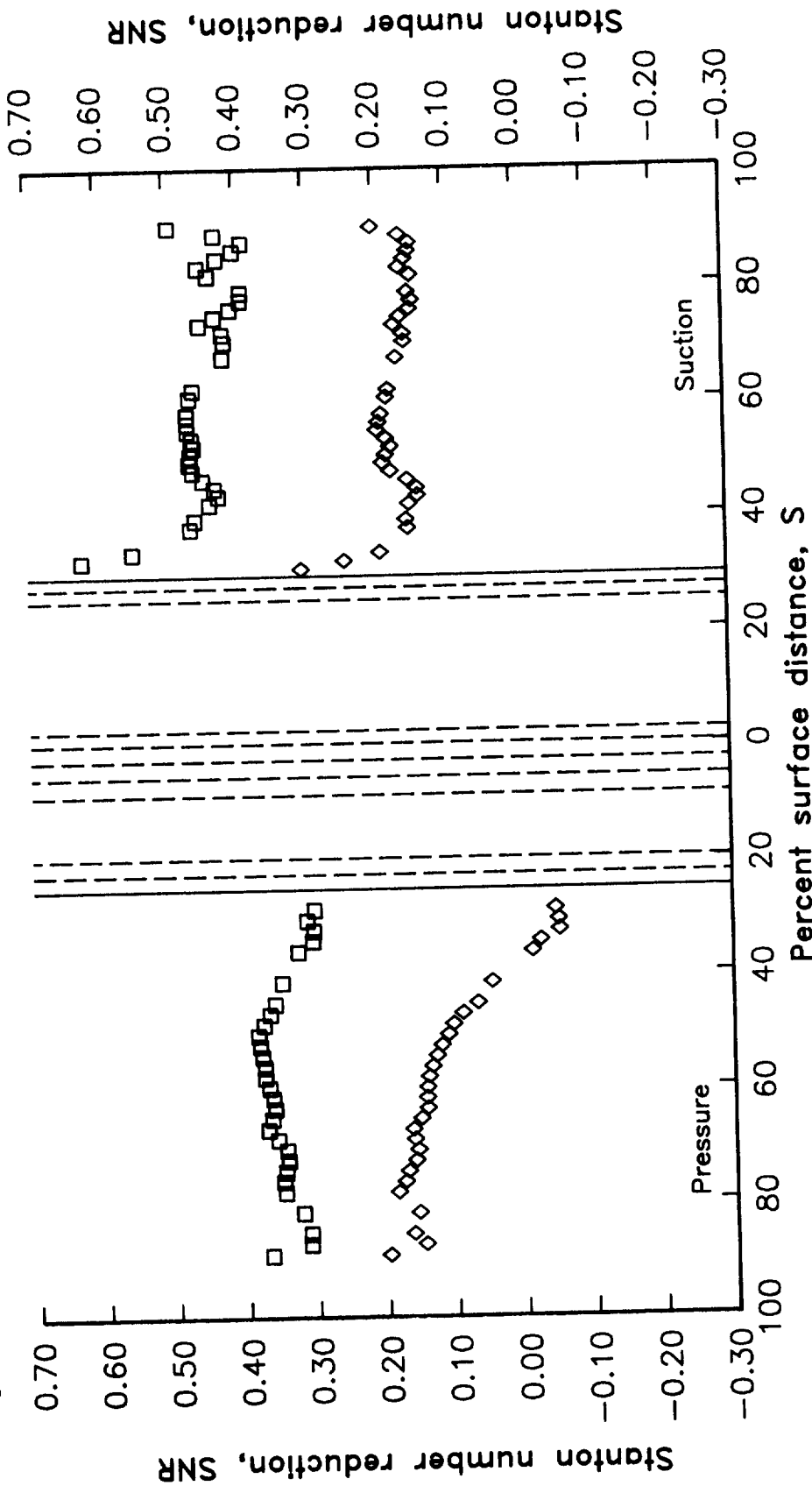


Figure 79. Effects of coolant-to-gas absolute temperature ratio variation on
SNR distribution -- series 45X05.

$Ma_2 = \text{VAR}$
 $Re_2 = 2.0 \times 10^{**6}$
 $P_{c,le}/P_t = 1.00$
 $P_{c,ds}/P_t = 1.02$
 $T_c/T_g = \text{MIN}$

Data	ID	Ma_2	Re_2	$P_{c,le}/P_t$	$P_{c,ds}/P_t$	T_c/T_g
◊	44103	.89	1.96E6	1.00	1.02	.68
□	34103	.75	1.97E6	1.00	1.03	.64

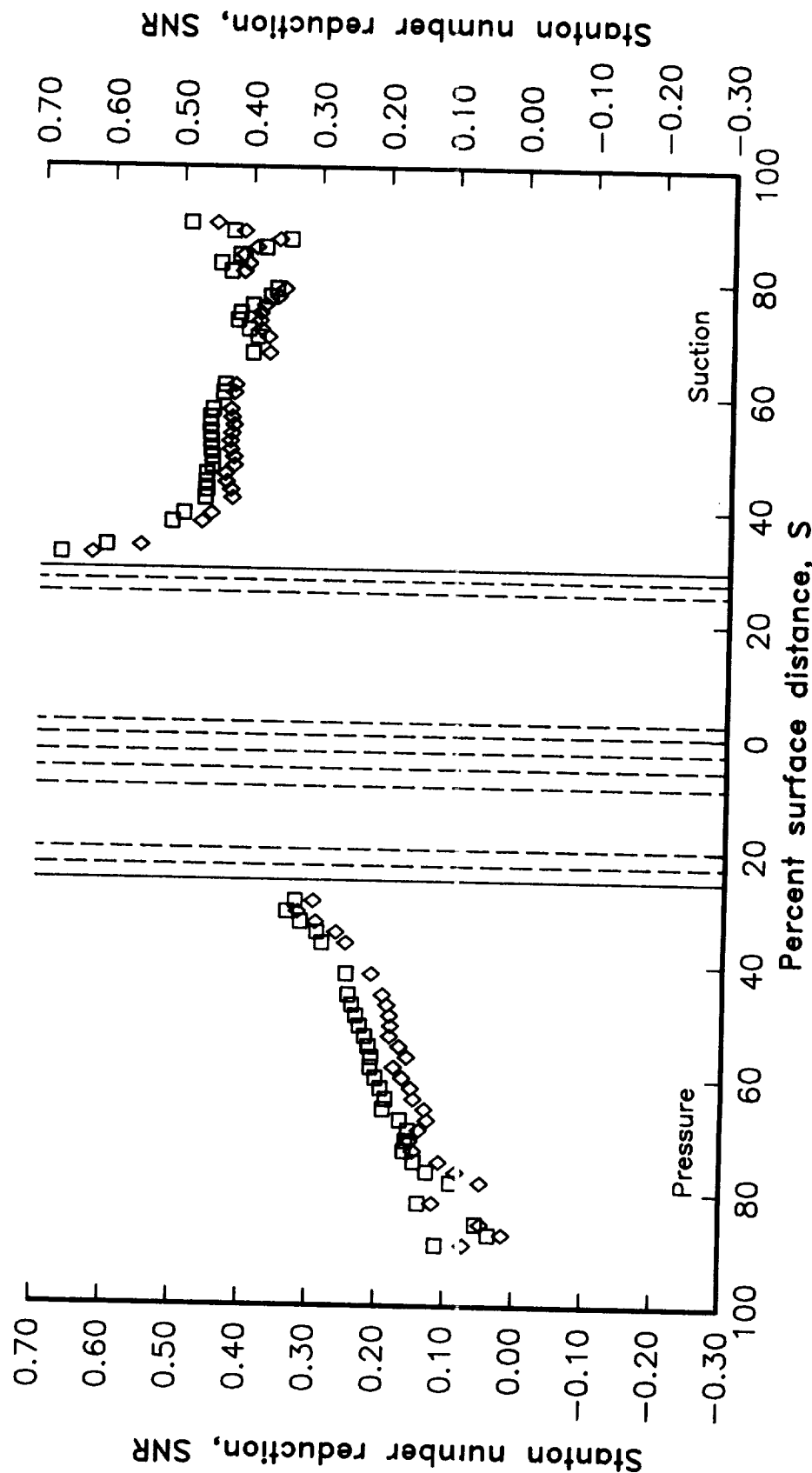


Figure 80. Effects of exit Mach number variations on SNR distributions
-- series X4103.

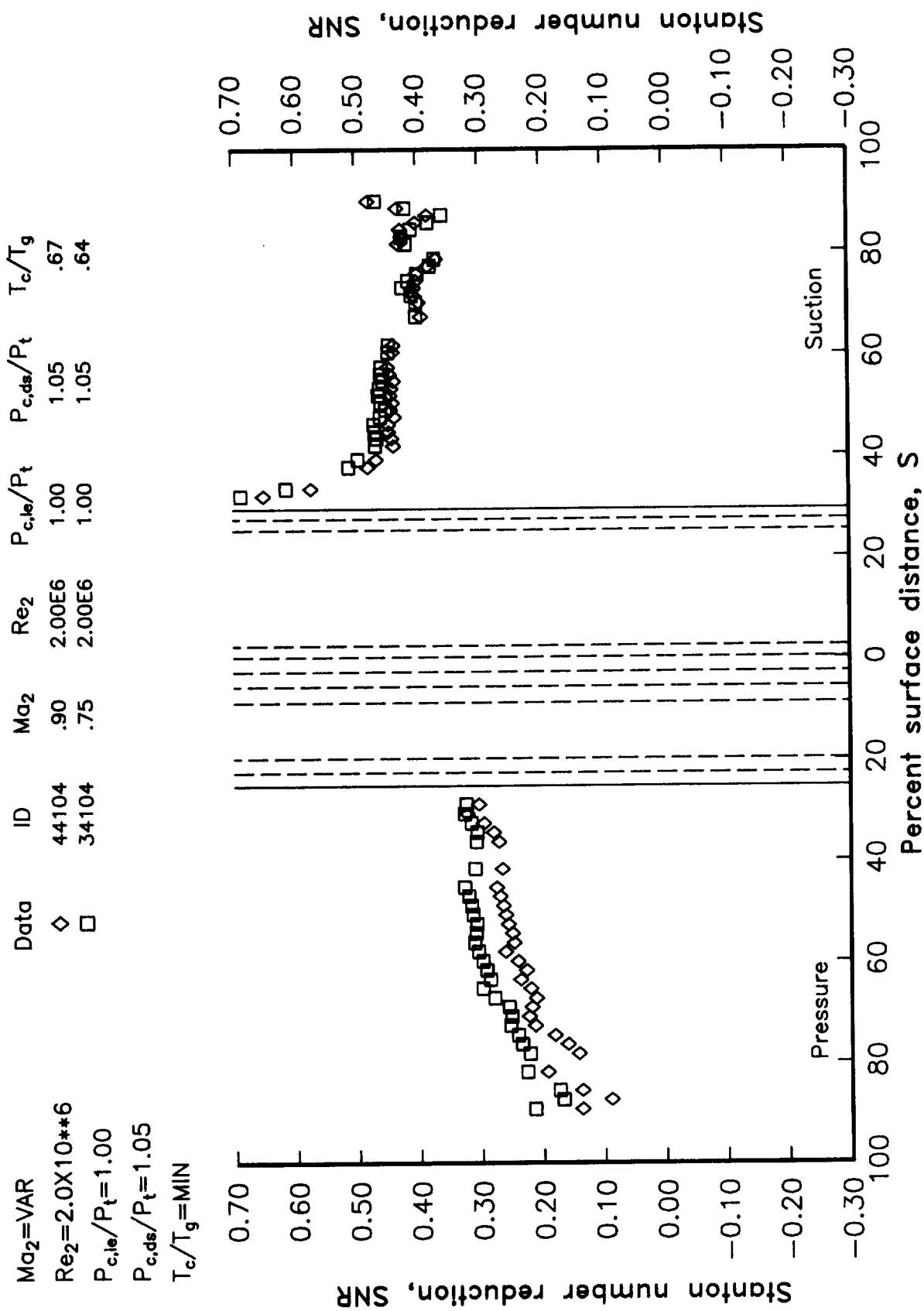


Figure 81. Effects of exit Mach number variations on SNR distributions
-- series X4104.

$M_{\infty 2} = \text{VAR}$	Data	ID	$M_{\infty 2}$	Re_2	$P_{c,\text{le}}/P_t$	$P_{c,\text{ds}}/P_t$	T_c/T_g
$Re_2 = 2.0 \times 10^{**6}$	◊	44105	.89	1.99E6	1.00	1.10	.68
$P_{c,\text{le}}/P_t = 1.00$	□	34105	.75	2.00E6	1.00	1.10	.66
$P_{c,\text{ds}}/P_t = 1.10$							
$T_c/T_g = \text{MIN}$							

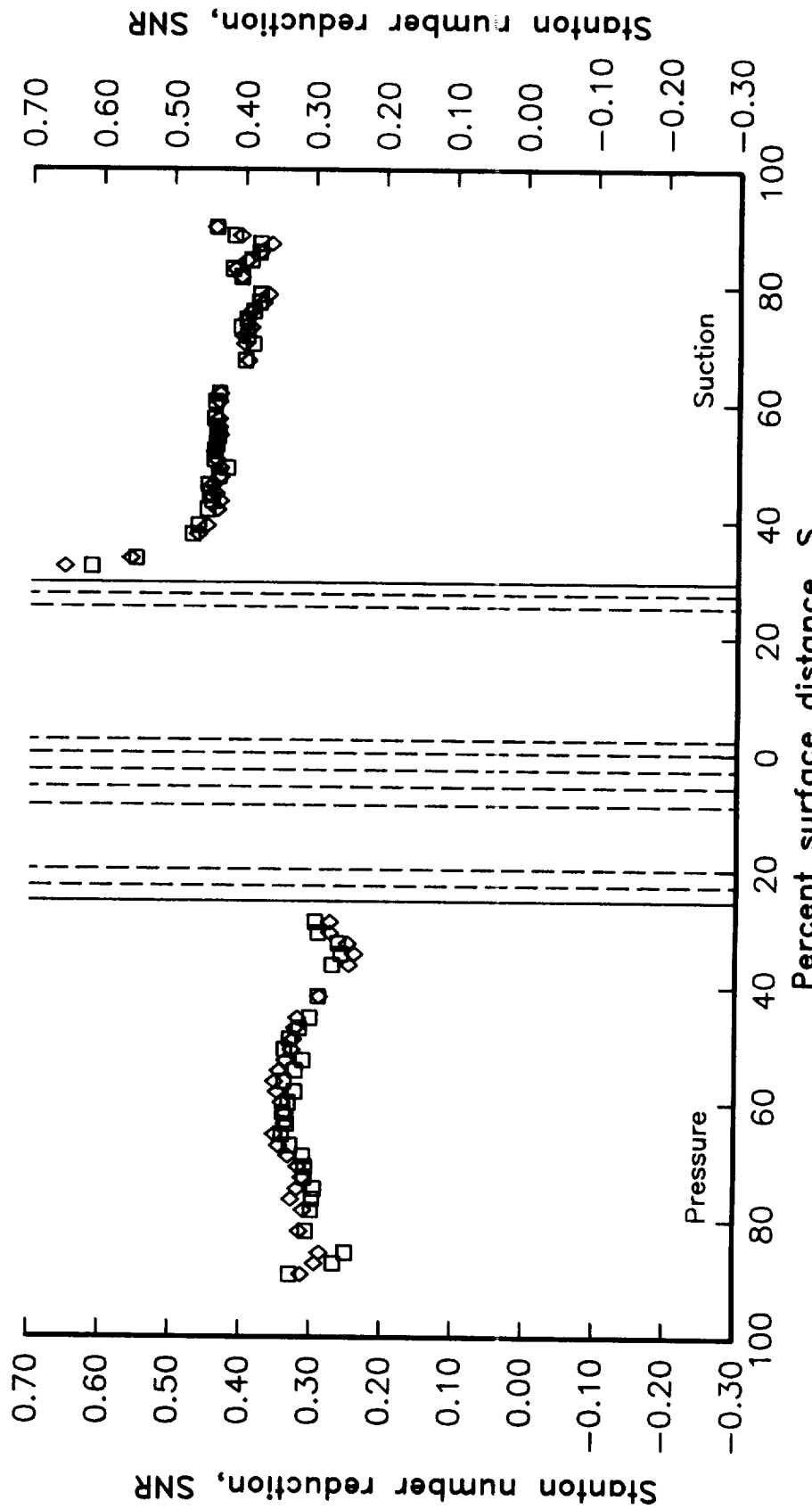


Figure 82. Effects of exit Mach number variations on SNR distributions
-- series X4105.

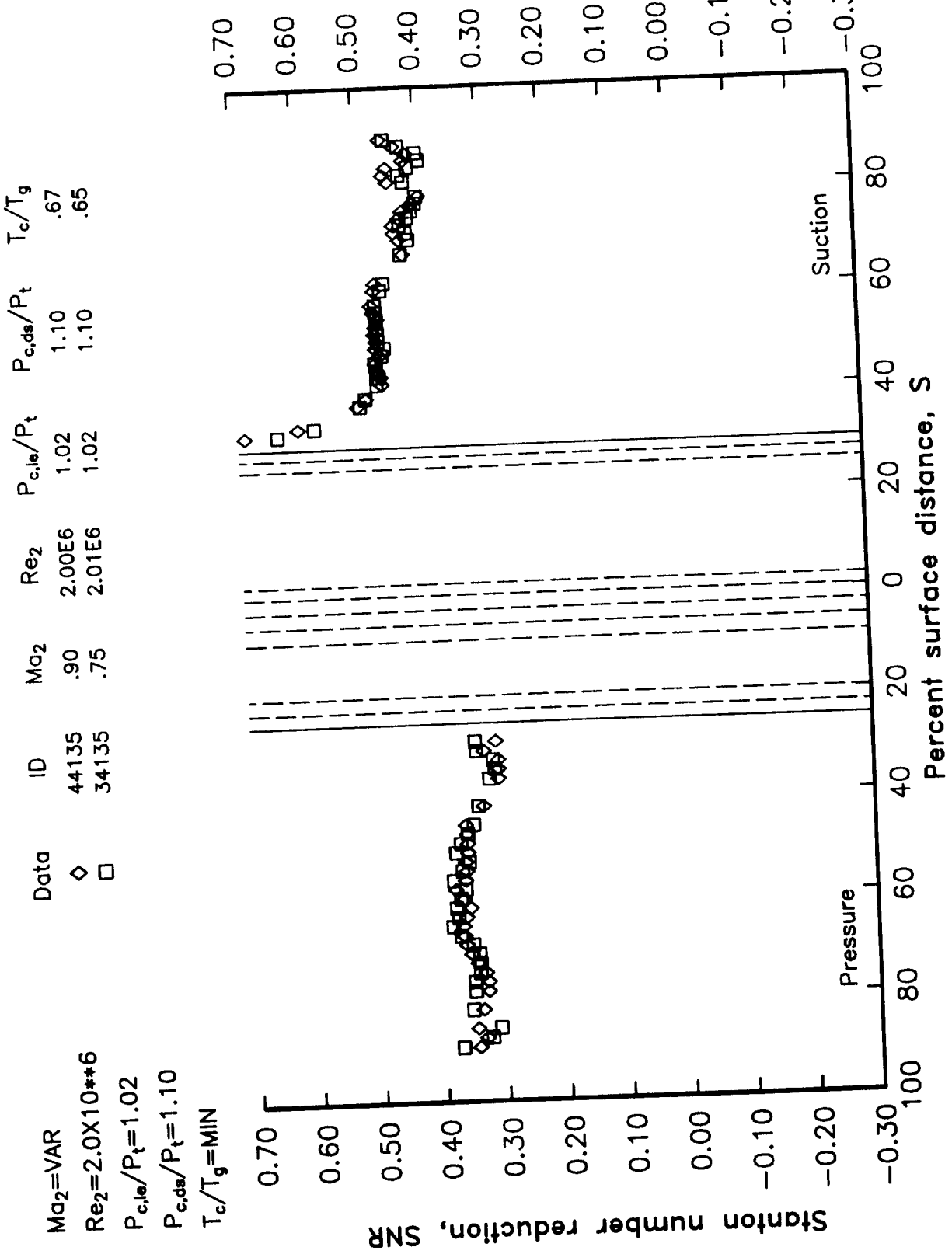


Figure 83. Effects of exit Mach number variations on SNR distributions
-- series X4135.

$Ma_2 = \text{VAR}$
 $Re_2 = 2.0 \times 10^{10} * 6$
 $P_{c,le}/P_t = 1.05$
 $P_{c,ds}/P_t = 1.10$
 $T_c/T_g = \text{MIN}$

Data	ID	Ma_2	Re_2	$P_{c,le}/P_t$	$P_{c,ds}/P_t$	T_c/T_g
◊	44145	.89	1.98E6	1.05	1.10	.68
□	34145	.74	2.00E6	1.05	1.10	.65

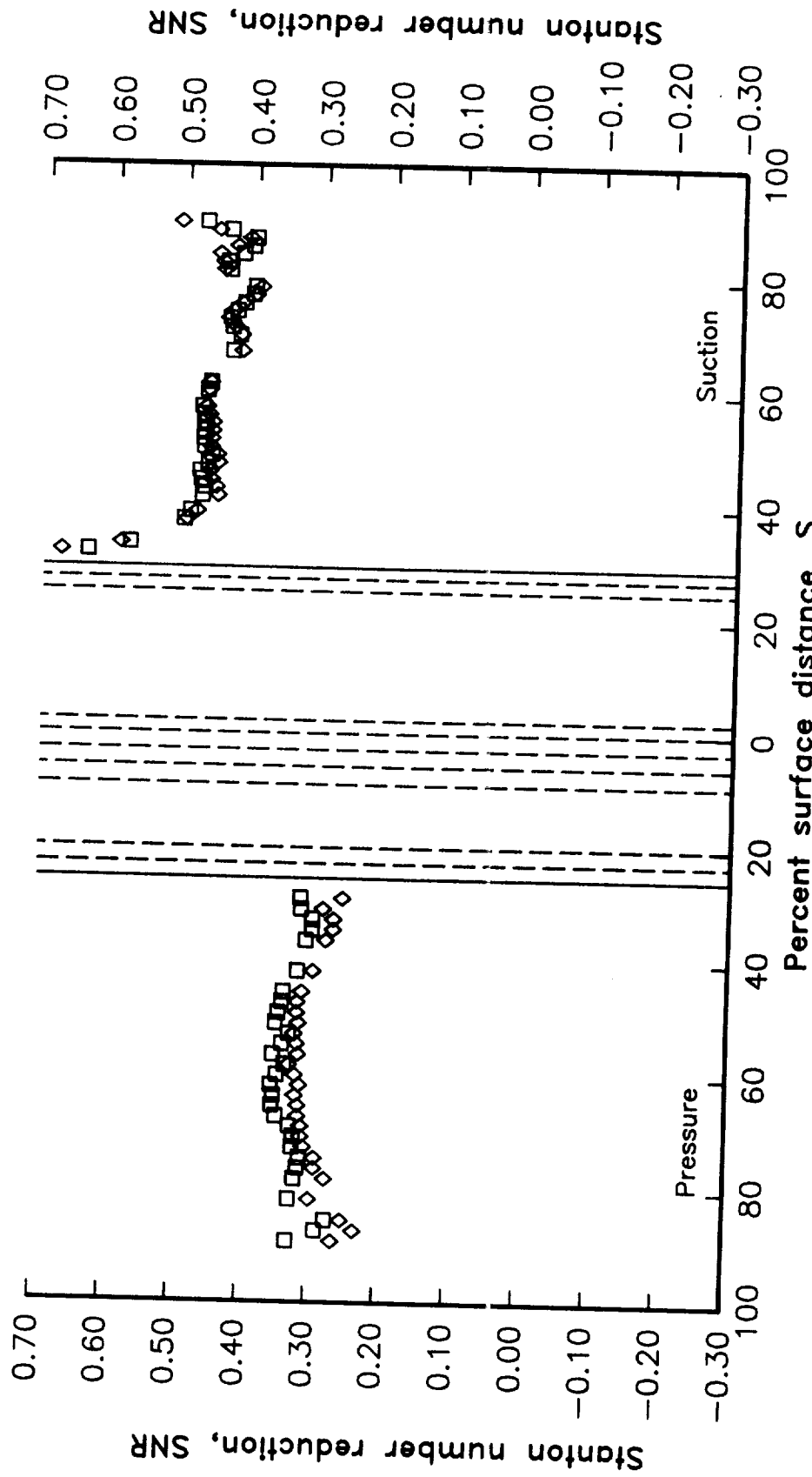


Figure 84. Effects of exit Mach number variations on SNR distributions
-- series X4145.

$Ma_2 = \text{VAR}$
 $Re_2 = 2.0 \times 10^{**6}$
 $P_{c,le}/P_t = 1.10$
 $P_{c,ds}/P_t = 1.10$
 $T_c/T_g = \text{MIN}$

Data	ID	Ma_2	Re_2	$P_{c,le}/P_t$	T_c/T_g
◊	44155	.90	2.00E6	1.10	.66
□	34155	.75	2.05E6	1.10	.67

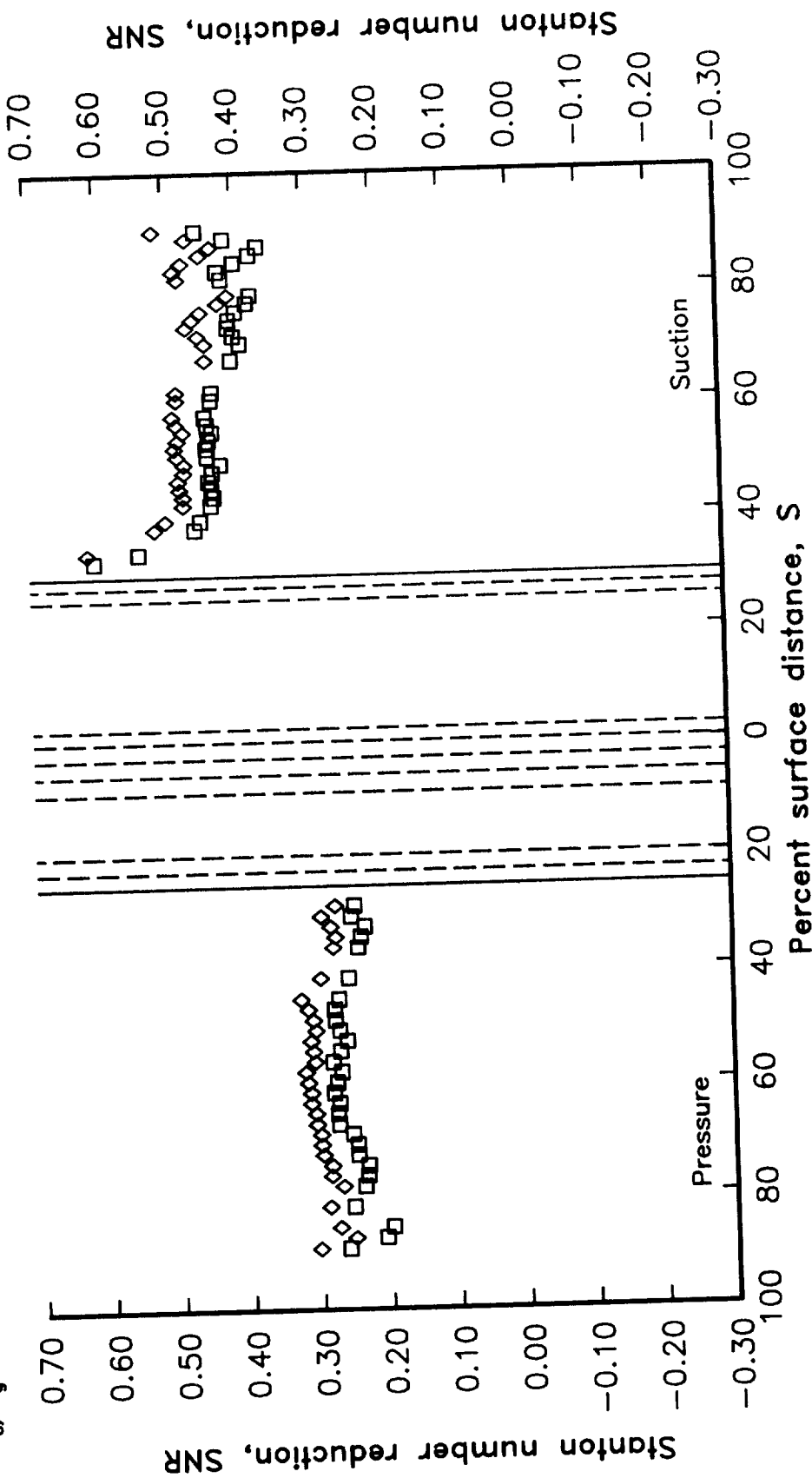


Figure 85. Effects of exit Mach number variations on SNR distributions
-- series X4155.

$Ma_2 = VAR$
 $Re_2 = 2.0 \times 10^{**6}$
 $P_{c,le}/P_t = 1.00$
 $P_{c,ds}/P_t = 1.02$
 $T_c/T_g = MAX$

	ID	Ma_2	Re_2	$P_{c,le}/P_t$	$P_{c,ds}/P_t$	T_c/T_g
◊	44303	.90	2.01E6	1.00	1.02	.84
□	34303	.75	2.00E6	1.00	1.02	.86

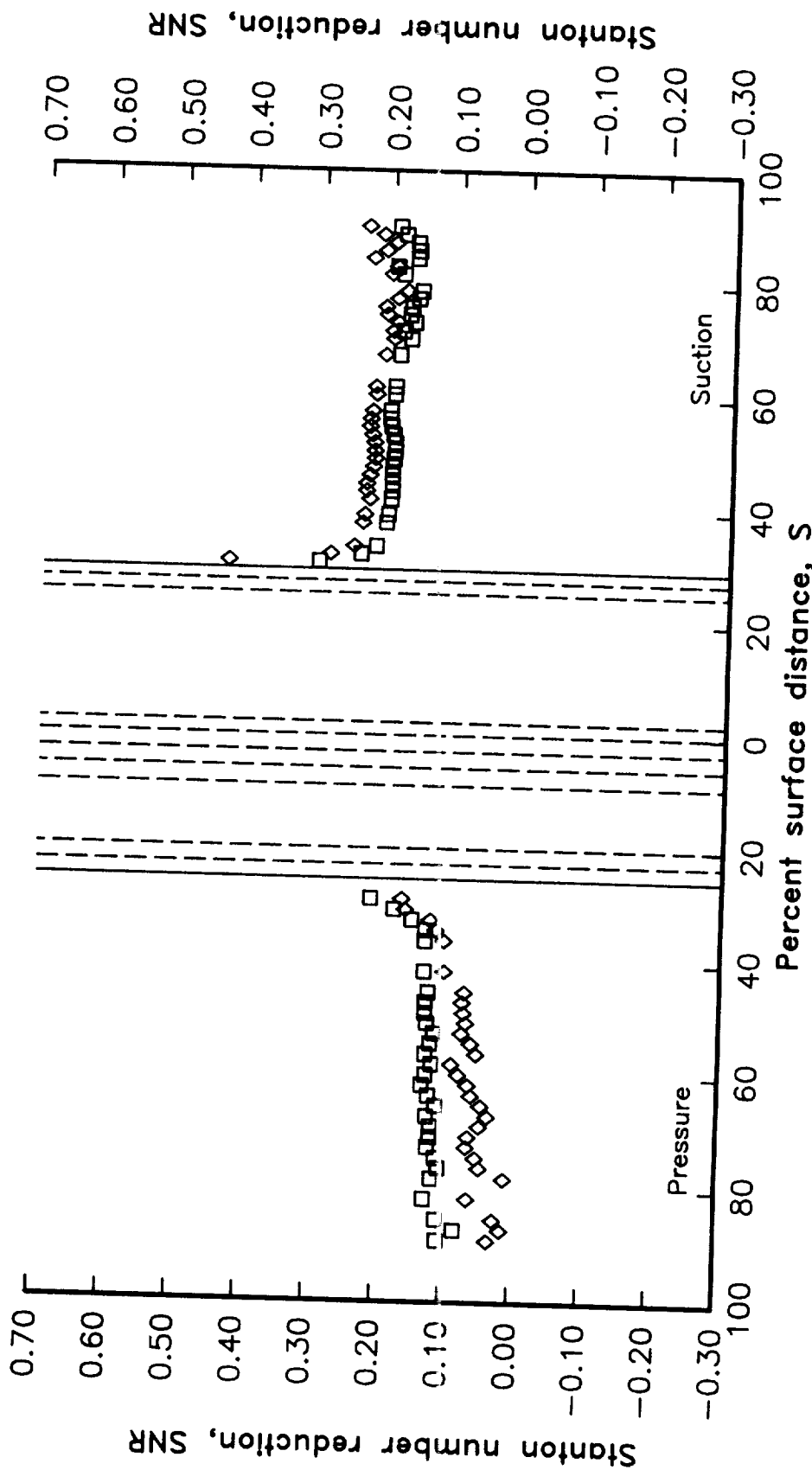


Figure 86. Effects of exit Mach number variations on SNR distributions
-- series X4303.

$Ma_2 = \text{VAR}$
 $Re_2 = 2.0 \times 10^{**6}$
 $P_{c,le}/P_t = 1.00$
 $P_{c,ds}/P_t = 1.05$
 $T_c/T_g = \text{MAX}$

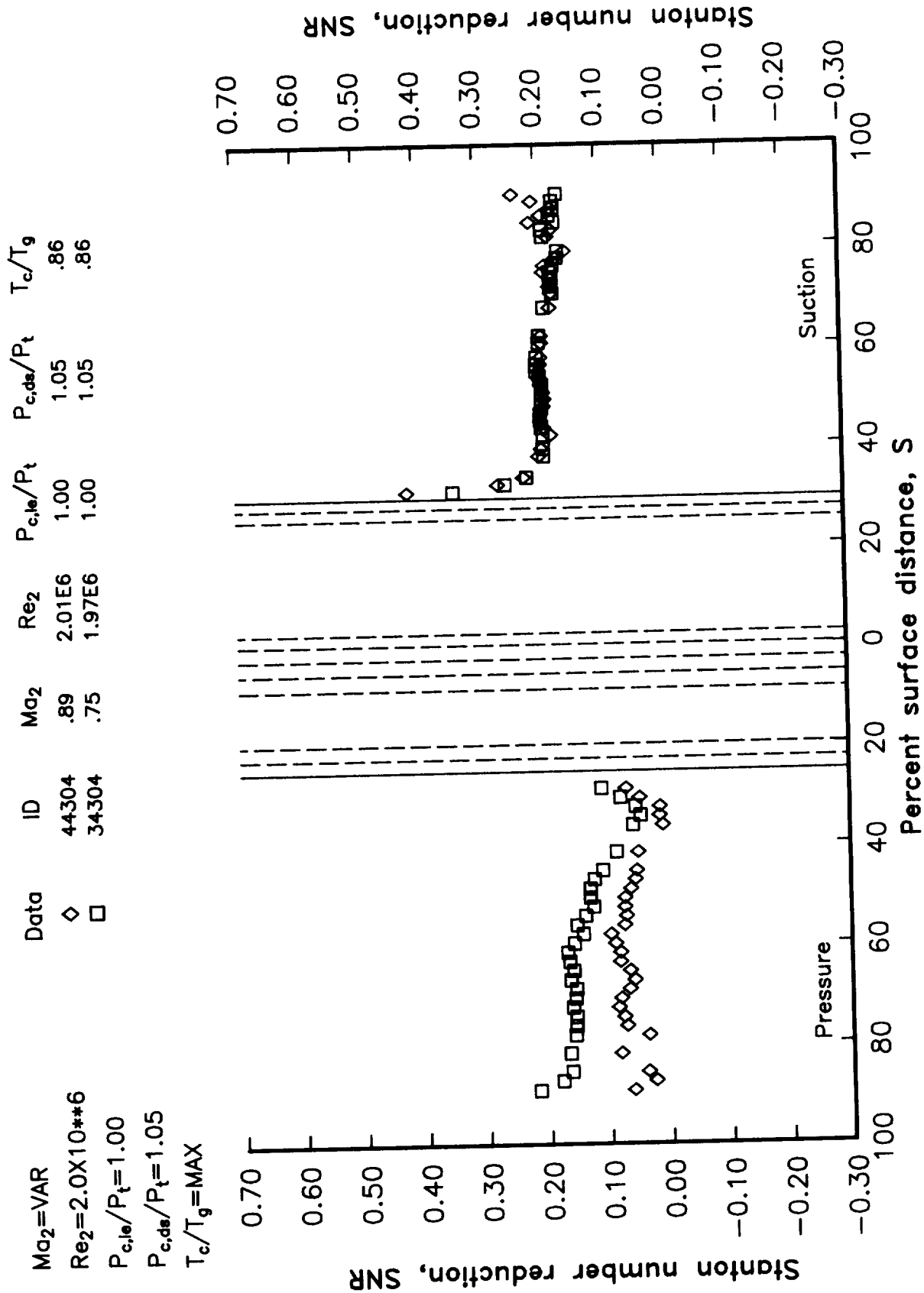


Figure 87. Effects of exit Mach number variations on SNR distributions
-- series X4304.

$Ma_2 = \text{VAR}$
 $Re_2 = 2.0 \times 10^{**6}$
 $P_{c,\text{le}}/P_t = 1.00$
 $P_{c,\text{da}}/P_t = 1.10$
 $T_c/T_g = \text{MAX}$

Data	ID	Ma_2	Re_2	$P_{c,\text{le}}/P_t$	$P_{c,\text{da}}/P_t$	T_c/T_g
◊	44305	.90	2.03E6	1.00	1.11	.85
□	34305	.75	2.03E6	1.00	1.10	.87

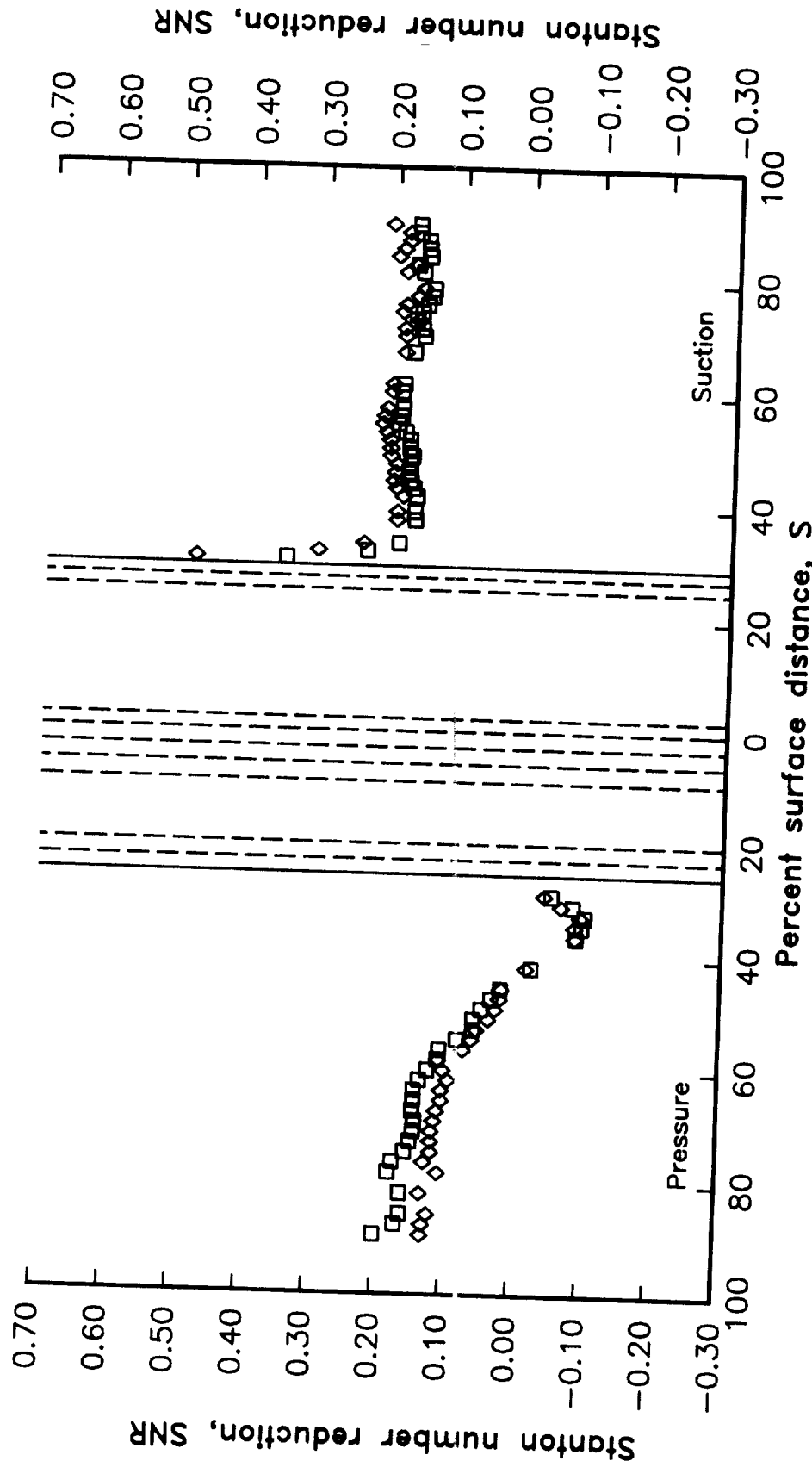


Figure 88. Effects of exit Mach number variations on SNR distributions
-- series X4305.

	$Ma_2 = 0.9$	$Re_2 = VAR$	$P_{c,ds}/P_t = 1.00$	$T_c/T_g = MIN$
Data	ID	Ma_2	Re_2	$P_{c,ds}/P_t$
Δ	45103	.89	2.48E6	1.00
\diamond	44103	.89	1.96E6	1.00
\square	43103	.89	1.49E6	1.00

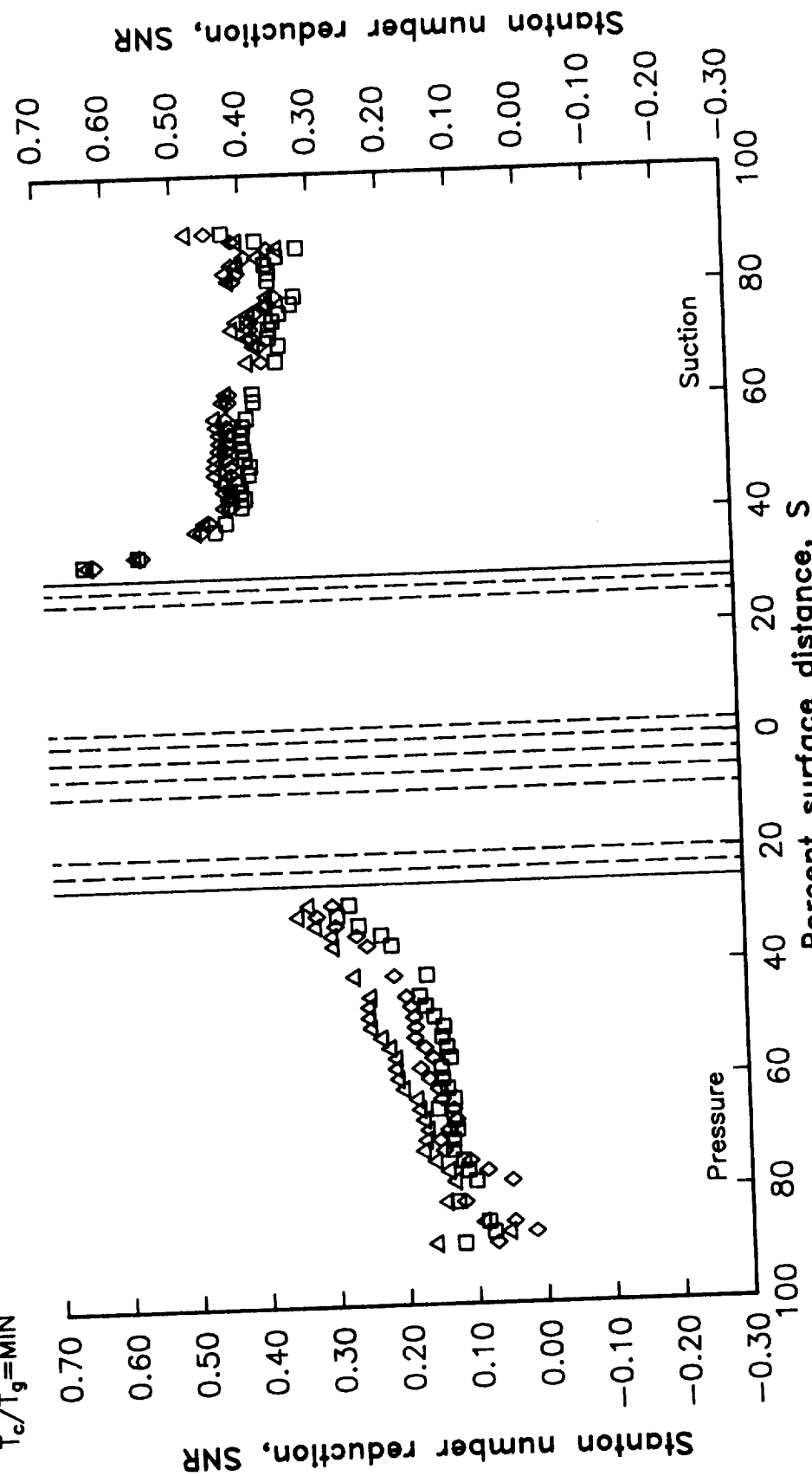


Figure 89. Effects of exit Reynolds number variations on SNR distributions
— series 4X10³.

$Ma_2=0.9$	Data	ID	Ma_2	Re_2	$P_{c,le}/P_t$	$P_{c,de}/P_t$	T_c/T_g
$Re_2=VAR$	△	45104	.89	2.49E6	1.00	1.06	.67
$P_{c,le}/P_t=1.00$	◇	44104	.90	2.00E6	1.00	1.05	.67
$P_{c,de}/P_t=1.05$	□	43104	.91	1.51E6	1.00	1.06	.67
$T_c/T_g=MIN$							

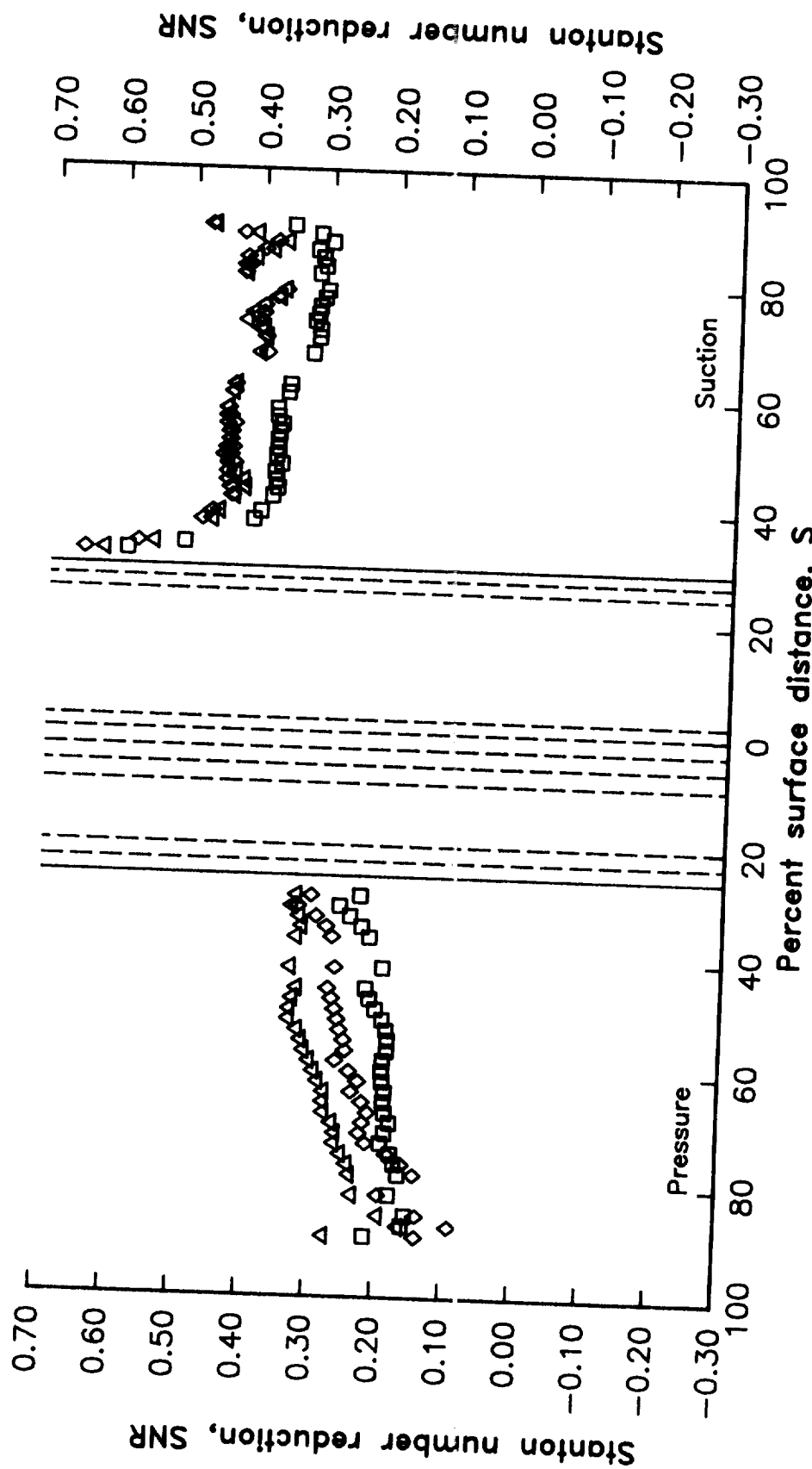


Figure 90. Effects of exit Reynolds number variations on SNR distributions
-- Series 4X10⁴.

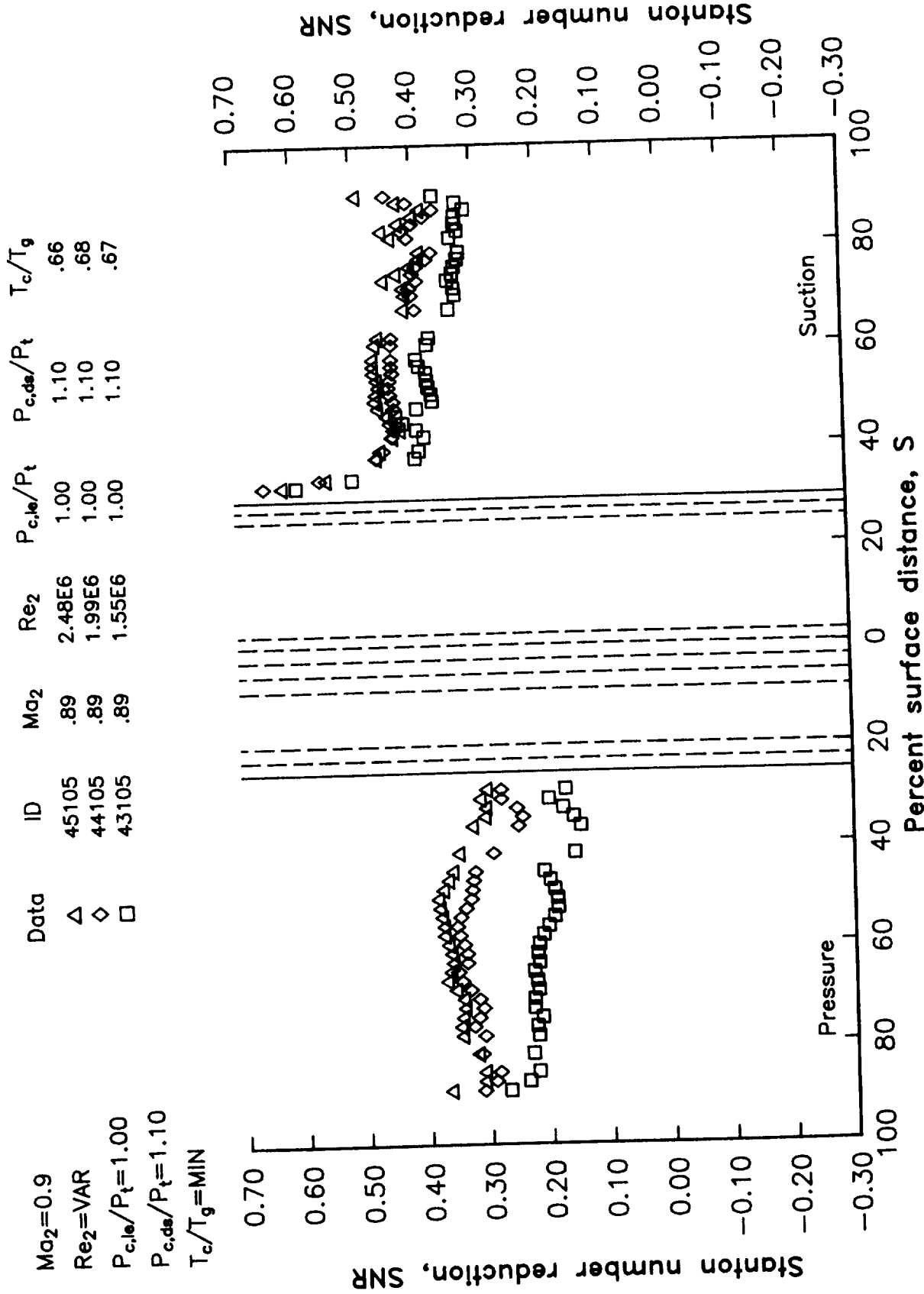


Figure 91. Effects of exit Reynolds number variations on SNR distributions
-- series 4X105.

$Ma_2 = 0.9$	Data	ID	Ma_2	Re_2	$P_{c,le}/P_t$	$P_{c,de}/P_t$	T_c/T_g
$Re_2 = VAR$	△	45135	.90	2.51E6	1.02	1.09	.64
$P_{c,le}/P_t = 1.02$	◊	44135	.90	2.00E6	1.02	1.10	.67
$P_{c,de}/P_t = 1.10$	□	43135	.90	1.52E6	1.02	1.11	.65
$T_c/T_g = MIN$							

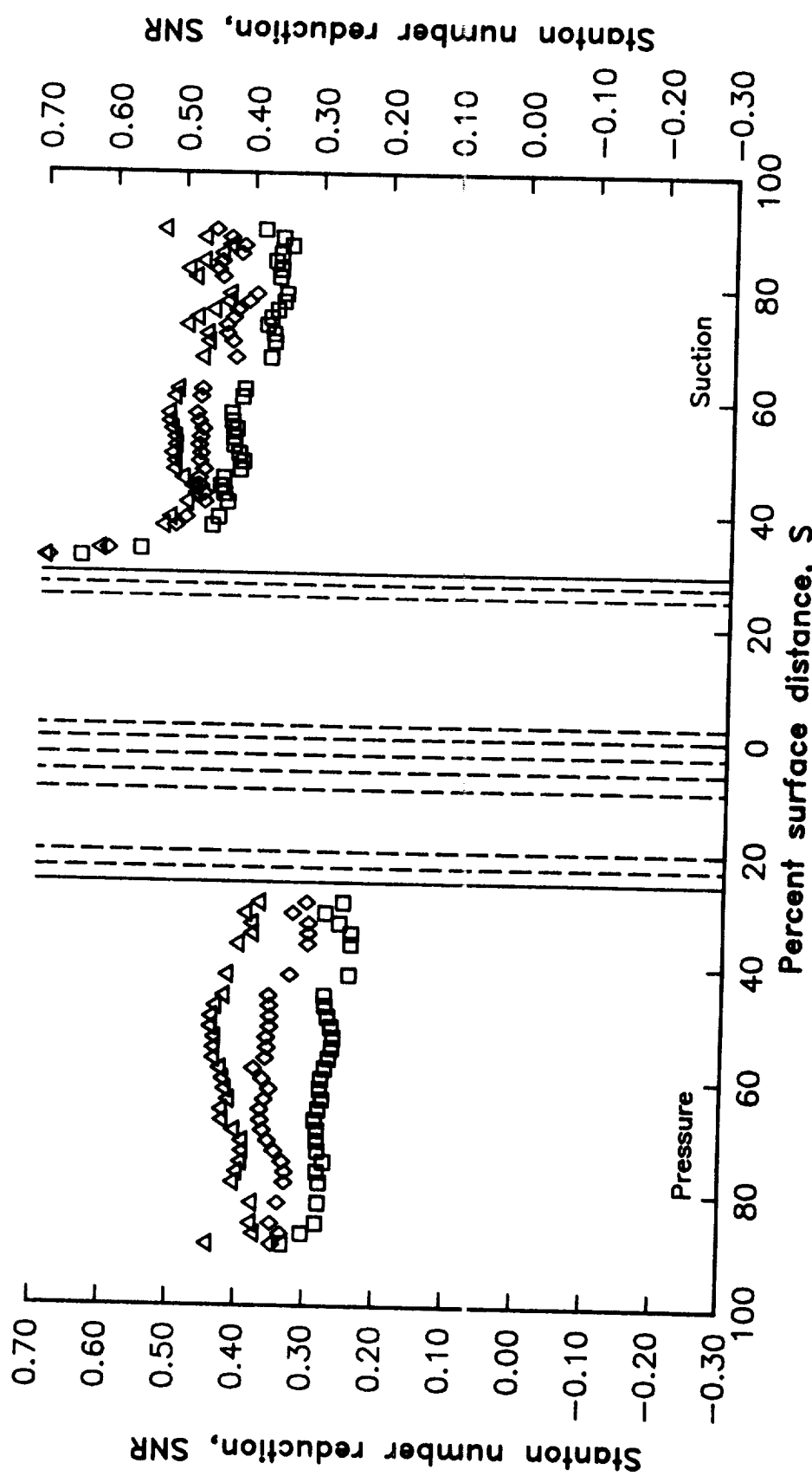


Figure 92. Effects of exit Reynolds number variations on SNR distributions
-- series 45135.
-- series 44135.

	Data	ID	Ma ₂	Re ₂	P _{c,dz} /P _t	T _c /T _g
Ma ₂ =0.9						
Re ₂ =VAR	△	45145	.89	2.52E6	1.05	.65
P _{c,le} /P _t =1.05	◊	44145	.89	1.98E6	1.05	.68
P _{c,dz} /P _t =1.10	□	43145	.90	1.52E6	1.05	.66
T _c /T _g =MIN						

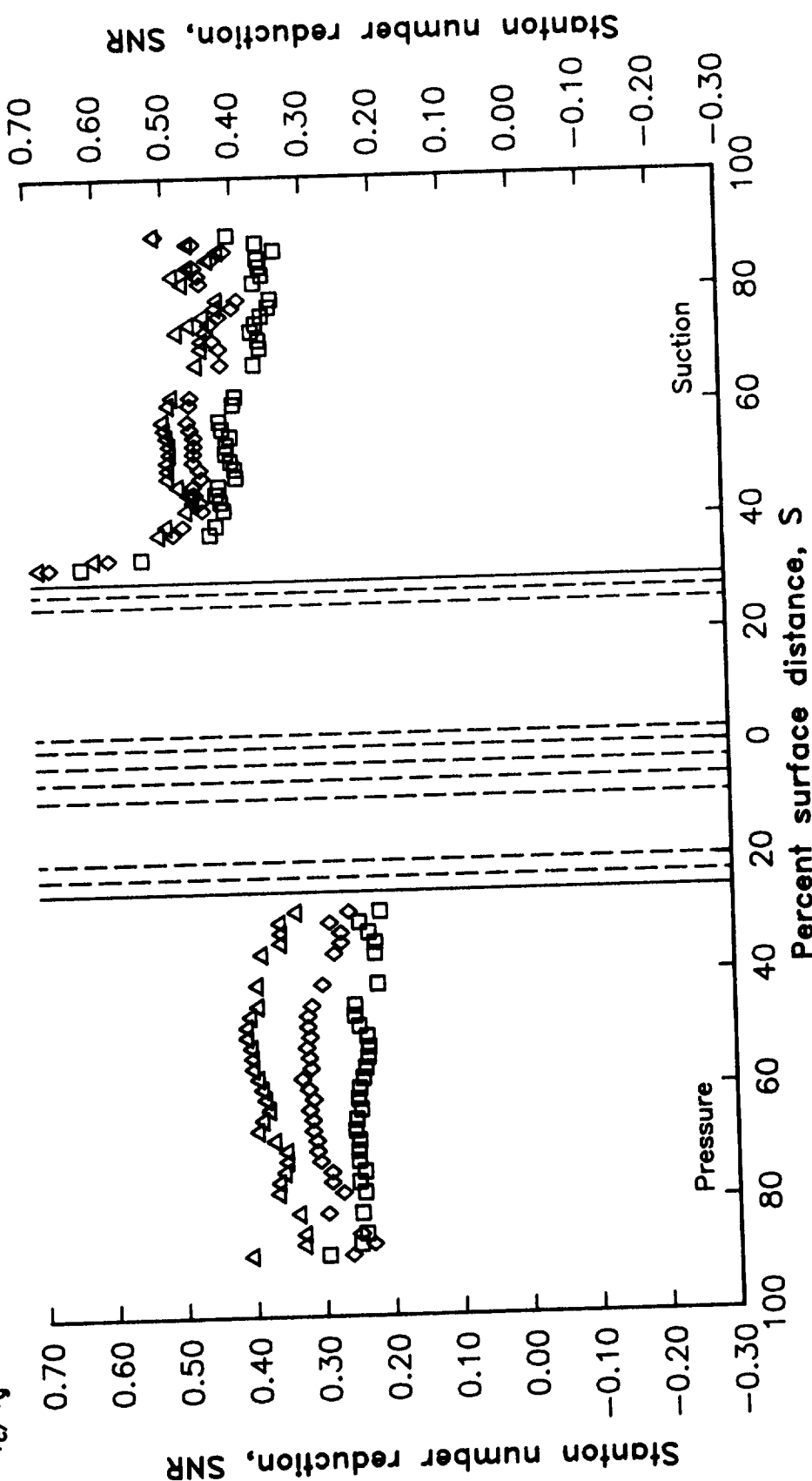


Figure 93. Effects of exit Reynolds number variations on SNR distributions
 — series 4X145.
 - - series 4X145.

$Ma_2=0.9$	Data	ID	Ma_2	Re_2	$P_{c,lo}/P_t$	T_c/T_g
$Re_2=VAR$	△	45155	.90	2.50E6	1.11	1.12
$P_{c,lo}/P_t=1.10$	◇	44155	.90	2.00E6	1.10	.66
$P_{c,ds}/P_t=1.10$	□	43155	.89	1.55E6	1.10	.66
$T_c/T_g=MIN$						

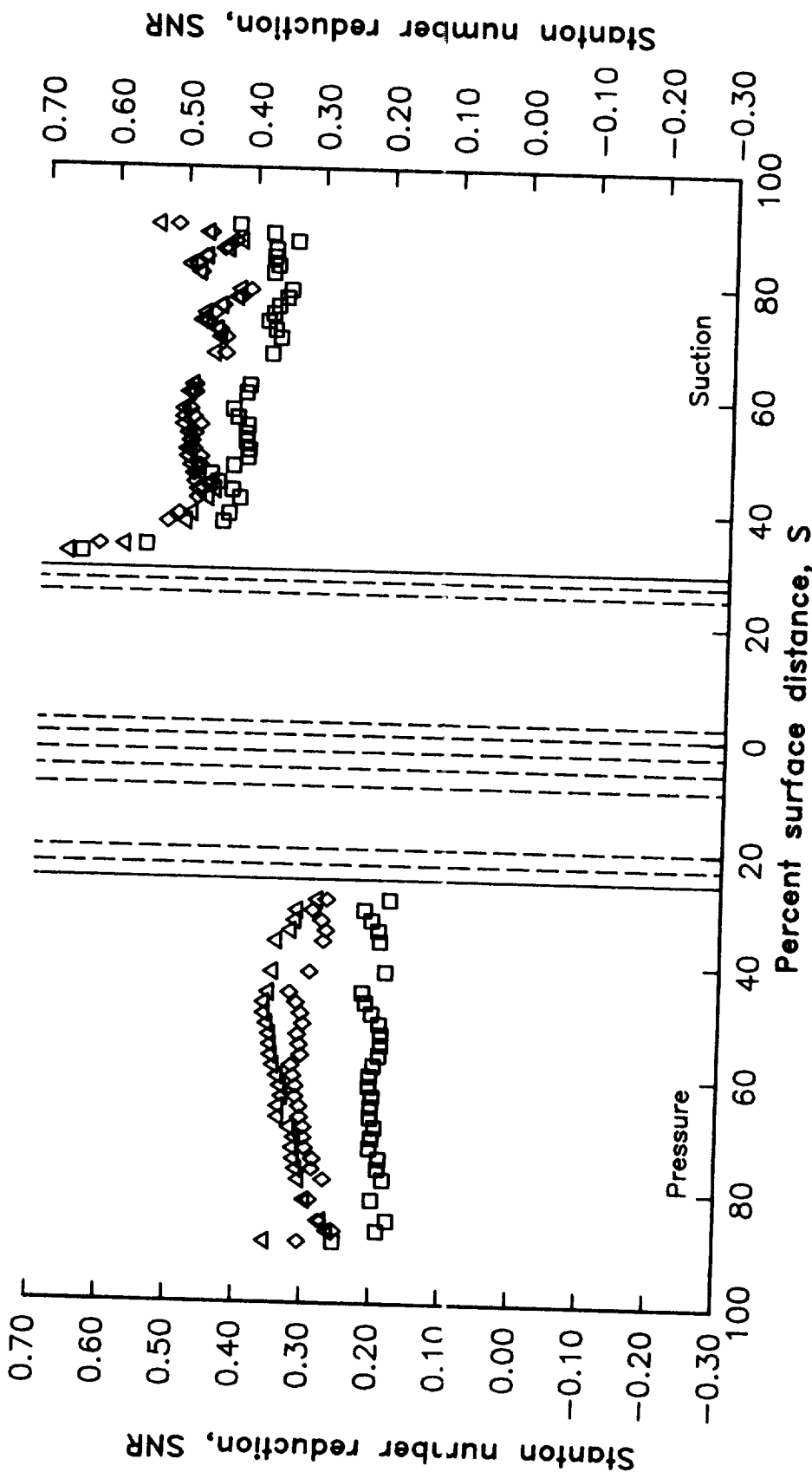


Figure 94. Effects of exit Reynolds number variations on SNR distributions
-- series 4X155.

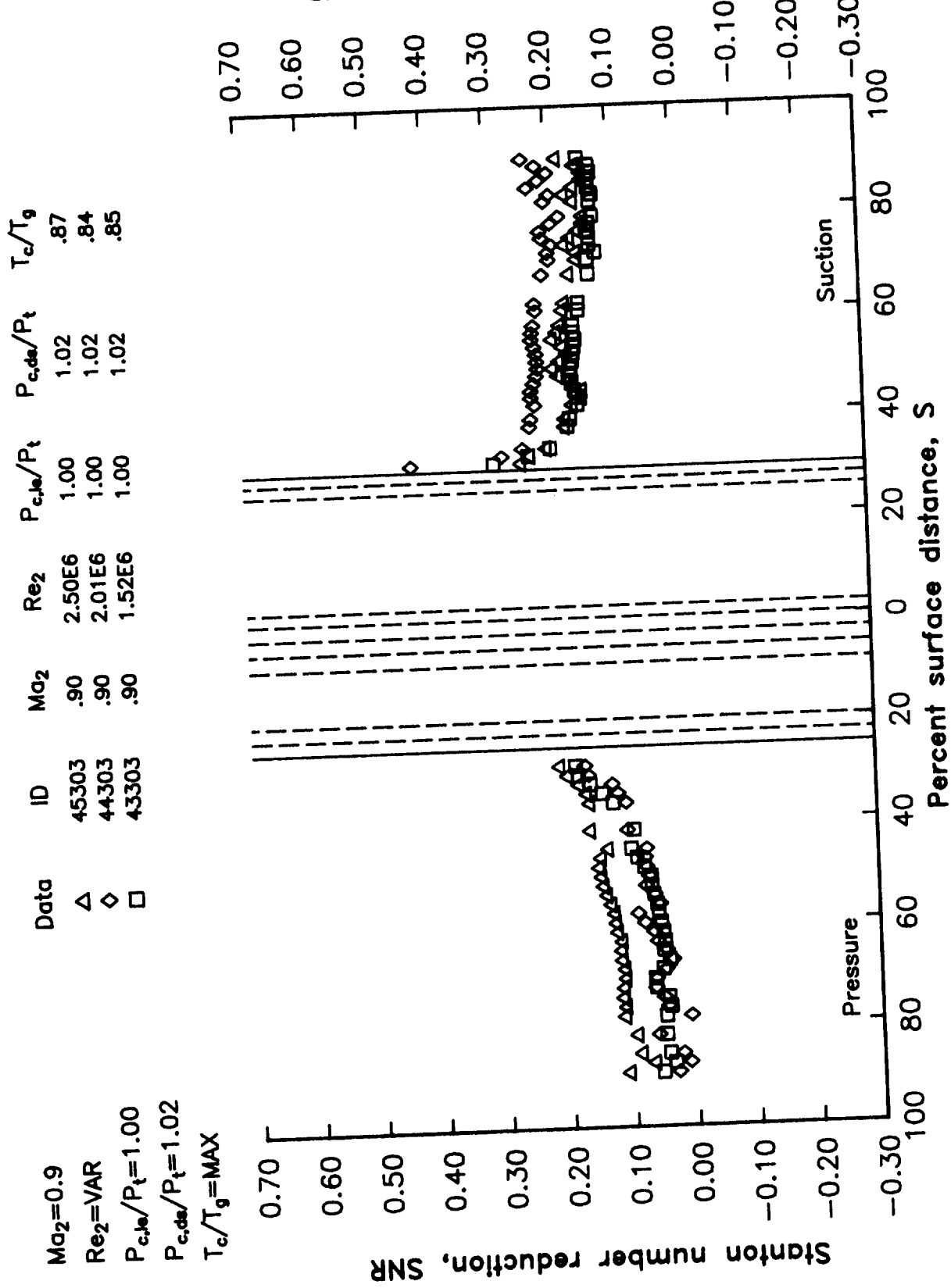


Figure 95. Effects of exit Reynolds number variations on SNR distributions
 — series 4X303.

$Ma_2 = 0.9$	Data	ID	Ma_2	Re_2	$P_{c,de}/P_t$	$P_{c,de}/P_t$	T_c/T_g
$Re_2 = VAR$.89	2.49E6	1.00	1.05	.89
$P_{c,de}/P_t = 1.00$	△	45304	.89	2.01E6	1.00	1.05	.86
$P_{c,de}/P_t = 1.05$	◊	44304	.89	1.52E6	1.00	1.05	.85
$T_c/T_g = MAX$	□	43304	.90	1.52E6	1.00	1.05	.85

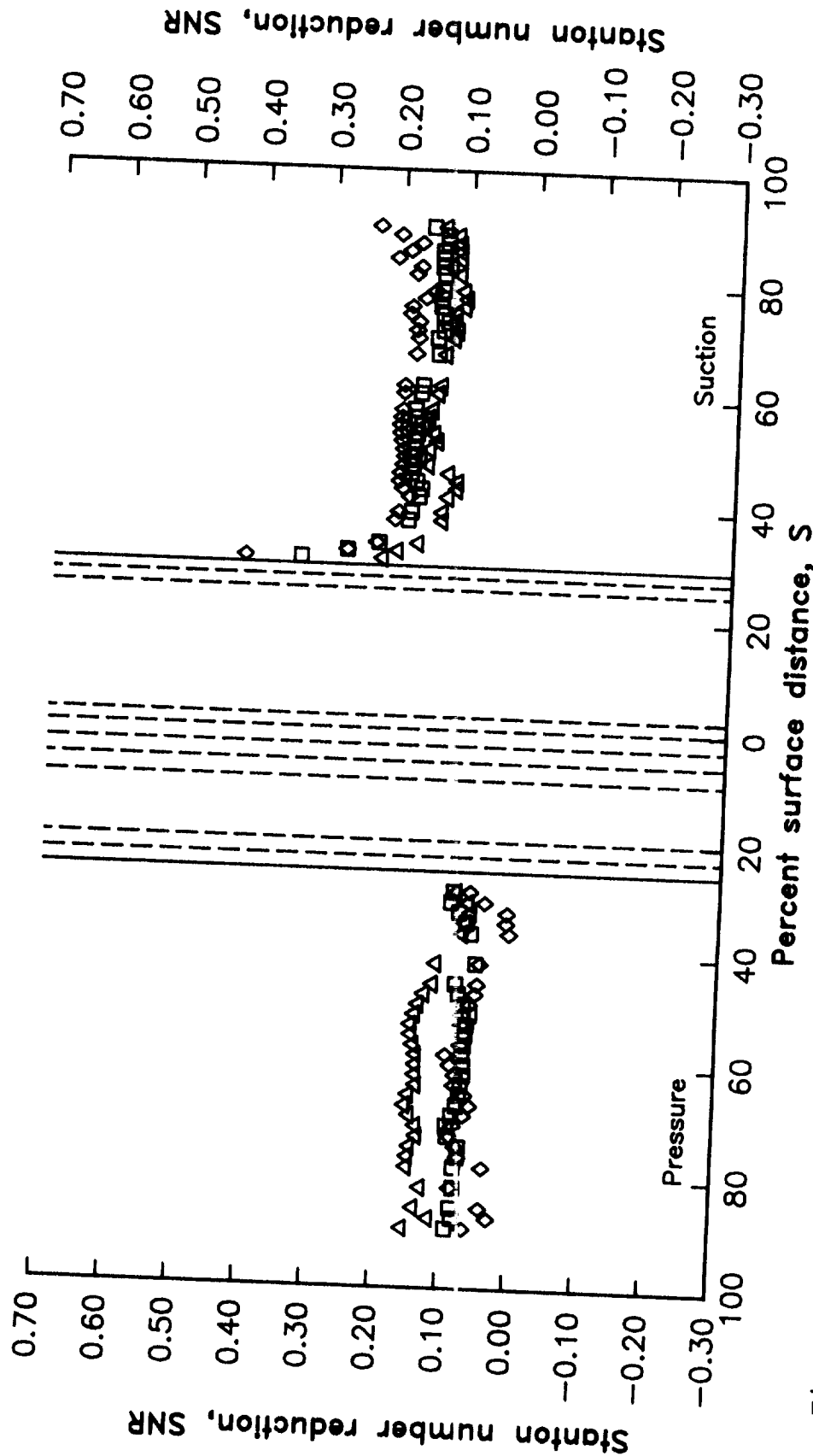


Figure 96. Effects of exit Reynolds number variations on SNR distributions
-- series 4X304.

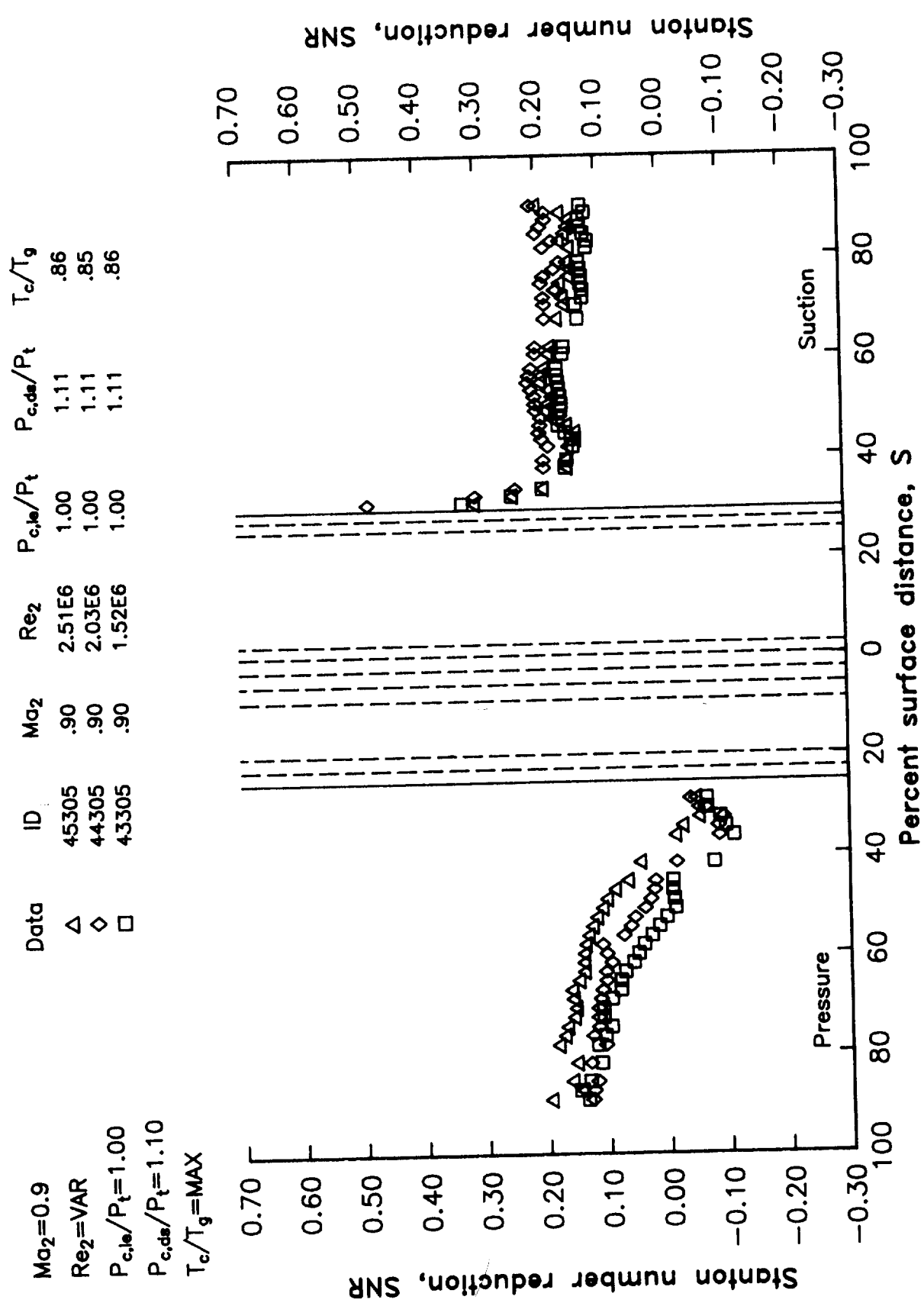


Figure 97. Effects of exit Reynolds number variations on SNR distributions

-- series 4X305.

APPENDIX C
TABULATED THROAT PASSAGE STATIC PRESSURE DATA

Tabulated throat passage static pressure data for each run code of the downstream and leading edge film-cooled C3X cascade are presented in Tables X and XI. These data sets are listed in run code order, and the actual operating conditions associated with each run code were given previously in Table VI. Table X contains the upper passage throat static pressure data while Table XI contains the lower passage data. Throat passage static pressure data are tabulated as static-to-inlet total pressure ratio versus percent surface distance from the upper vane surface midspan to lower vane surface midspan.

ORIGINAL PAGE IS
OF POOR QUALITY

Table X.
Upper throat passage static pressure data

RUN CODE	PERCENTAGE DISTANCE FROM UPPER VANE MIDSPAN TO LOWER VANE MIDSPAN VIA THE ENDWALL: TOTAL DISTANCE = 11.008 cm (4.296 in)	ENDWALL						PRESSURE SURFACE (LOWER VANE)							
		SUCTION SURFACE (UPPER VANE)	0.362	0.409	0.470	0.530	0.590	0.639	0.679	0.704	0.733	0.778	0.840	0.913	0.953
34000	0.131 0.171 0.245 0.306	0.657 0.654 0.637	0.656 0.680 0.690	0.698 0.703	0.701	0.680	0.662	0.661	0.652	0.670	0.673	0.663			
34103	0.664 0.664 0.665 0.662	0.658 0.662 0.667	0.662 0.687	0.697 0.706	0.711 0.712	0.692 0.671	0.668 0.659	0.668 0.659	0.678 0.682	0.682 0.668					
34104	0.658 0.659 0.656 0.652	0.657 0.659	0.683 0.692	0.701 0.706	0.707 0.707	0.687 0.665	0.661 0.652	0.671 0.675	0.675 0.661						
34105	0.661 0.663 0.661 0.654	0.665 0.686	0.695 0.704	0.708 0.705	0.686 0.667	0.664 0.657	0.675 0.676	0.676 0.663							
34135	0.661 0.663 0.661 0.653	0.664 0.685	0.695 0.704	0.708 0.705	0.691 0.673	0.670 0.663	0.681 0.682	0.682 0.669							
34145	0.667 0.668 0.666 0.658	0.670 0.690	0.700 0.709	0.713 0.710	0.691 0.673	0.670 0.662	0.649 0.649	0.670 0.660	0.673 0.660						
34155	0.657 0.659 0.657 0.638	0.661 0.684	0.692 0.700	0.704 0.700	0.683 0.662	0.658 0.655	0.671 0.674	0.674 0.664							
34303	0.658 0.658 0.654 0.637	0.656 0.680	0.690 0.699	0.703 0.701	0.681 0.663	0.662 0.653	0.671 0.674	0.674 0.664							
34304	0.657 0.657 0.653 0.636	0.656 0.680	0.690 0.698	0.703 0.701	0.680 0.662	0.661 0.652	0.670 0.673	0.673 0.662							
34305	0.658 0.658 0.654 0.637	0.657 0.680	0.690 0.699	0.703 0.701	0.681 0.663	0.662 0.652	0.671 0.674	0.674 0.664							
43000	0.557 0.560 0.555 0.557	0.569 0.583	0.594 0.602	0.607 0.598	0.584 0.564	0.565 0.564	0.574 0.573	0.574 0.560							
43103	0.565 0.567 0.564 0.564	0.570 0.592	0.603 0.611	0.615 0.612	0.591 0.568	0.564 0.562	0.571 0.571	0.571 0.565	0.571 0.565	0.571 0.565	0.571 0.565	0.571 0.565	0.571 0.565	0.571 0.565	
43104	0.555 0.557 0.552 0.555	0.568 0.582	0.592 0.600	0.605 0.597	0.583 0.562	0.563 0.562	0.671 0.674	0.674 0.662	0.671 0.662	0.671 0.662	0.671 0.662	0.671 0.662	0.671 0.662	0.671 0.662	0.671 0.662
43105	0.527 0.530 0.525 0.530	0.544 0.556	0.567 0.574	0.579 0.572	0.557 0.557	0.535 0.535	0.573 0.573	0.574 0.573							
43135	0.541 0.544 0.539 0.543	0.555 0.568	0.579 0.587	0.592 0.583	0.570 0.558	0.549 0.547	0.556 0.556	0.556 0.556	0.556 0.556	0.556 0.556	0.556 0.556	0.556 0.556	0.556 0.556	0.556 0.556	0.556 0.556
43145	0.541 0.544 0.539 0.543	0.556 0.569	0.580 0.588	0.593 0.584	0.570 0.558	0.548 0.547	0.556 0.556	0.556 0.556	0.556 0.556	0.556 0.556	0.556 0.556	0.556 0.556	0.556 0.556	0.556 0.556	0.556 0.556
43155	0.527 0.530 0.524 0.530	0.544 0.555	0.567 0.575	0.579 0.572	0.557 0.557	0.535 0.535	0.574 0.574	0.575 0.574							
43303	0.559 0.561 0.556 0.558	0.571 0.565	0.596 0.604	0.609 0.609	0.587 0.583	0.557 0.548	0.549 0.547	0.549 0.547	0.549 0.547	0.549 0.547	0.549 0.547	0.549 0.547	0.549 0.547	0.549 0.547	0.549 0.547
43304	0.559 0.562 0.557 0.559	0.572 0.587	0.597 0.605	0.605 0.602	0.588 0.567	0.568 0.568	0.575 0.575	0.575 0.575	0.575 0.575	0.575 0.575	0.575 0.575	0.575 0.575	0.575 0.575	0.575 0.575	0.575 0.575
43305	0.560 0.562 0.558 0.560	0.572 0.586	0.596 0.605	0.605 0.602	0.588 0.567	0.564 0.564	0.575 0.575	0.575 0.575	0.575 0.575	0.575 0.575	0.575 0.575	0.575 0.575	0.575 0.575	0.575 0.575	0.575 0.575
44000	0.563 0.564 0.559 0.559	0.571 0.589	0.600 0.608	0.609 0.601	0.587 0.566	0.567 0.567	0.574 0.574	0.574 0.574							
44103	0.566 0.567 0.563 0.556	0.577 0.595	0.605 0.613	0.615 0.608	0.588 0.566	0.568 0.568	0.575 0.575	0.575 0.575	0.575 0.575	0.575 0.575	0.575 0.575	0.575 0.575	0.575 0.575	0.575 0.575	0.575 0.575
44104	0.555 0.556 0.553 0.549	0.570 0.587	0.596 0.603	0.603 0.596	0.579 0.559	0.534 0.534	0.534 0.534	0.534 0.534							
44105	0.561 0.563 0.560 0.561	0.568 0.590	0.601 0.609	0.611 0.607	0.585 0.565	0.554 0.554	0.574 0.574	0.574 0.574							
44106	0.558 0.560 0.557 0.559	0.565 0.588	0.598 0.606	0.608 0.608	0.584 0.570	0.569 0.569	0.577 0.577	0.577 0.577	0.577 0.577	0.577 0.577	0.577 0.577	0.577 0.577	0.577 0.577	0.577 0.577	0.577 0.577
44107	0.564 0.566 0.562 0.564	0.570 0.592	0.603 0.613	0.609 0.609	0.586 0.563	0.563 0.563	0.566 0.566	0.566 0.566	0.566 0.566	0.566 0.566	0.566 0.566	0.566 0.566	0.566 0.566	0.566 0.566	0.566 0.566
44108	0.563 0.565 0.562 0.564	0.570 0.591	0.602 0.612	0.606 0.606	0.584 0.560	0.554 0.554	0.565 0.565	0.565 0.565	0.565 0.565	0.565 0.565	0.565 0.565	0.565 0.565	0.565 0.565	0.565 0.565	0.565 0.565

**ORIGINAL PAGE IS
OF POOR QUALITY**

Table X. (contd)
Upper throat passage static pressure data

RUN CODE	PERCENTAGE DISTANCE FROM UPPER VANE MIDSPAN TO LOWER VANE MIDSPAN VIA THE ENDWALL: TOTAL DISTANCE = 11.008 cm (4.296 in)	ENDWALL										PRESSURE SURFACE (LOWER VANE)						
		SUCTION SURFACE (UPPER VANE)					ENDWALL					PRESSURE SURFACE (LOWER VANE)						
		0.131	0.171	0.245	0.306	0.362	0.409	0.470	0.530	0.590	0.639	0.679	0.704	0.733	0.778	0.840	0.913	0.953
44133	0.545	0.547	0.544	0.542	0.562	0.579	0.588	0.593	0.594	0.588	0.572	0.548	0.546	0.532	0.554	0.555	0.541	
44135	0.536	0.557	0.555	0.551	0.572	0.589	0.597	0.603	0.604	0.599	0.581	0.557	0.557	0.544	0.565	0.566	0.551	
44144	0.557	0.558	0.554	0.548	0.569	0.586	0.597	0.605	0.606	0.598	0.580	0.559	0.559	0.546	0.568	0.569	0.554	
44145	0.566	0.567	0.563	0.556	0.577	0.594	0.605	0.613	0.614	0.607	0.588	0.567	0.568	0.555	0.576	0.577	0.563	
44155	0.559	0.559	0.555	0.548	0.570	0.588	0.599	0.606	0.607	0.599	0.581	0.560	0.561	0.548	0.569	0.570	0.554	
44203	0.555	0.556	0.552	0.545	0.564	0.584	0.595	0.602	0.603	0.599	0.579	0.555	0.553	0.540	0.562	0.565	0.552	
44204	0.554	0.555	0.551	0.543	0.563	0.583	0.594	0.601	0.602	0.598	0.578	0.554	0.551	0.538	0.560	0.564	0.550	
44205	0.557	0.558	0.554	0.546	0.565	0.586	0.596	0.603	0.605	0.601	0.581	0.556	0.554	0.540	0.563	0.566	0.553	
44303	0.555	0.556	0.552	0.545	0.564	0.584	0.594	0.601	0.603	0.599	0.579	0.555	0.553	0.539	0.561	0.565	0.552	
44304	0.562	0.563	0.559	0.551	0.569	0.590	0.601	0.608	0.611	0.607	0.586	0.563	0.561	0.547	0.569	0.573	0.560	
44305	0.561	0.562	0.558	0.550	0.569	0.590	0.601	0.608	0.610	0.606	0.585	0.562	0.559	0.546	0.567	0.571	0.557	
44306	0.560	0.563	0.559	0.561	0.567	0.590	0.600	0.608	0.610	0.605	0.583	0.562	0.559	0.535	0.567	0.571	0.557	
44307	0.560	0.562	0.559	0.561	0.567	0.589	0.600	0.608	0.610	0.604	0.582	0.560	0.552	0.534	0.561	0.565	0.552	
44308	0.566	0.568	0.565	0.566	0.572	0.594	0.605	0.613	0.615	0.607	0.585	0.563	0.561	0.547	0.569	0.573	0.560	
44333	0.554	0.555	0.551	0.544	0.563	0.584	0.594	0.602	0.603	0.599	0.578	0.555	0.552	0.539	0.553	0.557	0.544	
44344	0.561	0.562	0.558	0.550	0.569	0.590	0.601	0.609	0.611	0.607	0.585	0.562	0.559	0.535	0.567	0.571	0.554	
44355	0.561	0.562	0.558	0.550	0.569	0.589	0.600	0.608	0.610	0.604	0.582	0.560	0.552	0.534	0.565	0.569	0.552	
45000	0.540	0.544	0.540	0.545	0.560	0.575	0.586	0.593	0.595	0.588	0.571	0.537	0.541	0.533	0.550	0.550	0.536	
45103	0.556	0.560	0.555	0.558	0.571	0.589	0.599	0.607	0.609	0.601	0.583	0.556	0.557	0.532	0.561	0.565	0.551	
45104	0.555	0.558	0.554	0.557	0.570	0.587	0.598	0.606	0.608	0.600	0.582	0.554	0.556	0.532	0.567	0.572	0.558	
45105	0.557	0.560	0.556	0.559	0.572	0.590	0.600	0.607	0.610	0.602	0.584	0.553	0.557	0.531	0.565	0.566	0.553	
45135	0.553	0.556	0.552	0.555	0.569	0.586	0.596	0.604	0.607	0.599	0.580	0.549	0.552	0.537	0.560	0.561	0.548	
45145	0.558	0.561	0.557	0.561	0.574	0.590	0.601	0.609	0.612	0.604	0.585	0.554	0.558	0.531	0.566	0.571	0.553	
45155	0.553	0.556	0.552	0.555	0.569	0.585	0.596	0.605	0.607	0.598	0.580	0.549	0.553	0.536	0.564	0.566	0.551	
45303	0.550	0.554	0.549	0.553	0.566	0.584	0.594	0.601	0.604	0.595	0.578	0.553	0.551	0.531	0.548	0.559	0.547	
45304	0.554	0.558	0.553	0.556	0.570	0.587	0.597	0.605	0.607	0.599	0.582	0.554	0.555	0.530	0.563	0.565	0.551	
45305	0.551	0.554	0.550	0.553	0.566	0.584	0.594	0.602	0.604	0.595	0.578	0.550	0.550	0.537	0.559	0.560	0.547	

ORIGINAL PAGE IS
OF POOR QUALITY

Table XI.
Lower throat passage static pressure data

RUN CODE	PERCENTAGE DISTANCE FROM UPPER VANE MIDSPAN TO LOWER VANE MIDSPAN VIA THE ENDWALL: TOTAL DISTANCE = 11.008 cm (4.296 in)								PRESSURE SURFACE (LOWER VANE)									
	SUCTION SURFACE (UPPER VANE)				ENDWALL													
	0.047	0.086	0.160	0.222	0.267	0.296	0.320	0.362	0.409	0.530	0.590	0.679	0.704	0.733	0.778	0.840	0.913	0.953
34.000	0.602	0.606	0.606	0.605	0.601	0.602	0.599	0.603	0.624	0.658	0.669	0.667	0.652	0.654	0.660	0.641	0.668	0.681
34.103	0.610	0.613	0.613	0.612	0.608	0.607	0.599	0.607	0.630	0.667	0.680	0.675	0.660	0.662	0.668	0.650	0.675	0.688
34.104	0.604	0.608	0.608	0.606	0.603	0.602	0.594	0.602	0.625	0.663	0.676	0.670	0.655	0.657	0.664	0.645	0.671	0.684
34.105	0.607	0.610	0.610	0.609	0.605	0.604	0.596	0.603	0.629	0.666	0.679	0.674	0.650	0.661	0.668	0.649	0.675	0.687
34.135	0.608	0.611	0.611	0.609	0.606	0.605	0.598	0.603	0.629	0.666	0.678	0.674	0.659	0.661	0.667	0.648	0.674	0.687
34.145	0.614	0.616	0.616	0.615	0.611	0.611	0.603	0.608	0.634	0.670	0.682	0.678	0.664	0.665	0.672	0.653	0.679	0.691
34.155	0.605	0.608	0.608	0.606	0.602	0.602	0.594	0.600	0.626	0.663	0.674	0.670	0.656	0.657	0.663	0.644	0.671	0.684
34.303	0.606	0.608	0.608	0.607	0.603	0.603	0.598	0.598	0.623	0.660	0.671	0.670	0.655	0.657	0.664	0.645	0.672	0.684
34.304	0.603	0.606	0.606	0.605	0.601	0.601	0.596	0.597	0.622	0.659	0.671	0.668	0.653	0.655	0.662	0.643	0.670	0.682
34.305	0.606	0.607	0.607	0.606	0.601	0.602	0.597	0.598	0.623	0.660	0.671	0.669	0.654	0.656	0.662	0.644	0.671	0.683
43.000	0.624	0.508	0.509	0.506	0.499	0.502	0.507	0.518	0.534	0.565	0.577	0.571	0.561	0.567	0.570	0.551	0.584	0.603
43.103	0.512	0.513	0.512	0.511	0.505	0.508	0.511	0.516	0.530	0.571	0.586	0.576	0.567	0.570	0.578	0.558	0.589	0.602
43.104	0.663	0.506	0.506	0.505	0.500	0.501	0.505	0.511	0.531	0.565	0.578	0.572	0.562	0.568	0.572	0.552	0.585	0.605
43.105	0.715	0.501	0.500	0.498	0.491	0.492	0.496	0.503	0.524	0.556	0.566	0.558	0.551	0.559	0.565	0.545	0.582	0.601
43.135	0.832	0.503	0.502	0.500	0.495	0.496	0.500	0.505	0.525	0.558	0.569	0.563	0.555	0.563	0.567	0.548	0.583	0.602
43.145	0.795	0.503	0.502	0.500	0.494	0.495	0.499	0.505	0.526	0.559	0.571	0.564	0.556	0.563	0.567	0.548	0.583	0.602
43.155	0.729	0.500	0.499	0.497	0.490	0.491	0.495	0.501	0.523	0.555	0.566	0.558	0.551	0.559	0.565	0.545	0.582	0.601
43.303	0.912	0.508	0.509	0.507	0.502	0.503	0.508	0.513	0.532	0.566	0.578	0.574	0.564	0.570	0.574	0.555	0.587	0.606
43.304	0.907	0.509	0.509	0.507	0.502	0.504	0.508	0.513	0.532	0.566	0.578	0.574	0.564	0.570	0.574	0.555	0.587	0.606
43.305	0.902	0.510	0.510	0.508	0.502	0.503	0.508	0.513	0.532	0.566	0.578	0.575	0.565	0.571	0.575	0.555	0.588	0.607
44.000	0.510	0.510	0.510	0.509	0.500	0.504	0.509	0.517	0.532	0.566	0.580	0.576	0.562	0.565	0.573	0.553	0.592	0.609
44.103	0.509	0.510	0.510	0.509	0.502	0.506	0.509	0.512	0.532	0.569	0.583	0.581	0.566	0.570	0.577	0.556	0.595	0.612
44.104	0.505	0.506	0.505	0.504	0.497	0.500	0.504	0.509	0.528	0.565	0.578	0.574	0.561	0.565	0.573	0.552	0.594	0.611
44.105	0.509	0.510	0.510	0.509	0.508	0.501	0.504	0.507	0.513	0.528	0.567	0.581	0.569	0.564	0.573	0.551	0.592	0.607
44.106	0.508	0.509	0.508	0.506	0.498	0.501	0.504	0.511	0.527	0.564	0.579	0.574	0.566	0.573	0.575	0.554	0.591	0.610
44.107	0.512	0.514	0.513	0.509	0.499	0.502	0.506	0.514	0.529	0.569	0.583	0.574	0.564	0.567	0.575	0.554	0.592	0.611
44.108	0.514	0.516	0.514	0.509	0.498	0.502	0.506	0.513	0.529	0.568	0.582	0.574	0.565	0.565	0.576	0.553	0.592	0.611

ORIGINAL PAGE IS
OF POOR QUALITY

Table XI. (contd)
Lower throat passage static pressure data

RUN CODE	PERCENTAGE DISTANCE FROM UPPER VANE MIDSPAN TO LOWER VANE MIDSPAN VIA THE ENDWALL: TOTAL DISTANCE = 11.008 cm (4.296 in)																	
	SUCTION SURFACE (UPPER VANE)					ENDWALL					PRESSURE SURFACE (LOWER VANE)							
	0.047	0.086	0.160	0.222	0.267	0.296	0.320	0.362	0.409	0.530	0.590	0.679	0.704	0.733	0.778	0.840	0.913	0.953
44133	0.502	0.503	0.501	0.500	0.492	0.495	0.499	0.504	0.524	0.559	0.572	0.567	0.556	0.561	0.570	0.550	0.591	0.607
44135	0.506	0.506	0.505	0.504	0.497	0.500	0.504	0.509	0.528	0.565	0.578	0.573	0.560	0.564	0.573	0.552	0.592	0.608
44144	0.505	0.506	0.505	0.504	0.496	0.500	0.504	0.508	0.527	0.564	0.577	0.573	0.560	0.564	0.573	0.552	0.593	0.609
44145	0.509	0.510	0.509	0.508	0.500	0.504	0.508	0.512	0.532	0.568	0.582	0.578	0.564	0.568	0.576	0.555	0.594	0.610
44155	0.507	0.508	0.507	0.506	0.498	0.502	0.505	0.507	0.527	0.563	0.576	0.575	0.562	0.566	0.574	0.554	0.594	0.610
44203	0.507	0.508	0.507	0.506	0.498	0.501	0.505	0.506	0.526	0.562	0.576	0.574	0.561	0.566	0.574	0.553	0.594	0.609
44204	0.506	0.508	0.507	0.505	0.497	0.499	0.503	0.505	0.525	0.561	0.575	0.572	0.560	0.565	0.574	0.552	0.593	0.608
44205	0.508	0.509	0.508	0.506	0.498	0.500	0.505	0.507	0.527	0.563	0.576	0.573	0.560	0.565	0.574	0.552	0.594	0.608
44303	0.506	0.508	0.507	0.506	0.497	0.500	0.504	0.505	0.525	0.561	0.575	0.573	0.560	0.565	0.574	0.552	0.594	0.608
44304	0.510	0.512	0.511	0.509	0.502	0.504	0.508	0.509	0.529	0.566	0.580	0.578	0.565	0.569	0.577	0.555	0.596	0.609
44305	0.508	0.510	0.509	0.507	0.498	0.500	0.505	0.509	0.529	0.566	0.579	0.575	0.561	0.566	0.574	0.552	0.594	0.611
44306	0.511	0.513	0.512	0.508	0.502	0.503	0.505	0.510	0.526	0.566	0.581	0.572	0.562	0.565	0.573	0.552	0.594	0.609
44307	0.512	0.514	0.513	0.507	0.501	0.497	0.501	0.509	0.525	0.561	0.575	0.573	0.560	0.565	0.574	0.553	0.594	0.609
44308	0.516	0.518	0.517	0.510	0.500	0.504	0.506	0.512	0.529	0.569	0.584	0.576	0.561	0.566	0.574	0.552	0.594	0.611
44333	0.505	0.508	0.507	0.505	0.497	0.500	0.503	0.509	0.523	0.566	0.579	0.573	0.561	0.566	0.574	0.552	0.594	0.609
44344	0.508	0.510	0.510	0.508	0.500	0.503	0.507	0.508	0.528	0.566	0.581	0.572	0.562	0.565	0.573	0.552	0.594	0.609
44355	0.507	0.509	0.508	0.506	0.497	0.500	0.504	0.508	0.528	0.565	0.580	0.572	0.561	0.564	0.573	0.552	0.594	0.608
45000	0.508	0.506	0.510	0.504	0.497	0.499	0.505	0.515	0.530	0.567	0.580	0.576	0.565	0.566	0.576	0.553	0.592	0.611
45103	0.509	0.507	0.510	0.507	0.504	0.506	0.510	0.512	0.530	0.569	0.581	0.579	0.563	0.566	0.574	0.553	0.594	0.609
45104	0.511	0.508	0.511	0.508	0.504	0.506	0.510	0.513	0.531	0.571	0.585	0.586	0.569	0.570	0.576	0.554	0.596	0.610
45105	0.511	0.510	0.513	0.510	0.506	0.507	0.512	0.515	0.533	0.574	0.590	0.592	0.573	0.575	0.574	0.552	0.593	0.608
45135	0.509	0.506	0.509	0.507	0.502	0.504	0.509	0.512	0.530	0.571	0.587	0.588	0.570	0.572	0.579	0.554	0.596	0.605
45145	0.511	0.508	0.511	0.508	0.505	0.506	0.511	0.514	0.533	0.573	0.590	0.591	0.572	0.575	0.581	0.553	0.598	0.611
45155	0.510	0.506	0.510	0.506	0.502	0.503	0.508	0.511	0.530	0.571	0.587	0.589	0.570	0.572	0.579	0.554	0.598	0.609
45303	0.506	0.505	0.508	0.504	0.499	0.500	0.505	0.508	0.526	0.565	0.577	0.574	0.562	0.565	0.576	0.552	0.598	0.609
45304	0.510	0.507	0.510	0.506	0.501	0.502	0.507	0.510	0.528	0.566	0.579	0.577	0.563	0.566	0.576	0.552	0.597	0.610
45305	0.508	0.506	0.509	0.505	0.499	0.499	0.505	0.508	0.526	0.565	0.577	0.575	0.561	0.565	0.576	0.552	0.597	0.611

NOMENCLATURE

ACF	Aerothermodynamic Cascade Facility
ASME	American Society of Mechanical Engineers
ASTM	American Society for Testing and Materials
CA	chromel-alumel
CAD/CAM	computer-aided design/computer-aided manufacturing
c _{lnt}	coolant
c _p	specific heat at constant pressure
CPU	central processing unit
C _r	correction factor for thermal entrance region effects
CRT	cathode ray tube
D	cooling hole diameter
dT/dn	surface normal temperature gradient
FEM	finite element model
h	heat transfer coefficient
h _{FC}	heat transfer coefficient with film cooling
h/h ₀	normalized heat transfer coefficient
h _{NFC}	heat transfer coefficient without film cooling
h ₀	reference heat transfer coefficient for normalization
HP	Hewlett-Packard
LDA	laser Doppler anemometer
le	leading edge
M	mega
Ma	Mach number
Ma ₁	upstream or vane row inlet Mach number
Ma ₂	downstream or vane row exit Mach number
Nu _D	diameter Nusselt number

P_c/P_t	coolant-to-inlet total pressure ratio (blowing strength)
$P_{c,ds}/P_t$	downstream film coolant-to-inlet total pressure ratio
$P_{c,le}/P_t$	leading edge film coolant-to-inlet total pressure ratio
$P_{c,ps}/P_t$	pressure side film coolant-to-inlet total pressure ratio
$P_{c,ss}/P_t$	suction side film coolant-to-inlet total pressure ratio
P/D	hole pitch-to-diameter ratio
\Pr	Prandtl number
ps	pressure side
P_s	surface static pressure
P_s/P_t	local static-to-inlet total pressure ratio
$PT1$	cascade inlet total pressure
R	gas constant
Re	Reynolds number
Re_D	diameter Reynolds number
Re_1	upstream or vane row inlet Reynolds number
Re_2	downstream or vane row exit Reynolds number
S	hole spacing
S	percent surface distance
ss	suction side
S/D	hole spacing-to--diameter ratio
SNR	Stanton number reduction
St_{FC}	Stanton number with film cooling
St_{NFC}	Stanton number without film cooling
T	temperature
T_c	coolant plenum temperature
T_c/T_g	coolant-to-gas absolute temperature ratio (thermal dilution)
T_g	cascade inlet total temperature
$TT1$	cascade inlet total temperature

T_w	vane surface temperature
T_w/T_g	vane surface-to-gas absolute temperature ratio
u	freestream velocity
u_c	coolant velocity
x	streamwise coordinate
y	surface normal coordinate
ρ	freestream density
ρ_c	coolant density

REFERENCES

1. L. D. Hylton, M. S. Michelc, E. R. Turner, D. A. Nealy, and R. E. York, "Analytical and Experimental Evaluation of the Heat Transfer Distribution over the Surfaces of Turbine Vanes," NASA CR-168015, May 1983.
2. E. R. Turner, M. D. Wilson, L. D. Hylton, and R. M. Kaufman, "Turbine Vane External Heat Transfer", Vol. I, NASA CR-174827, July 1985.
3. A. B. Turner, "Local Heat Transfer Measurements on a Gas Turbine Blade," Journal of Mechanical Engineering Sciences, Vol 13, pp 1-12, 1971.
4. M. E. Crawford and W. M. Kays, Convective Heat and Mass Transfer, McGraw-Hill, 1980.
5. S. J. Kline and F. A. McClintock, "Describing Uncertainties in Single-Sample Experiments," Mechanical Engineering, January 1953.
6. L. D. Hylton, V. Nirmalan, B. K. Sultanian, and R. M. Kaufman, "Turbine Airfoil Film Cooling," Turbine Engine Hot Section Technology - 1987, NASA CP-2493, 1987.



National Aeronautics and
Space Administration

Report Documentation Page

1. Report No. NASA CR-182133	2. Government Accession No.	3. Recipient's Catalog No.	
4. Title and Subtitle The Effects of Leading Edge and Downstream Film Cooling on Turbine Vane Heat Transfer		5. Report Date November 1988	
		6. Performing Organization Code	
7. Author(s) L.D. Hylton, V. Nirmalan, B.K. Sultanian, and R.M. Kaufman	8. Performing Organization Report No. Allison EDR 13481	10. Work Unit No. 505-62-21	
9. Performing Organization Name and Address Allison Gas Turbine Division General Motors Corporation P.O. Box 420 Indianapolis, Indiana 46206-0420	11. Contract or Grant No. NAS3-24619	13. Type of Report and Period Covered Contractor Report Final	
12. Sponsoring Agency Name and Address National Aeronautics and Space Administration Lewis Research Center Cleveland, Ohio 44135-3191	14. Sponsoring Agency Code		
15. Supplementary Notes Project Manager, Herbert J. Gladden, Internal Fluid Mechanics Division, NASA Lewis Research Center.			
16. Abstract This report addresses the progress under contract NAS3-24619 toward the goal of establishing a relevant data base for use in improving the predictive design capabilities for external heat transfer to turbine vanes, including the effects of downstream film cooling with and without leading edge showerhead film cooling. Experimental measurements were made in a two-dimensional cascade previously used to obtain vane surface heat transfer distributions on nonfilm cooled airfoils under contract NAS3-22761 and leading edge showerhead film cooled airfoils under contract NAS3-23695. The principal independent parameters—Mach number, Reynolds number, turbulence, wall-to-gas temperature ratio, coolant-to-gas temperature ratio, and coolant-to-gas pressure ratio—were maintained over ranges consistent with actual engine conditions and the test matrix was structured to provide an assessment of the independent influence of parameters of interest, namely, exit Mach number, exit Reynolds number, coolant-to-gas temperature ratio, and coolant-to-gas pressure ratio. Data from this contract provide a data base for downstream film cooled turbine vanes and extends the data bases generated in the previous two studies. The vane external heat transfer data obtained in this program indicate that considerable cooling benefits can be achieved by utilizing downstream film cooling. The downstream film cooling process was shown to be a complex function of two competing mechanisms. The thermal dilution effect, associated with the injection of relatively cold fluid, results in a decrease in the heat transfer to the airfoil. Conversely, the turbulence augmentation, produced by the injection process, results in increased heat transfer to the airfoil. The data obtained in this program and presented in this report illustrate the interaction of these variables and should provide the airfoil designer and computational analyst the information required to improve heat transfer design capabilities for film cooled turbine airfoils.			
17. Key Words (Suggested by Author(s)) Turbines; Heat transfer; Film cooling; Airfoils; Cascades	18. Distribution Statement Unclassified—Unlimited Subject Category 34		
19. Security Classif. (of this report) Unclassified	20. Security Classif. (of this page) Unclassified	21. No of pages 175	22. Price* A08

